On the Analysis of the Disproportionate Structural Collapse in RC Buildings

Dissertation

zur Erlangung des akademischen Grades

Dr.-Ing.

an der Fakultät Bauingenieurwesen

der

Bauhaus-Universität Weimar

vorgelegt von

Name: Hatahet, Tareq

aus: Syrien

Weimar

Gutachter: 1. Prof. Dr.-Ing. habil. Carsten Könke.

2. Prof. Dr.-Ing. Uwe Starossek

3. Prof. Dr. Dipl.-Ing. Guido Morgenthal

Tag der Disputation 22. Jan. 2018

Ehrenwörtliche Erklärung

Ich erkläre hiermit ehrenwörtlich, dass ich die vorliegende Arbeit ohne unzulässige Hilfe Dritter und ohne Benutzung anderer als der angegebenen Hilfsmittel angefertigt habe. Die aus anderen Quellen direkt oder indirekt übernommenen Daten und Konzepte sind unter Angabe der Quelle gekennzeichnet.

Weitere Personen waren an der inhaltlich-materiellen Erstellung der vorliegenden Arbeit nicht beteiligt. Insbesondere habe ich hierfür nicht die entgeltliche Hilfe von Vermittlungs- bzw. Beratungsdiensten (Promotionsberater oder anderer Personen) in Anspruch genommen. Niemand hat von mir unmittelbar oder mittelbar geldwerte Leistungen für Arbeiten erhalten, die im Zusammenhang mit dem Inhalt der vorgelegten Dissertation stehen.

Die Arbeit wurde bisher weder im In- noch im Ausland in gleicher oder ähnlicher Form einer anderen Prüfungsbehörde vorgelegt.

Ich versichere ehrenwörtlich, dass ich nach bestem Wissen die reine Wahrheit gesagt und nichts verschwiegen habe.

Tareq Hatahet

Weimar, 06 Dec 2016

Unterschrift

Table of contents

Acknowledgments

Sponsor

Without the funding of the German academic exchange service (DAAD), the advancement of this contribution was impossible. The DAAD provided the financial support through the international PhD scholarship program.

Supervisor

Special support and encouragement of Prof. Carsten Könke accompanied the journey of the work. Prof. Könke offered me a unique autonomy and support which enabled this independent development, without such leadership, the direction could have been changed and I could have been diverted from my target. Throughout the numerous conversations and discussions, I would like to return here his broad prospective, wide knowledge, sharp feedback, and encouragement.

His support was not only unique at guide, advice and direction levels, he also enabled financial means covered additional expense of my residence in Weimar. Prof. Könke supported my life-long development in many occasions through continuous funding of my learning; e.g. in the course of the advanced modelling of material in Prague, the advanced integration techniques based on Runge-Kuta Method in Kassel, the C++ course in the TU Munich, and in the visualization course in Stuttgart.

Acknowledgeable contributions

I would like to acknowledge the valuable free student membership of the American Concrete Institute opens all the journal in electronic copies. Without this facilities, many for

the recent ACI publication of the structural journal could not be obtained and discussed which could have undermined the quality and value of this report.

Prof. Tom Lahmer supported me in a few occasions. He proof-read draft version of chapter 7 and te German summary, answered many questions in the stochastic simulations, shared his courses' material openly. These, alongside his open door, open heart, and elegant reaction accompanied the journey with powerful encouragement and coaching.

Mrs. Terber, the executive secretary of the institution, also supported me. Although I was 1/52+ of her workload, she was always there with a solution, help and understanding, not to report my super-broken German.

Prof. Timon Rabczuk also supported me, I had joined his finite element (FE) analysis course, and he directed me to focus on structural FE which is more efficient for comparative analysis of various collapse models.

I also would like to acknowledge; Dr. Sarah Orton, Dr. Yhai Bao, and Dr. Kai Qian, for openness and the response to my email questions. Their responses were also useful in the learning of the topic.

Prof. Uwe Starossek in the kick-off of the research proposal in July 2011, although I was unable to follow up in Hamburg, the discussions and directions given in the 2 hours meeting was highly motivating and helped shaping the aim of this research.

Prof. Denis Lam drew my attention to the topic in 2007, although the sole work we were able to do was in steel frames, he guided my learning of key concepts from his wealthy background in steel and composite construction. Dr. Mihail Pekoviskis, the supervisor of my master thesis, supported my learning of the concepts of the nonlinear dynamic and static simulation of seismic response of RC structures.

Prof. Kypros Pilakoutas, from the University of Sheffield, is also credited for the course material in advanced design of reinforced concrete structures.

Dr. Ayham Abdulsamad helped me obtain many research papers beyond the service provided in the university library.

Last, but not least, Mr. Feras Alkam shared his time, asking questions every morning the kept on coaching me to focus on completing this work since he joined Prof. Lamer's group.

Also, sincerely acknowledged the contribution of Mr. Daniel Haag, and Philip Hofer for the help translating the summary into German.

Forward

- To my parents, my wife; Lama, and my children; Shefaa, Abdulrahman, and Hanan.
- To my senior guide, Prof Könke.
- To the committees of the German academic exchange service (DAAD), Karim Said Foundation and to all former and current supervisors and peers.
- To Prof. Tom Lahmer, and to Prof Uwe Starossek.
- To the community of the structural engineers involved in the renovation of buildings, or even demolition of the war ruins.
- To my colleagues at the institution of the structural mechanics at the Bauhaus University, and to my friends Dr. Ayham Abdulsamad and Eng. Salah Muhammad.
- To everyone seeks peace, and would like to see the human in safe, settled, happy, and booming environment.
- To every innocent suffered an aggressive war. To everyone lost a dear, a property, or got disabled as a result of the abuse of the war.
- And to everyone delighted to see this work.

Please accept my sincere love, pleasure, respect and tempting contribution. This only happened because of the energy I tanked whenever I thought about you.

Chapter 1 Introduction

1.1. Introduction

Here the main aim of this research is identified with reference to a few key features of the problem in hand through which the motivation is developed. The motivation is to understand how the structural safety can be improved for unforeseen abnormal loading events. This motivation is explained through example case studies of partial collapse situations. The problem is then defined generalizing the spectrum of case studies into the concept of disproportionate partial collapse in structures. Lights are shaded on the chosen methodology, resources, and approaches, used along-side this work. An introductory definition, of some key terms, is presented alongside the organization of the text.

1.2. Motivation

Many partial collapse case studies were reported all over the world in which the sole incident can be referred to the mechanical reaction of an extreme event; an impact, a blast, a fire, or an earthquake, a few examples are reported in the following paragraphs. In

addition to those reported examples, similar partial collapse can result from an immediate dynamic complex input like the rocket hit. Or in contrast, rather quasi-static action, such as the structural damage results from accumulated damage of, for example, the settlement of supports (Historical Archive of the City of Cologne in 2009), or the wetting of timber roofs (Bad Reichenhall Ice Rink roof collapse in 2006). Amongst these cases, understanding the transition of the structure from its initial state, to the stable partial, or the full collapse state, is the motivation of this work. To evaluate the remaining proportions of the building, a combination of simulation and site observations is required. With this view, the following text aim at rigorous contribution to the body of knowledge.

1.2.1. Blast as a source of partial collapse

Well-known example is the partial failure of the corner pay of the multi-story apartment in London result from gas explosion in the kitchen. The failure is limited to the single corner bay, Figure 1.2-1, although it propagated vertically. The partial collapse did not propagate to the nearby bays because of the rather detachable masses of the prefabricated reinforcement concrete elements used in construction.

The Progressive collapse of mill building is a classic example of progressive collapse following the removal of a single element at the third level, Figure 1.2-2. It happened suddenly and apparently without warning and it was fortunate that nobody was inside and the debris did not hit the nearby houses.

Figure 1.2-1 Ronan-Point-Explosion in London (Sourceable industry news analysis, 2016)

Buildings, like this example, were not designed with robustness in mind and there was no structural continuity and limited bracing apart from façade walls. They were constructed, not always very well, for specific industrial purposes and are now used for a variety of functions including conversion into residences.

Figure 1.2-2 progressive collapse of mill building from (Structural Safety, 2013)

In the following a few sources of partial collapse are presented through which the author aims at defining the problem statement of this research work.

1.2.2. Terrorists attack as a source of collapse

In the 1995, terrorists attack the federal building in the city of Oklahoma, Figure 1.2-3, the massive explosion lead to the full collapse of the affected proportion. The remaining part was detached because of structural separation which fortunately saved the rest of the structure.

Figure 1.2-3 the federal building in the city of Oklahoma (Net World Directory, 2013)

The ruins of the Khobar Towers military complex in Saudi Arabia, Figure 1.2-4, after the terror attack. The figure shows full detachment of the front bay (wikipedia, 1996).

A building in Aleppo, Syria Figure 1.2-5, attacked by explosion (Anderson, 2012), the extend of structural damage does not cause a complete failure of a column, however, the long-term reliably of the structure after shock will require careful examination.

Figure 1.2-4 Khobar Towers military complex in Saudi Arabia (wikipedia, 1996)

Figure 1.2-5 Bombs in Syria affect governmental building from (Anderson, 2012)

1.2.3. Earthquakes as source of partial collapse

Earthquake results in different types of structural collapse (Scawthorn & Johnson, 2000). One of the reported example, Multi-story, east of Golçuk Figure 1.2-6, show a partial collapse of structure which result from the fault crossing the building. The continuity of the structural system seemed to reduce the tragedy and probability enabled someone to escape.

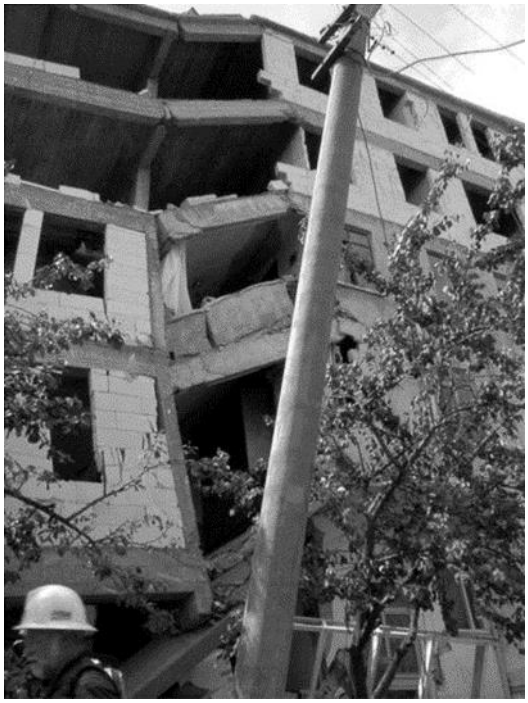

Figure 1.2-6 Multi-story building intersected by faulting from (Scawthorn & Johnson, 2000)

Another example of an earthquake induced partial collapse comes from Chile (2010 Chile earthquake, 2016). In the Figure 1.2-7, a soft-story mechanism spread over a significant proportion of the story area, although the mass of the above 8-9 stories is considerable, the structure remained stable without the full spread of collapse. It can be said the kinetic energy of the moving/rotating stiffness is less than the strain energy of the nearby structure that hold the collapsing proportion.

Figure 1.2-7 Partial soft-story vertical arrested collapse from (2010 Chile earthquake, 2016)

The ruins of the five-story office building, shown in the Figure 1.2-8, is another example of seismic collapse, Tangshan (Huixian & George W. Housner, 2016). The lower three stories had concrete columns, and the upper two stories were unreinforced brick without concrete columns.

Figure 1.2-8 Partial seismic collapse of building in china from (Huixian & George W. Housner, 2016)

1.2.4. Floods as source of partial collapse

Floods are another source of the partial collapse risk, in the example, the action of flow exceeding the well-known hydro-dynamic pushing force to evacuating the sub-soil and driving parts of the sub-structure. Although the full row of supporting element was moved out, Figure 1.2-9, the slab still hanged above by the tensile catenary of the continuous steel reinforcement. This example indicates the ability of the tensile catenary to take high dynamic action.

Figure 1.2-9 damaged by passage of debris-flow from (Wieczorek, Larsen, Eaton, Morgan, & Blair, 2016)

1.2.5. Fire source of the partial collapse

Fire, as it localizes for more than one hour, causes softening in the structural system, which can cause propagation of collapse. The damaged proportion can be see toward the top of the provided picture in Figure 1.2-10 (Kolkata, 2013). The long duration fire can cause stiffness softening of concrete and steel, therefore, the tensile catenary of reinforcement is a prime reaction mechanism in case of fire event.

Figure 1.2-10 Fire cause partial collapse of shopping building from (Kolkata, 2013)

1.2.6. The war source of partial collapse or full collapse

All the earlier given examples enjoy the definition of the rare even, and can be normally handled by the extreme event theories. However, when the rare terror event spans over the whole nation in wars, the high robustness of the human shelter become persistent problem, and therefore, it justifies serious and immediate efforts to increase structural robustness. No examples are reported here; the reader can use the image search function in any web search engine to find many examples.

The wars, in Syria as an example, left a huge number of half-ruined properties. Those properties, supposed to provide shelter, caused fatalities and permeant injuries due to partial or full collapse. For those two reasons, simulation of the collapse progression can aid decisions about the future of those ruins and guide the building standards for more robust shelter no matter how cruel the war crisis!

1.3. Statement of the problem

The challenge of the research is two folds; to find ways through which the robustness character of the building structures can be improved increasing resilience and human safety with minimal economic implication, and to address the analytical technique through which the later state of the remaining structure can be evaluated.

The collapsing structure will go through three phases; the immediate reaction to the abnormal event, also known by the direct reaction, the development of the mechanism

marked by large plastic deformations, and, at last, the transit from body motion to the static stable state. Assumptions were made to analyze the problem as explained in the following paragraphs, although the objectivity of these assumptions were revisited along this document.

1.3.1. The initiating event

Among the community of the progressive collapse practitioner, it has been accepted that the most rigorous analytical framework for the collapse safety assessment can be made regarding the unknown trigger event by removing certain part of the structure. The analytical framework is based on the following; elimination of supporting part of the structure; e.g. a column, then study the reaction through incremental nonlinear dynamic analysis (INDA) of the structure which is supposed to provide the alternate load path (ALP) (GSA, 2003). Therefore, the event is idealized here by removing columns or wall in the context of building structures.

1.3.2. The development of the collapse mechanism

Performing the prescribed INDA and investigating the actual ALP is straight forward when the design is checked for safe reaction as the damage is limited to predefined zones, in this case most of the structure will react in rather linear behavior, and few elements will go through some limited material nonlinear response.

In contrast to the ALP approach, simulating the event that causes partial collapse, or even a full collapse, will necessitate the modeling strategy to be ready to capture not only material nonlinearity, but also geometrical ones at any element of the structure. In application to the reinforced concrete (RC) structures, such INDA simulation presents an open challenge when the ALP is undefined. Undefined means the location and the extension of the plastic hinges is unknown. Therefore, the unknown collapse mechanism must be identified first, thereafter the ALP can be defined, and then the INDA can be performed. Finding the right ALP, and the reliable definition of its parameters, is a major challenge in this field to which major part of this work is dedicated.

1.3.3. The dynamic nature of the collapse progression

Ideally having the ALP in hand, between the two stable states of the structure; before and after the trigger event, there is dynamic response phase. The dynamic phase will depend on the level of damage in the ALP, for example, if small deformation was enough for the development of strong reaction mechanism, then this dynamic phase can be handled as a transit analysis with limited contribution of the motion. However, if system react with large deflection, the moving mass will go through a body motion phase before it lands on the transit analysis phase. The body motion phase was not handled before in the literature, therefore, the subject of this research will be to find an appropriate routine that describes the key parameters of the dynamic phase including the body motion effects.

1.4. Goal and objectives

There are a few existing simulation methods in the literature, these computational models are either limited to redundant mechanisms; e.g. models based on explicit integration schemes, or based on artificial parameters such as plasticity limiters or artificial element erosion parameters. Also, when continuum volume-base FE is used, simulation of the full size building structure become quite demanding making the task of evaluating different solutions and assumptions rather impossible. Also, existing models that use reduced finite element, e.g. based on structural beam column elements, were extended based on macro mechanical models based on multi-spring component assembly. These models required careful preprocessing of the limit state, and cannot adopts to various loading conditions that changes during simulation. Therefore, it is one of the concerns to find and evaluate a more appropriate modelling technique using the structural, rode-based, finite element method (SFEM).

With focus on the partial collapse, recent test benchmarks have been added to the literature, these new benchmarks point towards new critical targets of the simulation which were not handled before. Then, in this dissertation, these targets are identified, and used to validate the authors' new proposed model.

The probabilistic nature of the rare initiation event is well handled in the literature, but there is no evidence of well-structured framework that handles these uncertainties at both physical and modeling levels. Bearing in mind that the machismos are only identified with relatively recent test benchmarks, and the absence of the balanced modeling technique, one aim here is to take these developed simulation method, validate it to the new benchmarks, and roll it in structured assessment framework of structural robustness.

To isolate the modeling and physical uncertain parameters, sound analytical framework is needed. Although there are a few attempts to describe the key physical parameters affecting the collapse mechanism. Non-of-them, to date, is successful to describe the full response curve as each introduce a specific case problem at single pointwise of the response curve of the mechanism. Therefore, another aim here is to survey, describe, and develop a consistent analytical framework.

To summarize, the aim of this work is to reliably simulate the progressed development of the collapse mechanism and improve the judgment of the full, or partial, collapse potential of the reinforced concrete buildings as a disproportionate result of unspecified initiation event. Toward the goal, the following are the general objectives of this dissertation;

1. Identify the key parameters affecting the development of the collapse mechanism. And understand the limits and the sensitivity of each of them.
2. Develop a simulation technique through which the unknown collapse mechanism can be automatically identified.
3. Identify the limits of the simulation models, and handle modelling uncertainties isolating physical (mechanical) and modelling uncertainties.
4. Develop an assessment algorithm to identify the level of structural robustness.

In line with the goal statement, the objectives of the research will be more articulated considering the literature review which is the subject of chapter 2.

1.5. Methodology

The subject receives momentum and every week there are a few published contributions. Because the target of this research is the response at the full structural level, it encompasses a wide area of interest that made coping up with the momentum in the literature a difficult task, one can observe that many of the referenced articles are relatively recent. This caused the target to be realigned a few times throughout the progress of this work. Digesting the live literature, therefore, was a significant part of the development. The wealthy literature includes testing of components and structures, in addition to various simulation techniques. Chapter 2, presents an effort to bridge those literatures directly related to the contribution of this thesis. Based on the close examination of tests, a set of modeling quality criteria was established which is used to evaluate proposed simulation techniques. The last evaluation leads to further refinement of the research objectives which were used to elect the modeling strategy. While selecting the modeling tool, various complexities were faced. Many of these complexities can lead to a single problem known as a convergence problem. To aid the development process, and to enable stochastic analysis of the modelling parameters, structural finite element method (SFEM) were finally selected, it has also the appealing merits in case of seismic collapse analysis based on the dynamic time history. The geometrical nonlinear response in RC structure is unpopular problem because it fails at limited deformation, the at limited displacement, therefore, here new challenges have been handled, namely;

- The localized softening response and the objective unloading of the nearby element,
- Convergence problem in the softening phase and at the points of sudden change in element stiffness,
- Geometric transformation and the right choice of element discretization,

During simulation of local collapse mechanism, biased results were observed. These biases can be attributed either to the physical representation or to methodological based on the discretization of SFEM. To improve key parameter isolation process, simple, but novel,

analytical framework is perused in chapter 3 and Chapter 4, these procedures is used alongside benchmark tests to help improve the computational model based on SFEM. The structure of the SFEM is presented and discussed with validation benchmark in chapter 5.

Based on the test benchmarks, new analytical model, and the SFEM simulation strategy are developed. Uncertain parameters stem out modeling assumptions are identified in light with the regained limits of the developed SFEM models, and the analytical model pointed to the physical uncertain parameters. Then, uncertainties of physical and modelling source are identified and insolated, see chapter 6. Thereafter, new criteria of the overall structural robustness of progressive collapse is developed, this is linked to sub-modeling performance functions representing the three different phases of response, this performance functions are related to the modelling targets and presented for the first time in this report. The performance functions are presented by both deterministic and stochastic forms, both can be used for modelling, and/or, structures robustness alike. The structural robustness is presented; for a specific trigger point, and for the building. The presented indexes can objectively represent the favorable effects and coined to the opposite concept of the failure probability, or can be used as a risk index, these are presented in chapter 7.

1.6. Contributions

While targeting modeling at the building level, the contributions here are wide in scope from material failure up to full structural model. Alongside, the interest in the topic is increasing to the level that each week, there are a few relevant articles. Therefore, an attempt to present a state-of-the-art review and analysis is made although no guarantee can be made considering the limits of resources. Yet, all the chapters are original and presented for the first time in this document apart from the chapter 4, and parts of chapter 6 and 7, were presented in a former conference papers. The following contributions are here made;

- Structured review of the vibrant literature alongside the isolation of the key relationships. The recognized relationships were redeployed in target simulation criteria which describes the key modeling qualities necessary for progressive collapse

simulation. This set of modeling targets are nowhere discussed before in the literature, and therefore the first contribution to the current knowledge of the subject. These can be found in chapter 2.

- Based on the identified relationships, novel analytical framework based on simple procedures which describes the key parameters is developed and evaluated. The procedures match the test and provide quick learning portal which identify the key physical parameters through straight forward equations and procedures. However, these procedures cannot be used independent from higher order simulation in application to a RC building, it is still handful evaluating results of the structural FEM simulation, and guide the selection of the uncertain parameters that stems from the selected modelling strategy. Otherwise, uncertainty simulations could take the form of sophisticated numerical problem blind of the obvious principle relations. These are presented in chapter 3.
- As the slab grid reinforcement contributes to the absorption of the mechanical energy, simple analytical technique is developed and compared to benchmarks. The developed techniques answer the question of the rule of slab in the transition phase of progressive collapse, this question is raised a few times in the literature, and an answer is provided in the chapter 4. This comes along the line of identifying the principles that identify the key physical parameters.
- Structural element based FEM model using the Open Source program, the OpenSEES, is developed. It is capable of modelling, beam arching, objective softening, large deflection {non-linear geometry), and the cable catenary forces. The model is new in the sense of its domain of application and validation. Because, the presented models in the literature using the OpenSEES, or the SFEM in general, is either limited to quasi-linear response of the structure, or base on a mechanical macro models undermining the quality of the simulation where the loading condition at the key zones must be pre-processed and therefore the simulation cannot handle the

evolution of these zone naturally during simulation and moving from one phase of response to the other. The SFEM is presented in chapter 5.

- Because the progressive collapse is uncertain phenomenon, it is necessary to identify the source of uncertainties. Uncertainties are discussed for the first time in direct relation to the different modes of collapse mechanism. Simulation uncertainties are introduced recognizing the limits of the model. And a distinction between the model uncertain parameters, and the physical one is clearly established. The propagation of the modelling uncertainty is presented.
- Novel structural collapse robustness framework is developed and evaluated based on development simulation models and uncertain parameters. In this framework structured robustness indexes are collected on a uniform measure which can reflect reliability of the simulation, or the level of structural robustness. Through the decision tree, the link between uncertain parameters and the performance functions is established. And the performance functions are presented in both deterministic and stochastic form.

1.7. Structure of the thesis

In order to introduce the targets of this report, in Chapter 1, example problems are presented motivating and points towards future application. The problem statement is formulated in line with the current knowledge and the pursued development. Research objectives are articulated. An overview of the work methodology, and a summary of delivered contributions are also included. This chapter ends with overview of the thesis structure.

To sharpen the research objectives in an up-to-date target, in Chapter 2, review of the literature is presented including testing of components and structures, in addition to various simulation techniques. Solid conclusion is deduced based on firm test results, along the line, modeling qualities are developed guiding the survey of modelling strategies and more

precise research targets are concluded. The modeling qualities provided better insight into the limits of popular modeling techniques.

In Chapter 3, based on the firm test results, an analytical framework is developed that aims at isolating the key mechanical parameters in progressive collapse analysis. The model is novel, and compares well to test benchmarks linked to the mechanics of concrete structure at the level of bridging beam failure mechanism in both the arching and catenary. As an extension to the earlier chapter, Chapter 4, provide a simple model for the average slab contribution in the RC buildings, the models is discussed and compared to benchmarks.

While the presented analytical model in Chapter 3 is limited to simple cases, in Chapter 5, Computation based structural FEM model handling material and geometrical nonlinearity is developed based on the open source program; the OpenSEES (McKenna, Fenves, & Scott, 2000). The model, which is based on flexibility beam elements is presented, evaluated, and validated in this chapter.

While the progressive collapse simulation is rather complex, the sources of uncertain mechanical and modeling nature are discussed in Chapter 6. Sensitive parameters, of mechanical and modelling sources are discussed. Special attention is allocated to failure modes of columns in light with content of progressive collapse modelling using the structural FEM. While uncertainty can be handled through stochastic definition of key variables, performance functions are presented in chapter 7. These functions are also used in deterministic form defining a single robustness criterion for structural robustness. The criteria are provided from an event, or a specific trigger point, and for a building as a decision aid tool.

In Chapter 8, a summary of the presented models and finding is reported alongside some key conclusions. As result of this work, a few important future destinations are concluded. These are summarized by the end with some recommendations.

Chapter 2 Survey of the literature

2.1. Aim and abstract

The purpose of this section is to refocus the objectives of research in light of laboratory experiments and contemporary computer models. This survey prepares the ground for later developments reported in the following chapters.

The main assumption of the event independent approach is visited, thereafter, the benchmark tests are reviewed, and the key finding are summarized. Across the wide spectrum of contributing researchers, important results were structured and integrated aiming at understanding the subject. Based on finding, modeling criteria are developed for progressive and partial collapse simulation and presented taking their uncertain nature in mind. In light with the modeling criteria, or targets, different modeling approaches are surveyed and evaluated. Throughout this survey; reintegration, evaluation, and the refocus of objectives are reported as evolved. Refined set of research targets are concluded

2.2. The representation of initiating/trigger event

Design guidelines and standards accepted the use of quasi-static alternate load path (ALP) analysis for collapse safety and risk assessment in buildings. The quasi-static nature of the alternate load path analysis conforms to the fact the remaining strength of the blast or impacted structure is down to longitudinal reinforcement under the persisted axial force (Fujikake & Aemlaor, 2013). The buckled bars, and based on the intensity of the shear stirrups, provide a damping device. The quasi-static nature of the force redistribution during the full development of the collapse mechanism in redundant structures is confirmed by the relatively stable collapse of the half-scale 3x3 bays collapse test of the RC building, the second case reported in (Xiao, et al., 2015).

In fact, not only the shear reinforcement plays a main rule the residual strength of the collapsing column due to blast, the higher the axial load, the higher the ultimate strength of the column (Astarlioglu, Krauthammer, Morency, & Tran, 2013).

Therefore, the quasi-static remove of a column, or more, is justified to represent nonspecific abnormal threat of which the most severe scenario is the blast, and the blast effect can be confidently exemplified by quasi-static loading simulation of the ALP. Having said this about blast load, column removal can be presumed an envelope representation of other non-specific events which have less dynamic implications.

2.3. Tests and observations of collapse mechanisms

Accepting column removal as a reasonable representation of an abnormal event, many researches did explore the bridging actions after elimination of a single support or more. In the following an overview of these tests will be provided in association with the main finding. The following review is organized from the simplest test to the more complex ones. A summary of the main observations is made at the end of the section. Most of the following test are performed through quasi-static monotonic loading/displacement procedures unless specific loading procedures are referred to.

2.3.1. Tests of plane frames

The mechanism is the state of the sub-structure being in large deformation/deflection, which results from the flow, plastic deformation, of many elements enough to make the assembly irredundant, then in quasi-static motion.

The simplest form of mechanism is the one of the simple beam, in the simple beam a plastic-hinge forms at the point of the maximum bending moment. The mechanism is then consisting of three hinges; the two simple supports and the one at the point of the maximum bending. These are presented in the Figure 2.3-1 for simple beam.

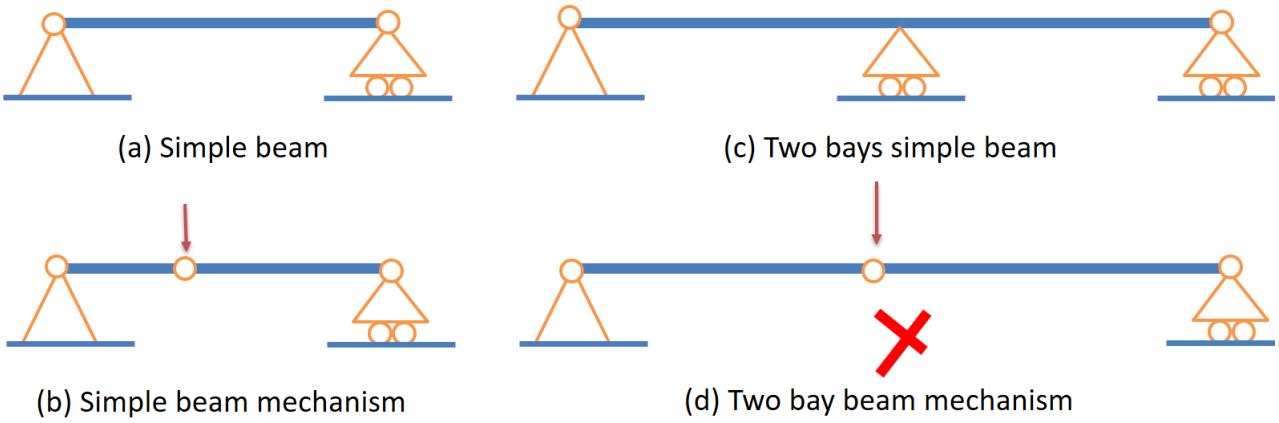

Figure 2.3-1 example beam mechanism in simple single, or double bay beam conditions

2.3.1.1. The simple beam conditions

The simplest mechanism of a continuous beam bridges over a missing column is the case of mechanism of a two bays beam. Where the stiffness of the joint at the middle lost column is higher that of that of the beam, plastic hinges forms at the both sides of the lost column forming the collapsing mechanism. One of these two hinges will break first due to imperfection causing an un-symmetric response even in a test set-up. In such a simple case the strength of the mechanism is down to the ultimate ductility of the weakest hinge. And the system will respond with a single peak of strength based on the plastic-bending strength of the assembly.

2.3.1.2. Improved boundary conditions

By increasing the translation stiffness, or rotation stiffness of the supports, the response of the assembly will change. Two peaks of strength are realized with the improved axial restraint of the assembly, the arching strength, and the tensile catenary.

If **rotational** constraints at boundaries are applied, due to the continuity of the frame action for example, the ability of the mechanism to redistribute the bending will be enhanced because of the improved redundancy causing the overall displacement **ductility** to increase. This may in turn be due to the improve in the arching strength of the assembly, but in fact it will increase the energy absorption capacity. Therefore, it is believed that it improves the dynamic damping rather than the static strength.

Unless the horizontal **translation** is also constrained, the second peak of the response, which is the **tensile catenary**, will not be observed if a tensile reaction in the support cannot develop. If compressive reaction can also develop in the support, the geometrical constraints of the beam between supports causes an axial force to develop in the form of an arch-like flow of compressive stress. This can improve the strength at the first peak, and this why the first peak is also regarded **as the arching strength**. Another factor can increase this arching compressive force, under high flexural deformation, the line of neutral axis shifts towards the compression zone, this shift indicates that the average strain in the beam section is in tension, and therefore the beam is increasing in length. Such phenomenon is regarded sometimes by the beam growth which adds to the developed resultant of shear force.

With rotational strains due to strong columns for example, two different detailing level tested by (Choi & Kim, 2011), their results confirmed the increased strength and ductility of the seismic detailed sample of the tested reinforced concrete beam. In both test specimens, the failure is shifted to the shear failure of the end-joints after the fracture of the main bending reinforcement with high shear forces applied to the joints. Another drawn conclusion is that, the higher the shear reinforcement of the beam the more energy were

absorbed by the joint showing relatively higher ductility in the frame assembly. Similar results are reported by (Lew H. S., et al., 2011) with improved seismic details and higher rotational stiffness by massive columns. In this test, the horizontal (translational) restraints were also provided which lead to a clear recognition of the second peak of strength result from the full deployment of the tensile catenary actions. The second peak was higher than the first in this test. The catenary action was also report by (Sasani & Kropelnicki, 2008). This tensile catenary is also reported in case of poorly detailed RC member by (Orton S. L., 2007) and (Bazan, 2008). Bazan pointed out the strength presence of compressive arching action in beams which may also result from beam growth similar to the arching strength concepts defined in slabs refereeing to the earlier works reported in (Park & Gamble, 2000).

Another advantageous contribution of the arching action reported through the increased translational restraints (Su, Tian, & Song, 2009) and (Yu & Tan, 2011). This compressive arching, based on component based mechanical model, showed less significant contribution when smaller span-depth ration is used (Yu & Tan, 2013). Another result obtained from (Tsai, Lu, & Chang, 2013) showed that the increased longitudinal reinforcement seems to increase the strength of the compressive arching, although it does not seem to increase the observed energy, this can be understood by the decrease in bending ductility results from high ration of reinforcement. Along the full path of the **response curve**, the stirrups, in both samples, played more tangible rule in the post-peak response while lower longitudinal reinforcement ratio is used (More ductile). To explore the rule of higher shear reinforcement ration and of effect of the span-to-depth ratio, they also tested another 6 samples (Tsai & Chang, 2015), the result confirms the minor rule of shear stirrups in prediction of the ultimate strength. And it points out that the arching improvement is less significant for shallower sections.

A high second peak of strength resulted from the action of the tensile catenary was also reported in 1-way bridge slab strip by (Gouverneur, Caspeele, & Taerwe, 2013). The tested case resamples the beam performance with minimum shear stress and at perfect translational constraint. The results emphasis the superiority of the mechanical strength of

the tensile catenary in the case of high span to depth ratio, however the structure is then considered out of service.

Therefore, both terms, the **compressive arching** and the **tensile catenary** has been introduced as observed by the tests. We shall take a closer look over each in the following sections.

2.3.1.2.1. Compressive arching in beams

In fact, the compressive arching is important when the design is the goal of the analysis, while the tensile catenary is a robustness advantage provided that it arrests the local failure. With attention to the high value of the ultimate strength of compressive arching, or called compressive membrane arching, researcher payed more attention to it.

With axial compressive deformation restrained, the compressive arching of beams was tested as a function of changing three parameters; the ratio of the bending reinforcement, the span-to-depth ratio and the loading rate (Su, Tian, & Song, 2009). The results showed that, for a constant support stiffness, the ultimate arching strength improves when reinforcement ratio increase or when the span-to-depth ratio decrease (in another word by the increase of the effective depth). They have also concluded that the loading rate has no significant effect on the ultimate arching strength, the studied loading rates were controlled at 0.2, 2, and 20 mm/s.

The effects of shallower span to depth ratios (shorter spans) on strength was tested by (Punton, 2014), the results assured that the compressive arching is more substantial for relatively lower span-to-depth ratio and for smaller ratios of longitudinal reinforcements, these results confirmed by other test and by simple analytical analysis. For Punton tests, stable failure after the ultimate strength was observed even for specimens with clear snap-through response. Such stable response may be understood by the bending dominated failure transition phase between the compressive arching and the tensile catenary.

To assess the influence of the ratios of longitudinal and transverse reinforcements, beams were tested by (FarhangVesali, Valipour, Samali, & Foster, 2013). The general statement of

their test report is that both reinforcement ratios has minor influence on the ultimate aching strength, this contradicts the generality of the earlier reported finding. We may understand that it is correct for the case of the longitudinal reinforcement because no increase of flexural stiffness occurs beyond the yielding of reinforcement. But, the generality of the result is not true in in the case of transverse reinforcement because; 5 out of 6 of tests showed no yielding of reinforcement at the end sections where stirrups are densified making it rather irrelevant because stirrups contribute to the flexural ductility only after the flow of the section in flexure. Therefore, it may be concluded here that no firm conclusion can be made based on this test. Rotationally restrained samples engaged the mechanism of four section only in the case of the test No. 6.

Taking the mechanical strength of the concrete as a variable, an almost linear relationship between the arching strength and the strength of concrete was confirmed by test of (Valipour H. , Vessali, Foster, & Samali, 2015). The same team reported that using fiber shear /confining reinforcement, an alternative for stirrups, does not seems to affect the behavior of the beam in a column loss situation, this is in the case of the ultimate compressive arching strength (Valipour, Vessali, & Foster, 2015). Nevertheless, it is understood that this improve the ductility.

To this end, the factors affecting the arching phase of the **single layer** beam mechanism are concluded as follows;

- Ultimate arching strength; which depends on
    - Axial compressive deformation constraints of the support lateral/horizontal translation.
    - Ultimate bending strength of the engaged sections in the collapse mechanism.
- Ductility of the arching phase; which depends on
    - Rotation constraints of supports. This will activate the contribution of the sections near supports in bending.

- The number of the engaged key section involves relatively large flexural rotation termed here by the **key sections**. These are the sections that involves yielded longitudinal reinforcements. This is can be understood with over all redundancy of the assembly.
- Transvers reinforcement improves section ductility at the key section that involves yielded longitudinal reinforcements.
- Presence of high shear deformation limits the ductile rotation of key sections.

2.3.1.2.2. Tensile catenary in beams

Although the tensile catenary was always recognized by most of the reported test so far, none of these commented directly on the parameters that affect the response in this phase. One of the exceptions (Yu & Tan, 2013) reported that the higher span-to-depth ratio, the better the chance in the development of the tensile catenary. Otherwise, for shear type of beams the tensile catenary is rather unlikely. Details of these tests are reported in Ph.D. thesis of Dr. Yu (Yu J. , 2012).

Although this is considered a **robustness parameter**, rather than a design one, EC and BS consider this sufficient for the collapse safety assessment in the case of structures at limited risk of abnormal events. Special interest of understanding this phase of response arises when we consider the question of whether the dynamic force that develops then in the catenary element will pull down the rest of the structure or not. In general term; will this force cause the vertical collapse to propagate laterally to engage more parts of the structure? In fact, there is limited experiments in the literature addressing this question.

To speculate some more information about the dynamic nature of the transition from the compressive arching to tensile catenary, the possible contributing factors are analytically listed;

- The anchorage and the Curtailment of reinforcements.
- The toughness of reinforcement
  - The yielding strength.

  - The hardening ratio.
  - The ultimate strength of the reinforcement.
  - The cut off (rupture of fracture) strain of the reinforcement.
  - The effect of the loading rate (strain rate) in the plastic response phase.
- The dynamic properties of the transition phase;
  - The mass to the ultimate strength ratio aggregated over the tensile reinforcements. This is the mass of the moving mechanism through the transition phase. Or it can also be defined by the ration of the target loading to ultimate catenary strength.
  - The loading speed. This can also be represented in relation to the effects of the strain rate.

2.3.1.3. Plane frame behavior

In order to explore the effect of beam extensions, also, (Yu J. , 2012) tested beams with full beam and column assembly. The wealthy test report confirms that the same pattern of response is observed; arching and catenary. Therefore, all the observed parameters influencing the repose reported in the previous section applied to the beam with extension tests.

As an extension work to Orton test of the poor detailed beams, comparison of 2 level frames, was tested (Stinger S. M., 2011) and (Stinger & Orton, 2013), the test shows the significant contribution of the proper detailing on the arching strength and the amount of energy absorbed by the bridging beam. A unique highlight of this test is the shift in the failure location from the face of remaining columns toward the bay, these points are rather associated to bar curtailments Figure 2.3-2.

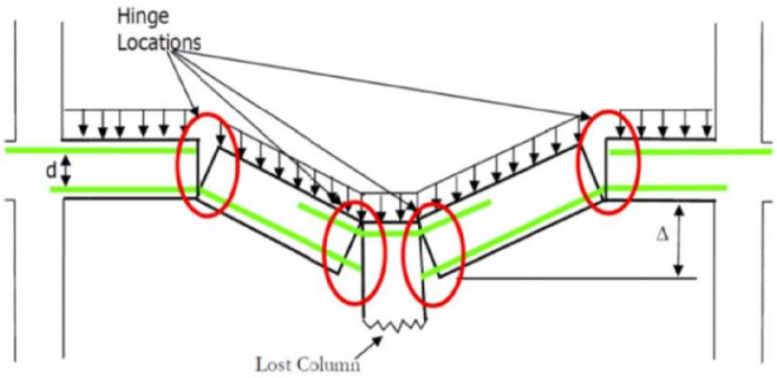

Figure 2.3-2 Adapted from (Stinger S. M., 2011), and (Orton S. L., 2007).

To explore the rule of constraints on frame, 2D frames were tested by (Yi, He, Xiao, & Kunnath, 2008) and (Stinger & Orton, 2011), these confirmed the existence of the same patterns of response. Additionally, it reveals that the increased level of plastic rotation, result from engagement of more plastic elements, is increasing the ductility of the mechanism, and apparently results from the increased chance of moment redistribution over more elements. This is a clear result of the test of (Yi, He, Xiao, & Kunnath, 2008).

2.3.1.4. Corner frame assemblage

While compressive arching and tensile catenary requires axial constraints of the beam/frame element, corner beam assembly sounds more vulnerable to collapse. Therefore, Quasi-static and dynamic tests of the corner beam assemblage (Qian K. , 2012) confirms that the main line of defense is the ultimate bending strength of the assemblage.

Building codes, such as (CEN, 2004), presumes that tying forces provided by reinforcement that deploy catenary action are sufficient for the provision of collapse resistance, but, in line with the above test results, if the acting collapse momentum passed the first quasi-static peak of response, will it stabilize at the catenary? The answer lays in; the correct representation of the restraints, appropriate model of RC plastic failure and may be in well representation of the slab contribution. These factors necessitate the 3D representation of the building model.

Therefore, if the simple beam assumptions are used for the design or analysis, it will preserve the advantageous contributions of the translational and rotational constraints of the connected substructure. These favorable end constraining effects will provide additional robustness beyond the design limits.

2.3.1.5. Dynamic tests of beam-frame assemblages

In an extension to the discontinuous frame (Stinger & Orton, 2013) test, a dynamic drop weight test is applied to similar frame 2 level 2 bay RC frame quarter scale sample (Orton & Kirby, 2013). The first and the second drop applied the same load, although the second drop is applied to non-virgin specimen. The third drop applied an increased load, but did not cause the frame to fail. The last, forth, loading drop caused the beam to fail the compressive arching, however the tensile catenary arrested the collapse, and the frame stabilizes. The test presents the different level of dynamic amplifications at various loading-response scenario in addition to the difference between the two beam layers. (Orton & Kirby, 2013) shows the dynamic amplification for reaction forces and displacement at different points as reported by the source. The amplification of the horizontal reaction force at the tensile catenary reached 2.18 and 4.49 for the top and bottom beams respectively. It must be stressed here that high horizontal stiffness was provided in the set-up of the test by the reaction frame.

Another extension of the corner-beam assembly is made for the experiment of the dynamic action (Qian & Li, 2012), the test series aimed at investigating the influence of the both longitudinal and transverse reinforcement in the dynamic response. To simulate the dynamic action, the target column was subjected to impact load of a heavy hammer. The process caused the reaction force in the removed column to drop out after only 3-3.5 milliseconds. Similar to trends observed in the twin static tests (Qian K. , 2012), beams failed in combined shear and bending. Also, due to the corner restraint, simulating the above column joint, the original negative bending moment, at the lost column corner, switched to positive bending where tension is at the bottom. Acceleration and displacement were reported and velocity were extracted.

	Drop 1	Drop 2	Drop 3	Drop 4
Vertical Disp.	-	1.08	1.11	1.08
Horiz. Disp. on top beam	-	1.09	1.04	1.44
Horiz. Disp. On bottom beam	-	1.10	1.09	1.46
Horiz. Load on top beam	-	-	1.82	2.18
Horiz. Load on bottom beam	-	-	-	4.49

(a) The factors of dynamic amplification

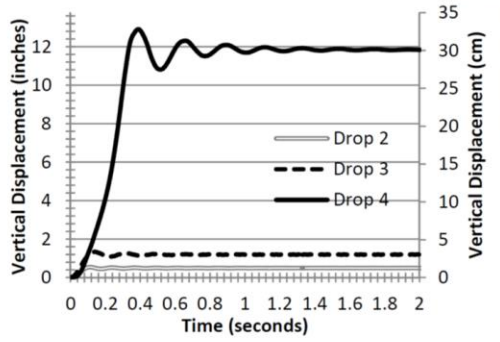

(b) The vertical displacement history

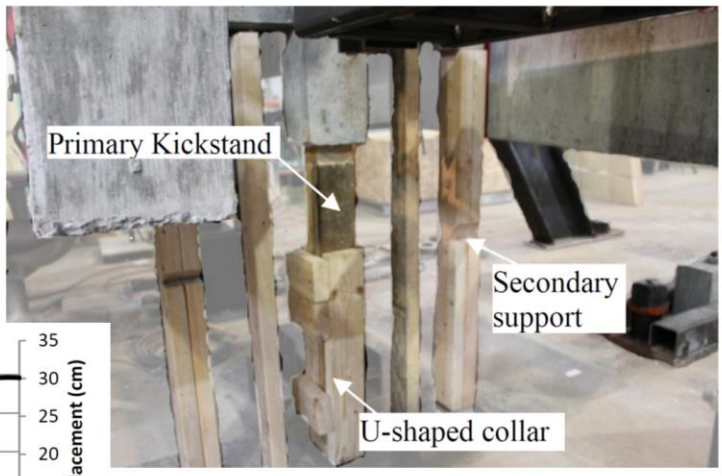

(c) The kick stand used for the dynamic application of the action

Figure 2.3-3 Adapted from (Orton & Kirby, 2013)

For the non-failed specimen DF1, maximum acceleration was recorded at 2.91g, and the maximum velocity was evaluated at 0.64m/s. Results indicated that, under the described dynamic action, seismic detailing improves the response of the assembly; the longitudinal reinforcement increases strength, and the transverse reinforcement reduces the cracks although the specimen suffers from the limited redundancy. To evaluate the difference between the dynamic and the quasi-static response, comparison with the static-twin series (Qian & Li, 2013) were made. Dynamic increase factor of load resistance is defined by the ratio of the static load capacity to the dynamic load capacity in strength, for this factor as an upper-bound value, at different detailing and loading, were reported 2.16, 1.38, and 1.46. Looking at the details of the specimen, it sounds that this factor is proportional either; to the bending strength, or to the stiffness. The first value is associated to the higher longitudinal reinforcement, and the third value is associated to the increase in transverse reinforcement when compared to the second value. Although the acceleration recordings of the other test are not reported, it is expected to follow the observed trends in dynamic increase factors. These results can be considered consistent with the understanding so far

that; higher ratio of longitudinal reinforcement reduces ductility, and improved transverse reinforcement increases it. And the improved ductility enhances energy absorption reducing the dynamic increase factor.

One of the closest test to the blast influence on a column damage presented in (Yu, Rinder, Stolz, Tan, & Riedel, 2014), two samples were tested, one remained within the compressive arching phase, and the other failed. The general conclusion of the reported test is the quasi-static testing procedures provided the comparable results to those reported by dynamic test. The test reported the dynamic forces developed in steel reinforcement in addition to the measured reaction force. Unfortunately, due to the test boundaries, the failed specimen did not reach the tensile catenary because it hit the ground, also the actual peak value of accelerations was not captured due to the limits of used accelerometer.

So far, all the earlier reported tests are made without slab element, in the following, tests included slab element are surveyed.

2.3.2. Test of slabs and slab-beam assemblies

In recognition of the additional favorable contribution of the slab element in 3D slab assembly with the famous texts of (Park & Gamble, 2000) and (Bailey, Toh, & Chan, 2008) regarding arching in constrained slabs, an outstanding test program conducted at Nanyang institute of technology in Singapore. One of reported results of (Qian & Li, 2012) showed that in corner slab assemblage, where neither translational nor rotational constraints at the beam ends is eventually provided, slab can contribute 35% up to 65% of the observed mechanical energy in the assemblage ductility.

Recently, the same group presented the results of multiple column removal on RC slab assembly (Qian, Li, & Zhang, 2016). Middle slabs with some restraints are tested by (Xuan Dat & Hai, 2011) and (Xuan Dat & Hai, 2013). These tests made researchers to make some confidence in expanding the concepts of yield-lines methods in slab to define the line of breaking in slab-beam assemblage (Hatahet & Könke, 2014b) and (Xuan Dat, Hai, & Jun, 2015), also reported for beams (Qian. & Li, 2013).

Slab can not only provide favorable reaction; it may also cause unfavorable pull out of the rest of the structure if the latter is unable to provide sufficient lateral resistance. Such investigation requires a full building assembly under examination.

2.3.3. Test of 3D RC frames and buildings

Under the column removal scenario, 10-story RC building was tested (Sasani, Bazan, & Sagiroglu, 2007). The edge B5 column, Figure 2.3-4 (C), was removed by explosion. The structural floor system was 1-way slab. The recorded results confirm the ability of the 10-levels Vierendeel to arrested collapse as only 6.4mm displacement is recorded at head of the lost column. The reporters confirm very high damping ration in response to the instantaneous remove of the column. Such high damping points to the plastic deformation of reinforcement over many plastic-sections of double curvature element with the moment frame Vierendeel over the axis 5, bay C-B.

Although the top bars were cut-off, the Vierendeel arrested collapse due to the high redundancy. Such high strain level confirms that the section is under full tension. Therefore, minimum bending resistance is expected at the top elements of the Vierendeel. Dr. Sasani in his report, also, pointed out to the risk of brittle failure due to limited encourage in slab reinforcement.

Another 6-story RC framed building is also tested by (Sasani M. , 2008). This time, the building tested in presence of the infill walls, and two adjacent corner columns, A2 and A3, were removed. Similar to the previous test, only 6.4mm deflection is reported pointing out again to the presence of bi-directional Vierendeel action over axis 2 and 3 Figure 2.3-5 (c). In his analytical model, infill wall was removed. Although the local failure does not propagate, the model showed that infill wall may reduce deflection significantly, therefore it must be included in analytical simulation with attention to the cracked state of the wall results from load redistribution and the deformed sate of the mechanism.

(a) West view of 10-story University of Arkansas Medical Center dormitory in Little Rock, AR

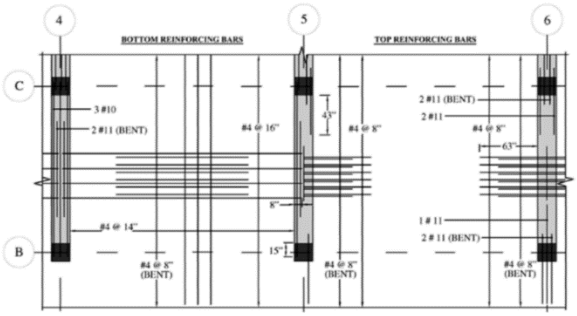

(b) Reinforcing detail for bottom (left) and top (right) of slabs and beams in second floor

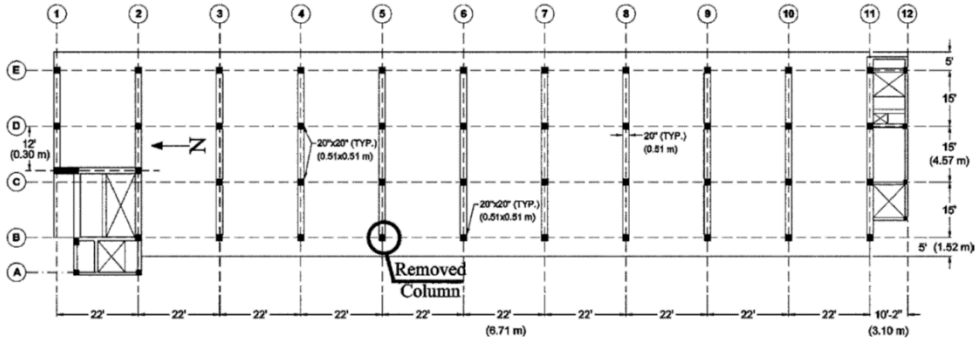

(C) Typical plan of the building showing 1-floor system.

Figure 2.3-4 Adapted from (Sasani, Bazan, & Sagiroglu, 2007)

The above two tests preset cantilever Vierendeel scenarios. Opposite Vierendeel test was also performed by Dr. Sasani (Sasani & Sagiroglu, 2010). In this test 20-story reinforced concrete building, Figure 2.3-6 and Figure 2.3-8, was studied under the case of an intermediate column removal. Similar to the two previous tests, the collapse was arrested at a very limited deformation of 9.7mm, and pavement value of only 5.1mm. It should be noted that after explosions, normally remain bent reinforcement of the column which can on source of the large damping observed in the measured response. The readings of sensors were reported at the 2nd and the 7th floors, through which difference in displacement is measured indicating tensile reaction in the remaining part above the lost column C3. Following the time history records of strain in the columns, it was found that the wave of the axial load propagating faster than the flexure. This was marked by the fact that the forces in the column dropped faster than the time needed for the full displacement to develop. In the discussion of their paper (Chen, Zhang, Sasani, & Sagiroglu, 2010), Chen suggested that the immediate compressive strain after 1 millisecond is understood by the

axial wave translate at 4000m/s in the concrete continuum that result from the blast wave. In contrary, he saw that 82% of vertical displacement reached after 5 milliseconds is not clear. This point suggests that the last 18% of the stable displacement is the result of moment redistribution along the Vierendeel due to the formation of plastic hinges, these, producing high damping, made the system to react relatively slowly. If this is true, it justifies the quasit-static tests reviewed so far in the previous sections.

(a) Center structure is studied

(b) Second floor of building

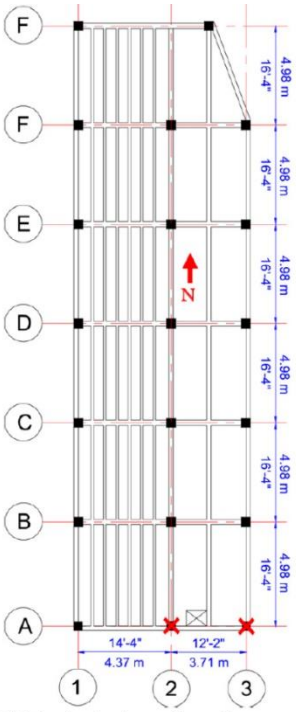

(C) Typical plan -first floor removed columns are crossed.

Figure 2.3-5 Adapted from (Sasani M. , 2008)

(a) Twenty-story Baptist Memorial Hospital.

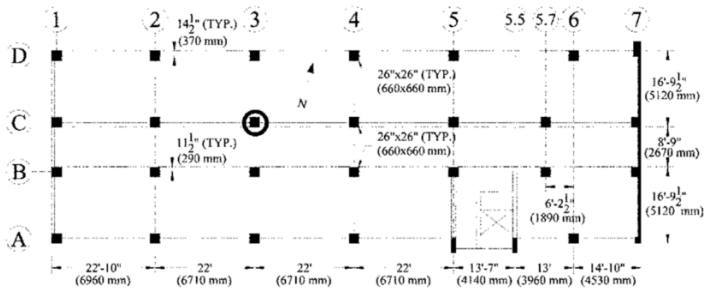

(b) Ground-floor plan of north-east wing of Baptist Memorial Hospital. Circled column was suddenly removed (exploded).

Figure 2.3-6 Adapted from (Sasani & Sagiroglu, 2010)

(a) Removed column before explosion (b) Removed column after explosion

Figure 2.3-7 Adapted from (Sasani & Sagiroglu, 2010)

Another RC building was tested (Morone & Sezen, 2014), 3-story 61.6x66.4m^2 shopping mall was subjected to the removal of three columns at the corner of the building Figure 2.3-8 (a). The numbers 1, 2, and 3 in Figure 2.3-8 (b) indicate the chronological remove of the columns. The columns were removed mechanically by pushing a jaw until concrete crush and reinforcement fracture, the process was quick, 1 seconds for the crush of concrete and the a few more for rupture of reinforcement. Strain measurements were made at the nearby column indicated by the location of the sensors shown in the Figure 2.3-8 (b). Due to the mechanical method of the column remove, the dynamic effects are not purely understandable, it is also noted that the floor is made of flat-slab panels. Therefore, the value of the provided test data is limited to the static displacement. It should be noted, though, that only on the first-floor wall were removed as can be seen in the figure XXXX (c) and (d). More results of the test were reported in (Morone D. J., 2012). More tests were reported by the same group (Wood, Lodhi, & Sezen, 2014), although little information about these tests were found.

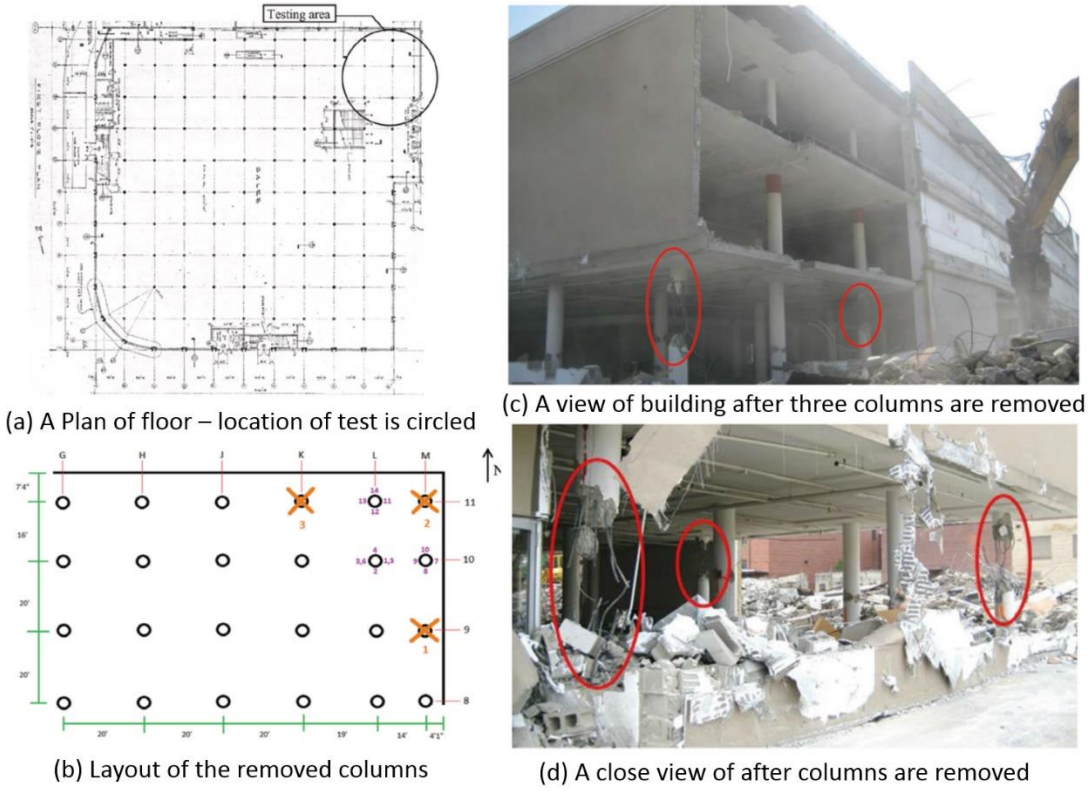

Figure 2.3-8 Adapted from (Morone & Sezen, 2014)

The national institute of technology recently provided test of three cases of full RC scaled building (Xiao, et al., 2015). Three scenarios were tested, corner, edge, and middle case of columns was instantaneously removed. In the first case, the system responded linearly without collapse. In the second case, two columns were removed subsequently, full failure mechanism was formed and no tensile catenary was possible because of the 3x3 bay frame, this leads the mechanism to keep deflecting without the support provided one of the temporary provided columns. In the third case; intermediate column was removed and compressive arching of the beams and slabs was able to hold the structure without collapse. Acceleration time-history was recorded in all tests and one of the outstanding finding of this test is that it confirms the quasi-nature of the progressive collapse even in second case where the collapse mechanism could have remained active.

Another reduced 1/3-scales 2x3 bay RC building model were reported (Wang, Chen, Zhao, & Zhang, 2015). The middle column removed suddenly, but only less than a millimeter was reported. The test was proceeded by quasi-static loading through hydraulic jack until the

damaged state. Damage pattern, in the Figure 2.3-9, reflect a shear failure at the top layer of beams' joint.

Another test is reported by (Vanadit-Ellis, Gran, & D. Vaughan, 2015) presents the case of the strong sub-structure. This reported test, in contrast to the earlier one, showed the case where reinforcement deboning dominated the response.

There is another evidence showing the strong vulnerability of the vertical collapse propagation through the shear failure of the above column in the case of corner column collapse (He & Yi, 2013).

Comments on the dynamic effects

Ruth, (Izzuddin, Vlassis, Elghazouli, & Nethercot, 2008) and (Orton & Kirby, 2013) discussed a simple method observe the dynamic increase factor of the applied forces in comparison with the conventional quasit-static simulation. But, as a result of the snap-through response, the increase in kinetic energy necessitate the dynamic analysis and suggest higher values of the dynamic force (Hatahet & Könke, 2014a). With distinction between the dynamic increase factor (DIF) of the force and displacement, analytically (Tsai & Chang, 2015) showed the variance of the force DIF along the full response curve, it also shows significant deviation from the analytical formula presented by (UFC, 2009).

With the attention to the difference in the arching and catenary phases of response, the dynamic increase factor shall be discussed further in the review of the analytical models below.

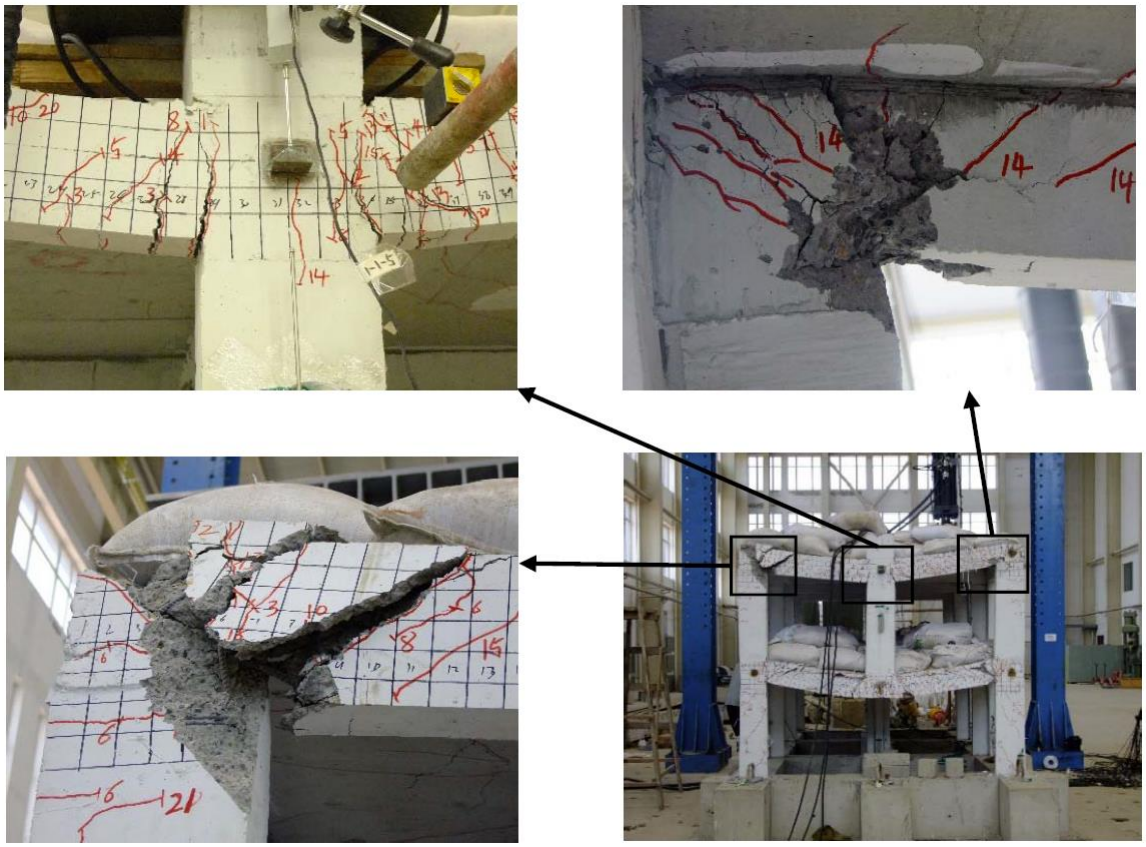

Figure 2.3-9 Adapted from (Wang, Chen, Zhao, & Zhang, 2015)

2.3. Summary on the observation on reported tests

Collapse vulnerability due to column failure depends on the location of the lost column, and on the degree of redundancy of the supporting system. Therefore, both factors are required for the assessment of the global progressive collapse robustness.

Test of beam element or sub-frames confirms the favorable strength enhancement result from compressive arching. This compressive arching is a function of the axial restraints of the beams or lateral supporting stiffness in frames. Although this compressive arching is more pronounced for short span-to-depth ratios, it is less significant for relatively shallower ratios. In general, the ultimate strength of the compressive arching improves while concrete strength and compressive reinforcement increase. Also the increase of the main tensile reinforcement ratios positively contributes but not beyond the balanced reinforcement ratio. Evident by test, the ultimate strength does not improve with the increased transverse

reinforcement unless this reinforcement was below a certain threshold. The threshold may coincide with the minimum reinforcement ration known in the ductile detailing standards of the shear reinforcement.

The rotational restraints of beam supports, or the increased stiffness of the sub-frames increases the ductility of the bridging assemblies. This is clear because it increases the number of plastic hinges in the assembly.

The tensile catenary is the second line of defense. However, this catenary cannot be obtained without sufficiently strong lateral restraints, sufficient anchorage or bonding in addition to the ductile classes of reinforcement. More attention is required for the short span-to-depth ratio beams, or shear beams, because none of these tested beams showed catenary strength higher than the arching strength. Such behavior in relatively short beams may cause the collapse proportion to be detached from the main structure.

All of the above observation, made by testing single bridging beam, are confirmed and coincide with the 2D frame test observations.

Floor element, e.g. cast in place RC slabs, plays important role in the 3D response, it does not only increase the redundancy. It may also have adverse effect in pulling down the remaining part of the structure. Evidences of such behavior was not provided to date in the literature.

Having found that the dynamic amplification of action is correlated with the increased stiffness, or even strength of the assemblage, the presence of slab element, or shear walls, may cause higher dynamic amplification for which there are no tests available to date to the best of current knowledge.

In test and observations of building behavior, structural Vierendeel action improves the chance of arresting the local failure in redundant buildings. Also, the spread of the axial loading wave is faster than the development of the vertical displacement. Because of dynamic remove of the column, the vertical displacement develops in two phases; the first

phase is semi-immediate, e.g. in the duration of 5 milliseconds, and the second phase is quasi-static which can be associated to the progressive development of the plastic mechanism.

2.4. The analytic approaches of the structural robustness

2.4.1. The developing analytical models

Most of the researchers who reported tested examples, followed their investigations by either analytical models, computer model or both. The following section will focus of the overview of the reported analytical models. The comprehensive model should hopefully replicate test observed behaviors at; element level and, the level of assemblage of floor elements and at the building level. The recognized benchmarks, outlined in the previous section, are the correct presentation of strength-deflection path of the collapse mechanism from the first yielding, through the ultimate strength with the contribution of the compressive arching, then post-peak until the point of fracture of the main reinforcement, and finally the balanced state of the tensile catenary when it exists.

2.4.1.1. The response at the levels of section and beam elements

The first relatively recent analytical model tried to approximate the prediction of the strength deflection of the beam arching and catenary is reported in (Orton S. L., 2007). Although the benchmark test is based on poor detailed beams, the analytical model well explained the rule of the longitudinal deformation in the overall deflection of the system. In the model the total displacement, in the tensile catenary at the point of the lost column, is the sum of the three components, joint/support rotation, bond-slip, and axial elongation of the beam assembly.

Concurrently, (Qian & Li, 2013), provided steps to describe the main points of the response curve, they presented their method on two abstract cases, one with fully restrained beam ends, and another with zero stiffness. Comparing the analytical model to their earlier test results, they have recognized the substantial contribution of joint deformation in the overall prediction of the deflection profile, and the role of restraints in the prediction of ultimate

strength. The concrete finding in the presented steps is that the ultimate strengths of the beam section at the location of the plastic hinges will allow an acceptable prediction of the full strength of the structural beam assembly.

The first who tried to trace the test results at different stages of the response curve and to compare them to the analytical model of the interaction diagram at the cross-section level was (Yu & Tan, 2013). They showed on the axial-bending interaction diagram that various repose patterns could be recognized, this is following either the crush of concrete, the fracture of the main reinforcement or even the improvement of the ultimate strength in presence of the increases of the axial force. Therefore, this result expands the earlier finding of (Qian & Li, 2013), that the plastic strength can be predicted. In conclusion; when the plastic failure mechanism is fully defined, the response curve can be followed further after the crush point of the concrete (the ultimate strength point), or even the fracture of the main reinforcement. But, it should be noted that this is limited under the condition of presence of axial compression bounded by the test set-up of their benchmark. To define the ultimate strength in recognition of the presence of the compressive arching, the same researchers (Yu & Tan, 2010) reported that Park method (Park & Gamble, 2000) gives not only an overestimate of the ultimate strength with 18% and an underestimate of the vertical deflection of the beam at this point, but also deviation in the proposed calculation concepts of the values of the constant used in their derived equation, these constant represents the ultimate compressive strengths at the end sections of the beam mechanism. The strength over estimate is understood within the scope of the upper-bound method based on rigid body movement which is also explained why displacement is under estimated having such simplified discrete analysis based on two elements only. The deviation is probably (Yu & Tan, 2010) a result of exclusion of the concrete softening or the relaxed stiffness of the reinforcing steel because of the relative bar-slip.

In the following a distinction between compressive arching, tensile catenary, and the transition in between shall be pursued separately.

2.4.1.2. The compressive arching

About the ultimate compressive arching in beams, (Merola, 2009) presented very detailed literature review of the analytical models of reinforced concrete response in compressive membrane and arching, and expanded the model of (Park & Gamble, 2000). In a trial of finding the point of the fracture of the main reinforcement, and concluding whether this fracture will occur within the compressive arching of the beam. The model showed an improvement gained from implementing modern prediction of the concrete strength block in bending over the method used by the developer of the model (Park & Gamble, 2000). Merola's model, concerned the effect of reinforcement ductility, proposes a method to predict the point at which the reinforcement would fracture during the compressive arching, was the first to address the sensible rule of reinforcement ductility in the compressive arching. Merola's work pointed toward the following conclusion, in order to obtain smooth transition from compressive arching to the tensile catenary reducing the dynamic effects, reinforcements must enjoy high level of ductility. The simulation by (Valipour, Vessali, & Foster, 2015) supports this in application to the top reinforcement contribution in the control of the end of the compressive arching phase. Such result is more pronounced with the increase of the longitudinal reinforcement ratio.

Arching in 1-way, or beam like, slabs was studied and analytically presented by (Park & Gamble, 2000), one of the main feature of this model is that it handles an elastic lateral translational stiffness of the supports. In the model, they have assumed uniform steel reinforcement, steel is at yielding in critical sections, and the beam between the critical section, strain-hardening of steel and tensile strength of concrete are neglected. In (Merola, 2009), the (CEN, 2004) concrete block instead of the ACI-318 is used. Also (Merola, 2009) recognized that with the increase of lateral stiffness, effects of creep and shrinkage on the ultimate strength can be more pronounced, she disregarded it in the model. For the tensile catenary, linear relationship was adopted from the same source of Park & Gamble model. The bar fracture criterion was based on the direct comparison of the elongated catenary to the maximum fracture length of the reinforcement bar that may be obtained from bar test

or a specifying standard. The unique advancement in (Merola, 2009) is that it tried to identify point of main reinforcement fracture in the compressive arching phase. The model relates the beam total deflection to an estimate of the total crack width at the critical section aggregated over the length of the plastic hinge. The result compares well with test data, this also reported by (Punton, 2014). Two practical conclusions made at the end of the parametric study; the steel ductility is vital in the development of the tensile catenary, and the steel curtailment of the bottom reinforcement over the remaining supports reduces the potential of the full mobilization of the tensile catenary, the results were also reported elsewhere. A unique result was to differentiate the two cases of bottom reinforcement fracture before or after the arching catenary and revealing that ductility of reinforcement is a key modeling parameter. These conclusions coincide with the postulations made in section 2.1.2.2 earlier.

Following the steps of the master model of park and Gamble, (Yu & Tan, 2014) expanded the analytical steps to address the partial rotational restraints alongside the variance in stress of the compressive steel.

In the scope of compressive arching, simulation of the rupture of reinforcement bars and the role of strain penetration in the analysis is pointed out by (FarhangVesali, Valipour, Samali, & Foster, 2013). The procedure for the analysis of the rupture of reinforcement was based on the work of (Lee, Chob, & Vecchio, 2011), the model considers the development of the average strain between cracks and include the tension stiffening effects. It sounds interesting to compare the model to the proposed rupture point by (Merola, 2009). The SFEM model of (Valipour, FarhangVesali, & Foster, 2013). The model is based on structural finite element; deformation of joint is modeled by discrete spring element mechanically representing the material behavior. The model matches the ultimate strength of the compared test results, although require improvement in the prediction of the post-peak descending part.

In focus on arching in beams which defined the opening of the transition phase, analytical model, developed by (Yu & Tan, 2014), advanced (Park & Gamble, 2000) work to include two important factors; the favorable rule of the partial rotational restraints, and the varying level of stress/strain of the compression reinforcement at the points of critical hinges. With the correlation of the arching strength of the assemblage to the compressive strength of concrete, the model showed an attractive match to the response in the immediate proportion aft the point C. Although it is not equally good in prediction of the deflection, the model can improve when the plastic rotation is actual aggregated over slightly larger proportion taking the length of the plastic hinge into account. This can be an immediate attractive improvement to the model (Yu & Tan, 2014). In their procedures, they assumed elastic-plastic without hardening of the reinforcement, bar buckling under compression was not considered, this is another need for the model to describe the transition phase toward the point of bar fracture.

2.4.1.3. The tensile catenary

Although the dynamic transition phase is key in the assessment of the stability of the tensile catenary, the analytic models are merely attempt to describe the static response and state of balance. Following the literature reported by (Merola, 2009) reporting over Meacham and Mathew (2006), the tensile catenary force in reinforcement cables relates to the invers of the vertical displacement in the Figure 2.4-1. Such an equation, used in the BS, does not hold true if the balance at the middle joint is evaluated, this is simply because there is no shear strength in the catenary, therefore, the equation of the moment equilibrium does not hold on model. Propose evaluation of the static evolution of the tensile catenary forces can be found in (Hatahet & Könke, 2014b). A contradicting conclusion is shown by (Stylianidis, Nethercot, Izzuddin, & Elghazouli, 2016).

The dynamic effects result from the transition phase shall be handled in the section 3.5 of the chapter 3, in which novel analytical procedures are developed and compared to benchmarks.

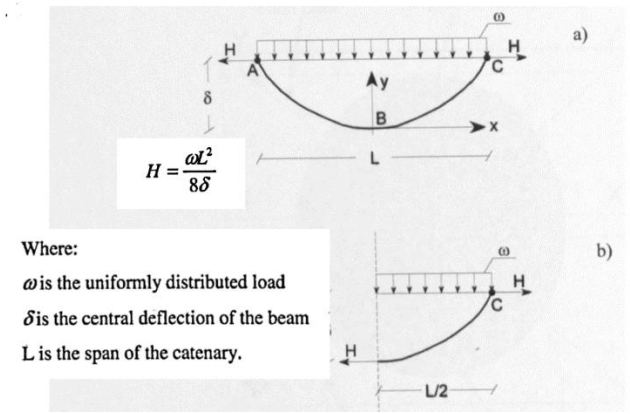

Figure 2.4-1 tensile catenary force as reported by (Merola, 2009)

2.4.2. The response at the level of floor assemblage

An expansion of the plastic mechanism concept, introduced earlier for beams, was redeployed by (Xuan Dat, Hai, & Jun, 2015) to predict the ultimate strength of slab-beam assemblage. The proposed steps are bounded by the difficulties defining boundaries and constraints of the slab in the real 3D simulation necessitate a staggered analysis approach of the structure. Also, they did not take into account the case of the tensile catenary.

Another model in the content of 2-ways slab membrane, see of example (Bailey, Toh, & Chan, 2008), show some enhancement of the bending strength of the slab. While the bending failure of slab in the arching happens at lower level of deflection than those of the beams, the beams bending mechanism remaining the controlling factor in the strength evaluation of the assembly as shown by (Xuan Dat, Hai, & Jun, 2015).

To isolate the model of slab in 2D, we, (Hatahet & Könke, 2014b), presented a simple analytical technique to include the tensile catenary of slab reinforcement in 2D frame simulation. The technique is based on the post-plastic analysis and uses the same assumption of the well-known yield-line theory in slabs in defining the lines of plastic rotation in the slab panels. The models are compared to two slab models; one with comer column remove, and the other with intermediate column removal.

2.4.3. Transition from arching to catenary

This refers to the proportion of the response curve between the points C and E by the transition phase. This phase is the focal for the assessment of **the dynamic collapse pull-down factor**. The last refers to the ratio of the lateral dynamic force demand to the ratio of the lateral dynamic strength and ductility of the remaining (stabilizing) part of the structure.

While the arching and catenary strength referred to by the key behavior assessment points the full curve were analyzed by (Stylianidis, Nethercot, Izzuddin, & Elghazouli, 2016). The presented analytical equations described most of the discussed factor related to the arching and tensile catenary failure progression in the beam assembly even though it was presented for steel frames. Apart from the connection behavior, most of the equations can be applied directly to the case of the RC bridging beam elements.

2.4.4. Summary

A few analytical models exist in the literature which can be used to explain the key response phenomena at the beam element level defining the arching and catenary points of the static response. However, none of the model describe the full curve in the case of the RC bridging beam assembly. It was also shown that the 3D contributions of slab and sub-frame elements are rather difficult to be analytically quantified limited the scope of the existing simple methods, e.g. handling the Vierendeel action in multi-story buildings. This necessitate the development of 3D computational models even though simple models can explain the key/sensible modeling parameters and therefore can help identifying key robustness indicators which is the farthest concern of this current work.

2.5. The sensitivity of the progressive collapse in RC buildings

In this section, evaluation of simulation alternatives is presented. It concludes with an informed simulation strategy that satisfies the overseen targets developed through the earlier surveys of the test literature.

2.5.1. The difference between demolition and progressive collapse

In building demolition, the collapse mechanism is predefined, therefore, the focus of the simulation is the relative motion of the falling fractured components. Also, the validation of these modes is merely based on visual inspection of the collapse process based on shots of high-speed cameras.

The progressive collapse mechanism is a property of the structure in reaction to a specified collapse trigger scenario. Therefore, the development and the propagation of the collapse mechanism is the unknown of the simulation. Also, partial or full failure of the structure is ought to be identified by the progressive collapse simulation. Then, the simulation must capture dynamic, transit motion, properties as well as it impact on the rest of the structure.

2.5.2. The objectives of the progressive collapse simulations

The correct predictions of the points of the global response curve is the main target of the simulation. In order to fully cover the development of the progressive collapse mechanism, we speculate here three different levels of presentation. For each of these, ab sub-set of criteria is here outlined. The first level of presentation is associated to the frame mechanism which will be regarded as the frame level objectivity. The second is related to the correct capture of the contribution of the floor and beams assemblages, and it will be regarded as the floor level objectivity. And the last one is related to the capture of global reaction at the level of the 3D building simulation model, and so called the global level objectivity.

In the Figure 2.5-1, an idealized version of a response curve is presented. The curve shows the change in the reaction force recorded while the displacement at the missed column location is increased in quasi-static manner. On the presumed response curve, four distich phased of response are recognized and presented in the Figure 2.5-1, these will be referred to in the following paragraphs.

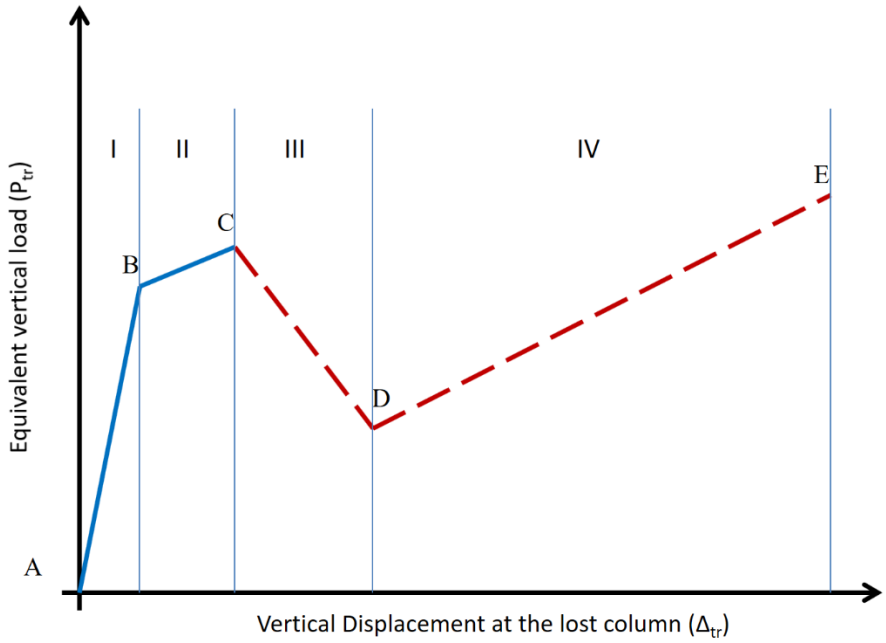

Figure 2.5-1 the phases of response shown on the Idealized response curve of the mechanism

2.5.2.1. The frame level objectivity

It has been shown, in the section 2.2, that the collapse mechanism passes through four distinct phases along the system response, also reported in (Hatahet & Könke, 2014a), it has been seen that for progressive collapse simulation special attention is needed in response phases II, III and IV;

In the phase II, between the yielding of the first contributing section and the full formulation of the failure mechanism, significant force redistribution takes place. This force redistribution will demand the following;

The gradual increase in the number of section that enter the post yielding points. This increase will require an iterative increased rate of displacement at the control point, with live update of the drop of stiffness at the yielding sections. This a very critical feature of the modeling tool, let us name this modeling feature; **phase II: the adaptive spread of plasticity.** Due to the increased number of involved sections that alter stiffness, an adaptive, growing model, is required. Hence, only at the end of this phase the size of the mechanism is defined

and this is the only possible point at which the component of the mechanism model is identified. To accurately observe the mechanical response at each contributing section, the following must be accurate modeled;

1. **The strain at which hardening in steel begin**, mapped to the strain at which the concrete crashes and whether this strain level can be reached for every tension bar in light with strength development length and bonding.
2. As the section goes beyond yielding, yielding locally spread. **In shear critical elements**, such a spread will decrease the shear span of the element. This is also referred to as the prediction of the length plastic-hinge.
3. Due to the increased rate of plastic strain, **large geometrical displacement must be considered**. This can lead to local softening of an element, while the global response is still hardening due to the high degree of redundancy. Local softens can present in two cases; softening in step column, or softening in beam element or local bridging assemble.
4. The model of the **RC column** must consider possible **modes of failure** as discussed in the paragraph 4.3 that discusses the concept of the step-column collapse.

In the phase III; directly after the point of concrete crash, reaction forces of the mechanism are decreasing, this is phase of the global softening therefore, let us name this target feature **phase III: the global softening**. Depending on the point where rupture strain is captured, this phase will be marked by either of the following events;

1. Gradual decrease in shear, then bending, stiffness due to interface friction/interlocking. This stiffness soon vanishes as a function of the offset displacement between the sides of the shear failure plan which normally follows the bending crash of concrete. It is worth to note here the role of the compressive arching force that increase the role of friction and interlocking.

2. Compression bars, in one hand, have a sharp jump in compressive demand, develop a buckling mode as a result of tangential displacement at the interface of the failure plane at the other hand. The buckling mode-shape is also linked to the strength and intensity of the local stirrups and the way bars and stirrups are constrained together. Hence, bars buckling model in light with constraints and the compression development length is needed in this part of the response curve.
3. Tests showed that the bottom strength point, D lowermost point of the softening response, is defined before the compression bar switches to tension and at the level of end deflection beyond the effective depth of the beam defining an analytical end of the arching effect. So arching ends first, however compression bars keep reporting some compressive stiffness indicating some residual bending stiffness by the point of the tensile cut of tension reinforcement layer. Therefore, the precise definition of the point D, describe the theoretical transition from arching to catenary, is bound by two events and defined a certain dynamic state;
    a. Before the point D, the tensile reinforcement will begin in fracture phase reducing its mechanical strength. Then, the point at which the reinforcement fracture is precisely required.
    b. After the point D, the compressive reinforcement will switch to catenary.
    c. At the point D, the collapse mechanism reaches the peak velocity and zero acceleration state at which the mechanism so the minimum strength.
4. This phase is marked by an overall lively changing negative stiffness, and an increased importance of the dynamic part of the balance equation. Therefore, clear distinction between pseudo time step and real temporal discretization is required.
5. Strain rate may also play a rule in the rapture strength of reinforcement
6. due to the presence of gravity field, and the sharp negative gradient of strength special numerical manipulation is required

In the last phase of the response, phase IV, pure dynamic analysis with initial velocity $V_{D,}$ at point D, must be performed. The stiffness of the system is the tensile stiffness remaining

catenary elements. We will call this target feature **phase IV: the dynamic state of catenary.** The feature requires clear view of;

1. The strain rate effect.
2. The maximum dynamic tensile strength that can be developed, which is the minimum;
    a. Catenary strength after compression, buckling and combined tension and bending,
    b. Bonding strength
    c. Reaction strength of the supporting structure with attention to chance of its softening

2.5.2.2. The floor level objectivity

The model of slab shall objective contributes through the following four distinct observations;

1. In the phase II above, while the size of the collapse mechanism is evolving, bending fracture and crashes take place forming clear lines of yielding. While any bending strength of the slab before this stage is negligible, these yield-lines define boundary initial cracking conditions defining potential extension lines for failure planes of the beams. Also, these crash-lines form a clear boundary for slab contribution to bending stiffness of the beams especially around the columns' heads.

2. In both phases II and III, before and beyond the peak response point, the stiffness of the slab contribution is almost constant in the phase II however inclination angle is required (Hatahet & Könke, 2014b); update of inclination is critical in the second model as well as the live update of the cut/ deboned bars. In the phase III the same applies.

3. About phase IV, the clear crash-lines define the location of combined tension and bending in bars. In this region, it is very likely that all the bars are in yielding causing almost constant contribution until these bars gradually cut off. The model definition

of this mechanical contribution requires lively update of the tensile strain state, bending, and the development length fully embedded in concrete. Again large geometric nonlinearity plays a role in this part.

2.5.2.3. The global level objectivity

The model should describe the composite behavior of the RC material as outlines above through computationally effective, an efficient, algorithm without compromising the scope and the quality of the result. The target of the simulation is to define the state of the building result from instantaneous remove of one, or more, of the supporting columns. The following criteria can be isolate from the earlier observations;

1. The time history state of the moving mass of the collapse mechanism
2. The time history state of the rest of the structure that may be pulled by the moving mass in case of the catenary.
3. The potential kinematics of the remaining mass under the collapse mechanism when the mass of the mechanism falls down.

Therefore, we have three general modelling targets that will be used to summaries the detailed sub-criteria above;

- Target 1; Phase II: the adaptive spread of plasticity
- Target 2; Phase III: the global softening
- Target 3; Phase IV: the dynamic state of catenary

Each of these targets has sub-discrete requirements which shall guide the assessment and the development of the computer modeling regime. These are summarized in the table below;

Table 2.5-1 Summary of modelling target of disproportionate collapse of RC assemble

Target 1; Phase II: the adaptive spread of plasticity
1. The strain at which hardening in steel begin
2. Large geometrical displacement
3. Modes of failure in RC columns
4. Shear interaction in shear critical elements
Target 2; Phase III: the global softening
1. Buckling of compressive reinforcement.
2. Post-peak concrete damage and failure.
3. The lowermost strength at the point D.
Target 3; Phase IV: the dynamic state of catenary
1. The strain rate effect, or the dynamic force increase factor.
2. Model of steel in hardening and softening.
3. Model the transition and the dynamic amplification factor.

2.6. Survey of the simulation techniques

In the following, the potential of each of simulation strategy is evaluated against the defined objectives outlines in the previous section. The purpose is to define the tradeoff simulation amongst the key factors aiming at balanced assessment of the risk and robustness of the progressive collapse in the RC frame buildings.

2.6.1. Finite element based simulation strategies

The reported simulation strategies based on the finite element methods can be classed based on the used software, or based on the used class of the solution procedures. Based on the solution strategy, we can classify the following;

1. Explicit dynamic analysis and with element erosion function for damage simulation. Examples; LS-Dyna (Bao, Main, Lew, & Sadek, 2014) and MSC.MARC (Xiao, Xin Zheng, Wan Kai, & Lie Ping, 2011). The general problem of the explicit schemes is the need for small time-integration step, when this disadvantage is weighted out by the robustness of the integration without convergence problems, this option become more attractive (Lu, Lu, Guan, & Ye, 2013). Compared to the named targets of the progressive collapse simulation, the Target 1, explicit integration cannot trace the full development of the mechanism of collapse because of the co-existence of plastic

deformation, hardening and softening at various location in the model, an implicit time solution steps is a must before the algorithms moves from the solid state to the flowing state. For example, although in the case of building denotation, collapse mechanism is prescribed, researchers recognized such limitation and used hybrid simulation to trace the local plastic deformation at section levels (Hartmann, Breidt, Nguyen, Stangenberg, & Höhler, 2008). The last fact significantly undermines the quality of the identified failure mechanism although it is still an attractive continuum-discontinuous modelling strategy and it is widely adapted by many researchers, e.g. NIST. Therefore, this school of simulation will undermine the objectives of the 'phase II', which will subsequently prevent the accurate prediction of the ductility even though it may predict the strength in the 'phase II' objective. This simulation strategy is the elite for the objectives of phase 'III and IV' because it is naturally describing the state of motion based on well-established Newton laws.

2. Explicit dynamic analysis based on reduced (macro) models. This class of models aims at reducing the computational cost of the continuum elements in comparison with the above class which is more generic. The use of macro- elements demands an overhead preprocessing calculating the equivalent properties of these elements. This fact compromises the quality of the modelling even further because it blinds the change in material behavior results from the change of the loading state which is unavoidable while the physical properties of the material chancing over the simulation. This, therefore, is more problematic in the phases 'I and II'.
3. Implicit quasi static analysis and with element erosion function for damage simulation. Examples include ANSYS, ATHENA, ABAQUS, and DIANA, see for example (Sasani & Kropelnicki, 2008) and (Sasani, Werner, & Kazemi, 2011). It is clear that the use of an implicit integration scheme improves the prediction of the collapse mechanism in addition to the benefits of the adaptive time stepping improving the simulation convergence. Therefore, these can be considered as the most

outstanding option fulfilling both Targets 1 and 2. However, there are three clear drawbacks;

a. Both the size of the unknowns and the convergence difficulties associated with the continuum implicit integration scheme and volumetric locking problems made the full model of structure a super challenge, which is still beyond the practical implementation, and therefore it is not recommended for robustness and sensitivity analysis proposed in the earlier section.
b. The need for full geometrical representation of the steel reinforcement in addition to the appropriate configuration of the bond and slip behavior of reinforcement,
c. Material failure is modeled through element erosion criteria which is based on local finite element variables (deformations), these local variables characterized by higher error order as error is normally controlled at the model level undermining the quality of the simulation of the progressive failure especially when the erosion function depends on the failure mode and strain rate which necessitate customized configuration at different locations,

4. The implicit quasi-static simulation based on reduced (macro) models e.g. (Bao, Kunnath, El-Tawil, & Lew, 2008) using; OpenSEES, SeimoStruct, and SAP2000. These models enjoy the limited number of unknowns in the problem. But, the presented models in the literature are merely validated after the arching point. Therefore, it may be good approximation for the phase 'I and II' of the ultimate strength although it is not the best for the collapse progression analysis as defined in the phases 'III and IV'. The reported models are merely valid for elastic response of the mechanism, not even providing full validation of the target 1. To the best of the current knowledge, reported models are only valid in the dynamic simulation of the elastic repose of the mechanism, and none of these even proposed a structured collaboration process before the validation. Therefore, this class is the least reliable option in terms of the

accuracy of the results although it may be expanded to reproduce the full development of the collapse mechanism.

5. Multi-simulation platforms based on explicit integration scheme, e.g. Ls-Dyna, FEAB (Hartmann, Breidt, Nguyen, Stangenberg, & Höhler, 2008) and multi-body models (Lu, Lin, & Ye, 2008). The presented application counter, in principle, the need for implicit integration aggregating of the reaction force in plastic hinges. But this is only reasonable when the failure mechanism is full predefined, because such procedure cannot discover the new location of a new plastic hinge. But, in the reported model these locations has been prescribed.
6. Sub-structured hybrid simulation based on implicit integration schemes; e.g. (Li & Hao, 2013). The presented model cannot predict the horizontal spread on the mechanism making a soft-story for example. Therefore, the model also fails at the target 1.

Another important observation is that although the dynamic effects of the moving mass of the mechanism are well defined, non-of the provided models in the literature integrate the real time and inertia effect in the simulation completely, which is supposed to describe the full response path over the 4 distinct phases. Instead, it was left out as a post processing task and the reported validating simulations provide checks only at specific points or response (Orton & Kirby, 2013). It shall be shown later that describing a single point; (force, deflection) see for example (Arshian, Morgenthal, & Narayanan, 2016), is very sensitive to modeling parameter and shall not be considered sufficient for the full check of the model quality.

Mapping the simulation surveys to the simulation targets defined in the earlier section and referred to at different phases of response in F. The above comments are regrouped and summarized as follows;

1. The high-resolution models suffer from significant convergence problems hinder the analysis of the problem at the building level, or when many component of the

mechanism is being analyzed. Such problem become more pronounced when the clear definition of many interacting material response is not well presented such as those described in the phase II and III refereeing to the phases of the response curve earlier. If the models are well presented in the simulation model, rate of convergence can be improved using adaptive step-size and line search algorithm.

In the third phase of response; stirrups, shear crack open and locking as well as the descending proportion of the steel strength curve, beyond the point of the ultimate strength, and the fracture stress-strain are all key parameters.

2. The multi-platform models, or those based on slave-master description of stiffness matrix, cannot represent the progressing of the inelastic material response to another part of the structure (Hatahet & Könke, 2014a).

3. The reduce models are limited to the details process of model reduction and does not represent the gradual changes in stiffness of in the third phase, which is important in the identification of the dynamic load increase factor of the tying force requirements. This has been denoted DAF in (Hatahet & Könke, 2014a).

When implicit simulation is not yet possible, the explicit techniques have been found attractive by wide range of audience. The disadvantages are;

1. Small time-step-size, attention to the error evolution and careful validation. These entire disadvantages make the practical application difficult and iterative based on experience and judgment. This point out the risk of human miss-interpretation and inaccurate implementation.

2. The multi-platform models are only valid when the collapse is assured a result of the analysis. Because, when the proportional collapse is expected, which is the case considered in this work, while the failure found a new stable position, significant inelastic and geometric nonlinearity took place which cannot be presented by the multi-body model unless further updating loop is made based on the high-resolution

model. It is also worth to indicate here that the validation of the proposed model (Hartmann, Breidt, Nguyen, Stangenberg, & Höhler, 2008) is based on visual validation of the modes of failure comparing simulation to shots of high-speed camera of the denotation projects.

3. The reduced model in this class is the most dangerous in terms of elaboration effort; however, it provides a valuable tool for deterministic analysis once the collapse machismo is defined. In other word, it is good strategy for the target 2 and 3. However, it is wrong in target 1 as multi-level plastic deformation exist and force redistribution is important.

2.6.2. Overview of the simulation alternatives to the classic FEM models

The FEM is the most developed and established with application to non-linear problems. It can be classed as an extension of the boundary element method (BEM). However, owing to the above defined targets, the standard FEM suffers specific difficulties as follow.

1. The need for the simulation of material discontinuity result from gradual cracking/softening, fracture/crush of compressed concrete and the rupture of reinforcement bars in tension.
2. Localizations result in severe mesh distortion especially when a full building model is developed using relatively fine mesh.
3. Large deformation in collapse problem imposes additional challenges to FEM models, for example the stiffness matrix will be asymmetric, and further iteration loops will be needed in the solver.
4. The need for artificial techniques to balance removed forces result from the deleted (eroded) elements due to the transit nature of the complete damage of the elements.

Before sinking in different formulation approaches, it is useful to discuss the disadvantages of the classic FEM in application to progressive collapse simulation. Where the drawbacks of the explicit methods were presented in the earlier section, improvement of the FEM is foreseen through the development of a full implicit solution.

2.6.2.1. Mesh-free, and the element-free Galerkin with the partition of unity

This is an extension of the FEM with the key difference that the integration of the weak form is performed over points in the material enriched by trial shape function to which a jump in displacement is introduced to simulate the partition of the body as the crack evolve (Rabczuk T. , 2013). Such technique will provide more flexibility in increasing the number of points at the localization regions, however such meshing flexibility is returned by the intense of the numerical solution for updating trial function. There is also no evidence in the literature of successful simulation of complete failure (or crush) of concrete in compression as most of the validations reflect single major crack in tension, see for example (Rabczuk & Belytschko, 2004), (Kaufmann, Martin, Botsch, & Gross, 2008) and (Wu, Ma, Takada, & Okada, 2016).

2.6.2.2. Discontinuous discrete element based simulation strategies

This family is popular in rock mechanism and geotechnical failure analysis. Although the name sound versatile and attractive for progressive collapse simulation, in general, these methods still to date require predefined lines of fracture at which the boundaries of element are drown. In addition, it increases the computational demand and solved by explicit time stepping schemes. Therefore, specially manipulation is required for these methods to capture an unknown failure mechanism, and its occasionally reunified with one of the superseding methods to handle cracks yet in tension.

2.6.2.2.1. General discrete element method (DEM)

It is called distinct element method by some other researchers (Cundall & Strack, 1979). The principle idea in this method is that the problem is idealized by moving boding with face interaction laws, an over view of the early generation can be found in (Hart, 1989). Sophisticated algorithms have been developed to detect interaction of the moving bodies (Glösmann, 2010), and the contact configurations, see for example (Jiang, Leroueil, Zhu, Yu, & Konrad, 2009) and (Kazerani, 2013).

2.6.2.2.2. Multi-body dynamics Method

In this model, the material is modeled as an assembly of rigid (none-deformable) discrete element connected by normal and shear springs. These models have been widely used and implemented in demolition simulation. Another name of this is the distinct element method. Recently, it appears in another name of the applied element method (Meguro & Tagel-din, 2002).

2.6.2.2.3. Applied element method

It is the same as the multi body method implemented in commercial software Extreme Loading System® in which models are developed for building simulations under blast and earthquakes. The software aimed at progressive collapse simulation, the validation examples, as shown from the website, include the collapse-failure modes of slabs, building demolition case studies, simulation of the pattern of the macro cracks at failure and bucking simulation applied to rubber material (Meguro & Tagel-din, 1999). In the literature, there are some work related to the improvement of crack pattern (Meguro & Tagel-Din, 1997), reduced bias of cracks, simulation using element structure based on Voronoi tessellation (Worakanchana & Meguro, 2008), large displacement analysis and non-linear buckling. It is difficult to follow the development in the direction due to the commercial nature of this application.

It is unclear how much the modeling method is sensitive to simulation assumptions. In a white paper of the software website, RC models are valid in prediction accurately the bridging forces in beam or the progressive collapse of the RC column which are critical in accurate prediction of the safety level against progressive collapse (El-Fouly & Khalil, 2012), however the validation is limited to a single bridging beam case and the response curve show a sharp ultimate strength point that can be only explained by the nature of the method. The absence of full validations can be alerting when the software claims fir for purpose in safety assessment of progressive collapse in buildings.

2.6.2.2.4. Discontinuous deformable analysis method

From its name, it considers the deformation of the bodies (elements) as compared to the simple version of the multi body method (Munjiza, 2004). The major development in this method driven by the tunnel models, slope stability analysis and rock failure models. Further development in the rock mechanics is taking the form of so called hybrid simulations. For examples, DEM-FEM, or called FDEM, in which the FEM is used to model the deformable body with the DEM simulation algorithm. It sounds extremely versatile to use hybrid simulation if one can imagine that material nonlinearity, small deformation, and discontinuities can be models using FEM and the large displacement and discontinuities are analyzed in the DEM in a single model, see for example an advanced multi-scale simulation from (Wellmann & Wriggers, 2012).

2.6.2.3. Particle models

Widely applied to soil models, particle models provided opportunity for concrete simulation at meso-scale level and to represent concrete crash under uniaxial compression as well as hydrostatic compression. However, unless the model used the exact scale of the material heterogeneous structure, cracks cannot be accurately modeled leaving it with two folds' problem of high number of unknowns and the need for explicit integration scheme.

One development is the discrete particle lattice model, which combines the lattice structure of the element to the particle model regulating the relationship between the particles and reducing the solution demands of the normal particle method. It also allows for further regulation of averaging material behavior (Cusatis, Mencarelli, Pelessone, & Baylot, 2011) and (Cusatis, Pelessone, & Mencarelli, 2011). The disadvantages of particle models are yet the phenomenal description of material mechanical rules rather than the intrinsic simulation of the cement past structure and the volumetric representation normally provided by higher resolution material models. The later also suffer from reliable model of the micro cracks caused in concrete by hydration, shrinkage and the lattice structure method

Instead of using continuum structure of the FEM, the material is modelled truss or beam element triangles in 2D of the element in 3D. Collapse can be simulated through gradual remove of the failing elements without causing severe instability in the simulation. Nonlinear formulation is applied through the failure criteria as defined to the discrete component of the lattice structure.

2.6.2.4. Multi-scale and hybrid simulation

In heterogeneous material, like concrete, the mesostructure of material play the major role in the actual material nonlinear behavior and strength dependence on the size of the sample, or what is known by the size effect. This was one reason to think of multi-scale simulation, bearing in mind that the meso-scale representation of the concrete results in millions of degrees of freedom, the need for strength simulation at macro level aspired such development (Koenke, Eckardt, Haefner, Luther, & Unger, 2010). When multi-scale is used, artificial methods will be required to couple the models without losing the physical meaning of the model and with smooth application of the mathematical solution.

So far, different advance modelling techniques has been roughly surveyed. With target of modelling the progressive development of the collapse mechanism, an implicit algorithm is recommended, although bridge scaling can offer comprehensive approach, the need for an adaptive scale bridging and computational cost are perceived as an advanced target. In this work, beam finite element is applied for simulation and it is surveyed in the following section in line with the modelling targets named in earlier sections.

2.7. Structural based finite element models (SFEM)

Dealing with progressive collapse encompasses that the FE model must handle the following problems from solution algorithm point of view;

1. The nonlinear material behavior at the section level
2. Geometric nonlinearity due to the P-Delta and cable/catenary tensile behavior
3. Large displacement and flow of material until the full catenary action is developed

Various nonlinear simulation techniques of the RC beam behavior were adopted in the literature, see for example one of the most outstanding works of (Talaat & Mosalam, 2008).

Considering the advantages of the reduced models in the parametric analysis, and within the time frame of this research, the structural FEM was selected for modeling of the problem. A well-structured review in the content was presented by (Filippou, D'Ambrisi, & Issa, 1992). Later, amongst the community of the structural FE, both displacement based (DB) and the flexibility based (FB) FEM structural beam/column formulation are widely studied in the seismic response simulation of structure under both static and dynamic loading. To couple the axial load and bending moment on the element the concept of section analysis associated to the response of the section through the known fiber bases beam/column element (FibE). Where the FibE is based on the uniaxial (1D) stress strain curve of the steel and concrete at the section level, it is regarded as inelastic FibE when an inelastic 1D material model is adopted. The concept of the inelastic FibE gained further attention as implemented in the FB beam formulation. The advantage of the FB over the DB beam element is that the force's equilibrium is strictly satisfied at the section and element level reducing convergence problems associated to DB element. However, FB doesn't provide full physical description of material deformation even at the section level therefore the evaluated deformation is purely virtual and therefore equilibrium must be established in the deformed configuration and updated along the evolution of the large displacement (Filippou & Fenves, 2004). Extensions of the FB was made for the large displacement and geometric nonlinear response based on the co-rotational beam element formulation (Alemdar & White, 2005) based on the work of (Crisfield, 1990) and (Crisfield, 1991).

While the development of full FEM simulation coded based on the flexibility based FEM is rather not popular, steps to incorporate the FB in displacement based FEM program was developed. And the FB beam/column element is now a known option in most of the displacement based FE codes. To embed the FB in DB program, element flexibility must be

converted into a stiffness, this normally done by taking the inverse of the value of the flexibility results from FB (Taucer, Spacone, & Filippou., 1991).

In nonlinear simulation, while plastic response of RC section is likely, the localization of the plastic-hinge can be simulated by either the lumped plasticity technique, or by the defining the plastic zone at the expected location of the developing hinge. Although the lumped plasticity offers an effective computing solution and was supported by many calibration studies, it decouples the automatic interaction of the axial-benign forces. In contrast, by defining a certain length of the plastic-hinge alongside the use of the FibE can automatically account for the axial-bending interaction while certain regulation routine is proposed, for example (Scott & Hamutceuogelo, 2008). A compromise of the two concepts exists through the use of the zero-FibE beam element embedded at the end of an elastic beam element; (Zhao & Sritharan, 2007), (Bao, Kunnath, El-Tawil, & Lew, 2008) and (Valipour, FarhangVesali, & Foster, 2013). Such a compromise suffered from difficulties in simulating element and system softening which required further calibration. A more representative formulation was based on predefined length of the plastic hinge based on empirical value or standard recommendations, it also undermines the merit of the axial-bending interaction at the critical sections. But, in progressive collapse simulation, the zone of plastic-hinge grows until failure and local unloading take place. Therefore, during the simulation, the growth, extension of the plastic-hinge influences the progressive development of the collapse mechanism.

Recently (Almeida, Das, & Pinho, 2011), and (Lee & Filippou, 2009), proposed methods for the extension of the plastic-hinge, but non-of these considered the evolution of the length as a natural output of the simulation. (Izzuddin & Einashai, 1993) considered the update of the mesh by adding nodes, (Lee & Filippou, 2009) use empirical equation for the hinge and (Almeida, Das, & Pinho, 2011) developed an adaptive strategy of the element response integration regularizing the element response for element softening, also regularized FB beam were also presented by (Scott & Hamutceuogelo, 2008).

2.8. Concluding remarks on the earlier surveys

Under the scope of this project the following concluding remarks are made at the end of the literature survey;

1. Modeling of the progressive collapse is sensitive to material and geometrical nonlinearities.
2. Modeling softening based on methods of continuum mechanics present major challenge in handling localization softening, large geometrical displacement and discontinuities
3. Limit-state macro-based models can only work for the decoupled analysis of the loading level.
4. Widely applied models are based on phenomenal empirical observation
5. Structural models, based on the empirical material models, is still subjective although a few objectivities based procedure are present. Objective models also depend on the nature of element implementation in FE. In particular, modelling failure modes in column element presents a major challenge.

The frame finite element, or the macro-element-simulation, unavailable yet, in spite of the nonlinear dynamic models which is only validated in the elastic reaction of the mechanism. Because the frame finite element still the most versatile and computationally acceptable, also it is extendable through multi-scale or hybrid simulation, we propose the development of this stream to simulate the problem of progressive collapse.

2.9. The focus of this research

The focus of this work, in light with learned literature above, is to model the quasit-static evolution of the collapse mechanism following the full path of response especially beyond the peak of the ultimate strength; including section softening and cable catenary at the 3D structure level using frame finite element. This simulation model is used to derive the dynamic effects based on the energy preservation principle. Calibrations of the model is

performed for objective hardening and softening. The simulation procedures are evaluated by the tests reported in the literatures.

The modeling strategy is used for numerical experiment of various sources of uncertainness and the degree of sensitivity of the results. Finally, the e outstanding robustness parameter affecting the collapse safety in building are concluded based on novel defined robustness indexes and performance functions.

In pursue of the outlined targets, the following chapter shall address rational analytical and the computational evaluation strategy of the collapse evolution in beams, frames, and buildings. This will be followed by modelling sensitivity analysis and concluded by key factors in the robustness of the structural robustness.

Chapter 3 Analytical Evaluation

3.1. Aim and abstract

The aim of this chapter is to simulate the quasit-static evolution of the collapse mechanism following the full path of the quasi-static large displaced response especially beyond the peak of the ultimate strength; including the flexural softening and cable catenary. The following formulation of the analytical relations bridges the needed emergent understanding of the progressive collapse mechanics to the mechanics of RC structures. These integrative procedures therefore explain the mechanical relationships. This formulation is perused based on the key mechanical relationships newly developed as an extension to, and an integration with, existing works presented in the literature. As compared to benchmark tests, the provided analytical procedures proved providing reasonable insight weighing some of the key mechanical parameters of the response curve introduced in the earlier chapter in Figure 2.5-1. However, it requires further development before being reliable for predicting unknown mechanisms.

3.2. Analytical evaluation based on beam structural mechanics

Based on the benchmark test performed by the NIST (Lew H. , et al., 2011), an idealization of the system can be proposed as outlined in the Figure 3.2 1. In the Figure 3.2-1(a), three phases of response were observed; these mapped to the idealized free-body diagrams introduced in (b), (c) and (d) for; the arching in the hardening phase 'I', the arching in the softening phase 'II' and the tensile catenary phase 'III' respectively. It hall be noted that there is one phase is omitted here, the linear elastic phase as compared to the four phases regarded in chapter 2. Each phase is schematically indicted on the response curve in the Figure 3.2-1 (a).

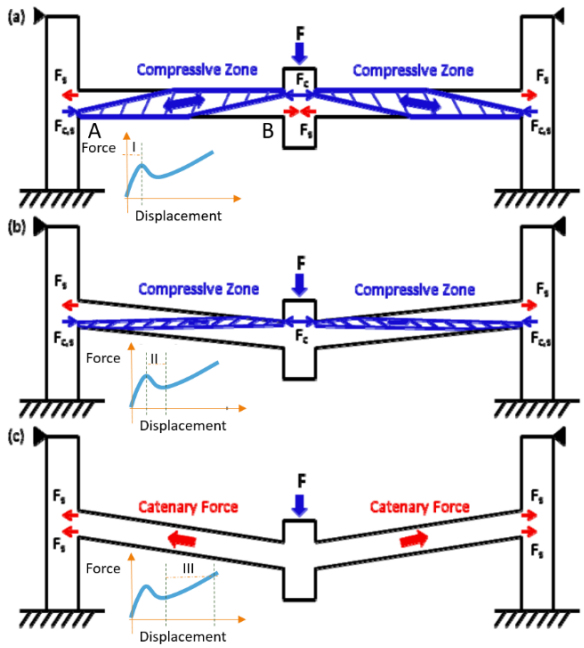

(a) Three stages of load transfer adapted (NIST, 2011)

(b) Arching in the hardening phase (I)

(c) Arching in the softening phase (II)

(d) Tensile catenary phase (III)

Figure 3.2-1 Idealization of the frame assembly in the main phases of the quasi-static response

In the idealization, half of the assembly AB is considered due to symmetry. A rigid beam element is considered with concentrated forms of axial and bending deformations located at each end A and B. These deformations result from the beam forces N_A, N_B, m_A, and m_B; which are the axial forces, and the bending moments, at the beam ends. Similarly, the same forces associated with deformation of the sub-frames are related here to the joint (J), and

therefore they have been named N_{JA}, N_{JB}, m_{JA}, and m_{JB}. Then, the deformation/force of the beams are related to the beam element and the sub frame deformations/forces will be associated to the joint (J). Load balance at each node is also shown between beam and joint forces.

In the following, each of the named phase will be discussed based on the principle of the mechanics of the idealized beam elements above. The master contributions in this section are expanded from the pioneer works of;

- (Park & Gamble, 2000) set the arching force equations,
- (Qian. & Li, 2013) who first reported the validity of the plastic analysis for progressive collapse situations and linked it to shear stiffness of joints and bar-slip deflection,
- (Yu & Tan, 2014) who examined the axial-flexure interaction at the point of ultimate strength, and
- (Stylianidis, Nethercot, Izzuddin, & Elghazouli, 2016) who implemented various response mechanisms; flexure, arching, and catenary, in coherent analytical framework in steel and composite type of structure.

As extension of these contributions, here the arching phase in RC beams is reevaluated and it is found that the arching strength is not only limited by the axial-flexure interaction, but also by the considerable eccentricity in defining the point of ultimate strength. In addition, the full behavior in the tensile catenary is well described covering the change in axial stiffness as a result of bar fracture. In addition, the body motion phase is newly adapted and shown to describe the recorded underestimation of the dynamic effects found by (Orton & Kirby, 2013). These are presented here for the first time.

To present these integrative procedures, basic mechanics of beam collapse mechanism is first presented covering arching and catenary, the high sensitivity to boundary conditions is discussed and the bonding stiffness, and the presence of shear stress are presented. Then, the dynamic implications are evaluated based on principle newton laws and integrated to the dynamic amplification evaluation. Finally, summary of the procedures is provided with

validation examples. In these examples, the results matched the modeling targets of phases II, III and IV as defined in chapter 2, in addition to the dynamic amplification. It also shows that the procedures can capture the change in the depth/span ratio.

3.2.1. Beam mechanism

Based on the nature of supports, three different types of beam mechanisms can be identified because of losing the support at point B, in the Figure 3.2 2, the beam ABC under the uniform distributed load (q) is considered. If the bridging beam ABC in (a), has simple support at A, both bending moment at the point A and the axial force are zero in the free-body diagram (FBD) in (b). In addition, the reaction at B is lost. At failure plastic hinge forms by the point B, and the plastic strength q_p that can be obtained using the 3 equations of the equilibriums;

$$q_p = \frac{2m_B}{L^2} \dots\dots (3.1)$$

The vertical deflection w can be evaluated through the principle of virtual work; balancing the external work of the active load q.L multiplied with the displacement/deflection w, with the internal work done by the deformation of the plastic hinge at B in this case; we obtain;

$$w_p = \frac{\emptyset_B m_B}{qL} = \frac{\emptyset_B}{2} L \dots\dots (3.2)$$

Where $\emptyset_B$ defines the rotation of the plastic hinge at the point B.

Equations, (3.1) and (3.2) reflect the 'phase I' of response including the two cases where the yield moment is formed, or where the ultimate state is defined.

The response curve can be recognized by three phenomena; the compressive arching, the tensile catenary, and the transit body motion in between them. Each of these will be discussed further in the following sections.

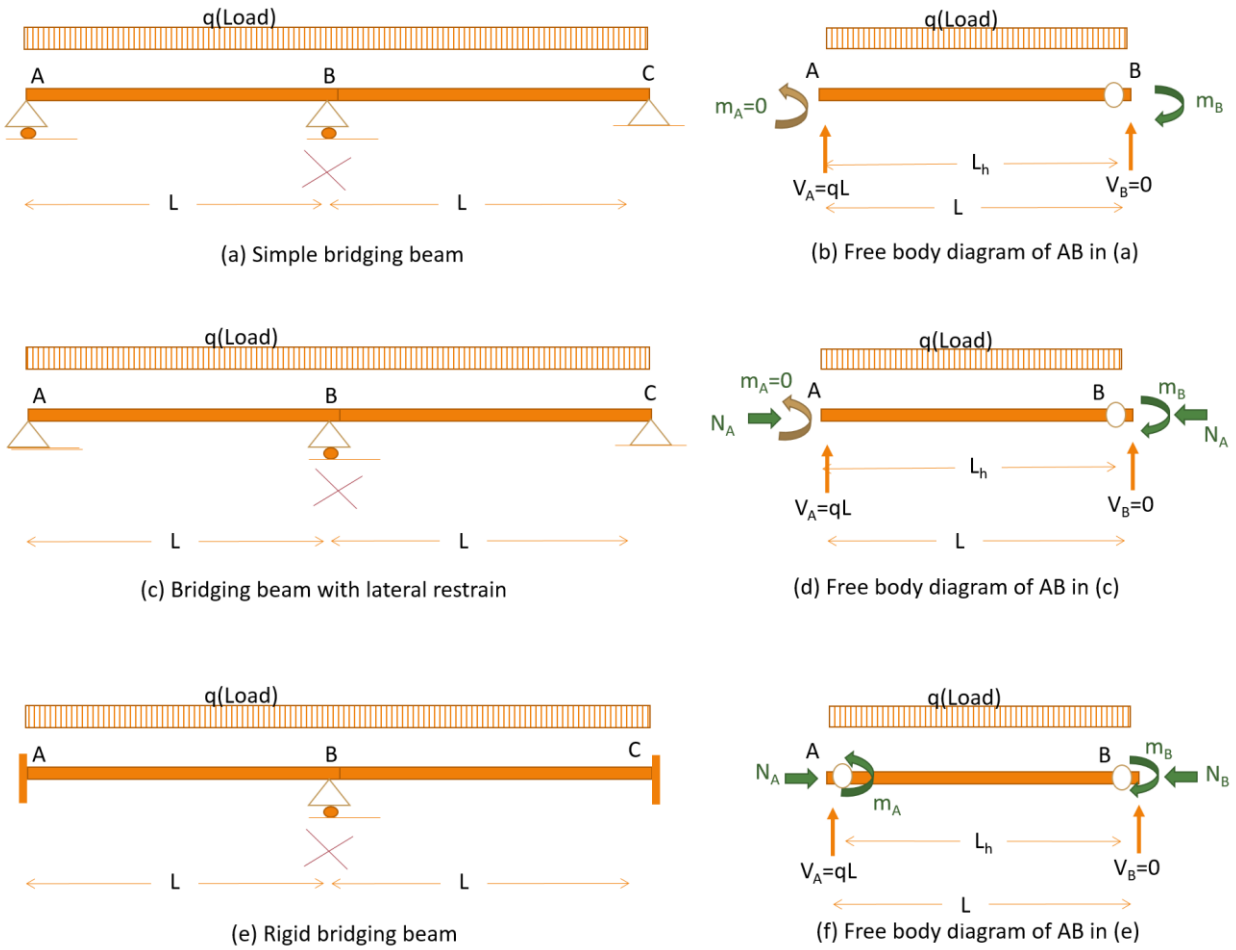

Figure 3.2-2 effects of the improved boundary conditions on the beam mechanism

3.2.1.1. Arching in beams with translation restraint

With lateral restraint, Figure 3.2-2 (c), the axial force develops as the point B moves downward. Due to geometric locking, see Figure 3.2-2, compressive force develops before the bending failure occur. If the system still in the hardening arching phase, the vertical displacement is small and the equation (3.1) does not significantly change. But the bending strength is down to the axial force $m_{B(N)}$, therefore we may obtain;

$$q_{p(N)} = \frac{2m_{B(N)}}{L^2} \dots\dots (3.3)$$

Another sequence of the geometric locking is that the beam will not deflect downward unless it deforms axially in compression because of the arching force N. This axial

deformation of the arch can be evaluated by the geometric analysis assuming fully rigid lateral constraints, see Figure 3.2-3 (Stylianidis, Nethercot, Izzuddin, & Elghazouli, 2016).

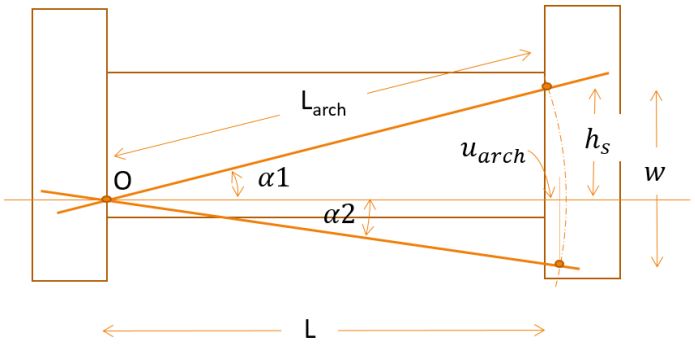

$$u_{arch} = -l_{arch}(\cos(\alpha 1) - \cos(\alpha 2))$$

$$\alpha 1 = \frac{h_s}{l_{arch}} \quad \& \quad \alpha 2 = \frac{h_s - w}{l_{arch}}$$

$$cos\alpha = 1 - \frac{\alpha^2}{2}$$

$$u_{arch} = -w\frac{2h_s - w}{2l_{arch}}$$

Figure 3.2-3 the geometric conditions of the arching in the beam mechanism

The axial deformation u_{arch};

$$u_{arch} = -l_{arch}\left(\cos(\frac{h_s}{l_{arch}}) - \cos(\frac{h_s - w}{l_{arch}}\right) \dots\dots (3.4)$$

This is valued in small rotation. The 'cos' function can be further approximated by second Taylor approximation;

$$cos\alpha = 1 - \frac{\alpha^2}{2} \dots\dots (3.5)$$

This makes the axial deformation;

$$u_{arch} = -w\frac{2h_s - w}{2l_{arch}} \dots\dots (3.6)$$

And the maximum deformation coincides with w=h_s;

$$u_{arch,max} = -\frac{{h_s}^2}{2l_{arch}} \dots\dots (3.7)$$

The above relation suggests that the axial arching deformation is a second order function of the arching depth. The arching deformation can be understood as an additional internal strain energy according to (Stylianidis, Nethercot, Izzuddin, & Elghazouli, 2016), presuming

$K_{axial,arch}$ is the axial stiffness of the beam element and the arching deformation is the largest deformation that the beam can absorb; using the virtual work principle, we can write;

$$\left(q_{p(N)}+q_{arch}\right)L\frac{w}{2} = \emptyset_B m_{B(N)} + K_{axial,arch}\frac{{u_{arch}}^2}{2} \dots\dots (3.8)$$

The, $\emptyset_B$, is the lumped rotation at the plastic hinge by the point B. This equation suggest that the deflection/strength can be superimposed; results from bending; of the first term, and the part that results from the arching mechanism. If we consider the arching part only, and seek the arching strength at balance through differentiating with respect to w, we obtain;

$$q_{arch} = \frac{K_{axial,arch}}{L{l_{arch}}^2}\left(w^3 + 2w{h_s}^2 - 3w^2h_s\right) \dots\dots (3.9)$$

This equation describes the additional strength results from the arching restraint which can be added to the bending strength to obtain the full strength of the beam mechanism. To obtain the local peak values, we differentiate and put to zero, the local max value of q_{arch} can be obtained at;

$$w_{arch,max} = 0.425h_s \dots\dots (3.10)$$

And the associated arching strength;

$$q_{arch} = 0.385K_{axial,arch}\left(\frac{h_s}{L}\right)\left(\frac{h_s}{l_{arch}}\right)^2 \dots\dots (3.11)$$

The axial arching force N;

$$N = K_{axial,arch}u_{arch} = -K_{axial,arch}w\frac{2h_s - w}{2l_{arch}} \dots\dots (3.12)$$

And a maximum theoretical value, when w=h_s, defines;

$$N_{max} = -K_{axial,arch}\frac{{h_s}^2}{2l_{arch}} \dots\dots (3.13)$$

When; $w_{arch} = 0.425h_s$, then;

$$u_{arch} = -0.335 \frac{{h_s}^2}{l_{arch}} \ldots\ldots (3.14)$$

$$N_{arch} = -0.335 K_{axial,arch} \frac{{h_s}^2}{l_{arch}} \ldots\ldots (3.15)$$

Then the arching force is also a second order function of the arching depth h_s. Equation (3.15) can be useful while calibrating the mode to test results, e.g. putting the measured axial reaction force in the balance equation can lead the equivalent arching stiffness if the arching depth can be defined.

The expression in equation (3.8) can be disputed if the arching reaction force is considered as an external force acting on the beam which convert the addition into subtraction at the other side of equation having the plastic external energy twice the internal elastic energy. Or simply cancels out if both are elastic, or both are plastic. Therefore, the derived expressions cannot always hold true. It can be easily shown that equation (3.15) can result in high/unrealistic arching force because the fore equilibrium at the section level here is not yet established.

3.2.1.2. Increasing ductility with rotation restraint

Adding rotational restraints add to the plastic strength as defined in equation (3.3) cause by the contribution of the bending moment at the end A in presence of the arching force N, see Figure 3.2-2 (e) and (f).

$$q_{p(N)} = \frac{2\left(m_{A(N)} + m_{B(N)}\right)}{L^2} \ldots\ldots (3.16)$$

To evaluate the vertical displacement, the same assumptions for equations (3.9) to (3.13) applies. With the only change to equation (3.8) adding the terms related to the plastic rotation at the hinge by the point A;

$$\left(q_{p(N)} + q_{arch}\right) L \frac{w}{2} = \emptyset_A m_{A(N)} + \emptyset_B m_{B(N)} + K_{axial,arch} \frac{{u_{arch}}^2}{2} \ldots\ldots (3.17)$$

The $\emptyset_A$ is the lumped rotation at the plastic hinge by the point A. This update makes no changes to the arching analysis mentioned earlier. The item q_{arch} is a 3rd order function of w, see equation (3.9), as well as u_{arch}. Therefore, solving equation (3.15) for a specific w required iterative procedures, which is best handled by assuming values of w and then checking the error in equation (3.15).

3.2.2. The first-order geometrical effects of the large arching force

In case of large arching force, or displacement, the additional bending moment result from the eccentric force will alter the balance equation in (3.16) to;

$$q_{p(N)} = \frac{2\left(m_{A(N)} + m_{B(N)}\right) - N.w}{L^2} \dots\dots (3.18)$$

Therefore, it is not only the ultimate arching axial forces is required but also the pointwise update of N is required maintaining the balance condition at the full beam element level.

3.2.3. Deformation of the sub-frame elements

The serial connection to the sub-frame elements add to the overall flexibility of the beam element. These effects can be reflected by updating the values of the axial arching stiffness $K_{axial,arch}$ and the lumped flexural stiffness by each end of the beam in the terms; $\emptyset_A$, and $\emptyset_B$.

3.2.3.1. Axial stiffness of the sub-structure

Suppose the lateral stiffness of the substructure at the joint A is K_{JA}. Then the equivalent axial stiffness of the arching mechanism becomes;

$$K_{eq} = \left(\frac{1}{K_{JA}} + \frac{1}{K_{axial,arch}}\right)^{-1} \dots\dots (3.19)$$

The values of the stiffness in equations (3.12), (3.13), and (3.15) updates;

$$N = K_{eq} u_{arch} = -K_{eq} w \frac{2h_s - w}{2l_{arch}} \dots\dots (3.20)$$

$$N_{max} = -K_{eq}\frac{{h_s}^2}{2l_{arch}} \dots\dots (3.21)$$

$$\left(q_{p(N)}+q_{arch}\right)L\frac{w}{2} = \emptyset_A m_{A(N)} + \emptyset_B m_{B(N)} + K_{eq}\frac{{u_{arch}}^2}{2} \dots\dots (3.22)$$

As a result of the reduced arching stiffness, lower values of the axial force N can develop in the assembly, this will, subsequently, affect bending stiffness and strength updating all the terms in equation (3.19).

3.2.3.2. Sub frame rotation

Similar to the updating defined in the section 2.2.1, the terms; $\emptyset_A$, and $\emptyset_B$ will be updated as a result of the additional flexibility of the rotating sub-frame. Due to symmetry, $\emptyset_B$ remain unchanged, and the equivalent total rotation by the point A; $\emptyset_{A,eq}$ becomes;

$$\emptyset_{A,eq} = \emptyset_A + \emptyset_{JA} \dots\dots (3.23)$$

Where, the $\emptyset_{JA}$ represent the sub frame lumped rotation encapsulated in the joint at A. This is true as long as the bending moment and the end A, and the Join A balance in the joint equilibrium, see Figure 3.2-2 (c).

Summary of the rigid body based beam mechanism is shown in Figure 3.3-1.

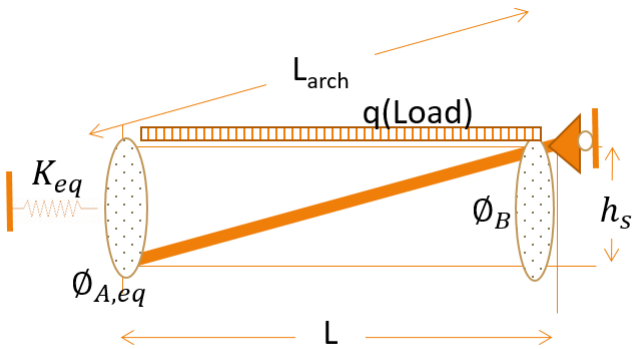

Figure 3.2-4 Schematic representation of the rigid body based beam mechanism

Both the equivalent stiffness and the lumped rotation present a modeling challenge. While all the earlier analytical formulation may valid for any forms of the structural system in

general, further insight is down to the specific form of construction in the following, the focus will be made on RC structures in line with purpose of this work. Based on the well-established principles of the RC design, the joint related mechanism will be discussed, then the plastic hinge shall be handled in detail in the following sections.

3.3. The suspended tensile catenary mechanism

Refereeing back to the third phase 'III' of the response outlined in Figure 3.2-1 (d), the tensile catenary force developed in the element can be related to the applied force by;

$$q_{t,cat} = 2\frac{N}{L}.sin \propto \cdots \ldots . (3.24)$$

Here $\propto$ defines the cord rotation. If second order approximation is also employed, tan $\propto$ = $\propto$ = sin $\propto$, then equation (3.21) becomes;

$$q_{t,cat} = 2\frac{N_{t,cat}}{L}.\frac{w}{L} \ldots \ldots . (3.25)$$

The axial stiffness is also the serial contribution of a few element which will be referred to by $K_{eq,t,cat}$. By integrating the serial contributions into the axial elongation; u_{elong}; the catenary force is then;

$$N_{t,cat} = K_{\mathrm{eq,t,cat}} u_{\mathrm{elong}} \ldots \ldots . (3.26)$$

And from the geometry and second order approximation of the cos, see Figure 3.2-3;

$$u_{\mathrm{elong}} = L(1 - cos \propto) = \frac{w^2}{2L} \ldots \ldots . (3.27)$$

Then the equation (3.22) reduces to;

$$q_{t,cat} = K_{\mathrm{eq,t,cat}}.\left(\frac{w}{L}\right)^3 \ldots \ldots . (3.28)$$

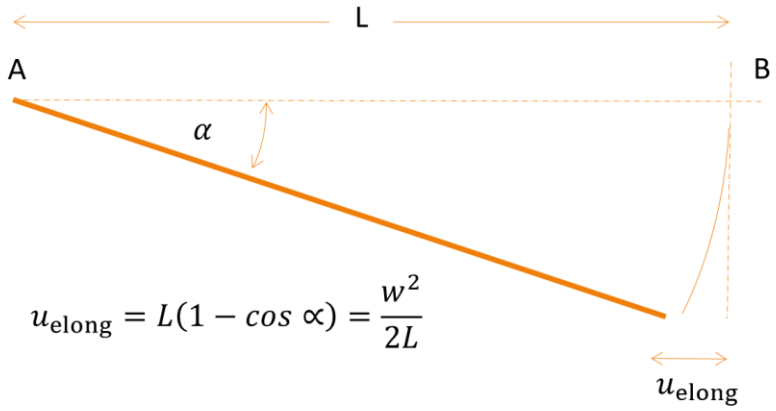

Figure 3.3-1 the geometry in the suspended tensile catenary mechanism

The approximation in (3.25) shows that the value of the tensile catenary force is a third order function of the vertical drift ration w/L provided the deflection w is small with reference to the beam length. The, $K_{\text{eq,t,cat}}$, takes different values according to the changing from elastic to plastic and strain hardening. Therefore, multi-step analysis is needed, see section 3.6.3 and Table3.6-1. In fact, the little reduction in $K_{\text{eq,t,cat}}$, will not only have linear effect on the catenary strength $q_{t,cat}$. But it will also relax the w making the strength a forth order function to the stiffness. Therefore, the bonding stiffness at different loading state is another key parameter, these are visited in section 3.4.2.1; Bar-slip and de-bonding at joint, for the complete reference to known related parameters.

3.4. Principles in the RC behavior analysis

In this section, the identified key stiffness and rotation variables will be discussed in the light of the RC design practice.

3.4.1. Analysis of the critical zone

Critical zones are those parts of the structure that develop nonlinear behavior which localize the rate of deformation due to the gradual, or even prompt, reduction in stiffness. Such high nonlinear response, can be regarded as progressive damage, is proceeded by the progressive failure of strength through normally regarded by softening. There are numerous approaches in the literature used addressing the modelling question, the models

range from pure phenomenological; such as the classical plastic analysis principles of concrete to the high definition computational models, e.g. (Bazant & Brocca, 2000), (Grassl, 2004) , (Bažant & Caner, 2005), (Grassl & Jiraesek, 2006), and (Jiang & Wu, 2012). Where the last are iterative and computationally intensive, it is vulnerable to computational stability result from the strict continuum modelling in flow and failure simulation, the earlier is simple but it depends on high level of judgement and provide upper bound approach which compromises the compatibility in favor of the explicit solution. We are seeking reliable computational model with minimum preliminary judgment and explicit computational efficiency. Because the target is to derive the full strength-deflection curve of the quasi-static response of the mechanism, both strength and associated deflection; or deformations, must by reliably derived. This focus in maintained in the following section although in the normal design, only the strength conditions are analyzed in the limit state.

3.4.1.1. Axial-flexural interaction

The concept of the axial force bending moment interaction is well established especially in the design of RC columns. The core idea is based on Bernoulli beam assumption that the section remains flat before and after deformation, through which the strain is distributed over the full depth. From the given strain at the key points of the section, stress is evaluated based on the explicit 1D law of material, and these stresses are integrated over the section obtaining axial force and bending moment strengths of the section. This state-determination process in the section necessitate the check of the equilibrium of internal forces making the solution of the tow balance equations iterative, which depends on the initial guess. Building-up such a nonlinear solution routine can compromise the reliability of the procedures, especially in the case of the prompt change of the material stiffness unless high number of control point are used compromising the computing attraction of it. A few exiting procedures were proposed to handle such a drawback, see for example (Monti & Petrone, 2015). In the referenced work, closed form solution was derived for bending strength and rotations of the section at yielding and ultimate state in presence of the axial load. In their derivations, fixed location of the centroid of the compression zone is assumed

at 0.33 from the depth of the compression zone; y_y, and 0.4 for the centroid in ultimate state based on the idealized shape of stress bock suggested in the (CEN, 2004). Also, the high order form of the balanced equation is reduced by the Taylor expansion around the point at the middle of the effective depth; d_y, presuming an initial guess value of $y_y/d_y = 0.5$.

$$\frac{y_y}{d_y} = \xi_y$$

$$= \frac{n_{sy} + {\xi_0}^2\left(2\bar{\varepsilon}^2\xi_0 - n_{sy} - \mu_{s,y,c}\right) + \mu_{s,y}\left(1 + \eta\zeta + \beta(1+\zeta)\right)}{2n_{sy} + 2\xi_0\left(\frac{3}{2}\bar{\varepsilon}^2\xi_0 - n_{sy} - \mu_{s,y,c}\right) + \mu_{s,y}\left(2 + \eta(1+\zeta) + \beta(3+\zeta)\right)} \dots\dots (3.29)$$

For;

$$\mu_{s,y} = \frac{A_s f_y}{b d_y f_c'} \dots\dots (3.30)$$

$$\mu_{s,y,c} = \mu_{s,y}(1 - \eta + 2\beta) \dots\dots (3.31)$$

And the $\mu_{s,y}$ and $\mu_{s,y,c}$ are the mechanical reinforcement ratios of the tensile reinforcement and the volumetric confining steel respectively with reference to the effective depth d_y.

Obtaining the approximated value of; y_y/d_y. Then the yield curvature is found;

$$\varphi_y = \frac{\varepsilon_y}{d_y}\frac{1}{1 - y_y/d_y} \dots\dots (3.32)$$

The equation indicates that the yielding section rotation is related to the ratio of the height of compressing stress zone to the effective depth.

In the case of the ultimate state, cover spalling can be assumed, the height of the compression zone; with zero axial force, is assumed $0.4d_y$.

$$\varphi_u = \frac{\varepsilon_{cu}}{d_u}\left(\frac{0.8 + 4\beta\mu_{s,ult}}{n_{s,ult} + \mu_{s,ult,c}}\right) \dots\dots (3.33)$$

In this equation ε_{cu} is the ultimate strain value of concrete core which is confined by the shear reinforcement A_{ws}. This is normalized to the tensile reinforcements A_s by the ratio; $\beta = A_{ws}/A_s$.

The, $n_{s,ult}$, is the normalized axial load to the concreted compression force at the ultimate state, note that the concrete cover is neglected here. And the $\mu_{s,ult}$ and $\mu_{s,ult,c}$ are the mechanical reinforcement ratios of the tensile reinforcement and the volumetric confining steel respectively with reference to the effective depth d_u, these ratios are defined;

$$\mu_{s,ult} = \frac{A_s f_y}{b d_u f_c'} \dots\dots (3.34)$$

$$\mu_{s,ult,c} = \mu_{s,ult}(1 - \eta + 2\beta) \dots\dots (3.35)$$

And the bending moment at yielding and ultimate can be obtained integrating the sum of moments over the cross-section provided that the axial load is known. The assumptions of the depth of the concrete zone at yielding and ultimate states is bounded by certain range of the concrete reinforcement ratio and that concrete cover is not more that 10% of the section depth. The section ductility can be then worked out;

$$\mathbb{R}_{s,ult} = \frac{\varphi_u}{\varphi_y} \dots\dots (3.36)$$

To identify the bending strength at first yielding and the ultimate state the standard section analysis procedures can be followed in presence of prescribed value of the axial force. However, (Monti & Petrone, 2015) also suggested closed form equations in-line with used assumptions earlier regarding the centroid location of the compression zone in concrete. The resisting moment need to be considered about the point of neutral axis of the section avoiding the analysis of the equivalent eccentricity initiated by the arching conditions. The height of the compression zone can be evaluated based on the identified section rotation at ultimate state;

$$d_u = \frac{\varepsilon_{cu}}{\varphi_u} \dots\dots (3.37)$$

Then the bending moment resistance of the section can be aggregated around the point of the neutral axis, y_i is used here referring to the force F_i, where the later can be either the tensile force in main steel reinforcement, the compressive forces in concrete, or in the compressive secondary reinforcement. Then;

$$M(N) = \sum F_i y_i \dots\dots (3.38)$$

The steps discussed in this section utilize the axial force as a given input, but in collapse mechanism analysis, different values of the axial force may be associated at the point of yielding and ultimate strength. Therefore, the axial force values used in their procedures must be aligned with the arching analysis introduced in section 2.1.1. Another critique of the introduced section analysis is that it is only viable as long as the shear stress does not significantly jeopardize the material law. This is handled in the following section.

3.4.1.2. Shear-axial-flexural interaction

Coupling of the shear/stress or strain can classically be made in 2D using the Mohr compatibility circle, or using Rankine failure criteria coupled with Strut and Tie (S&T) model, such models are common for beams with small shear span and relative small ratios transverse reinforcement. 3D continuum or plasticity based models of concrete failure exists for example; Droger-Prager with capping curve; e.g. (Jiang & Wu, 2012). to the micro-plane, or the 5M models, of (Bažant & Caner, 2005) describing the solid state of concrete. Again iterative procedure is required for of the reported simple and complex methods. One of the most reported strategy in the 2D membrane is the modified compression failed theory developed by (Vecchio & Colliins, 1986) and co-workers. All of these master contributions have its advantages in certain application. However, for the sake of computational efficiency it is here foreseen through some preliminary assumption about the mode of failure that can be made within acceptable level of error. In the context of the structural reinforced concrete, reader is encouraged to look at (Hsu & Mo, 2010). Based on this reference, shear flexure interaction can be prepared though either; the rotation angle S&T model, fixed angle S&T model and/or the softened membrane S&T model. For each of

these models, an update of the material law in line with compatibility and stress distribution can be made (Hsu & Mo, 2010). Where the fixed angle S&T is a development of the rotating angle version and the latter is simpler, both are limited by the fixed value of the ultimate strain making the post peak behavior rather brittle when large deformation is considered in match with current need. The softened membrane S&T provide the most rigorous model although sub solution iterations are required solving 21 equations at each step in the section analysis and a few of these equations are nonlinear. Therefore, we need to simplify such procedures in line with beam/column application. For state determination, at least three additional parameters should be solved for; the shear strain at the section, the strain in the transverse reinforcement, and the crack/stress field rotation angle. Then based on the perfect bond between stirrups and concrete assumption, material law of concrete is updated and the final stiffness and forces of the section can be obtained (Mullapudi, Charkhchi, & Ayoub, 2009).

These 2D membrane based models received attention in focus on the shear walls. In contrast, RC columns are special cases, because in addition to the rule of the shear span, the ratio of the transvers reinforcement and the level of the axial load play important roles, not to mention the bi-axial effects and torsion. For more detailed discussion about modes of failure in columns, refer to section 6.4.3.

In beams, with shear span rations less than 4, modes of failure can be similar to those of columns with low axial load level. The shear-flexure interaction occurs at an offset approximately equally to on-half of the effective section depth. But, when the span is doubled because of a column loss, the shear stresses in the critical sections also doubles alongside the quadrat-doubled flexural cracking.

The softened membrane model (SMM) can predict the ultimate shear capacity and the post peak behavior using the calibrated modified Poisons ratio Zhu and Hsu (2002). In beam element, the presence of high shear stresses will cause a reduction in the strength of

concrete (Hsu & Mo, 2010). Within the SMM framework the stress-strain curve of concrete can be updated by introducing a softening factor; ς, which reflects shear softening where;

$$\varsigma = \left[\frac{5.8}{\sqrt{f'c}} \leq 0.9\right]\left[\frac{1}{\sqrt{1+400\bar{\varepsilon_1}}}\right]\left[1-\frac{\alpha_{r1}}{32^0}\right] \ldots\ldots (3.39)$$

Where; $\bar{\varepsilon_1}$ is the principle strain, and the; α_{r1}, is the rotation angle of the principle plane. The softening factors applies to both the ultimate strength and the strain at which the ultimate strength is obtained. In the beam problem, the principle strain ca be calculated from;

$$\bar{\varepsilon_1} = \frac{1}{1-\mu_{12}\mu_{21}}\varepsilon_1 + \frac{\mu_{12}}{1-\mu_{12}\mu_{21}}\varepsilon_2 \ldots\ldots (3.40)$$

Where; $\varepsilon_1$and ε_2 are the smeared strain in the beam element in the main and transverse directions respectively. μ_{12}, and μ_{21} are the modified SMM ratio;

$$\mu_{12} = 0.2 + 850\varepsilon_s, \qquad for\ \varepsilon_s \leq \varepsilon_y \ldots\ldots (3.41)$$

$$\mu_{12} = 1.9 \qquad for\ \varepsilon_s > \varepsilon_y \ldots\ldots (3.42)$$

$$\mu_{21} = 0.2 \ldots\ldots (3.43)$$

Where; ε_s, is the strain in the reinforcement which ever yield first. In the case of the ultimate strength, reinforcement can be assumed in yielding. Therefore, putting static values back, a reduced version of the equation can be reproduced;

$$\bar{\varepsilon_1} = 1.613(\varepsilon_1 + 1.9\varepsilon_2) \ldots\ldots (3.44)$$

And

$$\alpha_{r1} = 0.5tan^{-1}\frac{2\gamma_{12}}{\varepsilon_1 - \varepsilon_2} \ldots\ldots (3.45)$$

At the point of the ultimate strength of concrete, and assuming strain in transverse steel half of the yielding strain of that in concrete, we get an approximation of; $\varsigma = 0.47$. Then up-to 53% of the mechanical strength may be lost as a result of high shear stresses.

Therefore, high shear stresses shall not be excluded in contrast with some suggestions in the literature.

3.4.1.3. The plastic hinges

In this section, we aim at finding the length of the beam proportion over which the softened flexural stiffness will evolve. This length is sometime coinciding with the definition of the plastic hinge common in equivalent static seismic analysis. The outstanding difference from the common plastic hinge is that it cannot be prescribed, because, in progressive collapse mechanism, this length keeps increasing until the localized region unloading. With reference to the response curve, the correct representation of the length evolution of the plastic hinge is the main variable in accurate prediction of the point C. Therefore, an adaptive algorithm of the plastic hinge is needed. Because in the full CM, a few localized regions will develop different loading combination for each level of deflection.

The variable length of the plastic-hinge (PH) in an RC member can be defined by the length of the proportion of the structural member over which any cross section engages yielded reinforcement and therefore sudden decrease in bending stiffness. It is clear that the length of the plastic hinge is a function of; element geometry, detailing, material properties, and the level of damage, in addition to the loading conditions. The concept of the RC element ductility provides a rationale understanding of the effect of details and geometry including some of the mechanical properties of materials, these were addressed in section 3.4.1.1; Axial-flexural interaction. In contrast, the damaged state of the RC element can be related to previous steps of the loading history and the associated state of deformation. While the mechanical strength will not directly affect the length of PH, the descending part of the flexural stiffness can play a role, especially when the ultimate strength is less than the yielding strength. Graphical representation of all factors that can be related to the length of plastic hinge is replicated in Figure 3.4-1. In the figure, the factors affect the PH grouped into two main categories; strength and deterioration related, and the ductility related. The strength related factors are handled in here in this section. The damage related, will be touched on in the next chapter. And, the ductility related factors are listed with some

related key symbols of important parameters. The symbols are explained in the list of symbols and it will be explained whenever reused in the following paragraphs.

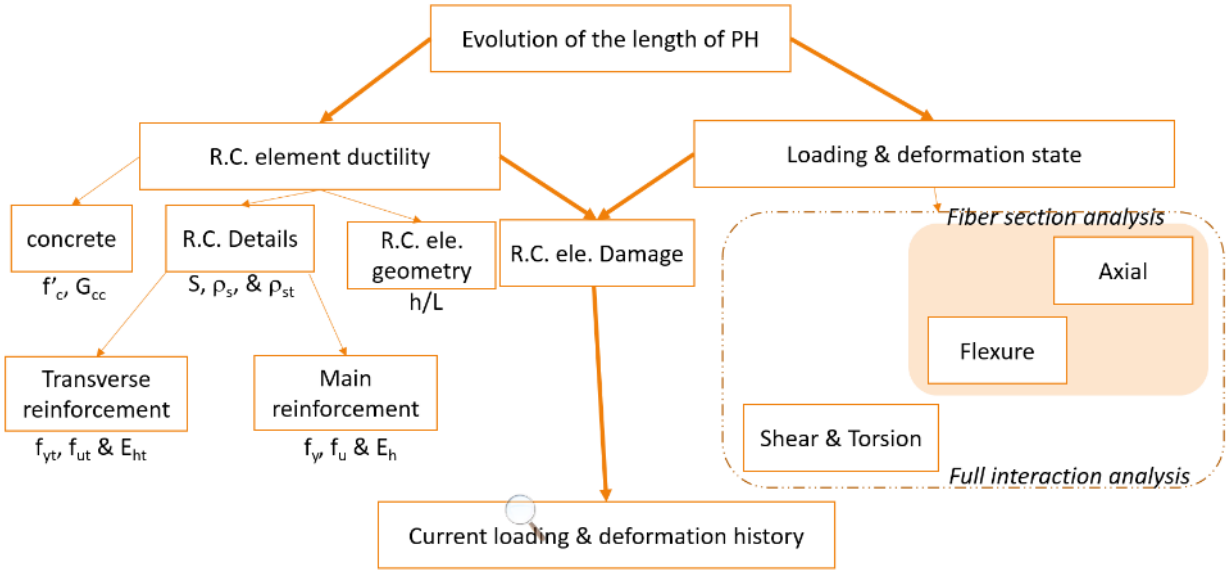

Figure 3.4-1 Different factors affecting the evolution of the length of the plastic hinge in hardening

Trials to identify the plastic length and the plastic rotation capacity in reinforced concrete structures is proved to be an open problem. Because single formula for all cases is not yet available as it not only depends on loading to strength ratios, but also on all the parameters that govern the amount of strain energy dissipated by the virtue of progressive failure, for example; in the compressive arching, crashing energy in concrete G_{cc} is related to yielding strength of stirrups. Another inherited limit to available formulas, according to (Merola, 2009), is that the benchmark tests used in the development of many of them, are bounded by load displacement control which disables the track of softening response due to concrete crash, or spall.

Based on the observed frame/beam elements behavior reported in chapter 2; this is the compressive arching phase of the progressive collapse of the structural assemblage. Surveying these tests lead us to make these preliminary observations; **The Section ductility** is increased with the increased shear reinforcement up to the point at which shear-axial interaction is negligible in the concrete continuum when the stirrups are capable enough to

take all the shear forces. Such effects is seen up to the point of the ultimate strain improvement of the concrete in compression result from section bending.

In the content of the target progressive collapse simulation, no short spans are expected because the assumption of a column loss implied doubling the span to depth ratio (L/h). Therefore, the target of this section is identifying a method of implementing rational values of length of PH to predict the arching strength of a beam mechanism in which the shear interaction can be neglected, Figure 3.4-1.

From the left side of the figure 3, the 'f' is stress value associated to concrete strength, and reinforcement yielding and ultimate strength, E_h is the hardening ratio, these are present for both main and transvers reinforcement spaced at 'S' distance and defined by geometric reinforcement ratios of ρ_s and ρ_{st} respectively.

The analytical plastic hinge length is the value required for drift/deflection prediction at the element tip, this is popular in the seismic analysis of bridge piers. In such pier element, high axial load and lower span-to-depth ratio are present, although this is not the case in double-beam bridging mechanism. For beams, most recent reported empirical formula was made by (Panagiotakos & Fardis, 2001). A summary of these formulas in beams and columns adopted from (Zhao, Wu, Leung, & Lam, 2011) is shown in Figure 3.4-2. The equation of; (Bae & Bayrak, 2008), consider the effect of high axial loading and (Coleman & Spacone, 2001) gave attention to the concrete softening region. Seeing the ductility as one key parameter, the only equation that provide a window for this perception is the (Coleman & Spacone, 2001) equation in which the fracture energy and the strain of the residual stress of concrete are considered. These can be aligned with the increased values of uniaxial confined concrete model (Mander, Priestley, & Park, 1988). In contrast, their equation disregards the loading state of the element.

Beams	Corley (1966)	$0.5d + 0.2\sqrt{d}\,(z/d)$
	Mattock (1967)	$0.5d + 0.05z$ (for RC beams)
	Paulay and Priestley (1992)	$0.08z + 0.022 d_b f_y$
	Panagiotakos and Fardis (2001)	$0.18z + 0.021 d_b f_y$
Columns	Priestlley and Park (1987)	$0.08z + 6d_b$ (for RC columns)
	Coleman and Spacone (2001)	$G_f^c / \lvert 0.6 f_c^{'} (\varepsilon_{20} - \varepsilon_c + 0.8 f_c^{'} / E_c) \rvert$
	Bae and Bayrak (2008)	$l_p/h = [0.3(p/p_o) + 3(A_s/A_g) - 1](z/h) + 0.25 \geq 0.25$
	Sheikh and Khoury (1993)	$1.0h$ (for columns under high axial loads)

Figure 3.4-2 Empirical equations of PH length adopted from (Zhao, Wu, Leung, & Lam, 2011)

Figure 3.4-2 list proposed equation by different researches describing the length of the plastic-hinge. In the figure, d stands for the effective bending depth of the section, z is the lever arm, d_b and the f_y are the depth and the yielding strength of the reinforcement bar. G^c_f, f'_c, ε_{20}, ε, and Ec are the compressive fracture energy, compressive strength, strain at residual strength of 20% and at ultimate strength, and the tangent modulus of elasticity of concrete respectively.

None of these empirical equations in Figure 3.4-2 provide an acceptable representation of the plastic hinge in the content of the progressive development of the failure mechanism because it cannot be built to handle different distributions on internal forces. Therefore, for a single beam element to do the job under prescribed number of integration points, the interpolation must objectively allow for the reasonable representation of the different phases of response. In this case the evolution of plastic hinge must be handled analytical over the axis of the beam.

Among many existing empirical equations (Bae & Bayrak, 2008) and (Zhao, Wu, Leung, & Lam, 2011), none seems to have sound link to be integrated into analytical simulation. In the following, analytical formulation of a simple, but relevant, analytical expression for the plastic hinge length is proposed. It has the following two advantages;

1. Suitable to be linked to the element state determination.

2. Associates the bending length the element b_l, which defines the length of the proportion of the element under homogenous bending by the point of contra-flexure.

Assume the plastic hinge region as shown in the Figure 3.4-3, the element AB is a single element representing the plastic hinge at the ultimate limit state. V_u and V_y are the shear forces associated to the limit states of; ultimate strength and yielding respectively. The shear forces are the results of the element balanced forces associated to the bending ultimate strength M_u, and the bending section resistance at yielding M_y respectively.

Assuming a linear distribution of the shear forces, Figure 3.4-3 (a), the shear force value anywhere over the element AB, V(x) can be written;

$$V(x) = V_u - ((V_u - V_y)/L_p)x \quad \ldots\ldots (3.46)$$

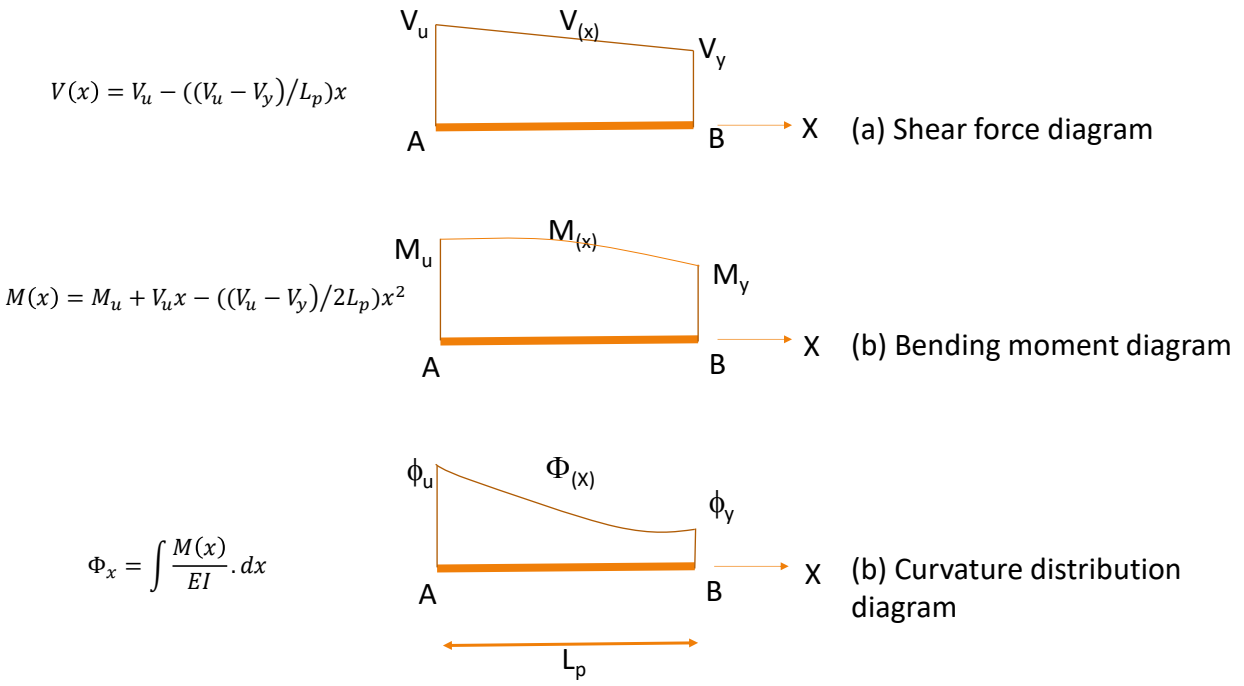

Figure 3.4-3 shear, bending and flexure diagrams of the PH zone at the ultimate limit state

Based on the classical Euler-Bernoulli beam theory, bending moment can be derived integrating the shear forces over the domain, with attention to the boundary conditions at A;

$$M(x) = M_u + V_u x - ((V_u - V_y)/2L_p)x^2 \quad \ldots\ldots.(3.47)$$

This equation shall satisfy the conditions at B as well, therefore;

$$M_y - M_u = ((V_u + V_y)/2)L_p \quad \ldots\ldots.(3.48)$$

The last expression makes some sense defining the plastic hinge length by the double the ratio of the subtraction of the ultimate and yielding bending strength to the sum of shear forces at the two situations. Although it reports a negative value of the length which can be understood relative to the point B at which the conditions are utilized. The above expression can be naturally related to element state determination although some approximation yet exists because of the assumption of the linear distribution of the shear forces

It is beyond this text to do a thorough validation; however, the expression can be evaluated follows. Consider the bridging beam in Figure 3.4-4 (a). At the ultimate bending state, bending diagram is shown in (b). Let the length AO by the length of the beam proportion under single-bending direction b_l. Then, if study the free body-diagram of the elements AO and BO, without external loading, taking the sum of moments around the point O, the following expressions can be made;

$$M_u = V_u b_l - N\Delta_O \quad \ldots\ldots.(3.49)$$

$$\mathrm{M_y} = \mathrm{V_y}(\mathrm{b_l} - \mathrm{L_p}) - \mathrm{N}(\Delta_\mathrm{O} - \Delta_\mathrm{B}) \quad \ldots\ldots.(3.50)$$

Where Δ_O and Δ_B are the displacements at points O and B respectively and N is the value of the normal force. For simplicity in evaluating the expression, let us assume that displacements, or normal force, are small enough to neglect. If hardening ration of the section bending strength M_u/M_y can be approximated at 1.15, for example, combining the three last expressions will lead to the following result;

$$L_p = 0.122 b_l \quad \ldots\ldots.(3.51)$$

Where, b_l, of the order of the half of the element length in the case of double curvature element, the plastic hinge is of the order 0.06 of element length, see (Bae & Bayrak, 2008) and (Zhao, Wu, Leung, & Lam, 2011) for examples. The derived expression seems to be appropriate for both beams and columns governed by bending failure where L_p is related to external element forces satisfying balance with the internal forces in presence of relatively low axial force.

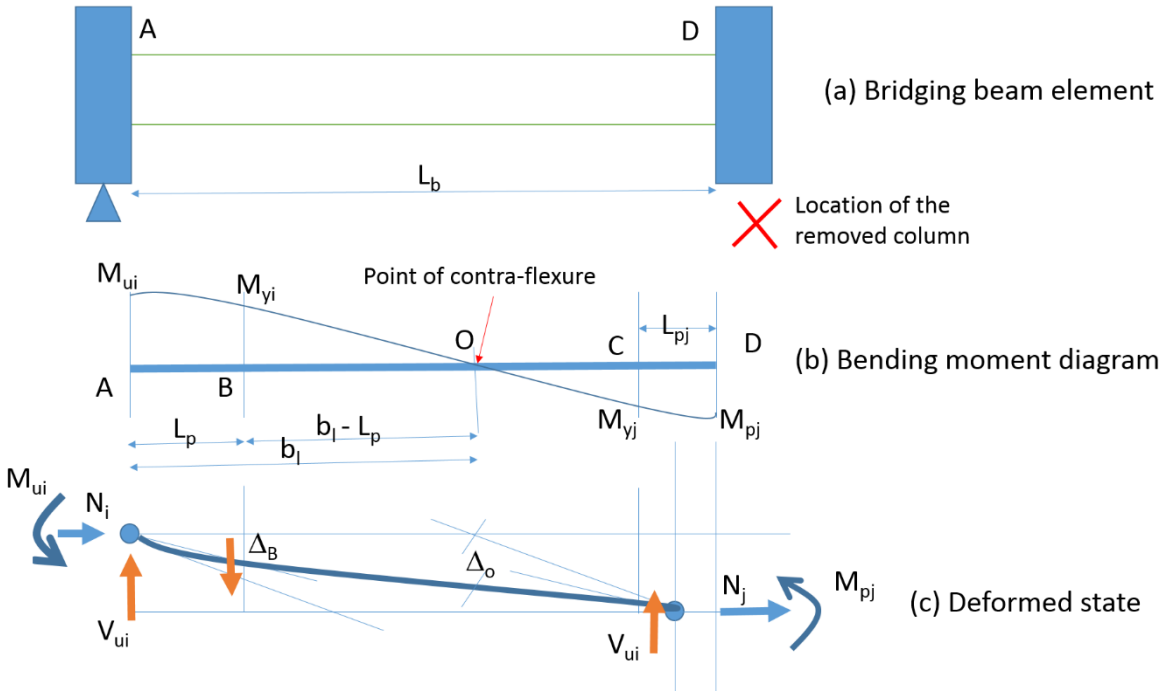

Figure 3.4-4 Analytical verification of the derived expression of the length of the plastic hinge in beams

In direct association to the tensile yielding strain and ultimate strain in concrete under bending, the two critical values of curvatures may be derived linking bending and axial forces using the procedures in section 3.4.1.1.

In order to quantify the total amount of plastic element rotation, one option is to use the direct integration of curvature over the hinge region. This can be done through direct integration of the bending distribution, when fully defined, provided that the ultimate and yielding rotations are evaluated in section 3.4.1.1;

$$(EI\Phi)_x = \int M(x).dx \quad \ldots\ldots (3.52)$$

Compared to the criteria defined above for the factors affecting the length of the plastic hinge, Figure 3.4-1, the derived expression naturally considers many of the named factors, but the shear interaction and the effect of shear confinement are decoupled. Therefore, pre-processing of these two effects must be pre-analyzed and can be included in the material model of concrete;

- Higher confinement can be reflected by an increased value of the cut-off strain of uniaxial model of concrete. There are a few existing methods, see for example the (FIP-MC, 2010).
- High shear stress, when coupled at the fiber level, will reduce the ultimate stress capacity of concrete and the thereafter the softening branch. This was introduced in section 3.4.1.2.

3.4.1.4. Handling softening in the flexural stiffness

Beyond the point C, in the response curve Figure 2.5-1, rapid failure of the flexural stiffness can be associated to many inter-related phenomena e.g. bucking of compressive reinforcements, sliding, and friction of the remaining concrete and the dowel-action of the aggregates as well as the transverse reinforcements. Full model of all of these factors is an interesting challenge although it does not thoroughly affect the important following points of rupture of reinforcement, catenary balance station and the dynamic implication of the body motion and the transit repose. However, it is worthwhile to trace the developments of forces in both tensile and compressive reinforcing bars. The remaining toughness in the catenary reinforcement is important, because it is required to identify the point at which the tensile reinforcement will rupture, and the state of the compressive reinforcement by this point to evaluate how this will affect the following path of the progressive failure in particular.

With regard to the state of the tensile reinforcements, let us name the strain in this outermost steel layer at the point of concrete ultimate strain, flexural failure, by $\varepsilon_{y,f}$ referring to appoint in between the yield and fracture strain of steel; ε_y and ε_f respectively. Then;

$$\varepsilon_{y,f} = \varphi_u(d_u - y_u) \ \ldots\ldots (3.53)$$

The ultimate rotation of the section; φ_u, is defined by the equation (3.30) in section 4.1.1.

If we assume a static value of; $y_u = 0.6d_u$, simple benchmark can be made at

$$\varepsilon_{y,f} = 0.6.\, d_u.\, \varphi_u = 0.6.\, d_u.\, \varphi_y.\, \mathbb{R}_{s,ult} \ \ldots\ldots (3.54)$$

The $\mathbb{R}_{s,ult}$ is the rotational ductility of the given section. Now if; $\varepsilon_{y,f} > \varepsilon_f$, the reinforcement layer is expected to fail before this point, this is a brittle design which uncommon in RC design. Otherwise, the additional axial elongation due to the plastic deformation can be evaluated based on the length of the plastic hinge L_p;

$$\Delta_{s,y,f} = L_p\left(\varepsilon_f - \varepsilon_{y,f}\right) \ \ldots\ldots (3.55)$$

This is can be controlled against the value of axial elongation at the theoretical point of unloading to decide whether rupture will occur before or after the point of full axial unloading D.

In case of the compressive reinforcements, due to arching action, high compressive force may still exist just after the crash of concrete causing kind of dynamic compressive impulse load on the compressive reinforcement. The static resistance of these bars in compressive may be evaluated using an explicit integration procedure such as those suggested by (Potger, Kawano, Griffith, & Warner, 2001).

Let us consider the buckling load of the compression bars, (Potger, Kawano, Griffith, & Warner, 2001) developed model which has further been implemented in combined model to capture shear-flexure interaction by (Lodhi & Sezen, 2012). The model is based on

simplified up-date of the stress-strain design curve of the compressive steel bars as shown in Figure 3.4-5.

At the point A in figure 4-5, buckling of bar under compression force begin, the point A is defined by the buckling strain ε_{sb} and from the ideal non-buckling stress strain curve the associated stress is defined at f_{sb}. The point A can be before or after the idealized yielding point depending on the quality of concrete cover. The buckling strain can be evaluated by (Potger, Kawano, Griffith, & Warner, 2001):

$$\varepsilon_{sb} = \varepsilon_{cu} + f_1 f_2 f_3 f_4 f_5 \ \ldots\ldots (3.56)$$

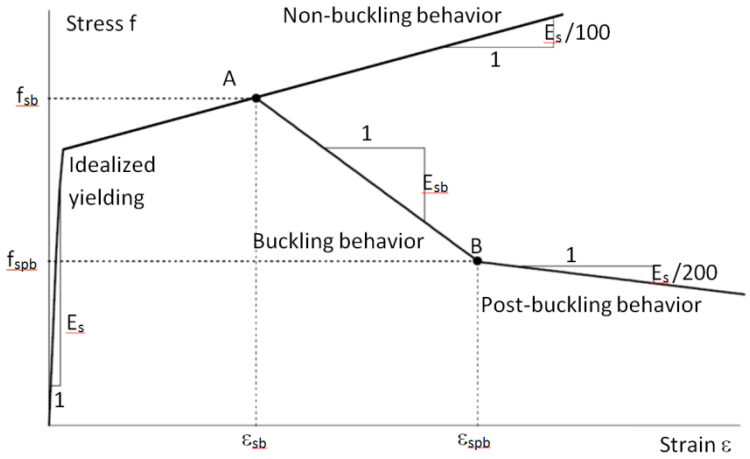

Figure 3.4-5**:** Buckling stress-strain curve of reinforcement bars adapted from (Potger, Kawano, Griffith, & Warner, 2001)

Where; ε_{cu} is the ultimate strain of concrete cover, and f_i are factors proposed in the source to account for stirrups support, shear reinforcement ration, position of the bar, type and strength of concrete and finally the strength and type of reinforcing steel bar.

At the point B, the post buckling idealized curve begin assuming tangent as a ratio from the E_s, which is the steel modulus od elasticity. At the buckling curve, which divert from point A to B, negative modulus of elasticity is defined E_{sb}. The value of the E_{sb} can be evaluated from the equation (Potger, Kawano, Griffith, & Warner, 2001);

$$E_{sb} = -100\varepsilon_{sy}\left[\frac{1}{\sqrt{1+{lamda}/{200}}}-1\right]E_s \quad \ldots\ldots(3.57)$$

Where: $lambda = \frac{\propto s}{i_b}$ as α=1 for corner bar, and α=0.5 for internal bars. S is the spacing distance of stirrups and the i_b is the radius of gyration of the steel bar.

3.4.2. Deformations at the boundary of the beam

The purpose of this section is to provide rational analytical procedures for the additional flexibility/stiffness results from the certain mechanisms of the sub-frames. In sections; 2.2.1 and 2.2.2 respectively, the contributions of the sub-frames translational and flexural stiffness are linked to the arching and flexural stiffness and rotations. Also, in the tensile catenary phase, the ultimate tensile force develops in steel reinforcement depends on the bonding strength, on addition, the overall catenary displacements relay on the bar-slip evolution along the process. In the following paragraphs, a method for the bar-slip and the shear strength check at the joints will be provided. The 3D analysis of the contribution of the sub frames will be left to chapter 4.

3.4.2.1. Bar-slip and de-bonding at joint

In the following, evaluation of slip is presented in flexure and axial catenary. In both cases, it reduces to analyzing the slip at different level of the active tensile force. Therefore, the presented procedures are related to the key changes of material states at the yielding and the ultimate strengths.

3.4.2.1.1. By the point of the flexural yielding strength

For the yielding displacement ${w^{Kai}}_y$, (Qian & Li, 2013) proposed the following equation for the restrained cantilever beams which is adapted from (Paulay & Priestley, 1992), as part of the total displacement:

$${w^{Kai}}_y = \frac{L^2}{6}(2-\aleph)\varphi_y + \frac{3}{5}Ll_{py}\varphi_y \quad \ldots\ldots(3.58)$$

Where the yielding rotation φ_y is the rotation of the main section at which it reaches yielding, and the; l_{py} is the length of the plastic hinge (Paulay & Priestley, 1992). The, $א < 1.0$, is used referring to the flexural stiffness ratio of the secondary section to the main section which enters the yielding phase first in the two sections mechanism. However, in the equation used by (Qian & Li, 2013), it is not clear how the plastic hinge will develop while the definition of the yielding rotation implies that; $l_{py} = 0$. To rationalize this, the slip of reinforcement bars which occur by this reference level, rather than the formation of the plastic hinge over a certain length of the beam, is the key responsible behavior (Sezen & Moehile, 2004). In their work, they showed that more than 30% of displacement would result from slip of the bars. It has been assumed linear bonding stress distribution with two distinct phases; when the rotation of the section is less than the φ_y and when it is more. In this model, the strain is assumed linearly distributed over the length of the beam as the bending moment will linearly vary over the length of the beam as a result of end concentrated load. In (Sezen & Moehile, 2004), it was concluded the following equation:

$$w_{slip} = \left(\theta^{E}_{slip} + \theta^{M}_{slip}\right)L \quad \ldots\ldots (3.59)$$

$$\theta_{slip} = \frac{\varepsilon_s f_s d_b}{8(d - h_{ec})\sqrt{f'_{ck}}} \quad \ldots\ldots (3.60)$$

Where

- w_{slip} is the displacement results from slip of reinforcement bars
- θ_{slip} is the section rotation as a result of slip of reinforcement bars, M for main section and E for the end section,
- ε_s is the strain in steel reinforcement bars,
- f_s is the stress in steel reinforcement bars.
- d_b is the diameter of the steel reinforcement bars.
- f'_{ck} is the characteristic compressive strength of concrete,
- d is the effective flexure depth of in cross-section,
- h_{ec} is the height of compression zone in cross-section,

Then final, instead of the second term in equation (3.2), equations (3.3) and (3.4) are proposed replace and to contribute to the total at-yield displacement; w_y;

$$w_y = \frac{L^2}{6}(2 - \aleph)\varphi_y + \left(\theta_{slip}^{E} + \theta_{slip}^{M}\right)L \ \ldots\ldots.(3.61)$$

The shear displacement will be assumed negligible at this state as can be also observed in (Sezen & Moehile, 2004).

3.4.2.1.2. By the point of the flexural ultimate strength

Following the point at which yielding of the main section begins, the yielded proportion of the beam mechanism evolves in the L_{PH}. Also, the softened flexural stiffness localizes at the contributing plastic hinge.

The approximation value of the ultimate displacement w_u can be obtained from adding the relaxation of the slip of reinforcement bars to the area of the plastic hinge and the flexibility of the plastic hinge as follows:

$$w_u = \frac{l_n^2}{6}(2 - \aleph)\varphi_y + \left(\theta_{slip}^{E} + \theta_{slip}^{M}\right)l_n + \frac{3}{5}Ll_{PH}\varphi_y \ \ldots\ldots.(3.62)$$

Both θ_{slip}^{E}& θ_{slip}^{M} must include the 'plastic' slip as explained in (Sezen & Moehile, 2004):

$$\theta_{slip} = \frac{d_b}{8(d - h_{ec})\sqrt{f'_{ck}}}\left[\varepsilon_y f_y + 2(\varepsilon_s + \varepsilon_y)(f_s - f_y)\right] \ \ldots\ldots.(3.63)$$

Where f_y and ε_y are the yielding stress and strain of steel reinforcing bars respectively.

The ultimate load of the assembly may be predicted by the equilibrium equation as follow;

$$P_u = -N_x w_u + \frac{M_x + M'_u}{L_n} \ \ldots\ldots.(3.64)$$

Where;

- P_u is the ultimate applied load associated to RL2.
- w_u is the ultimate displacement.

- M'_u is the ultimate bending strength of the main section where the plastic hinge was formed.
- M_x is the bending moment developed in the beam section near the lost column.
- N_x is the arching force developed at the ultimate point before strength degradation.
- L is the clear span of the beam.

If we accept the ω_u remains with two variables M'_u and M_x depends on the value of the arching compressive force N_x. If the last is known, the two bending moments can be found from the direct section analysis at both ends in presence of the axial compressive force. In fact, if the Vierendeel action is considered, axial force can not only result from the arching action, but it will also result from the balancing bending moment of the Vierendeel, for example, if 2-story building is discussed, horizontal balancing reaction force of H_b will be required at the end of the beam in each level: $H_b = \frac{2pL}{h}$ Where h is the story height of the second floor, this force is favorable in compression at the lower level, but it is not at favorable in tension at the higher levels (above levels).

Nevertheless, if a single story is assessed, or the last level only, only the arching will remain in interest as a result of the residual rotational stiffness at the end of the beam to which the cast in situ-slab will have a contribution.

Concentrated load is used in the test instead of uniformly distributed load the case of load transferred from floor panel. It is also worth noting that shear strain can cause concrete to crush before the design ultimate strain in concrete is developed, especially when the behavior of confined-concrete is considered known as shear-flexure interaction effects see section 4.1.2.

3.4.2.1.3. By the point of the tensile catenary strength

On sections 3.4.2.1.1 and 3.4.2.1.2, the bar slip is analyzed under the scope of the localized flexural rotations by the joint. Here, the same principles, equations, can be used but with

focus on the resulted overall axial stiffness of the reinforcement bar under high tensile forces. Explicit expressions can be based on any standard analysis procedures.

3.4.2.2. Shear strength of the joint

Although, (Qian & Li, 2013) provided a method to take such factor into account, it is beyond the current text to discuss it in detail. Because, in shear deformation at joint can be considered small in comparison with bar slip, and the ultimate strength can be checked to identifying the maxim force developed in reinforcement using an approximate expression or even by using high-definition simulation. Therefore, it can be isolated out of the flow of the progressive collapse analysis.

3.5. Evaluation of the bridging beam and catenary mechanisms

The motivation of this section is the fulfillment of the target 3, of the modeling targets in Chapter 2. It was shown by (Orton & Kirby, 2013) that high dynamic amplification factors are recoded after the arching failure. Such high values, reached 4 in test, is alerting, because the (CEN, EN 1990 - Basis of structural design, 2002) regarded the tensile catenary as a line of defense in building category A and B2. Here an explanation is provided.

3.5.1. Static transition from arching to catenary

This phase is marked by the lowermost point of the response curve D. This point is perceived to be the transition point at which the axial compression force will transfer to axial tension, and therefore it defines the start of the tensile catenary phase.

The approximation of the cosine function, Figure 3.2-3, defines a loading and unloading phase of the compressive arching in beams. From the theory of equation (3.4), full unloading of the arching compressive force occurs when displacement w gets into the $2h_s$. Therefore, after this point all sections of the beam will switch to tension assuming zero average axial force at the named point. Because, the tensile bending reinforcement was in tensile yielding at $w=h_s$, the plastic deflection will localize in this reinforcement layer first, meanwhile the tensile force switches to tension in the other layer of reinforcement in the

section and the hardening/softening state. Therefore, the difference of rupture strain, and the current strain here is important, or in more precise term, the remaining energy before the full rupture of the *secondary* reinforcement is required the right prediction, see the following section.

$$\Delta\varepsilon_{c,f} = \varepsilon_f - \varepsilon_{c,2hs} \quad \ldots\ldots (3.65)$$

Where;

- $\Delta\varepsilon_{c,f}$ is the remaining strain to the point at which secondary bar fracture (rupture) is expected,
- ε_f is the strain at bar fracture (rapture of reinforcement in tension, and
- $\varepsilon_{c,2hs}$ is the strain on the tensile reinforcement at the point where the vertical deflection w=2h$_s$.

Similarly, the remaining energy before the full rupture of the main reinforcement can be evaluated with reference to the pit of the ultimate strength having pronounced effects on the tensile stiffness in the catenary phase.

$$\Delta\varepsilon_{t,f} = \varepsilon_f - \varepsilon_{t,ult} \quad \ldots\ldots (3.66)$$

Where;

- $\Delta\varepsilon_{t,f}$ is the remaining strain to the point at which main bar fracture (rupture) is expected,
- ε_f is the strain at main bar fracture (rapture of reinforcement in tension), and
- $\varepsilon_{t,ult}$ is the strain on the tensile reinforcement at the point where the ultimate arching is recorded.

The arching fore is then zero, which can be evaluated by the approximate equation (3.9), figure (3.2-3), by replacing w wth 2hs. And the reaction/strength force can be evaluated by the catenary equation (3.25) and figure (3.2-4);

$$q_{t,cat,hs} = K_{\text{eq,t,cat,hs}}.\left(\frac{2h_s}{L}\right)^3 \quad \ldots\ldots.(3.67)$$

The correct use of the above equation is down to the right evaluation of the term $K_{\text{eq,t,cat.hs}}$ at this point bearing in mind that the value depends on the average state of the contributing components; yielding/hardening/softening, in addition to the slip and buckling of reinforcement.

In the above equation the displacement is assumed, but with the appropriate evaluation of the; $K_{\text{eq,t,cat.hs}}$, it may be concluded that the zero-axial force is associated rather deferent level of deflection.

3.5.2. The body motion in transition from arching to catenary

Discussing the case of catenary is considered a general form of the dynamic response if the mechanism stabilizes in flexural/arching phase. The valley CDE presents the loss of the strain energy which will be replaced by pure kinetic energy.

The loss in strain energy can be evaluated by the area under the line DE. This can be graphically obtained by the algebraic aggregation around the point C;

$$E_{lost} = \left(q_{p(N)}+q_{arch} - q_{t,cat,hs}\right)(h_s) + \left(q_{t,cat} - q_{t,cat,hs}\right)(w_{cat} - h_s) \quad \ldots\ldots.(3.68)$$

However, it does not consider the dynamic parameters. The kinetic energy, linearly dependent on the moving mass, M_{cm}, of the collapse mechanism (cm), is a second order function of the of the movement velocity v_{cm};

$$E_{k,cm} = \frac{1}{2} M_{cm}.{v_{cm}}^2 \quad \ldots\ldots.(3.69)$$

Where;

- E_{lost} is The loss in strain energy result from the response valley CDE.
- $E_{k,cm}$ is the kinetic energy of the collapse mechanism [Joule].
- M_{cm} is the equivalent mass of the collapse mechanism in motion, and
- v_{cm} is the velocity of the moving collapse mechanism.

The above equation is the correct choice if the motion is well defined by the vertical translation. However, in case of corner type of mechanism, the kinetic energy may be better described by the rotational mass and the circular velocity.

If we apply an energy conservation law; the deflection at the point of catenary, w_{cat}, can be evaluated of the velocity of the collapse mechanism is known. When the traveled distance is defined by $(w_{cat} - h_s)$, the elapsing time is needed to find the unknown velocities. If the cm will pass to the tensile catenary, or to the point E, the motion that the M_{cm} transfer will pass through 4 subsequent phases, not including the dynamic transit phase. These phases are summarized in the Table 3.5-1 below;

Table 3.5-1 key points of the response curve

Phase	Location	Distance	Time	Velocity	Acceleration
	A	0	0	0	0
1	AB	w_{AB}	t_1	v_1	a_1
yielding	B	$w_A=w_y$	t_B	v_B	a_B
2	BC	w_{BC}	t_2	v_2	a_2
Static-strength	C	$w_C=w_{ult}$	t_C	v_C	a_C
3	CD	w_{CD}	t_3	v_3	a_3
Unloading	D	$w_D=w_{hs}=2h_s$	t_D	v_D	a_D
4	DE	w_{CD}	t_4	v_4	a_4
Static-catenary	E	$w_E=w_{cat}$	t_E	v_E	a_E

If the duration of each phase is known, velocity can be integrated from the traveled deflection, the distances in the table, but we have no information about the durations making the problem unbounded. To improve the situation, the pseudo-accelerations at the points B, C, and D, can be evaluated from the balanced energy principle based on the difference between the work of external energy and the strain energy, which balances the kinetic energy. Then, if velocities at points B, C, D, and E, are defined, durations can be found using the average value in each phase, and then the pseudo-accelerations can be integrated.

Generalized formulation can be based on the concepts of the total potential energy must balance with the strain and kinetic energies; the 'tot' refers here to the total value aggregated over all phases outlined in the Table 3.5-1;

$$E_{ptn} = E_{tot,k,cm} + E_{tot,st,strain} \ \ldots\ldots (3.70)$$

Where;

- $E_{ptn} = M_{cm}.g.w_{bal}$ is the potential energy of the mechanism balances at w_{bal}.
- $E_{tot,k,cm}$ is the aggregated total of kinetic energies over passed phases of response.
- $E_{tot,st,strain}$ is total strain energy absorbed by the static response of the system. This is the full area under the response curve of the quasi-static simulation or test.

It is worth to point out here that the M_{cm}, like the applied load, is uncertain value. And, it varies, similar to the strength, over the response curve between the points B and C. Nevertheless, by the point C, where all the plastic components of the cm is defied, fixed value of M_{cm} is found.

We can also distinguish two cases; the cm entails large plastic deformations, or the cm is irredundant. In the first case, the deflection at the local ultimate strength can be deduced from the w_{bal} with limited error, whereas it is not for the second one, the last is represented in the equation of the E_{loss}, and then the $w_{bal}= w_{catl}-h_s$.

Refereeing back to the energy balance equation, the loading velocity by point E; v_E can be obtained based on the M_{cm} and the equivalent static loading demand. Let us assume that the average reaction force over the full reaction response curve can be defined by; α, then the equation above can be rewritten;

$$M_{cm}.g.w_{bal} = \frac{1}{2}M_{cm}.{v_{cm}}^2 + \alpha.M_{cm}.g.w_{bal} \ \ldots\ldots (3.71)$$

Rearrange the equation results in;

$$v_{cm} = \sqrt{2(1-\alpha)g.w_{bal}} \ \ldots\ldots (3.72)$$

And; α can be defined by;

$$\alpha = \frac{\int P.dw}{M_{cm}.g.w_{bal}} \ \ldots\ldots (3.73)$$

Where; $\int P.dw$, is the integration of the strain energy under the response cuve of the quasi-static response.

An approximation of the problem can be made, dropping out the time (durations), by the Galileo's Kinematic equations, if an average acceleration can be assumed for each phase of the motion, an upper-bound limit for the loading velocity v_{ub} can be then wirten;

$$v_{ub} = \sqrt{2ax} \quad \ldots\ldots (3.74)$$

Where x refers to the travelled distance and can be replaced by an appropriate choice of w. The above equation assumes zero initial velocity. For non-zero initial velocities; standard laws of motion can be used. An upper-bound, conservatism, evaluation of the additional loading speed at the balanced point can be made assuming a=g and x= w_{bal} =w_{cat}-h_s.

Comparing equations; (3.72) & (3.74);

$$a = \left(1 - \frac{\int P.dw}{M_{cm}.g}\right) g \quad \ldots\ldots (3.75)$$

Therefore, approached for analyzing the motion state of the cm was introduced aiming at the concluding the loading velocity by the point E. The two approaches can be used in parallel for the evaluations of the level of the system dynamic redundancy which will be introduced in chapter 5.

3.5.3. Transit analysis

This phase supersedes the balanced state whether in flexural/arching or catenary phase of response. The analysis starts with the value of the initial velocity found in the previous section, and the generalized solution of the transit equation can be described by sine function in order to obtain the maximum dynamic increase factor of the force and the displacement as a final control making sure that the static balance point can be attained.

Similar procedures were used by (Li, Lu, Guan, & Ye, 2014). Although they did not refer to intermediate body motion phase proposed in the earlier section, they have proved their analytical steps by simple SFE fiber beam element model in which time dependent material

properties was implemented. However, there is no physical evidence of the loading speed, and there is also no information about the modeling parameters of the dynamic incremental analysis, e.g. what value of the damping is used. The Figure 3.5-1, show the simplified SDOF model adapted from (Li, Lu, Guan, & Ye, 2014). The main difference here is that the transit analysis will start with the initial velocity which need to be identified analytically or experimentally. Analytical method was presented in the former section to evaluate this velocity.

The static reaction force and displacement of the response curve are yet defined, the target is to identify the dynamic amplification factors (DAF) increasing the reaction force (DIF^F) and displacement (DAF^D). Assuming the damped single degree of freedom in the Figure 3.5-1, the magnitude of the additional displacement result from the transit analysis can be evaluated by (Li, Lu, Guan, & Ye, 2014);

$$\rho = \sqrt{{w_0}^2 + \left(\frac{\dot{w}_0 + w_0 \xi \omega}{\omega_D}\right)^2} \quad \ldots\ldots (3.76)$$

Then,

$$DAF^D = \frac{w_{bal} + \rho}{w_{bal}} \quad \ldots\ldots (3.77)$$

Where; $\dot{w}_0$ is the initial velocity evaluated in section 5.2, w_0 is initial displacement which can be assumed zero, w_{bal} is displacement at balance, ξ is the ratio of structural damping, ω and ω_D are the rotational velocities of the undamped and damped system respectively, which can be evaluated by.

$$\omega = \sqrt{K_{eq}/M_{cm}} \quad \ldots\ldots (3.78)$$

$$\omega_D = \omega\sqrt{1 - \xi^2} \quad \ldots\ldots (3.79)$$

The DIF^F can be evaluated using the concept of pseudo action. Alternatively, the increased demand in displacement can be compared to the remaining strain capacity of reinforcement to judge if the catenary will cut-off.

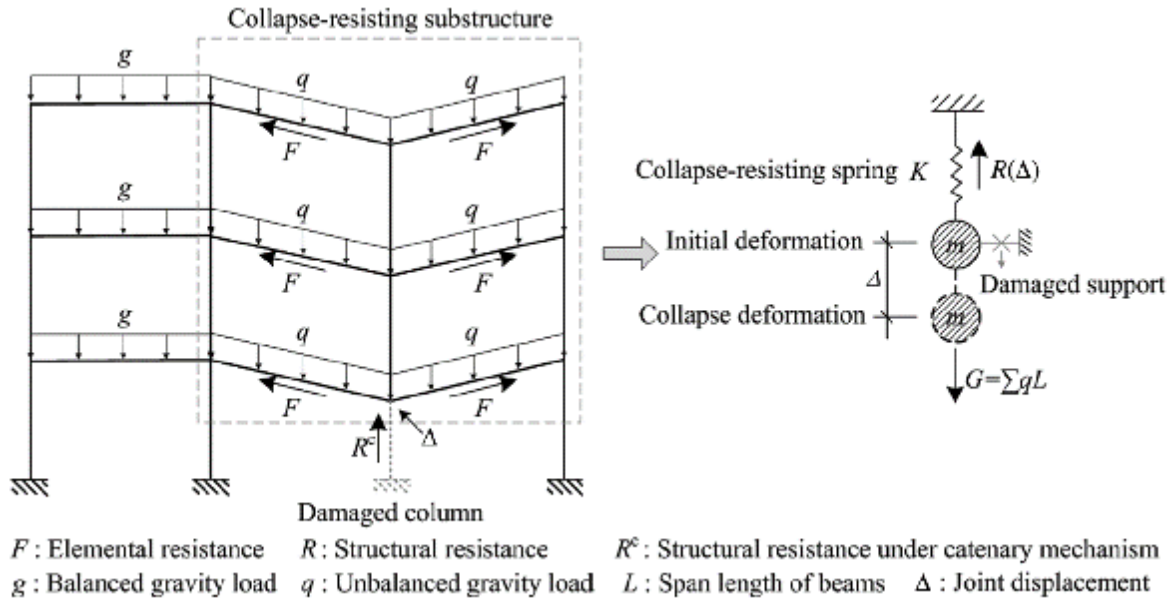

Figure 3.5-1 Equivalent SDOF of a sub-frame RC structure under tensile catenary (Li, Lu, Guan, & Ye, 2014)

The increase factor of the reaction force can be considered based on the strain rate rules of the material law,

3.5.4. Stable equilibrium

This point, if it exists according to section 3.5.3, can be defined by the end analysis of sections 3.5.4, in which the final deflection w and velocity are the key parameters. Again they are a critical function of the appropriate assumption of the mass M_{cm}. The static equilibrium is satisfied only when the dynamic increased action does not supersede the dynamic strength of the material.

3.6. Summary of procedures

In the earlier section, the upper-bound equations were derived defining the interrelation s of key response factors. In this section, explicit procedures are presented in summary of

the developed analytical evaluation algorithm. The proposed procedures are implemented in Matlab. The steps, starting with values control displacements at w^i;

1. Find the appropriate value of arching force,
2. Then, the axial flexural interaction procedures can be processed,
3. The main reinforcement rupture point is analyzed, and
4. The development of the tensile catenary forces can be evaluated.

3.6.1. Model calibration steps

Although there were many tests reported in the literature, not all of the reports stated all of the key modeling parameters, presumable, these were unknown being the outputs of this chapter.

The model is very sensitive to the boundary conditions, the active strength of concrete, and the size of the localization zone. Therefore, the model is recommended to be calibrated in the following order when some of these factors are missing;

1. the equivalent arching stiffness,
2. the arching depth h_s,
3. the softened concrete strength due to shear, a couple of iteration loops will be required,
4. the flexural or the rotational stiffness of the sub structure,
5. the plastic hinge length,
6. bonding/deboning axial stiffness of reinforcement under the tensile catenary, and finally;
7. the localization length of the reinforcement must be identified.

It worth to point out here that the steps from 1 – 4 are naturally handled by the proposed structural FEM model developed in chapter 5. However, the equivalent arching and rotation stiffness are in the following example approximated based on the known test results. The arching depth is defined from the test boundaries; a linear softening of concrete strength is

assumed. Steps 5, 6, and 7 will required additional attention and shall be discussed later in the same chapter.

3.6.2. Deriving the response curve for a given beam mechanism

As mentioned earlier, while the displacement w^i are the input of the procedures, the total reaction force can be aggregated as a natural contribution of three elements; the arching strength, the flexural strength and the tensile catenary strength. Although, the tensile catenary can be neglected while ($w^i < h_s$), the arching can be considered fully unloaded, and therefore can be neglected while ($w^i > h_s$). Having used the simplified steps of Monti, linear interpolation is used to obtain values of the bending strength and rotations between the point of zero bending and yielding strength, as well as, between the yielding and the ultimate strength (step 5 in the Table 3.6-1 the list of the required steps to obtain the quasi-static response curve), the evaluated rotation at each point is used as a basis for this interpolation. Table 6-1 lists of the required steps to obtain the quasi-static response curve.

Table 3.6-1 the list of the required steps to obtain the quasi-static response curve

Step	Formula	Equation ()
1	Assume values for w^i [mm]	
2	Equivalent stiffness; $K_{eq} = \left(\frac{1}{K_{JA}} + \frac{1}{K_{axial,arch}}\right)^{-1}$	3.18
3	Arching force $N^i = K_{eq} w^i \frac{2h_s - w^i}{2l_{arch}}$: $w^i < h_s$	3.20
4	Bending resistance at N^i; M_y , M_u	3.32, 3.33, and 3.38 (section 6.2)
5	Linear interpolation of the M^i between 0, M_y and M_u	
6	$K_{eq,flx} = K_y = \frac{My}{\varphi_y}$: $M^i < M_y$ and $K_{eq,flx} = K_u = \frac{Mu}{\varphi_u}$: $M_y < M^i < M_u$	Equivalent bending stiffness
7	$\varphi^i = \frac{2w^i}{L} - \theta_{slip} = \frac{M^i}{K_{eq,flx}}$	Repeat 5, 6, and 7 until single value of M^i obtained
8	$q_{p(N)} = 2\,\frac{m^i{}_{A(N)} + m^i{}_{B(N)} - N.w}{L^2}$	
9	$K_{\mathrm{eq,t,cat}} : \varepsilon_{yf}$	Depends on steel material law (section 6.2)
10	$q_{t,cat} = K_{\mathrm{eq,t,cat}}.\left(\frac{w}{L}\right)^3$: $w^i > h_s$	3.28
11	$q_{tot} = q_{p(N)} + q_{t,cat}$	

3.6.3. The points of ultimate strength of the quasi-static response

These are the points C and E of the response curve, representing the arching/flexure strength and the tensile catenary strength respectively.

For the point C, it is the ultimate strength result from the combined bending mechanism and the compressive arching. Therefore, the highest value recorded over the steps 8 and 9 of Table 3.6-1 is the repetition of the ultimate strength when small displacement steps are used. If the bending stiffness of the sub-frame is small, the ultimate strength point will coincide the arching strength point provided that lateral translation is sufficiently restrained. And vice versa, if no lateral stiffness is there the ultimate strength is then associated to the point recognized by the bending mechanism at the ultimate rotation of section added to the slip rotation.

With regard to the point E, full loading history of the secondary reinforcement is needed, which is marked by the following points;

1. Stress/strain state at the point of concrete failure
2. Buckling in presence of high arching, or compressive force, with spaced stirrups,
3. Stress/strain state at the point of rupture of the main reinforcements,
4. Yielding in tension
5. Hardening in tension
6. Softening, and
7. Rupture strain/strength

Each point is related to the one before, and they can all be handled by conditional analysis of the axial tensile force in relation to the right phase of the 1D material law, until the full path is defined. It is important here to point out that conditional analysis may be also applied to equivalent stiffness of the sub-frame in the section 6.1, because failure of the joint in shear, and/or bar de-bonding will not only alter the deflection, it may also prevent the development of the full strength. In the conditional control procedures, the active stiffness of the catenary is updated whenever; the average elastic strain passes the cracking

point of concrete then whenever the tensile force develops higher the yielding and the strength limits of reinforcement.

3.6.4. The body motion phase and the loading velocity

The aim of this analysis is to conclude the loading velocity just before the dynamic transit phase around the final balanced state. This velocity forms, therefore, the initial condition of the transit analysis. The velocity, discussed in section 3.5.2, can be found by;

$$v_{cm} = \sqrt{2(1-\alpha)g.w_{bal}} \ \ldots\ldots(3.80)$$

And; α by;

$$\alpha = \frac{\int P.dw}{M_{cm}.g} \ \ldots\ldots(3.81)$$

Where g is the gravity acceleration and the integral refer to the total strain energy absorbed by the system.

3.6.5. The dynamic increase factors based on transit phase

Once the mechanism is fully formed, the active mass can be identified and the transit phase can be idealized to a single degree of freedom with the initial velocity; v_{cm}. The expressions are summarized in section 3.5.2.

3.7. Validation

3.7.1. Case of axial arching and tensile catenary

The benchmark here is based on the test date reported by (He & Yi, Discussion of 'Slab Effects on Response of Reinforced Concrete Substructures after Loss of Corner Column', 2013). In their test Summary of the detailing of the tested samples are presented in Figure 3.7 1 and the geometry is shown in Figure 3.7 2. In the tests, B2 and B6 have the same properties making some sort for range for comparison. While B3 is an improvement of reinforcement ratio, compared to B2 and B6, the B4 and the B5 can be used to evaluate of the effects of different grades of reinforcing steels. The arching strength is provided by the

pins at the middle of the section height, Figure 3.7 2, although a side moment of 2.5mm and 2.2mm, for B2 and B6 respectively, were reported in the test. Therefore, the axial stiffness of the support can be predicted assuming linear relation if the ultimate arching force is known.

Using the procedures in section 3.6.2, the full reaction force-displacement curve is derived.

Properties of reinforcing steel and concrete

Material	Items		Measured values		
			HRB400	HRB335	HPB235
Steels	Yield strength/MPa		445	372	351
	Ultimate tensile strength/MPa		579	539	533
	Ratio of elongation	δ_5	29.7%	28.1%	26.1%
		δ_{10}	23.4%	22.5%	21.3%
Concrete(C30)	Cubic compressive strength/MPa		32		

Detail information of designed specimens and load capacity

NO.	steel class	Steel ratio	Beam section	Ultimate load capacity (kN)		Maximum Displacement(mm)
				Hinge support	Simple support	
B2	HRB400	0.7%	Figure (b)	113	37	372
B3	HRB400	1.4%	Figure (a)	184	74	410
B4	HRB335	0.7%	Figure (b)	99	31	421
B5	HPB235	0.7%		98	29	452
B6	HRB400	0.7%		115	37	393

Note: Ultimate load capacity of simple support is computed by the plastic methods, and others' are test value.

Figure 3.7-1 the detailing of the tested samples adapted from (He & Yi, 2013).

The position of the pin support reduces the effective depth of the arch in section, named h_s earlier, from the effective depth to a one half. The pin constrains both horizontal and vertical translations. With the pin support, taking one half of the beam mechanism because of symmetry, only one location of the plastic hinge is expected by the middle joint which is in line with the test result. No information about the transvers reinforcement provided in the report and the ultimate strength of concrete cylinder is assumed 30MPa. Results are compared here in Figure 3.7-3, and Figure 3.7-4. The load is applied monotonically over the middle point

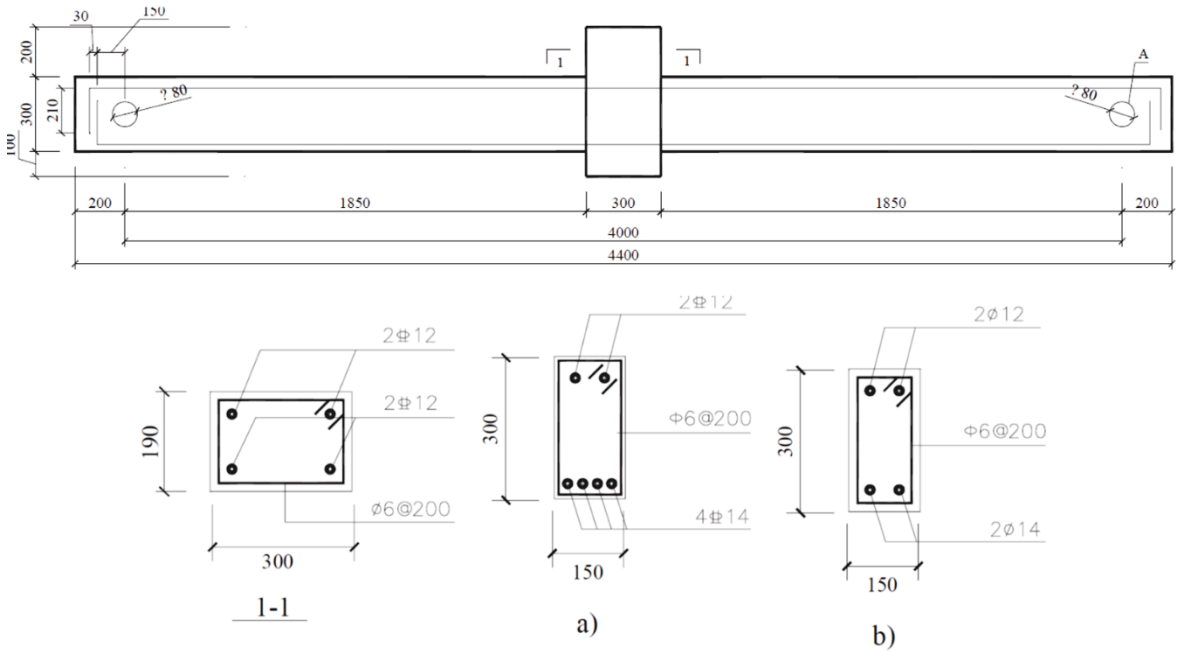

Figure 3.7-2 the geometry of the tested samples adapted from (He & Yi, 2013).

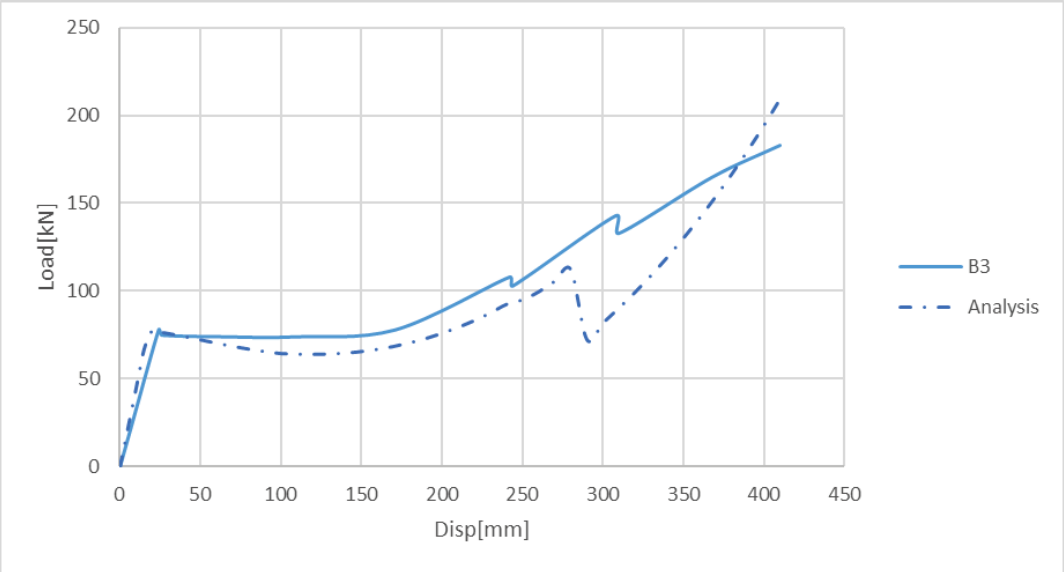

Figure 3.7-3 Comparison between analytical procedures and B3 test of (He & Yi, 2013).

While trying to obtain matching results, the support stiffness and therefore the arching axial force, and the bonding stiffness played a very critical role in changing results. Therefore, accurate information about the actual equivalent stiffness of the sub-structure is essential for getting somehow close results. Also, an artificial linear bending damage function were

assuming from the point of the ultimate bending strength to the 1.2 of the depth of the section.

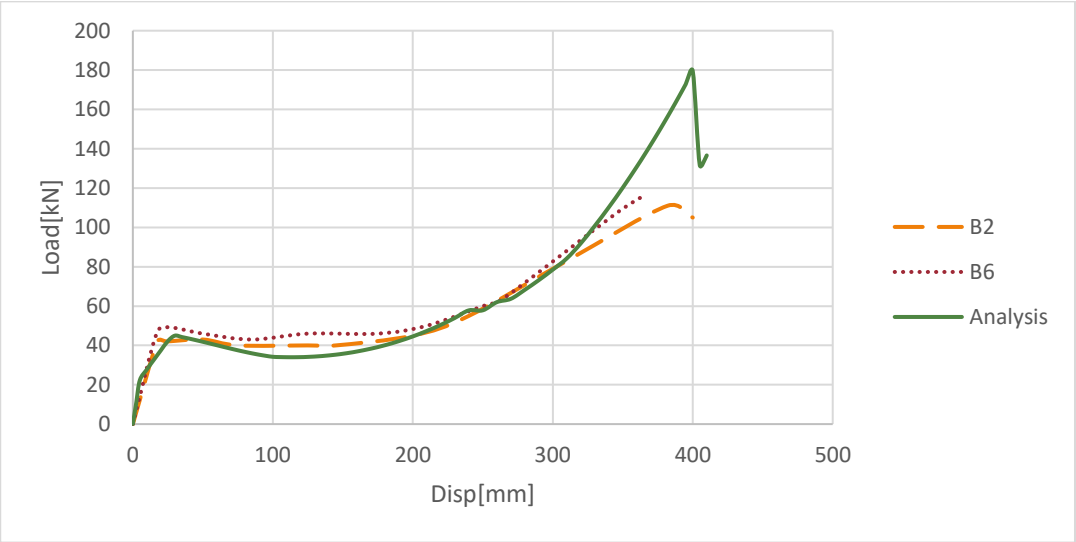

Figure 3.7-4 Comparison between analytical procedures and B2 & B6 test of (He & Yi, 2013).

With regard to the ultimate strength of the point of the tensile catenary, in addition to the equivalent active stiffness, the shape of the response curve and the assumed length of localization zone are also important information. Where these cannot be here objectively handled no additional effort is made here to improve the result.

3.7.2. The case of different depth to span ratio

The bench mark for this validation is chosen from the data of (Su, Tian, & Song, 2009b). In their tests they have observed the effects of three variations, the reinforcement ration, the span-to-depth ratio, and the loading rate. The focus of this section is on the effects of the beam span to depth ratio, which is the A3, B1, and B2 of the reported results. The test details are provided in the Figure 3.7-5. And results are compared in the Figure 3.7-6.

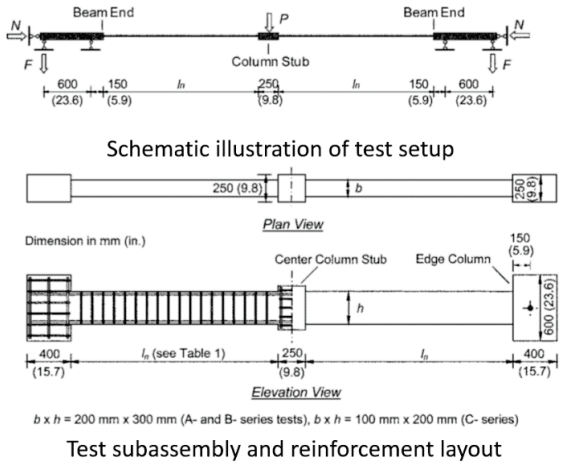

Specimen properties

Test	b x h, mm (in.)	l_n, mm (in.)	l_n/h	f_{cu}, MPa (psi)	Longitudinal reinforcement and ratio		Ties
					Top	Bottom	
B1	150 x 300 (5.9 x 11.8)	1975 (78)	6.58	23.2 (3360)	3ϕ14, ρ = 1.13%	3ϕ14, ρ = 1.13%	ϕ8 at 100
B2	150 x 300 (5.9 x 11.8)	2725 (107)	9.08	24.1 (3500)	3ϕ14, ρ = 1.13%	3ϕ14, ρ = 1.13%	ϕ8 at 120
A3	150 x 300 (5.9 x 11.8)	1225 (48)	4.08	39.0 (5660)	3ϕ14, ρ = 1.13%	3ϕ14, ρ = 1.13%	ϕ8 at 80

Reinforcement properties

Steel type	Diameter, mm (in.)	Yield strength, MPa (ksi)	Ultimate strength, MPa (ksi)	Elongation, %
ϕ8	8 (0.31)	290 (42)	455 (66)	33
ϕ12	12 (0.47)	350 (51)	540 (78)	26
ϕ14	14 (0.55)	340 (49)	535 (78)	27

Figure 3.7-5 information of the test specimen from (Su, Tian, & Song, 2009b)

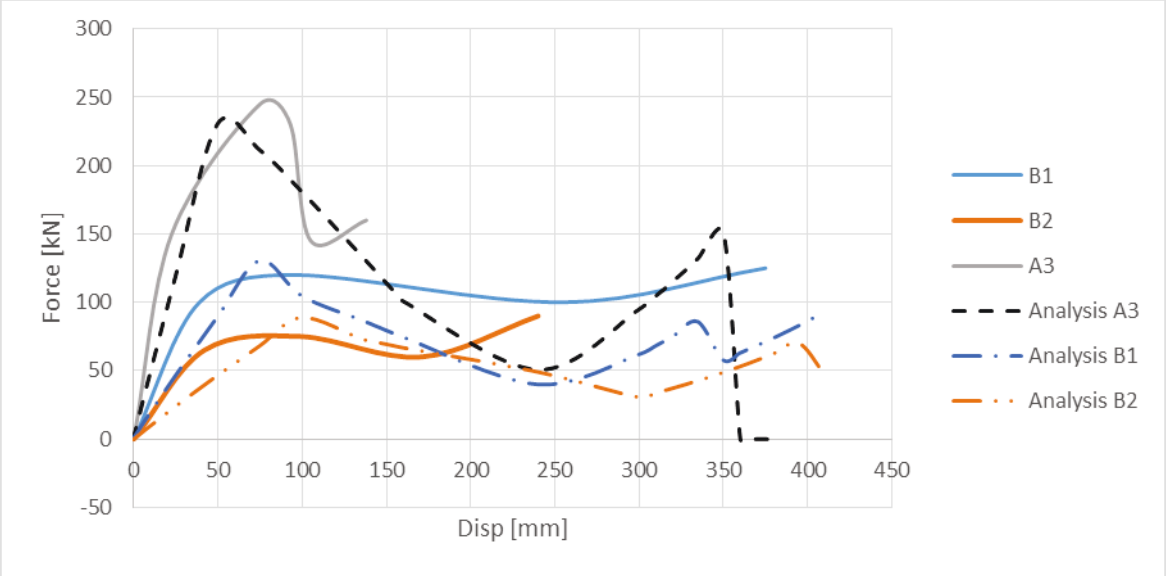

Figure 3.7-6 comparing the analytical model to the test specimen from (Su, Tian, & Song, 2009b)

It can be observed that the arching strength only match in the case of A3, while the discrepancy increases with the increased shear stresses as the span increase towards B1. With regard to the tensile catenary, only B2 showed relatively a good match, it similar to the calibration example above, while the B1 and A3 show complete wrong prediction. The test did not focus on the tensile catenary.

3.7.3. The case of the dynamic increase/amplification effects

To evaluate the dynamic effects in the state of arching and catenary, only one report found to date in the literature with clear experimental evidence. 2D RC frame were tested (Orton & Kirby, 2013), in the well reported test, scattered values of the DIF and DAF were recorded. The analysis disadvantage of the reported results is that the data obtained after the arching failure, of the 4th drop, were based on the damages state of the assembly after three different loading cycles.

While no thing has been reported here about progressive damage, it can be shown that the DAF ranges from 2.2 to the 4.25 when we used the proposed procedures in section 6.5. Therefore, the inclusion of the body motion phase can explain the shortcoming of the procedures suggested in (Orton & Kirby, 2013), although the use of the direct integration of the response curve provide a sound approximation where no free motion transition phase exist. Therefore, here is shown that for progressive transfer from arching to catenary, the inclusion of the body motion phase is more realistic.

3.8. Summary

In this chapter, procedures for the plastic mechanism of the progressive collapse, referred to by 'cm', were presented which can be built into an integrated analytical framework. The procedures address all the key mechanical parameters of progressive collapse as learned from the surveyed test of bridging beam mechanism discussed in chapter 2. These are the ultimate strength of concrete, the reinforcement ratios, in addition to the effects of the boundary conditions on the arching and catenary in terms of strength and deflection. The newly developed procedures is validated through benchmarks covered different detailing and span/depth ratio of the bridging beams. The developed analytical relations are presented here for the first time covering the full range of the repose targets including the dynamic amplification in the tensile catenary phase which includes the body motion phase. The last, cannot be modeled the current incremental dynamic approach although it is very popular in the literature.

The provided procedures give reasonable results and generally hit the named targets in Table 2.5-1 although it requires assumption not normally available without higher level simulation, or test information regarding the stiffness of the boundaries. Nevertheless, a few key parameters were successfully examined, and the parameters can be confidently used from preliminary design and analysis while other unknown assumption can be fixed for the sake of comparison and evaluation.

Although the developed relationships are powerful analyzing various conditions by rather simple formulations, collaboration of the model still require a considerable amount of expert judgment, e.g. the flexural damage and the ultimate displacement at catenary, which inhibit it from being used to accurately predict the strength or even the displacement capacity independent from some test results. Another disadvantage, the 2D and the 3D interaction with the other parts of the structure makes the implementation rather complex and tedious. Therefore, in chapter 5, simulation of progressive collapse using structural finite element shall be presented.

Chapter 4 Slab contribution

4.1. Aim and abstract

Progressive collapse simulation in reinforced concrete building is a challenge due to the complex inelastic behavior of the composite material, large deformation, body motion, transit phenomenon and the size of the full building model; it becomes even more challenging when the collapse due to an extreme seismic excitation is simulated. 2D models of multi-story building are very common in academic literature, but the contribution of the RC slab to progressive collapse is not yet considered in 2D to the best of the authors' knowledge. One reason is the absence of alternative model to represent slab contribution in 2D, simple method which includes slab tensile catenary contribution in the 2D progressive collapse simulation of the RC building, is here presented. Using the proposed method, the tensile catenary forces can be evaluated as compared to two tests from the literature. The far aim is to support stochastic analysis of progressive collapse safety in RC buildings.

Researcher reported the significance of slab contribution in the progressive collapse of the RC buildings, e.g. (Salem, El-Fouly, & Tagel-Din, 2011). The slab can also have a negative

effect in case the continuity of reinforcement may pull the sub-structure leading to complete collapse. Therefore, an attempt is made here to analysis how the lab contribution can be quantified.

The role of slab in bridging over the lost column(s) is studied by many researchers in the context of monotonic increasing load simulating column lose, see for example the contributions of (Dat & Hai, 2011) and (Qian & Li, 2012). The role of slab in frame simulation can be recognized in two folds; the added strength to the monthly beam element, and the slab contribution to the catenary forces. The later has not received enough attention by researchers. Although the work done by the NIST (Main, 2014) uses the fiber-shell element and smeared definition of the reinforcement, the relative course mesh used in slab elements, the damage functions, and the use of explicit dynamic simulation undermines the efficiency and the affordability of the use of these models by wider public.

4.2. The simple model of the slab contribution

As mentioned earlier, the first fold is the slab contribution to the beam strength, this is normally considered by the well-known 'T' section of the beam with the so called effective breadth contribution both in tension and compression. Although this problem can be straightforward in frame, attention must be made for the change of the effective breadth of the flange in tension under various level of loading, because the active area of the reinforcing steel bars may change and subsequently alter the mode of the response of the section. This observation was reported by (Ning, Qu, & Zhu, 2014) with strong critique to the validity of the strong-column weak beam assumption which is popular amongst the community of the seismic design of buildings.

As first fold seems to be addressable, the focus here is on the second fold which is the role of slab reinforcement throughout the tensile catenary stage. Before going into detail, it is worth to note that the failure mechanism passes through three distinct phases of response as the displacement of the joint above the lost column is increases, the first phase is the yielding mechanism marked by the formation of bending plastic hinges, the second is the

arching, bridging or call the compressive catenary, and the last is the tensile catenary in reinforcement. Where the focus is made here on the tensile catenary, a review of other modes of response can be found in earlier chapters and in (Hatahet & Könke, 2014).

4.2.1. The contribution of the slab reinforcement in the tensile catenary

Both the abnormal event, or the collapse trigger, and the progressive collapse propagation are dynamic phenomenon, so the proper assessment of the role of slab requires quantifying the amount of energy absorbed by the slab reinforcement. According to (Qian & Li, 2012) up to 65% of the post peak energy absorbed by the slab reinforcement although no lateral support was provided to the slab in the test setup. If these supports are provided, according to reported photos by news agencies about Syrian war[i], the slab reinforcement may not only pass through the full dynamic catenary forces but it may also hang up the remaining masses. The dynamic energy absorption is made by the yielding of reinforcement due to the large displacement of the assembly after the ultimate strength or the first peak (Hatahet & Könke, 2014).

Using tests in literature, the corner slab assembly will be discussed first then the cases of the edge and middle slabs will be generalised.

4.2.1.1. The case of the corner slab assembly

Assume the total tensile catenary force developing in the reinforcement of the slab is F_{sr}, in the 3D, the vector of F_{sr} rotates with the increased displacement of the catenary assembly, then the total force, at a single slab, is;

$$\overrightarrow{F_{sr}} = \overrightarrow{F_{xr}} + \overrightarrow{F_{yr}} \qquad (4.1)$$

Where; F_{xr} and F_{yr} are the reinforcement in the x and y directions respectively. Force is evaluated by the stress multiplied by the area of reinforcement provided in each direction. Assume that; A_{xr}, and A_{yr}, are the equivalent reinforcement areas in the x and y directions, and all reinforcement are in the yielding stress state at f_y, the magnitude of the total force is;

$$\|F_{rs}\| = \sqrt{\left(A_{xr}f_y\right)^2 + \left(A_{yr}f_y\right)^2} \qquad (4.2)$$

Pulling out the yield strength result in;

$$\|F_{rs}\| = f_y\sqrt{(A_{xr})^2 + \left(A_{yr}\right)^2} \qquad (4.3)$$

The facts that hardening contribution is relatively small and that both x and y reinforcement enjoy the same geometrical deformation, both legitimise the assumption that f_y is uniform. The remaining challenge is to define the equivalent area of reinforcement 'A_{eqs}' in each direction. This can be defined by the length of extension of the plastic yield-line of the collapsing slab panel (He & Yi, 2013), (Qian & Li, 2012) and (Dat & Hai, 2011). The application of the yield-line theory, (Park & Gamble, 2000), will enable the prediction of the yield-lines before the simulation. To explain this, consider the corner panel and the presumes yield-line in Figure 4.2-1 (a), the total resultant force of F_{rs}, will pass through the point D at the middle of the slab diagonal AB which is the defined the yield-line assuming uniform distribution of the reinforcement.

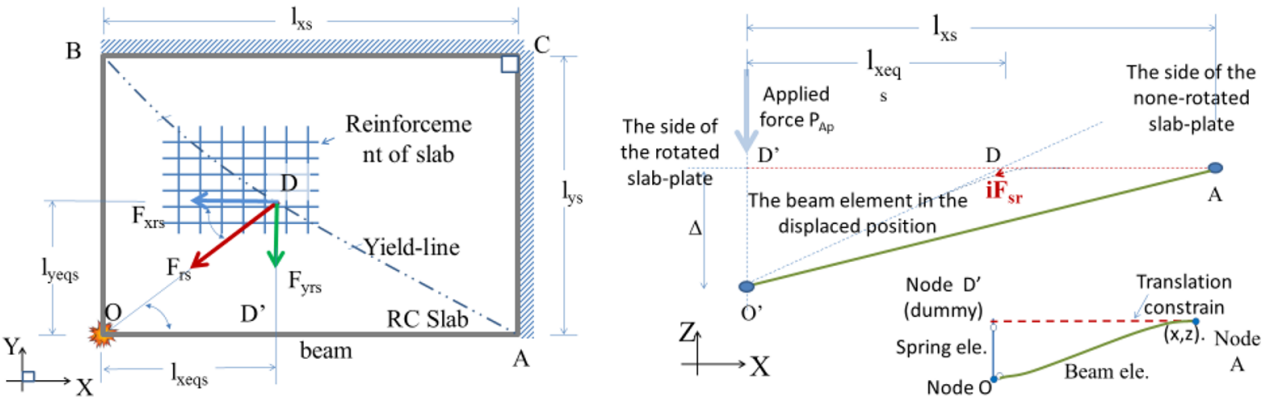

(a) Corner slab panel under the lose of corner column support

(b) The equivalent bar (truss), beam element, and the dummy (node D') in 2D FEM discretization

Figure 4.2-1 the simplified slab model for 2D FEM simulation of the corner slab assembly

To evaluate the slab contribution in each of the idealized 2D frame models in the x and y; direct projection of the force is performed. First the reaction resultant force, F_{rs}, will be

assumed concentrated at the head node of the lost column 'O', the projection of the force over the planes xz can be written as, dropping off sign of vector magnitude;

$$F_{xrs} = F_{rs} \cos\left[\tan^{-1}\frac{l_{ys}}{l_{xs}}\right] \qquad (4.4)$$

Here; l_{xs} and l_{ys}, are the dimensions of the slab. Assuming that there is little hardening in steel, the total force is almost constant, so both projections are also almost constant.

The 2D contribution of slab catenary forces can be presented by an equivalents spring element, figure 1 (b), with an equivalent area of reinforcement A_{xeqrs};

$$A_{xeqrs} = \sqrt{(A_{xr})^2 + \left(A_{yr}\right)^2} \cos\left[\tan^{-1}\frac{l_{ys}}{l_{xs}}\right] = const \qquad (4.5)$$

To quantify the contribution of the dummy spring element D'O in figure 1 (b), the projection of the force in the z direction must be obtained. The direction of the resultant force, in the zx plane can be assumed DO'. So, the tensile reaction force in Z direction can be found by direct z projection.

We need to predict the full energy contribution; if the above formulation allows for the force contribution to be reliably simulated; therefore, an adjusted strain response is required bounded by the yielding and hardening limits. Before dealing with this, let us map the contribution of the slab to the full response of the structural assembly. Assume that the response curve of the full assembly as shown in the figure 4.2-2 (b) (Hatahet & Könke, 2014), the curve describes the displacement history of the head n-ode of the lost column O, Figure 4.2-2 (a). Assuming the total equivalent applied vertical load is P_{Ap}, figure 2 (b), and the vertical displacement of the joint O is Δ, the P_{Ap} & Δ response curve for the failure assembly is idealized. This is proposed by (Park & Gamble, 2000), analysed (Qian & Li, 2013) and tested; for frame assembly (Yu & Tan, 2011), (Qian & Li, 2013) & (Lew H. , et al., 2011) and for floor and beam assemblages (Dat & Hai, 2011) & (Qian & Li, 2012). The points B, C, D & E, defines the states of; the first yielding (y), ultimate strength of local collapse (LC) mechanism (or assembly), end of failure (f) (or the beginning of the catenary), and the

ultimate catenary stage (Cat) respectively. It is important to note that this curve is valid by tests for mechanisms involve single story; there is no to-date any similar curve derived for a full mechanism involving a few stories apart from what is presented in (He & Yi, 2013). So, it is assumed here that the trends can be generalised. Having defined the characteristic points of the response curve, we can now address the displacement contribution of the slab reinforcement.

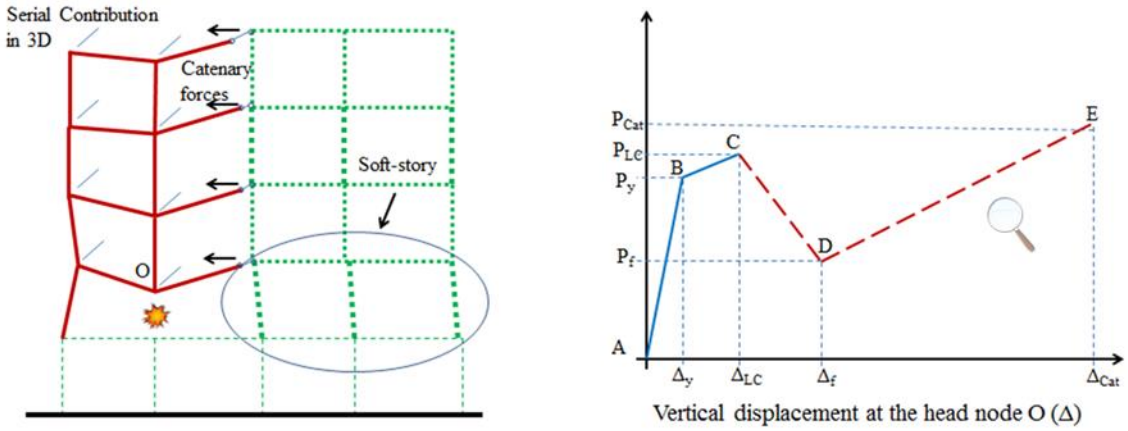

(a) Catenary case – progression of the collapse to soft-story

(b) Idealized response curve of the structural assembly

Figure 4.2-2 local collapse caused by assuming the loss of single column below the point O

The formation of the braking-lines in slab, initialised by the yield-lines, will concentrate the reaction force in reinforcement bars, before projecting the displacement (strain); when are the bars developing yielding stress? In fact, this will not happen simultaneously for different lines of reinforcement. But as the plastic flaw is localised in the breaking-lines it can be proven that by the point D, of the response curve in Figure 4.2-2, defined by the fracture of main beam reinforcement, a complete flaw of the slab reinforcement can be guaranteed. The proof lays in the fact that all the bars in each direction, say x for example, will have almost the same rotation angle, hence the same bending, and so the same strain demand. Let us explain why and show the limiting values of the yield and ultimate strains in relation to the response curve.

To quantify the contribution of the dummy spring element, the projection of the force in the z direction must be obtained. Referring to an idealised response curve in the Figure 4.2-2 (b), In the case of the segment D-E of the response curve, full equilibrium can be established at any section, and the resultant force in bars can be assumed taking the direction of the DO'.

These idealisations are valid if the horizontal reaction is constant as shown earlier, that means after the FEM model define the stable position; either before point C or E in the curve, another analysis must be run making sure the rest of the structure provides sufficient lateral strength. To generalise the case, we need to predict the minimum value of the displacement associated to the point C of the response curve; Δ_{LC}. Consider the single story segment in the Figure 4.2-3, beyond the point of the concrete crashes in the beam, the collapsing assembly switches to the body motion stage, in particular, the slab plates and the attached beam ruins will rotate in 3D defining a line of rotation. In the case of corner panel, the line of rotation passes through the centre of rotations of the two beams of the corner assembly which is in turn parallel to the breaking-line of slab panels. What happens moving from the point C toward D in the response curve is eventually an increase in the offset of the line of rotation away from the parallel centre of the localised strain, breakage, of the slab reinforcement.

To find out the strain response of the slab reinforcement, we need to take the above assumption of the parallel axis of rotation and accept that the rotation angle is uniform over the whole breaking-line, in Figure 4.2-3. As the rotation angle is constant, the strain profile of all bars can be analysed based on the strain profile in the cross section at the node A. In the Figure 4.2-4 (a), the ultimate state of the section is shown which is associated to the point C of the response curve in the Figure 4.2-2 (b). At the minimum strength point D. The offset is defined by the curvature, or the radius of rotation, at which the main bar of beam reinforcement fractures, this is shown in the Figure 4.2-4 (b).

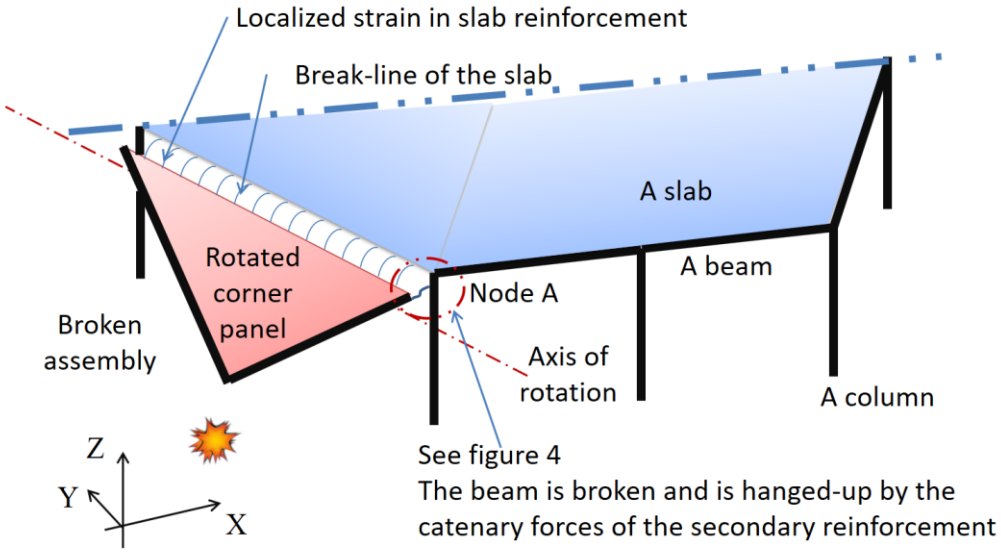

The localized catenary in the slab reinforcement in the case of corner column lose

Figure 4.2-3 single story segment – the case of corner assemblage failure

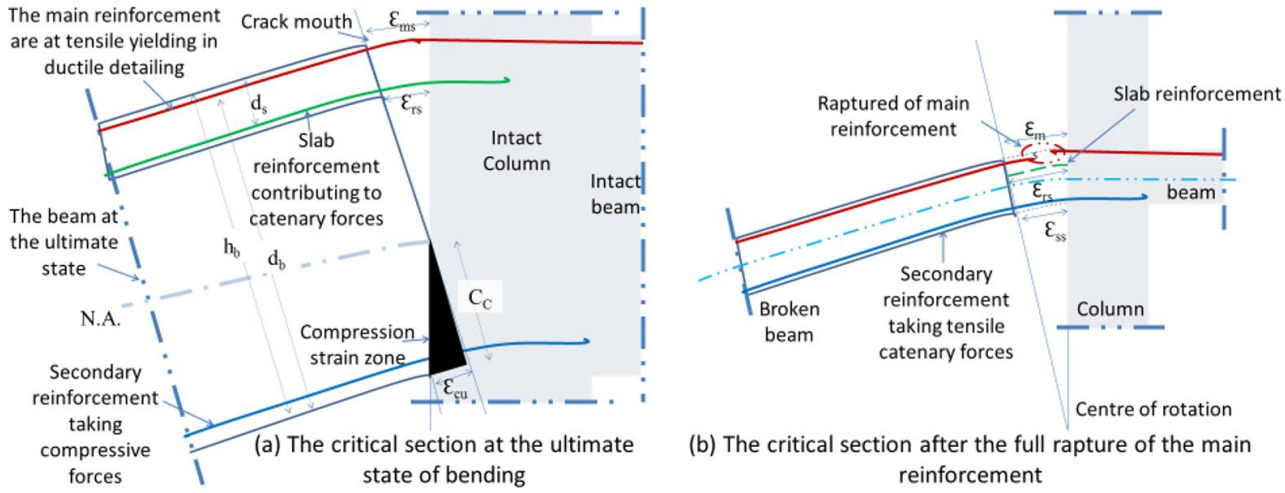

Figure 4.2-4 failure of the beam at the node A in; the ultimate state (a) & the tensile catenary (b).

At the ultimate state, the offset of the centre of rotation coincide the neutral axis (N.A.) of the section. The geometrical data is known; height of the beam h_b, the effective depth of the beam d_b, also for the slab h_s and d_s. Also, the height of the compression zone C_c can be found based on reinforcement ratio. Therefore, based on Figure 4.2-4 (a) at the face of the

column, the strain of main reinforcement 'ε_{ms}', as well as the most adjacent slab reinforcement 'ε_{rs}', can be related to the ultimate strain at concrete crash 'ε_{cu}';

$$\frac{\varepsilon_{cu}}{C_c} = \frac{\varepsilon_{ms}}{d_b - C_c} = \frac{\varepsilon_{rs}}{d_b - d_s} \qquad (4.6)$$

To show that it is a valid hypothesis that the slab reinforcement is in yielding, let us have a bottom-line look on the design practise of solid-slab supported beams, It is justified to presume that the effective depth of beam is three times that of the slab, also, the height of the compression zone will never be more than $0.45d_b$, by replacement;

$$\frac{\varepsilon_{cu}}{0.45d_b} = \frac{(\varepsilon_{rs})_{min}}{d_b - d_b/3} \leftrightarrow (\varepsilon_{rs})_{min} = 1.48\ \varepsilon_{cu} \qquad (4.7)$$

This means that no matter how brittle the concrete, the adjacent slab reinforcements are in yielding from the point C of the response curve.

4.2.1.2. The case of the edge or intermediate slab assemblies

The generalization of the introduced elements above to the case of edge or intermediate slab lays in the yielding-lines defining the breaking-lines of the slab at which the strain is localized. Depending on the ratio between the dimensions of the slab, these lines will be aligned toward the lost support, the case of lateral unrestrained slab is studied by (Dat & Hai, 2011) and (Dat & Hai, 2013), the reported yield-lines match the yield-lines of slab without beams (Park & Gamble, 2000). Those yield-lines for the case of edge slab and intermediate slab are shown in the Figure 4.2-5 (a) and (b) respectively. It worth to be note here that the rotating plates (panels) defined by the lines of yielding required yield-lines to formulate on the boundaries as well. Also note that Figure 4.2-5 (b) show the pattern observed in the test of (Dat & Hai, 2013), while is Figure 4.2-5 (a) is hypothetical assuming weak detailing at the sides of the point O.

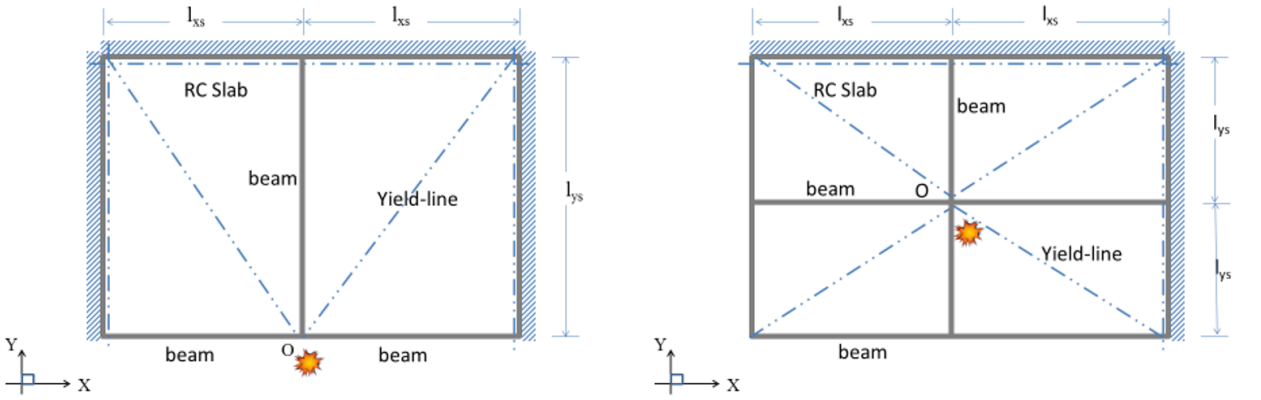

(a) Possible yield-lines in the case of an edge column lose (b) Yield-lines in the case of an intermediate column lose

Figure 4.2-5 Yield-lines of RC slab in the case of the edge assembly (a) and the middle assembly (b)

Where the yield-line theory is based on the principle of the minimum energy, why it does not develop in the direction of the alternate diagonals? The reason is that the initiation of these lines is linked to the weak beam section, for example, in the tests of (Dat & Hai, 2013), the beam broken near the lost column because half, or even one-third of the bottom middle reinforcement of the beam are normally detailed above the support, which also vulnerable to bar de-bonding. Otherwise, for example if retrofit strategy like (Orton S. L., 2007) is applied, the yield lines may shift to the alternate diagonals.

Before going back to the issue of the slab representation in 2D, it is important to refer to the fact that the yield-lines discussed here in the (b) of the Figure 4.2-5 is based on the test result of (Dat & Hai, 2013), their finding is limited to the first peak, the point C, of the response curve in Figure 4.2-2 (b) which, said before, can be represented by the contribution of the flange in the T-section. Although no tensile catenary is clear in the test, it believed that it was due to the lack of the continuity of slab restraints over the boundaries.

Now to derive the contribution of the slab reinforcement, presume that; (1) the panels provide sufficient bond to the reinforcement, (2) for the catenary tensile forces to mobilize the stability conditions must be satisfied at both inner and outer lines of yielding, shown in

the Figure 4.2-5. Note that, the stronger the boundary frame, by the lateral restrains; (the hatched area in the Figure 4.2-5), the higher the tensile catenary forces that can develop.

If lateral restraints are provided and the tensile membrane stress is uniformly distributed, the minimum catenary tensile forces can be evaluated using (Usmani & Cameron, 2004). However, when localised bar bending is present like our case, the deformed shape of the reinforcement is different. Therefore, the derivation of the stress and strain response is different. Unlike the corner slab; the strain in bars will vary across the inner breaking-lines of the slab, because it depends on; (1) the presence hogging reinforcement of the slab, (2) the development of the full strength and so the bonding development length under the high tensile catenary forces. We will begin with assuming these conditions are being observed and the following fits within the area of the application of its assumptions.

In Figure 4.2-6, the tensile catenary of the edge slab is considered, note that the horizontal constrains are assumed to be provided at the edges AE and BC (match the Figure 4.2-5 (a)). With the increased deflection the lines of breakings open making a plane defined by EO'O'$_1$ and CO'O'$_2$ in the Figure 4.2-6 (a). The 1 and 2 is used here to refer to the case of two different spans of the slab; l_{x1s} and l_{x2s}. It is worth to mention that the drawn collapse mechanism is based on the assumption that failure will occur in the beam AB at the sides of the middle joint O. Although this agrees with solid slab yield-lines, it can only be guaranteed when; $l_{ys} > l_{x1s} > l_{x2s}$.

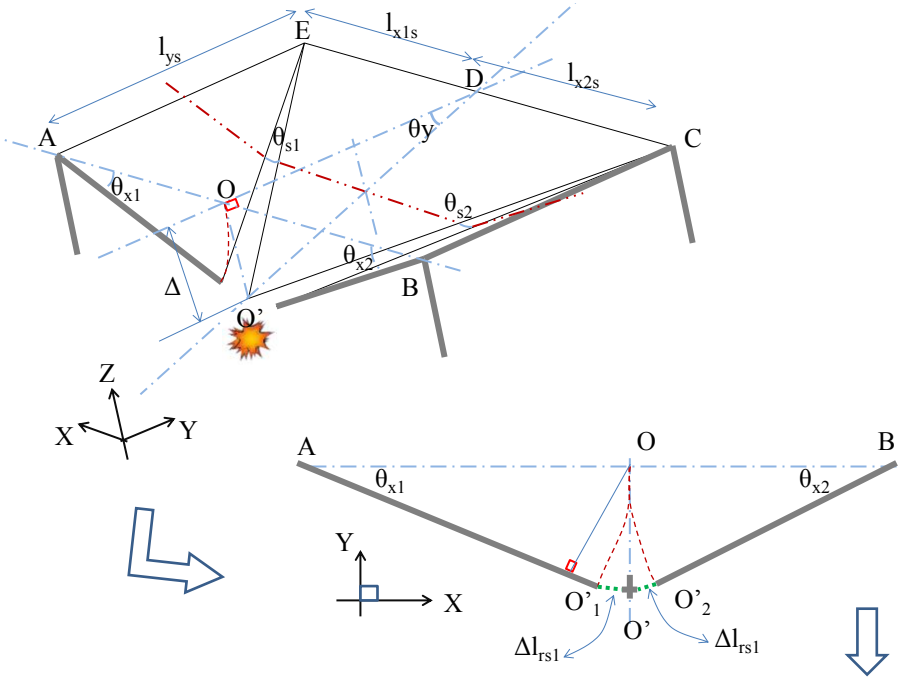

(a) Breaking-lines in the case of edge slab assembly

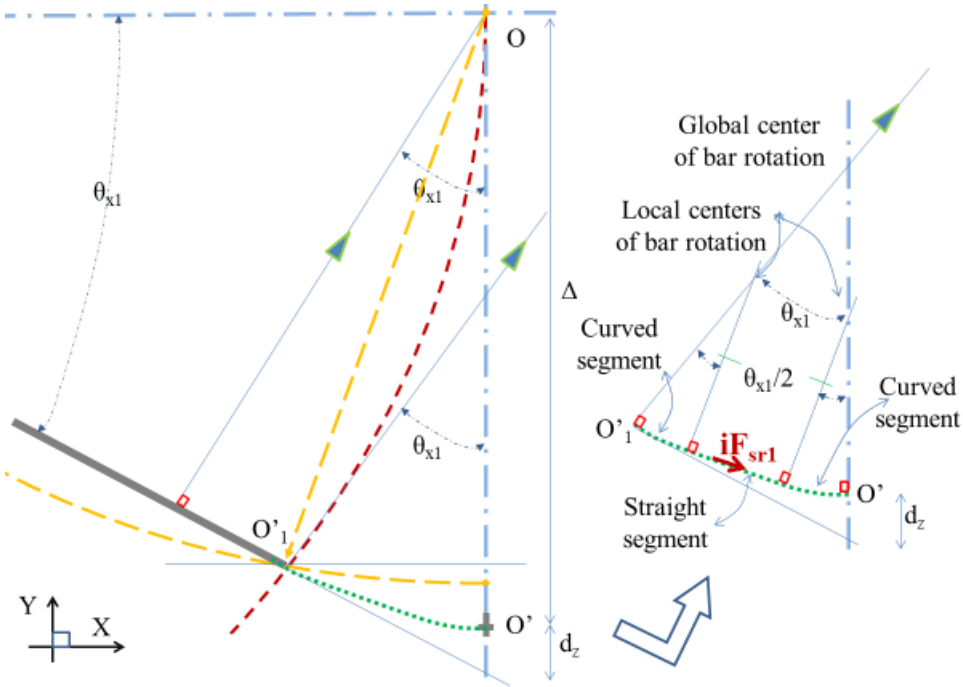

(b) Compatibility of reinforcement under combined tension and bending

Figure 4.2-6 the breaking-lines in case of edge assembly (a) and the compatibility conditions (b).

To evaluate the contribution of the slab reinforcement, the extension in length of each bar must vary from zero, at points E and (the corners) to the maximum value joint offsets $O'O'_1$

and O'O'$_2$ named Δl_{rs1} and Δl_{rs2} respectively which are the bases of the triangles EO'O'$_1$ and CO'O'$_2$. But the extension is not due to pure tension, bar bending is also occurring at each side at the connection points of the bars with slab panels, see figure 6 (b), the path of the bar deformation O'O'$_1$ can be presumably a compound of three segments; two symmetric curves and a straight line. It worth to note here that the precise prediction of the location of O' required knowledge of the two symmetric curvatures of the reinforcements, then the target is to define the unit vector $\mathbf{iF_{rs}}$, see Figure 4.2-6 (b). As no information about the bar bendability is currently in hand, we aim at providing a reasonable prediction of the location of O' and define the direction of the $\mathbf{iF_{sr}}$ identical to the direction of the O'$_1$O'. The direction $\mathbf{iF_{sr}}$ will be approximated here by the average of; (1) the direction of the tangent of the circle of the centre at O and radius of OO'$_1$ at the point O'$_1$, named $i_{\perp OO'1}$, see Figure 4.2-6 (b), and (2) the direction of the vector AO'$_1$; (this approximation can be only justified by the provided visualisation).

$$\overrightarrow{F_{sr1}} = \overrightarrow{\iota^{\perp}{}_{OO'_1}} + \overrightarrow{\iota_{AO'}} \qquad (4.8)$$

$$\overrightarrow{\iota F_{sr1}} = \overrightarrow{F_{sr1}} / \|F_{sr1}\| \qquad (4.9)$$

The location of the dummy joint is also defined at the node O; the head of the column. And to represent the reaction force developed in slab reinforcement, a spring element with non-linear stiffness properties must be defined. The function defines the vertical equivalent reaction force F_{zsr} as a function of the vertical displacement Δ and the direction AO' for the segment D - E Also the degradation due to progressive fracture of the rows of the reinforcement can be evaluated within the triangles EO'O'$_1$ and CO'O'$_2$.

The FEM discretisation and the shape of the force displacement curve of this element are shown in Figure 4.2-7.

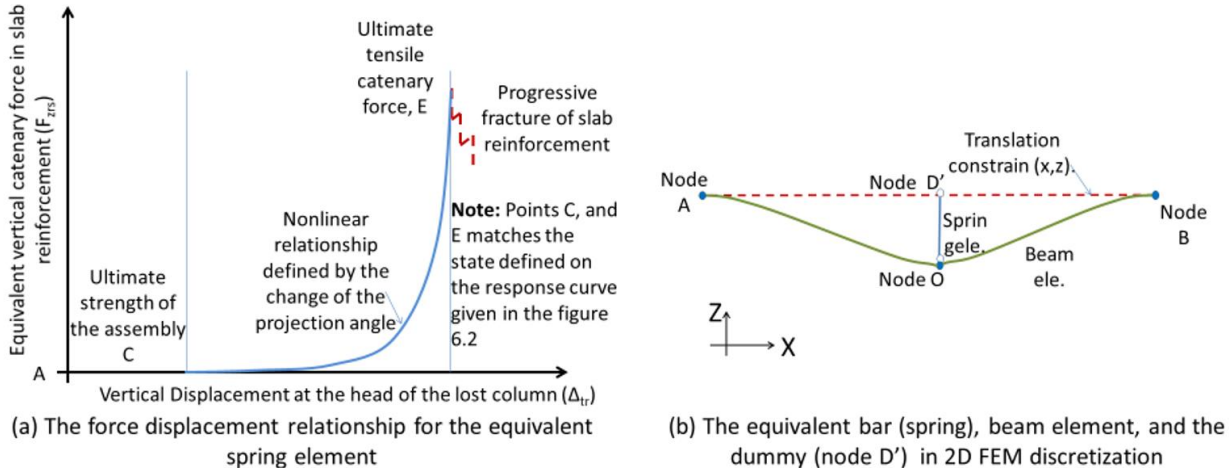

Figure 4.2-7 The simplified slab model for 2D FEM simulation of the slab assemblies

4.3. Summary of the procedures

The phenomenal behaviour of the proposed dummy element is defined by the derivation of the force displacement history curve, shown in Figure 4.2-7 (a) prior the 2D FEM modelling. Therefore, either a set of ready values can be given in pre-defined response curve, or these values can be embedded in either displacement based FEM formulation or in the force based. For the segment D - E as static equilibrium can be defined; the resultant force will take the full direction of the idealised element rotation.

4.4. Validation of the proposed method

4.4.1. The case of the corner slab

The proposed concept of the simplified model is compared to the test by (Qian & Li, 2012). In this benchmark, two sets of corner bare frame, and corner slab assembly are tested. The beams are assumed continuous over the provided column supports. The corner joint under which the comer column is removed, was rotationally restrained simulating the action of the above Vierendeel action that obtained from 3D model. Three test pairs can be used; two square corner slab assembly and a single rectangular where tested with and without the slabs. If the repose of the bare assembly were subtracted from the response of the full assembly, Figure 4.4-1 (a), the net contribution of the slab element is obtained, see Figure

4.4-1 (b) as highlighted by the (slab – frame) curve. These are compared to the results of the proposed method shown in the predicted curve, highlighted (prediction).

In the proposed method, we assume full contribution of slab reinforcement justified by the continuity of the slab through the diaphragm. In test, stress/strain in all reinforcement where not available, because of the lateral reaction forces were only provided at the frame corners of the test setup, rather than the slab edges. Another factor, the assumed truss element does not consider bending deformation an evenly distributed amongst deferent bar elements. Therefore, these results considered useful only as an average strain energy contribution.

It is worth to note here that the bare frames in the test did not consider the contribution of the flanged section (converted 'L'). Therefore, the overall mismatch can be also understood by the missing flange contribution, but in the catenary stage, which is the focus here, both tests S1 and S3 show an overestimation, which can be understood by the fact that the lateral support is only provided through columns at which joint failure in compression was reported by the source. In the case of S2 and F2, having ductile detail of the joint and higher transverse reinforcement increased the consumed energy, therefore the prediction shows a conservative result. The case of S3 represents the rectangular slab case. The flange contribution of these tests was discussed in (He & Yi, 2013).

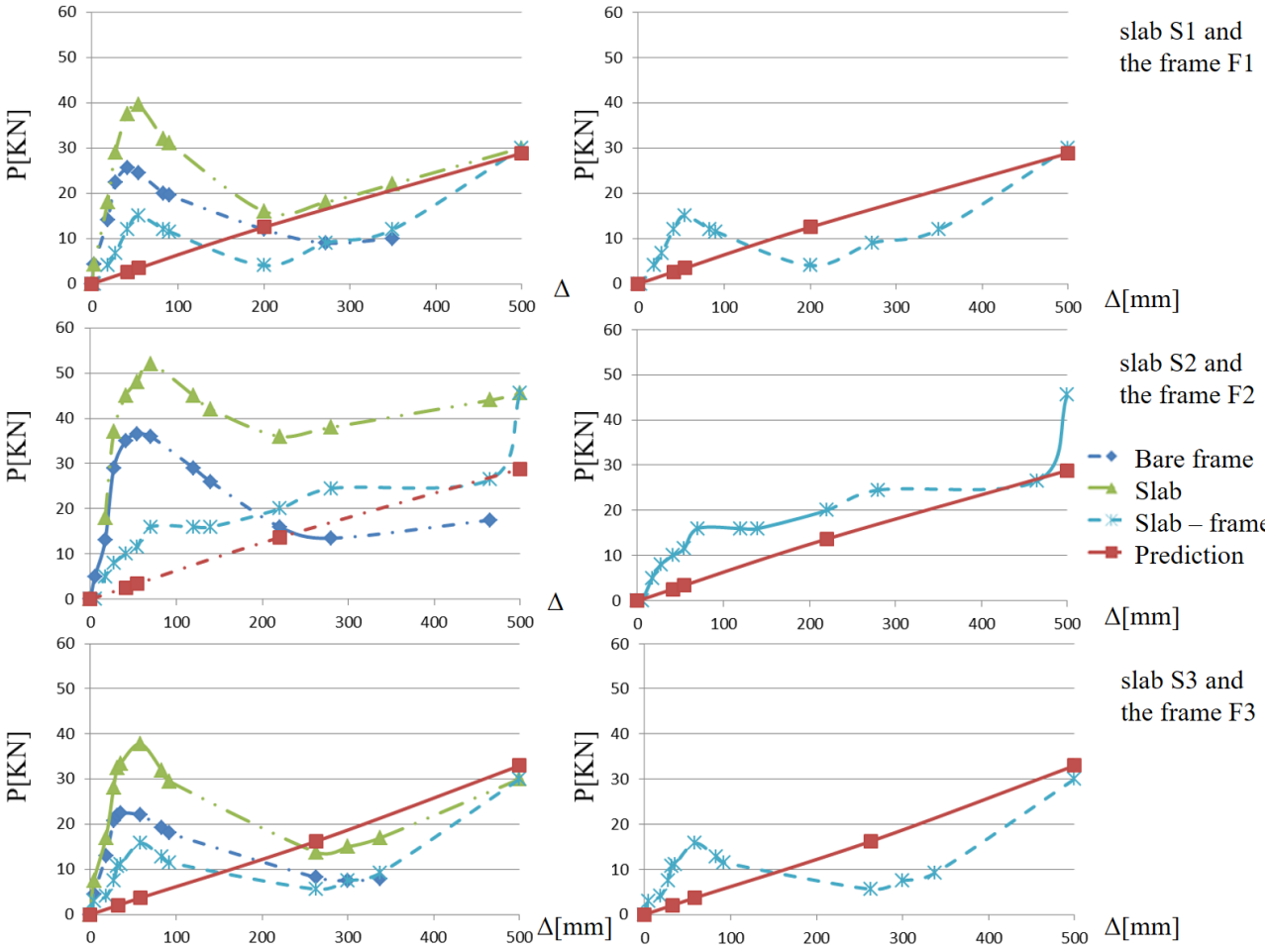

(a) Test results of (Qian and Lin, 2013)

(b) Comparing the prediction of the proposed method and the subtraction of the beam contribution from the contribution of the slab

Figure 4.4-1 the comparison of the proposed method with test in the case of the corner assembly.

4.4.2. The case of the edge or the intermediate slab panels

For the tensile catenary forces to develop, test must be arranged for the deflection of four times the effective depth of the slab or more. The slab strip tested by (Gouverneur, Caspeele, & Taerwe, 2013) until the full fracture of reinforcement. The strip was continuous beam with axial translational restraints at the supports, this is required for the full catenary strength to develop. The one-way slab strip was broken in three parallel lines, if the total tensile catenary forces are aggregated at the middle of the strip, these compares to the test

data as shown in the Figure 4.4-2. The results presented in the figure is only based on the tensile reaction force evaluated as an average of the force in the two longitudinal reinforcement layers with hardening included, neither bending contribution due to coupled force nor the contribution of the distribution bars were included.

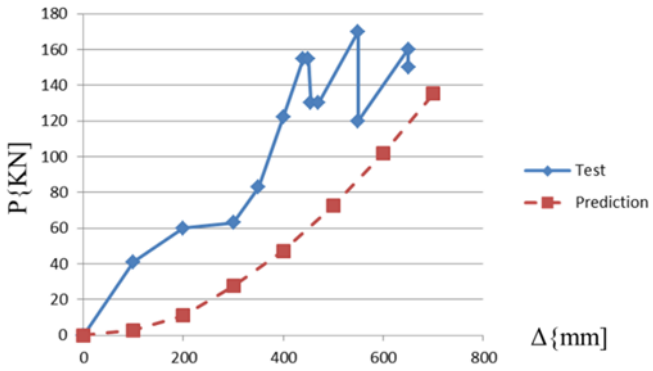

Figure 4.4-2 the comparison of the proposed method with test in the case of the slab strip

4.5. Comments on the results

Further validation is required with limits on strain and bar fracture implemented as proposed. Due the limited test data of the slab with beams and without beams, including the complete tensile catenary, further slab testing is also required.

The developed approach require attention to the provided horizontal restraints which is made here based on judgment of the shape of yield-lines, prior knowledge of the weak sections and the contributing active yield-lines is essential. Although these limits the proposed approach, it remains valuable when the instability result of local failure is dynamically analyzed. In this case, the tensile catenary forces contribute to the damping and reaction forces making the evaluation of the dynamic increase factors more realistic.

4.6. Summary

Non-linear spring element is proposed to simulate the tensile catenary forces develops in the reinforcement of the RC slabs under large deflection proposed. The element is suitable for nonlinear static as well as dynamic frame FEM simulation promoting comparative

deterministic analysis of various structural solutions even in 2D. Therefore, the model is simple and efficient.

Although the model was validated as compared to 2 tests from the literature, considerable judgement is made defining the yield-lines and the plastic hinge location, which indicates the need for further validation tight to availability of further specific slab testing. Also, the proposed model assumes that the flange and arching actions can be included in the beam FEM element, for example using the fibre section combining the action of bending and compression.

Chapter 5 Structural FEM model

5.1. Aim and abstract

In the earlier sections, the principle mechanics of the progressive collapse in the RC bridging beam and beam slab assembly is thoroughly discussed, and the advantages and the shortcoming of the basic analytical relationships are evaluated in the light of some benchmark data. A few of the identified shortcoming can be handled within the scope of the structural FEM. Namely the automatic consideration of the axial-flexural interaction using the fiber section, and the evaluation of the boundary conditions as full frame models can be used, and at last the evaluation of strain in material fiber can be more systematically traced using the standard discretization of the FEM procedures at each point of integration.

While the use of beam element will compromise some important geometrical information, a novel modeling strategy is presented here suitable for being used for the overall robustness assessment at the full-scale of RC building structures. Although similar type of models is concurrently presented by (Livingston, Sasani, Bazan, & Sagiroglu, 2015) and (Arshian, Morgenthal, & Narayanan, 2016). In the first report, buckling of reinforcement

and various boundary conditions were analyzed but the model validation is limited to basic beam mechanism. In the second report, the researcher uses the model to evaluated different modelling strategies however the presented benchmark is limited to the test of quasi-linear structural response although in 3D. In both reports, there is no clue about how the objectivity of the non-linear simulation is handled, also the location of the integration points and the plastic-hinge were not reported.

In the following, full review of the of the background of the chosen modelling strategy is presented including the formulation of the beam element and the information exchange between the main solution algorithm and the element state determination. This is critical in evaluating the scope of the used technique and its limitation.

The following presentation will start from the section level, then the element and the algorithm. Then, two benchmarks are reported; the first cover the case of the simple bridging beam mechanism, and the other present the case of sub beam-column frame assembly.

5.2. The section response and the plastic-hinge

The value of isolating the analysis at the section level form the FE lays in exploring the capabilities of the section in redistribution of the internal forces throughout the response and the section wise damage evolution. In addition, the evolution of the plastic hinge in the beam element can, based on section behavior, be described. The response at the section level will be handled through the standard fiber section procedures, some important remarks are reported. Then the evolution of the plastic hinge shall be considered by the combination of the short beam discretization and the objectivity control strategy. Beams are discretized based on force beam element which is also presented in details in this chapter.

5.2.1. Notes on the response at the section level

In the current structural bending design of RC beams or columns, the section analysis is well established in coupling the axial-flexure interaction. This, well recognized in the interaction

diagram of columns, provided the foundation for the development of the fiber-based beam/column elements. The latter is widely adopted in structural analysis software. Although the axial-flexure interaction handles the cases where little shear forces are applied, the interaction with the shear stresses is less of interest of this section. Because the shear contribution is pronounced in the following two cases and non-of is critical of the beam problem;

- With short span of shear, a traditional example is the response of shear walls or short columns,
- Researches recognized that the shear interaction is also triggered with the large deformation of the section this well understood as the tensile cracks grow over substantial proportion of the section. Therefore, phenomenological approaches were developed to associate the strain in the tensile reinforcement to the shear strength. This phenomenon is of my interest as I believe it may help describe the progressive failure of the beam element by defining the point C and the following response Figure 5.2-1. The overviewed test data is chapter 2 indicates that the presence of the translational restraints, which increases the ultimate arching capacity, may also cause failure at smaller deformation values, this shall be also discussed further in this section.

If all the evolving damage will happen in the vicinity of a single section, the description of the post peak response is needed within the section analysis. The post-peak proportion of the theoretical response curve of the progressive collapse mechanism shown in the Figure 5.2-1, this is simplified by the line CD.

For the section model to represent the descending part CD, material model must describe the post peak, un-reversible damage, and must allow the solution algorithm to follow the negative stiffness value, or in another word, it must calculate the progressive damage and handle the non-absolute value of the section stiffness. The flexibility based beam element is used and reviewed below for this purpose alongside special interaction algorithm.

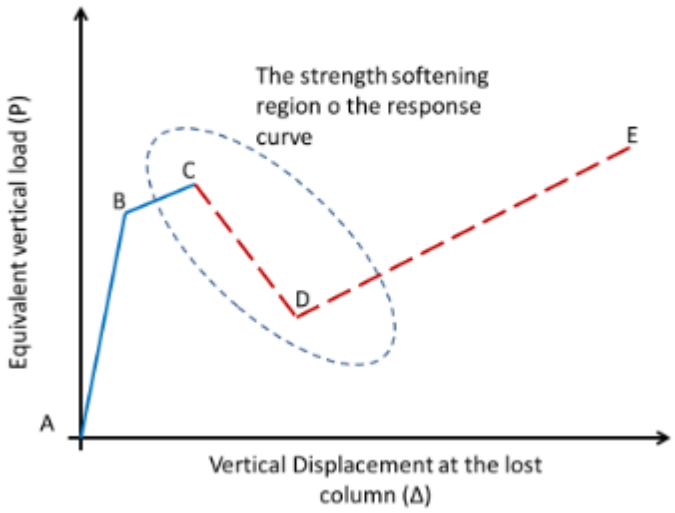

Figure 5.2-1 the post-peak proportion of the quasi-static response curve of the collapse mechanism

Within the fiber-section algorithm, fibers will cut-off; eroded, when a specific crash limit is reached. Damage criterial, alongside material model developed in (Talaat & Mosalam, 2008) can be implemented. This damage is reflected at the level of each of the failing fiber and over the therefore naturally over the full section response.

5.3. The response at the finite frame element level

An overview of the formulation of the beam/column element based on force based and displacement based interpolation can be found (Filippou & Fenves, 2004) in the content of the seismic response simulation of structures. Summary of these procedures and equations are collected in the Figure 5.3-1. Vectors v and p refer to element displacements and forces respectively. These are obtained from the global displacements u and the global forces through a series of geometrical transformations. Through the element information; v and p; and the local section information can be obtained either through the displacement interpolation, in the case of the displacement based element DBE, or by the force interpolation, in the case of the flexibility based beam element FBE. Then section deformations are obtained based on the material law. Provided that the force equilibrium

can be satisfied, the section, and then, the element stiffness can be concluded and submitted to the global processing loop. See Figure 5.3-1.

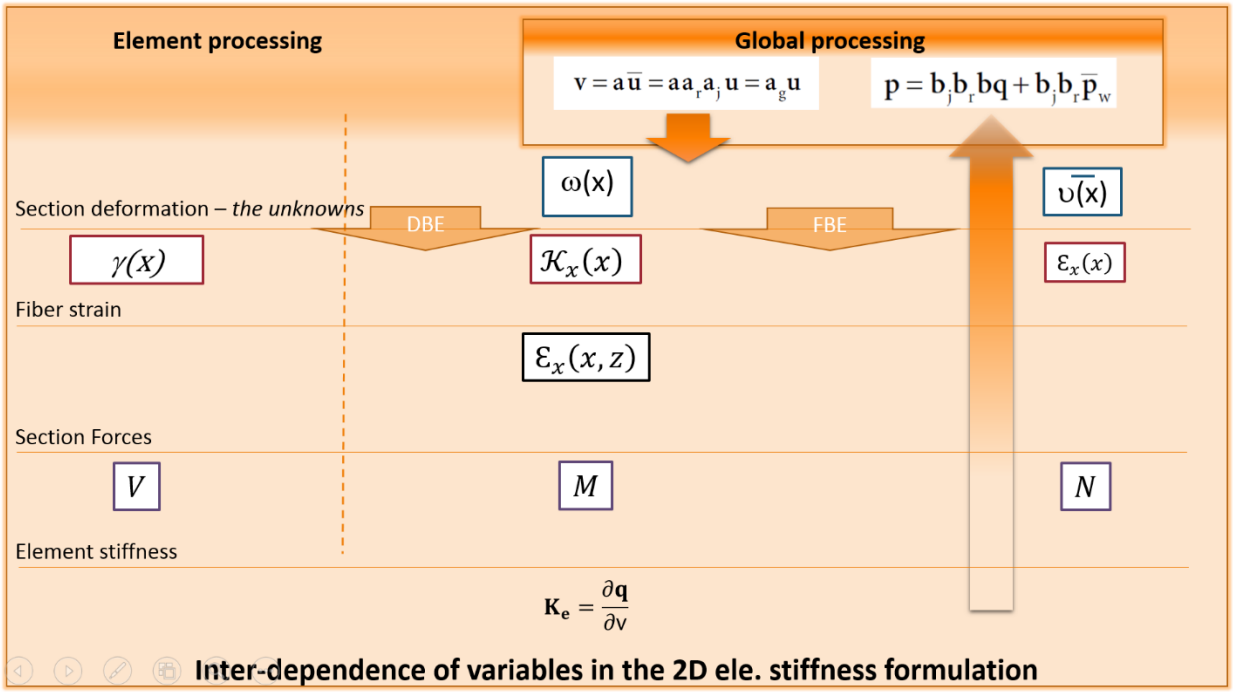

Figure 5.3-1 an overview of variable in the beam finite element model

Although the FE method is displacement based, FBE gained high attention over the DBE in the field of seismic response simulation of RC structures. The FBE and DBE differ in the way it handles the interaction between element displacements, collected in v, and the section deformations. The last are the unknowns of the element state determination process, refer to Figure 5.3-1. Merits of the FBE, over the DBE, lays in the focus on strong equilibrium satisfaction through direct interpolation of internal forces imposing strains over the section level. The strain/deformations, the additional unknowns, must satisfy the section kinematics of the 1D material law, and aggregate loads and stiffness which are in balance with the eternal loads. The process of embedding FBE in standard FE code received sufficient attention with a few consistent two and three filed variation formulations. However, integration algorithms of the nonlinear response remain bound by specific application. In OpenSEES, for example, the FBE is implemented in small deformation state limiting the chance of the FBE in the plastic localization problem in addition to the well-

known convergence issues related to the implemented integration algorithm. This convergence problem is related to the required solution of the nonlinear system of the balance equations of the element forces, external forces and the section forces. The equation is show over the FBE arrow in Figure 5.3-2.

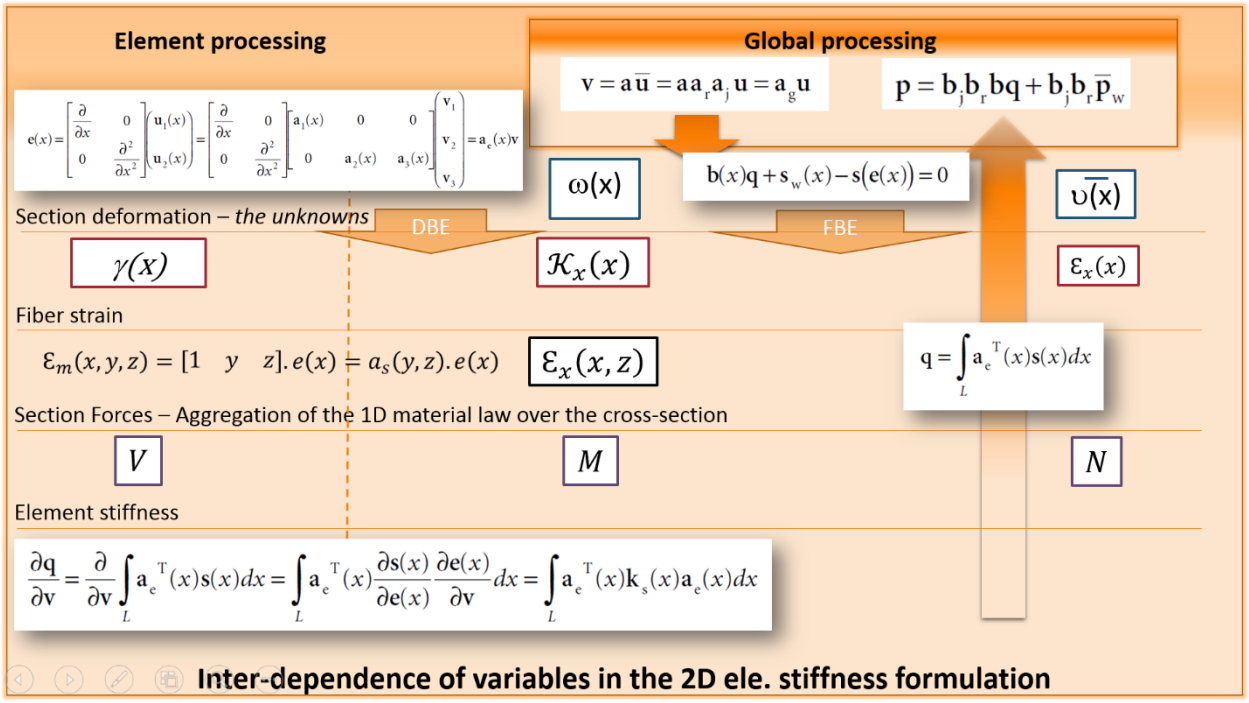

Figure 5.3-2 handling of unknown section deformations and stiffness in the DBE and the FBE

The development of the FBE is based on of the major benefit of avoiding the need for mesh refinement in the displacement based beam formulation required to capture the distribution of curvature at extreme conditions although the size of the nonlinear balance equations become more demanding.

In contrast, the approximation of the co-rotational transform is based on small deformation, then for large deformation at the hinge regions alongside the large displacement under collapse situation a few number of elements will be required compromising the merits FBE. Another complication associated to few FBEs, in addition to increased computational cost, is the vulnerability of the integration algorithm of section unloading when more than one integration point is located in the softening PH region.

Collecting benefit of both, mixed formulation is also popular in literature in which the force, the displacement, and/or the section deformations are dealt with as independent fields at the element level. It worth noting here that, the procedures implemented in the OpenSEES correspond to the equations shown Figure 5.3-2.

To satisfy the progressive collapse simulation needs, both formulation is a candidate. Both require derivation for large deflection and moderate deformation. And both suffer from the contradicting needs; of the a few element discretization for the approximation of large displacement by the corotational transformation, and the need for a single element for systematic handling of plastic hinge evolution. Where the DBE impose the kinematic relation based on standard theories of the beam defamation limiting the use in large deformation as mesh refinement is a non-sense under the Euler-Bernoulli beam hypothesis which based on beam as a slender segment. The FBE is more flexible in the abrupt change of curvature but it is more vulnerable for computational instabilities. Close look at the element formulations is perused in the following section for the complete reference.

5.3.1. Displacement based fiber section element

Summary of the different frame based, or structural, FEM implementations can be also found in (Gharakhanloo, 2014) and (Le Corvec, 2012). The figure shows the two most used elements implemented in the OpenSEES, the figure is adapted from (Filippou & Fenves, 2004).

5.3.1.1. Kinematics of large curvature beam element

The following beam-column element is based on Euler-Bernoulli beam theory; let the displacement field be:

$$\boldsymbol{u}(x) = \begin{bmatrix} u(x) \\ w(x) \\ v(x) \end{bmatrix} \dots\dots (5.1)$$

The u(x) is the axial, and w(x) and v(x) are the transverse displacements in the z- and y-direction respectively. The deformation vector of the section is at large deflection can be

written based on the extension of the Euler-Bernoulli beam theory and, on the von Kármán strain, also can be derived from the three-dimensional Green-Lagrange strain by neglecting the second derivative of the axial deformation about the axial displacement:

$$\mathbf{e}(\mathrm{x}) = \begin{bmatrix} \mathcal{E}_a(x) \\ \mathcal{K}_z(x) \\ \mathcal{K}_y(x) \end{bmatrix} = \begin{bmatrix} \frac{\partial u(x)}{\partial x} + \frac{1}{2}\left(\frac{\partial^2 w(x)}{\partial x^2}\right)^2 + \frac{1}{2}\left(\frac{\partial^2 v(x)}{\partial x^2}\right)^2 \\ -\frac{\partial^2 w(x)}{\partial x^2} \\ \frac{\partial^2 v(x)}{\partial x^2} \end{bmatrix} \dots\dots (5.2)$$

The $\mathcal{E}_a(x)$ is the value of the strain at the origin including the non-linear geometries, for any point of the section discretized by fibers, the deformation along the normal is defined by at the fiber m;

$$\mathcal{E}_m(x, y, z) = \mathcal{E}_a(x) + y\mathcal{K}_z(x) + z\mathcal{K}_y(x) \dots\dots (5.3)$$

$$\mathcal{E}_m(x, y, z) = [1 \quad y \quad z].\, e(x) = a_s(y, z).\, e(x) \dots\dots (5.4)$$

The, $a_s(y, z)$, is called the section kinematic matrix.

With regard to section forces:

$$\boldsymbol{s}(x) = \begin{bmatrix} N(x) \\ M_z(x) \\ M_y(x) \end{bmatrix} \dots\dots (5.5)$$

And the constitutive equation for the section is applied in a linearized analysis stepping;

$$\Delta\mathbf{s}(\mathrm{x}) = \mathbf{K_s}.\, \Delta\mathbf{e}(\mathrm{x}) \dots\dots (5.6)$$

And the $\boldsymbol{K_s}$, the material stiffness matrix, is therefore defined by;

$$\boldsymbol{K}_s = \frac{\partial s}{\partial e} = \begin{bmatrix} \frac{\partial N}{\partial \mathcal{E}} & \frac{\partial N}{\partial \mathcal{K}_z} & \frac{\partial N}{\partial \mathcal{K}_y} \\ \frac{\partial M_z}{\partial \mathcal{E}} & \frac{\partial M_z}{\partial \mathcal{K}_z} & \frac{\partial M_z}{\partial \mathcal{K}_y} \\ \frac{\partial M_y}{\partial \mathcal{E}} & \frac{\partial M_y}{\partial \mathcal{K}_z} & \frac{\partial M_y}{\partial \mathcal{K}_y} \end{bmatrix} \dots\dots (5.7)$$

We will use the **bold** letter to refer to **matrix** differentiating them form the vectors in normal, and the *scalar* in *italic*.

This generalized/global displacement field u is normally related to the nodal displacement v through;

$$\boldsymbol{u}(x) = \boldsymbol{a}(x).\mathbf{v} \ \ldots\ldots(5.8)$$

The matrix $\boldsymbol{N}(x)$ contains the shape/interpolation functions for each displacement. Also, in association with the local displacement at the element level, the section vector of deformation e(x) is derived from the vector of nodal displacement ***v*** by;

$$\mathbf{e}(\mathrm{x}) = \boldsymbol{a_e}(x).\mathbf{v} \ldots\ldots(5.9)$$

The matrix ***B(x)*** presents the combination of (5.1) and (5.2) above containing the first derivative of the axial displacement shape function, and the second derivatives of the transverse displacement shape functions.

The linearized section forces become therefore;

$$\Delta\mathbf{s}(\mathrm{x}) = \boldsymbol{K_s}.\boldsymbol{a_e}(x).\mathbf{v} \ \ldots\ldots(5.10)$$

And the nodal forces q can be obtained based on the principle of virtual displacement as

$$\boldsymbol{q} = \int \boldsymbol{a_e}^{\boldsymbol{T}}(x).\boldsymbol{s}(x).dx \ \ldots\ldots(5.11)$$

And finally, the element stiffness matrix can be derived through;

$$\mathbf{K_e} = \frac{\partial \mathrm{q}}{\partial \mathrm{v}} = \int \boldsymbol{a_e}^{\mathbf{T}}(\mathrm{x}).\mathbf{K_s}.\boldsymbol{a_e}(\mathrm{x}).\mathrm{dx} \ \ldots\ldots(5.12)$$

Due to discontinuities in the stress field in RC structures analytical integration is not possible, therefore these are replaced by numerical integration.

5.3.2. Flexibility based fiber beam element

In the FBE, the section forces are evaluated based on the interpolation of the element forces;

$$\boldsymbol{s}(x) = \mathbf{b}(x).\boldsymbol{q} \ldots\ldots (5.13)$$

The, $\mathbf{b}(x)$, is the matrix that contains the interpolation functions.

$$\mathbf{b}(x) = \begin{bmatrix} 0 & 0 & 1 \\ \frac{x}{L} - 1 & \frac{x}{L} & 0 \end{bmatrix} \ldots\ldots (5.14)$$

And then the linearized section deformation is found by;

$$\Delta\boldsymbol{e}(x) = \boldsymbol{f_s}(x).\Delta\boldsymbol{s}(x) = {K_s}^{-1}.\Delta\boldsymbol{s}(x) = \boldsymbol{f_s}(x).\boldsymbol{b}(x).\boldsymbol{q} \ \ldots\ldots (5.15)$$

Where the; $f_s(x)$, is the section flexibility matrix known in the flexibility method. Now based on the principle of the virtual forces, the vector of element deformations can be evaluated integrating section deformations over the length of the beam element;

$$\boldsymbol{v} = \int \mathbf{b}^T(x).\boldsymbol{e}(x).dx \ \ldots\ldots (5.16)$$

And therefore the element flexibility matrix f_e can be also obtained integrating the section flexibility;

$$\boldsymbol{f_e} = \frac{\partial \boldsymbol{v}}{\partial q} = \int \mathbf{b}^T(x).\boldsymbol{f_s}(x).\mathbf{b}(x).dx \ \ldots\ldots (5.17)$$

The analytical expressions in the above equations can is normally replaced by the numerical integration aggregating the response of sections, and then the integration points at which the section material laws are evaluated are the control points of the beam.

5.3.2.1. The interpolation of the force field

Forces are internal and external. The internal forces, or termed the generalized stresses, are defined in the content of the fiber section as the integration of the stresses over the cross section. The main advantage of generalized stress interpolation is the strict satisfaction of the equilibrium in the deformed state of the beam element.

The changes of these forces over the element length depends on the external load, the material stiffness; damage and plasticity, in addition to loading/unloading result from the

localization progressive failure of the element. Therefore, force interpolation must allow the changes in the generalized force field results from any changes of any combination of these. The interpolation of the force field as prescribed in 3D beam element

$$\mathbf{b}(x) = \begin{bmatrix} 0 & 0 & 0 & 0 & 1 \\ 0 & 0 & \frac{x}{L} - 1 & \frac{x}{L} & 0 \\ \frac{x}{L} - 1 & \frac{x}{L} & 0 & 0 & 0 \end{bmatrix} \quad \dots\dots (5.18)$$

5.3.2.2. Approximation of the equilibrium equations in the deformed state

Let us define the vector of element nodal forces in the local coordinates $\bar{P}$. In 2D, the vector contains 6 members, two displacements, and one rotation for each node ordered from 1 to 6. These can be linked to the three element forces collected in the vector q: axial force and two bending moments by the following set of equations (Filippou & Fenves, 2004);

$$\bar{P} = \begin{bmatrix} \bar{P}_1 \\ \bar{P}_2 \\ \bar{P}_3 \\ \bar{P}_4 \\ \bar{P}_5 \\ \bar{P}_6 \end{bmatrix} = \begin{bmatrix} -\frac{L + \Delta\bar{u}_x}{L_n} & -\frac{\Delta\bar{u}_y}{{L_n}^2} & -\frac{\Delta\bar{u}_y}{{L_n}^2} \\ -\frac{\Delta\bar{u}_y}{L_n} & \frac{L + \Delta\bar{u}_x}{{L_n}^2} & \frac{L + \Delta\bar{u}_x}{{L_n}^2} \\ 0 & 1 & 0 \\ \frac{L + \Delta\bar{u}_x}{L_n} & \frac{\Delta\bar{u}_y}{{L_n}^2} & \frac{\Delta\bar{u}_y}{{L_n}^2} \\ \frac{\Delta\bar{u}_y}{L_n} & -\frac{L + \Delta\bar{u}_x}{{L_n}^2} & -\frac{L + \Delta\bar{u}_x}{{L_n}^2} \\ 0 & 0 & 1 \end{bmatrix} \begin{bmatrix} q_1 \\ q_2 \\ q_3 \end{bmatrix} = \mathbf{b}_u q \quad \dots\dots (5.19)$$

Based on Taylor Series, an approximation can be obtained, but such approximation, will disregard the axial deformation term which hinder the simulation of the tensile catenary.

In the above equation the, the $\mathbf{b}_u$ matrix replaces the **b** in the case of small deformation. Also, based on the principle of virtual work, it can be seen the matrix $\mathbf{a}_u$. relating the vector of element deformations *v* to the element end node displacements in local coordinates $\bar{u}$, is a conjugate of the $\mathbf{b}_u$, and those can be related by the matrix transpose operation;

$$\mathbf{a}_u = {\mathbf{b}_u}^T \quad \dots\dots (5.20)$$

Where;

$$v = \mathbf{a}_u \bar{u} \quad \dots\dots (5.21)$$

$$v = [v_1 \quad v_2 \quad v_3]^T \quad \dots\dots (5.22)$$

$$\bar{u} = [\bar{u}_1 \quad \bar{u}_2 \quad \bar{u}_3 \quad \bar{u}_4 \quad \bar{u}_5 \quad \bar{u}_6]^T \quad \dots\dots (5.23)$$

5.3.3. Handling material nonlinear response

From numerical procedure point of view in the structural FE, the nonlinear material behavior is; either traced by the solution of the numerical nonlinear equation in FBE, or imposed by the interpolation of the beam deformation in the DBE. Whereas there is no guarantee for convergence in the first approach, the second approach is vulnerable to higher residual in the element balance equation leading to wrong results especially in the softening response. To counter this problem, in the state of large bending deformation in the critical zones, the force beam element is only based on two integration points approximating the material response by the imposed linear force interpolation. The advantage is here that the FBE is free from the compatibility condition of the standard Eelier Bernoulli beam assumption, compared to DBE. Although such an application does not provide full description of material damage, it shows an acceptable approximation in the following validation section.

5.3.4. Handling geometric nonlinear response

While the beam element transfer into tensile catenary, the co-rotational geometric transform is used (Crisfield, 1991).

5.3.5. Objective Response

To avoid the localization of deformation in a single FBE element, procedures, suggested by (Coleman & Spacone, 2001), are used here.

To predict the point of reinforcement rupture, an adjacent of the gauge length and the localization length in comparison with the distance of different integration points must be adapted.

5.4. Validation of the model

In Chapter 3, the test of (He & Yi, Discussion of 'Slab Effects on Response of Reinforced Concrete Substructures after Loss of Corner Column', 2013) were used to benchmark the proposed analytical model. To illustrate the advantage and the disadvantage of proposed modeling strategy based on the standard OpenSEES, the Figure 5.4-1 shows the comparison of the model result to the test benchmark. The use of higher hardening ration of the steel provides better results in the early part of the tensile catenary, while it diverts so high in the later proportion. This is understood by using constant hardening ration for the simplified model of reinforcing steel (Steel02) which is not developed for the tensile catenary analysis. The material model named (reinfSteel), supposed to provide better matching of material behavior at large displacement showed convergence problem when used with the FBE. This is a major drawback in this simulation when the tensile catenary is the key part of the problem. The 1D model of concrete is (Concrete01) as no tensile strength is here considered.

Over the plastic hinge region, four integration points is used divided over two FBE. The first integration point brought close to the critical section, at 50mm offset from face of the support, to observe point of ultimate strength. The distance between the two sub-sequent points of integration is used to adjust the material law for concrete as proposed by (Coleman & Spacone, 2001). Also, plastic-flow of the steel reinforcement will localize at a single integration point, therefore no further preprocessing for the material law is here required.

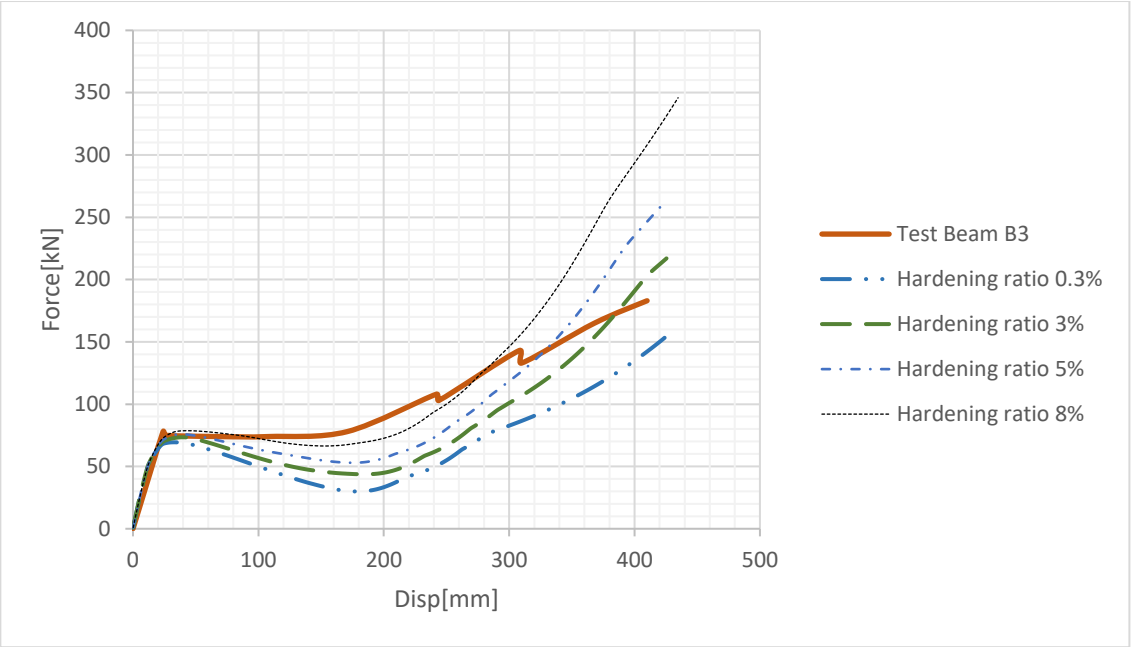

Figure 5.4-1 comparing the OpenSEES models at different hardening to the test (He & Yi, 2013).

To show the merit of simulating using the structural FEM, compared to the analytical frame work in chapter 3, the sub-frame assembly tested by NIST (Lew H. , et al., 2011) is here used. The SFEM models fooled the same process is used in the earlier benchmark; in terms of material models and element discretization.

The test benchmark is conducted on two different detailing levels of the frames with special detailed moment frame (SMF), and without seismically detailed, or so-called intermediate frame, conditions (IMF). The SMF and IMF refers to the special detailed moment frame, and intermediate detailed moment frame respectively. The material data are summarized in the Figure 5.4-2. And the detailing of the test specimen IMF and SMF are provided in the Figure 5.4-3 in order. Test is performed by quasi-static incremental pushing of the middle joint.

Specimen	Compressive Strength psi (MPa)		Split-Cylinder Tensile Strength psi (MPa)
	Footings	Beams and Columns	Beams and Columns
IMF	5700 (39)	4700 (32)	450 (3.1)
SMF	5300 (37)	5200 (36)	420 (2.9)

Average compressive and tensile strengths of 6x12 concrete cylinders at the time of testing

Heat	Bar Size	Yield Strength, f_y ksi (MPa)	Ultimate Strength, f_u ksi (MPa)	Rupture Strain†
A[1]	8	69 (476)	94 (648)	21 %
B[2]	9	67 (462)	93 (641)	18 %
C[3]	9	70 (483)	100 (690)	17 %
D[4]	10	73 (503)	106 (731)	16 %
E[5]	4	76 (524)*	103 (710)	14 %
F[6]	4	79 (545)*	98 (676)	15 %

Average mechanical properties of reinforcing bars

* 0.2 % offset yield strength
† Gage length: 8 in (203 mm)
[1] Top bars in beam of IMF specimen and all beam reinforcement in SMF specimen
[2] Bottom bars in beam of IMF specimen
[3] Vertical bars in columns of IMF specimen
[4] Vertical bars in columns of SMF specimen
[5] Ties and stirrups in IMF specimen
[6] Ties and stirrups in SMF specimen

Figure 5.4-2 the summary of material data of the two-test specimen of (Lew H. S., et al., 2011)

After collaborating the rotation of the sub-frame rotation, the test results are compared to the analytical procedures in the Figure 5.4-4 for the IMF and SMF respectively.

The presented results are made without further attempt to collaborate them showing the blind output comparison of unknown solution. In the case of the IMF, the comparison shows better results as compared to the SMF. One reason may be that the joint model is disregarded in the model. Because of the high specification of reinforcing steel in the SMF, the joint is expected to engage higher level of rotation and shear damage which is not included in the simulation.

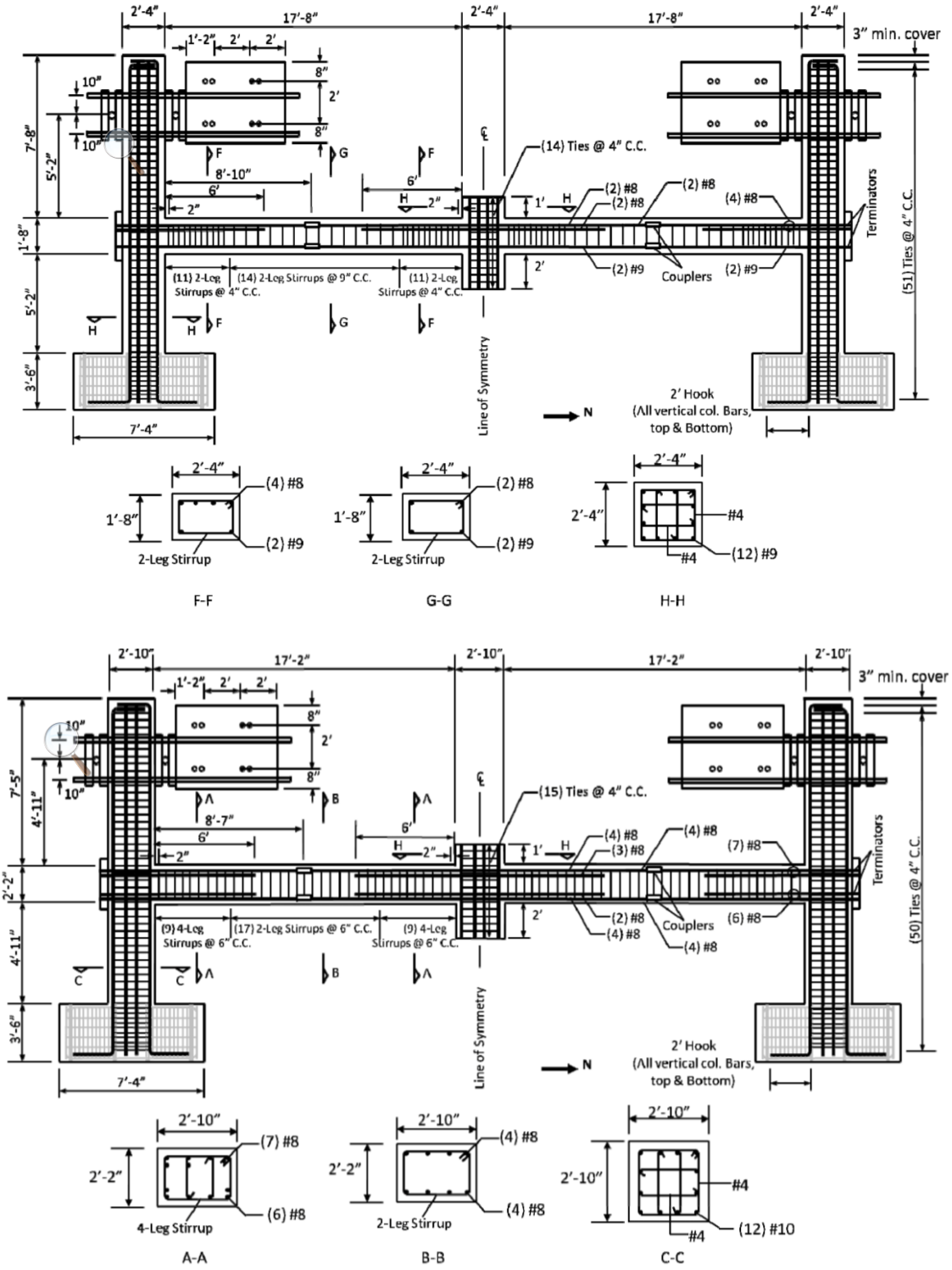

Figure 5.4-3 Detailing of the test specimen IMF, above and the SMF, bottom, (Lew H. , et al., 2011).

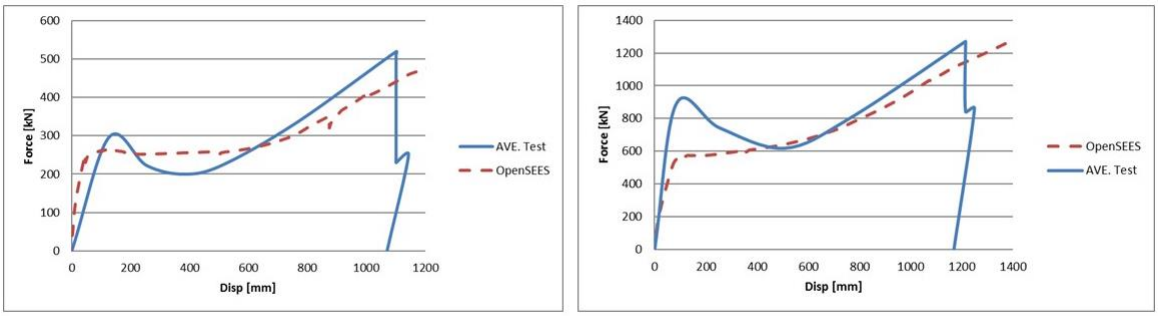

(a) The intermediate moment frame IMF (b) The special moment frame SMF

Figure 5.4-4 comparison of the standard OpenSEES model and the NIST test frame assembly

5.5. Summary and observations

The SFEM model based on FBE shows reasonable results, and the accuracy can be improved careful discretization. Compared to higher order FEM models, the SFEM still provide an efficient strategy bearing in mind the limited physical description of the erosion function, limiters of plastic deformation, and none objectivities of explicit integration schemes in rather solid problem. At the other side, it is shown that there is no need for artificial macro-element at the face of supports for the arching collapse and tensile catenary simulation in contrast to what perceived by (Bao, Lew, & Kunnath, 2012) and (Valipour, FarhangVesali, & Foster, 2013).

In comparison with the analytical model presented in chapter 3, while analytical formulation help double checking the correctness of input information, the SFEM possess the following attractive advantages.

- The boundaries of beam assemble can be modeled using structural FEM, the assumption needed about the equivalent stiffness of substructure is not any more cumbersome.
- The precise strain of the reinforcing steel is better predicted of the tensile catenary phase. However, the standard models of steel in OpenSEES will require special manipulation to match the real behavior to the rupture strain.

Referring to the modeling targets in Table 2.5-1, the quasit static simulation, presented in this section, performs the targets 1 and 2, and may be promising tool provided that complete set of key factors are sufficiently presented, yet the level of approximation is still questionable. To match all the targets confidently careful extension of the model is required, for e.g. the models of the joint, the column failure modes, and the floor element. And , regarding the target 3, the dynamic transition that includes free body motion/falling is required as already discussed in section 3.5.2.

Chapter 6 Uncertainty in modeling

6.1. Aim and abstract

The earlies sections show that the model of disproportionate collapse is possible yet require further development. To guide these developments, the uncertainty of the key modelling qualities must be mastered. The importance of this need stems out from the high sensitivity of the design and the safety assessment decision which is based on modelling. The far aim of this section is to identify the key modelling parameters in light of the sensitivity of the disproportionate collapse.

This chapter begins with isolating the key parameters, in the following sections, sensitivity of the risk independent approach is visited in terms of the impact of the chosen trigger point in the case of a RC multi-story building structure. The last shows that different trigger point will prescribe different component of the alternate load path (ALP). Then, the uncertainty results from the uncertain modeling parameters are analytically examined based on 2D frame example. These effects are reflected on the idealized structural response curve of the collapse mechanism with special attention to the need for well-defined column model.

6.2. Classes of uncertain parameters

Simulation of the collapse progression, like any other type of physical simulation, suffer from uncertainties. Apart from the possibility of human errors, a distinction between three type of uncertain parameters may be made;

1. **Mechanical (aleatory)** parameters of statistical/stochastic nature, e.g. material mechanical strength of concrete and the ultimate deformation steel, and the active load. These can be confidently measured, although they are uncertain. Therefore, they can be classified as a stochastic variable. Such uncertainty approached in literature by (Arshian, Morgenthal, & Narayanan, 2016) and (Yu, Lu, Qian, & Li, 2016). However, the following uncertainties are yet not discussed in the literature.
2. **Embedded (epistemic)** modelling parameters which are uncertain in nature. These are the physical quantities that perceived to present a key system parameter. For example, the displacement of the beam element at yielding, the system ductility, the length of the ***plastic hinge***, or even the dynamic increase and magnification factors. These are a hygiene factors which depends not only of the stochastic variables above, but also on the quality of the modelling strategy.
3. **Modelling** uncertain parameters. These are the results of the simulation, e.g. the reaction force or the total displacement and/or deformation of the simulated system. These are obvious to observe as a result of simulation, and the its impact on the decision is handled through what is known be ***performance functions***. This type is most difficult to handle, not only because of the composite nature of the uncertainty being based on the combined uncertainties of the above two categories, but also, it is difficult to find a solid benchmark to give a static prediction of the amount of the uncertainty. And the decision is based on them.

In fact, the quality of the analysis strategy is a minimization problem of the uncertainties, in particular, in the third category which inherits uncertainties of the first and the second. Therefore, the far aim of this chapter can be compressed in reducing the molding/analysis

uncertainties. To counter the absence of the analytical solution, or the solid test benchmark at the full-scale building level, different analysis strategy can be used and compared. Although it sounds straightforward, many of the modeling alternatives inherits some similar source of uncertainties. Thus, sound study of the modelling strategy is the firm prerequisite for successful uncertainty analysis, these are the most ambitious target of this section.

In the previous section, an overview of reported tests was presented. Here, I would like to reuse the leaned lessons by test in the context of progressive collapse analysis of RC building structure. Through this reflection, further analysis of the current research needs and the well-known principles are recycled in favor of the research goal. While the state of collapse, or of the static stability, is associated to the clear definition of the dynamic state of the collapse mechanism, two qualities must be handled in general;

1. the correct prediction of the collapse mechanism, the target 1 in Table 2.5-1, and
2. the correct description and assessment of the static and dynamic phenomena are the top challenges of this report. This can be understood in line with the target 3 of Table 2.5-1 realizing that target 2 is naturally embedded in the target 3.

While the statistical nature of the mechanical parameters is handled in standard design codes. The focus is given here to the parameters which are uncertain related to the safety assessment and the modelling strategy.

6.3. The sensitivity in the perceived safety of ALP

Provided that the element removal is an acceptable representation of a wide range of collapse specific trigger, the intensity of the collapse hazard or consequences will vary not only as function of the characteristic of the building, but also according to the point where the element is presumed to be removed. According to the location of the removed element, different analysis trigger scenarios are defined in the next section and two classes of material and structural parameter is distinguished.

6.3.1. The effect of changing the location of assumed loss of a single column

An earlier discussion of the following paragraphs was presented (Hatahet & Könke, 2014a), the similar analysis of the effects of the changing the column location was also reported later (Sagiroglu & Sasani, 2014), in their work they have use sab model and the conclusion supports our earlier (Hatahet & Könke, 2014a) and the following contributions.

Hypothetical 3D model-view of a multi-story building is shown in the Figure 6.3-1. In the assumed example the building is assumed ideally symmetric with a uniform; bay size and story height, reducing the number of alternative scenarios. The case of single column loss will be regarded in the following by Key Triggering Scenarios (KTSs), although here single column is handled here, it can be expanded to two or three column removal following the same structure. The identified KTSs are listed below; in the list numbers are allocated to each unique case of a possible loss of a single column element;

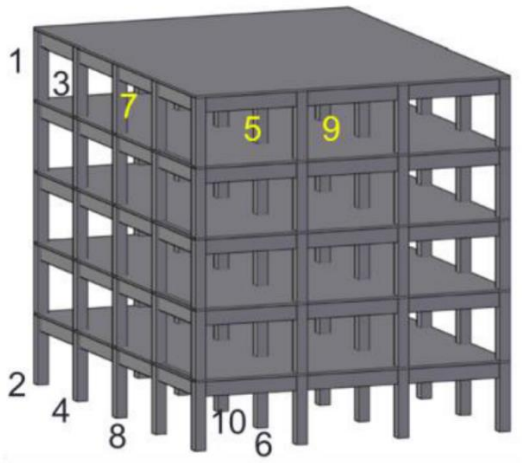

Figure 6.3-1 an example of the possible column removal scenarios

1. Corner top-level column (CT)
2. Corner bottom-level column (CB)
3. Near-corner top-level column (NT)
4. Near-corner bottom-level column (NB)
5. Inner-corner top-level column (IT)
6. Inner-corner bottom-level column (IB)

7. Edge top-level column (ET)
8. Edge bottom-level column (EB)
9. Middle top-level column (MT)
10. Middle bottom-level column (MB)

These the above KTSs are tabularized in Table 6.2-1 to explain the different resistant contributing phenomenon; these are labeled with reference to its location at the grid and at the two outermost cases; the most top level and the bottom one presented in Figure 6.3-1. The rows, of the table 1 present various sources of favorable modes of altering resistance (FMAR), these FMAR are a few un-observed phenomena in normal design practice using standardized structural analysis methods for RC structures. These FMAR rowed in table 1, in which the term altering indicates inherent contributions to structural robustness, are;

1. The compressive arching of the beams (CA-B), also referred to by compression membrane of the beam or the bridging action. For which horizontal support is required see for example (Yu & Tan, 2011).
2. The bending moment redistribution in beams (BMR-B) for which rotational stiffness of support is required (Qian. & Li, 2013) especially end joints.
3. The tensile catenary action in beams (TCA-B) for which the stiffness of the horizontal support is required. Sometimes it is called tensile membrane action (Bazan, 2008)
4. The compression membrane of the slab (CM-S), also called compressive arching or the bridging action. For which horizontal support is required (Park & Gamble, 2000), and (Bailey, Toh, & Chan, 2008).
5. The bending moment redistribution in slabs (BMR-S) for which rotational stiffness of support is required (Xuan Dat & Hai, Experimental study of beam–slabsubstructures subjected to apenultimate-internal column loss, 2013).

6. The tensile membrane action in slabs (TMA-S) for which horizontal support is required. Sometimes it is called tensile catenary action (Usmani & Cameron, 2004), and (Xuan Dat & Hai, 2013)
7. The presence of strong wall-panels or (SWP) (Talaat & Mosalam, 2008).

Table 6.3-1 Trigger scenarios and favorable modes of altering resistance (FMARs)

	CA-B	BMR-B	TCA-B	CM-S	BMR-S	TMA-S	SWP
CT - Corner top-level column	-	-	-	-	-	-	-
CB - Corner bottom-level column	PVA	PVA	PVA	PVA	PVA	PVA	ULs
NT - Near-corner top-level column	-	-	-	-	-	-	-
NB - Near-corner bottom-level column	PVA	PVA	PVA	PVA	PVA	PVA	ULs
IT - Inner-corner top-level column	-	FULL	-	-	FULL	FULL	-
IB - Inner-corner bottom-level column	P	FULL	-	P	FULL	FULL	ULs
ET - Edge top-level column	-	SD	-	-	FULL	FULL	-
EB - Edge bottom-level column	P-SD	SD	-	SD	SD	SD	ULs
MT - Middle top-level column	FULL	FULL	FULL	FULL	FULL	FULL	-
MB - Middle bottom-level column	FULL	FULL	FULL	FULL	FULL	FULL	ULs

- The (**Full**) indicates that the favorable action is fully deployed
- Partial (**P**) or partial due to Vierendeel actions or (**PVA**)
- **ULs** indicating that wall panels contribute to the upper levels only
- The favorable effects are available only in a single direction (**SD**)

Table 6.2-1 leads to conclude that the top-levels possess less potential of redundancy due to less FMAR. In contrast, triggers at the top-levels are not the most critical if the consequences are considered; bearing it is less likely to spread the collapse over a large service area. Whereas if triggers are applied at lower level, the vertical spread of the mechanism will result in more spread of damage in terms of the gross service area causing more severe consequences which may, even more, spread horizontally.

6.3.2. The key structural parameters (KSPs) for defined trigger scenario

We have gathered that the problem is two folds, where designers concern about the strength of the structural system under presumed scenario, risk analyst wants to address the question of 'what if it goes wrong/'. In such study a structural parameter, e.g.

mechanical strength of concrete or yielding of steel, can be sorted in two distinguished classes;

1. Design parameters (DPs); these are considered when well-established concepts of structural analysis are used, e.g. virtual work method. DPs are well defined by design guidelines and standards although these are changing with advancement of knowledge.

2. Robustness parameters (RPs); these provide an altering source of structural safety which is used to quantify the preserved strength (robustness) to an up-normal load beyond the design as defined in the DPs. these RPs are associated to the FMARs. The RPs are those explored by current researchers are corner stones in finding the answer to the 'what if' question of the collapse risk analysis.

Hence, in future, when a RP become will established, these may be included in the design guidelines, then it becomes a DP. Also, DP cannot be RP or wise-versa.

So, the numerical values of the provided robustness indicators in (7.3.5) are current values mapping the design now-how although it is still valid as benchmarks for; the level of robustness beyond design, and the level of development in the design practice. Having said this, it is also required to quantify the level of safety by design, and the level of safety by robustness, and the proportion of each with respect to the total preserve of safety. To illustrate the proposed framework, an example 2D frame is used as a case study.

6.4. The embedded modeling uncertainty

IN the following subsections, the uncertainty is presented analytically from the sensitivity of the simulation/analysis result to hidden modelling or simulation assumptions. The need for this evaluation stems out from the identified drawback in various modelling techniques as shown in chapter 2 and 5 alike. To comprehend the risk in modelling, discuss three key possible wrong decisions. These are;

1. The correct identification of the collapse mechanism,

2. The right interpretation of the full response path; the quasi static transition between the compressive arching and tensile catenary, and the perception of the dynamic amplifications.
3. The level of rigorous in the column modelling.

The above list is not more than example key points, others may be found with experiments; e.g. the presence of the infill-walls will alter the mode of failure, or by experienced investigation based on specific modeling toll or strategy.

6.4.1. The collapse mechanisms (CMs)

The collapse mechanism is the part of the structure including all members which experience non-linear response in material and geometry due to the assumed triggering scenario (KTS). Figure 6.4-1 illustrate an example collapse mechanism of a simplified 2D frame structure (a) in two possible further collapse propagations (b) and (c).

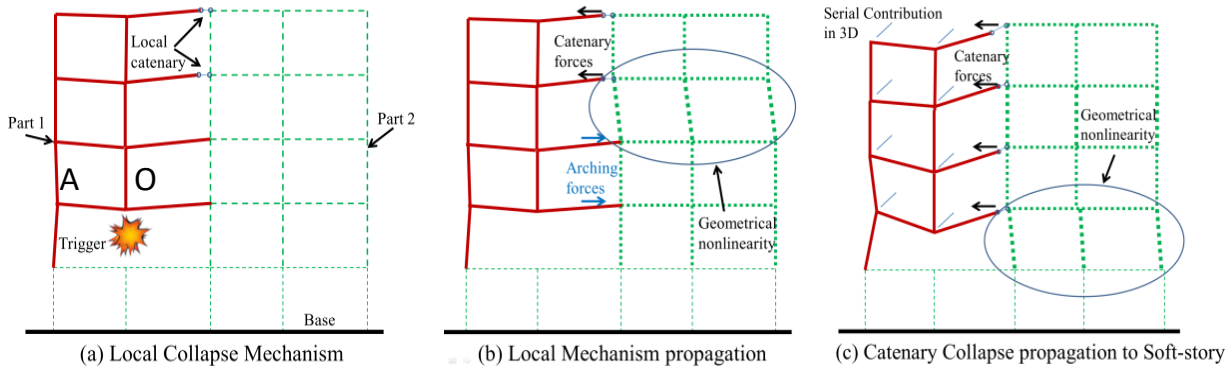

Figure 6.4-1 an example of collapse mechanism and two propagation scenarios

In Figure 6.4-1 (a), part 1 of the structures undergoes large displacement and therefore the analysis of this part must encounter for both nonlinearities; material and geometrical, while Part 2 does not nonlinearly response. In (b), the structural frame above, or the Vierendeel, bridging over the lost column develops tensile dominant forces at the upper beams being a cantilevering Vierendeel due to the lack of the lateral strength at the left side. These tensile dominant forces can result in an early catenary of the top two layers of beams. Also, such a couple of compressive, at the lower fibers, and tensile forces may develop soft-story mechanism which in turn undergoes large displacement, meaning that the key mechanism has spread to part 2. In (c), an alternative development of (a), part 1 is developing full

catenary over the four layers if loaded beyond its bending/flexural strength. Alternatively, if the acting mass of the mechanism passed the first peak of strength associated to the combined bending and arching, the full catenary forces at all levels of the beams are balanced by a set of tensile forces causing a soft-story at the bottom which also undergoes nonlinear geometrical response in the Figure 6.4-1 (c).

Those two simple examples points to the following;

1. Material and geometrical non-linearity are presents anywhere in the building model.
2. Progressive collapse model should accurately capture the possible single-column failure; at the left of the figure, or the sub-floor softening, at the right-hand-side of the figure. The failure of the latter can be derived from the single column failure; therefore, it will be discussed further later, and it will be regarded as a step column failure.

These points add to list of molding requirements of confident progressive collapse simulation in buildings.

6.4.2. The reaction curves of the progressive collapse in buildings

The analysis of progressive collapse in RC buildings ends at the point where the extent of damage result from the Trigger is defined. But, the reaction of the building to specific trigger depends on the articulation of the potential energy, and the exchange of the strain and the kinetic energy. Therefore, progressive collapse analysis is time-dependent problem unless the absorbed strain energy remains in the hardening reaction phase. Therefore, the analysis demands clear description of the energy exchange over process/history of the reaction. Due to the complex of test, it was shoe that results were approached either; through a quasi-static test set-up, or through dynamic loading and displacement or acceleration measurements. The links between the two is used to evaluate the dynamic implications of the problem when quasi-static procedure is performed perceiving that static analysis is simpler. In the following, reaction curves are classed in two groups; quasi-static and

dynamic. It should be noted that the following definition of the reaction curves is introduced as a description of the structural response of a building assembly although it is generally based on test results of fewer components.

6.4.2.1. The reaction curve of the quasi-static behavior

In the following a linear version of the force displacement curve is used. The curve resembles the observed patterns in the quasi-static test surveyed in the earlier sections.

To describe the overall response of the collapse mechanism, global response curve will be defined showing the quasi-static load-displacement path with two peaks of strength; the ultimate strength at C, and the dynamic ultimate strength of the catenary reinforcement at the point E, in the Figure 6.4-2. If the active loading level is higher from both peaks of strength, the trigger scenario will result in the full collapse of the superstructure above the floor of the trigger point.

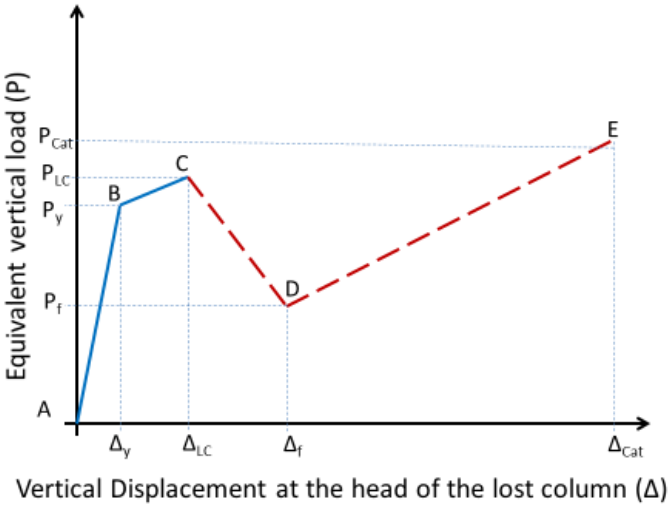

Figure 6.4-2 structural response curve of the forming collapse mechanism

Assuming the total equivalent applied vertical load is P_{Ap} which result from the elimination of the column at trigger point O, Figure 6.4-2, and the vertical displacement of the joint O is Δ, the P_{Ap} & Δ response curve for a forming mechanism will be idealized as shown in Figure 6.4-3. This is proposed by (Park & Gamble, 2000), analyzed (Qian. & Li, 2013) and tested; for

frame assembly (Yu & Tan, 2011), (Qian & Li, 2013) & (Lew H. , et al., 2011) and for floor and beam assemblages (Xuan Dat & Hai, 2013) & (Qian & Li, 2012).

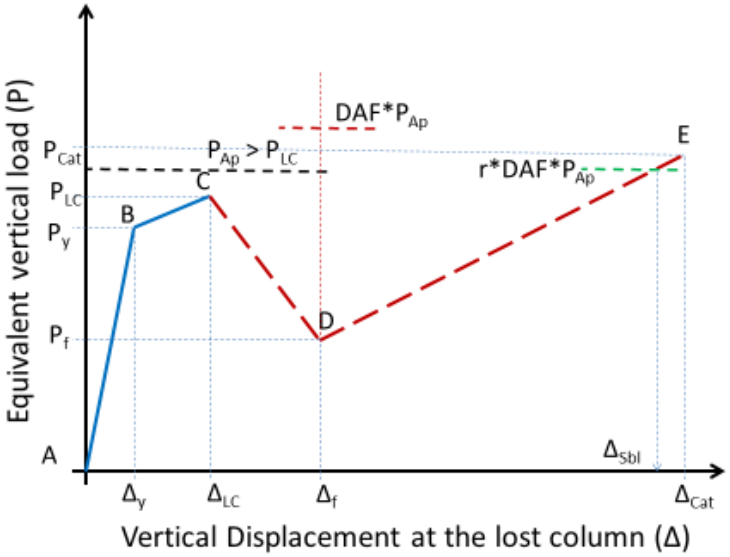

Figure 6.4-3 the dynamic amplification factor and the strain rate effect

The points B, C, D & E, defines the states of; the first yielding (y), ultimate strength of local collapse (LC) mechanism, end of failure (f) (or the beginning of catenary), and the ultimate catenary stage (Cat) respectively. It is important to note that this curve is valid by tests for mechanisms involve single story; there is not, to-date, any similar curve derived for a full mechanism involving a few stories apart from what is presented in (He & Yi, 2013) and (Xiao, et al., 2015). So, it is *assumed* here that similar trends can be observed by test or computer simulation.

A few researchers, e.g. (Punton, 2014), observed that if an early cut-off (rupture) of the tensile reinforcement occurs, the proportion CD will, then, show a snap-off point at which the bar rupture is clear observed on the reaction curve. This additional point is normally associated to the use of law ductility reinforcement. It will significantly affect the dynamic effects. Therefore, I shall stop at this point in more details later.

It is also important to highlight that if a single story-level was analyzed, the proportion ABC can be derived using relatively simple analysis, but if many layers are involved, e.g. Figure

6.4-1 (a), to derive the point C, significant material and geometrical nonlinearity take place across many contributing structural elements due to the local catenary at some components. For the part CDE, the structure will not only involve large geometrical nonlinearity, but dynamic analysis will be also required to include the inertia forces from the displacement (Δ_f -Δ_{LC}) of the mechanism mass at gravity acceleration (following the path CD). Also, the mass will reach loading speed at point D, then, the material strain-rate effects become essential to predict the point E. So, in Figure 6.4-3, when the equivalent load (P_{Ap}) is applied larger than the local mechanism strength, $P_{Ap} > P_{LC}$, the loading demand increases by the dynamic amplification factor (DAF) due to the inertia forces. If the favorable effect of increased strength of steel strain-rate effect is quantified in (r): r<1, the loading demand become r*DAF*P_{Ap}. If the last is less than the P_{Cat}, the local mechanism will not collapse. And the RP will be here defined by the vertical displacement at which the mechanism reaches a stable position is Δ_{Sbl}, Figure 6.4-3.

The response curve can be developed for either; a single independent trigger scenario or for any combination of any two adjacent columns, e.g. eliminating both columns under the points A and O, in Figure 6.4-1 (a), can follow the same analogy.

Visiting the above definitions of the KSPs, it can be noted that factors involved in obtaining response at points 'B' are, to-date, DPs. From C and beyond, FMARs contribute significantly and therefore there are many RPs which require reliable representation. However, the compressive catenary in beams (CA-B) has received significant attention, it is still a RP until a reliable standardized formulation became available.

Having defined the components of the idealized response curve for a general collapse mechanism, robust analytical formulation of strength and deflection response will be required which the subject of the author efforts following this point.

6.4.2.2. The reaction curves of the dynamic behavior

In chapter 3, we pointed out to the dynamic amplification factor (DAF) at the catenary point, I assumed that the equivalent dynamic load 'Py' maybe well-established using the current

state of knowledge provided that the reaction of the collapse mechanism remains in the arching-hardening phase.

In summary, the dynamic effects involve the equivalent dynamic increase of both load and displacement, also these dynamic effects are different when the reaction of the assemblage/mechanism is in the compressive arching or in the tensile catenary stage. Therefore, 4 different dynamic factors must be recognized, and all the parameters influencing these dynamic factors shall be accurately established. There were reported in chapter 3.

6.4.3. One column step propagation of the collapse trigger

The transfer from the point B to C, in the quasi-static reaction curve, is defined by the path from the beginning of the plastic deformation to the full development of the collapse mechanism. So far, the issue was addressed because of column loss. But what if the first lost column result in a single second column? And what if more than a single column is failed? The single column propagation will alter the failure mechanism engaging further plastic deformation of more elements, this is regarded here with the one step propagation, and the second lost column is regarded as the step column scenario. In the following, the earlier example will be expanded to discuss the possible consequences of the failure of a step column. The motivation is to identify potential loading states trying to name the bottom-line modeling requirements for progressive collapse analysis. As it will be shown later, the building/frame model of disproportionate progressive collapse is uncertain form the capability point of view of when the failure in RC column plays a significant rule.

When a supporting column is lost, below the point O in Figure 6.4 4 (b); the nearby supports will take additional load to keep the rest of the assembly in static balance as possible. Additional loading demand, result from the dynamic load, or the speed of loading. This is another phenomenon which can be addressed through transit analysis. Let us call the column, which is the focus of this section, the step column, the ‘step’ will hint that it is the case of progression of collapse. It also makes a clear distinction from the trigger column.

The step columns in the Figure 6.4 4 (b), depending on the location of the lost column, will take additional loading demanding higher strength in;

1. Shear and bending (case 1 directly above point O)
2. Combined flexure-shear- compression at the column AB,
3. Compression and side sway, or what is known as the (P-□□ effects. Also, demands in increase in the axial compression results in the column CD and below
4. It is also possible, depending on the size of the building, that soft-story mechanism forms shown between the levels 3 and 4 in the figure (b).

The global response curve earlier, distinguish different phases of repose of the collapse mechanism, Figure 6.4 4;

- Phase I: the semi-elastic hardening
- Phase II: the plastic hardening
- Phase III: the softening
- Phase IV: the plastic hardening in the catenary

Going back to the idealized response curve in the Figure 6.4 4 (a), the response of the collapse mechanism (shown in red in the Figure 6.4 4 (b) may stabilize in the phase II, or phase IV. The dynamic increase demand of on the mechanical strength will depend on the phase of the response precisely on the stabilizing phases the II or IV. The example case given in the Figure 6.4 4 exemplify the case of the column AB compressive softening while the collapse mechanism is still in phase II of the response curve. Other propagation scenarios may exist depending on the nature of the supporting structure.

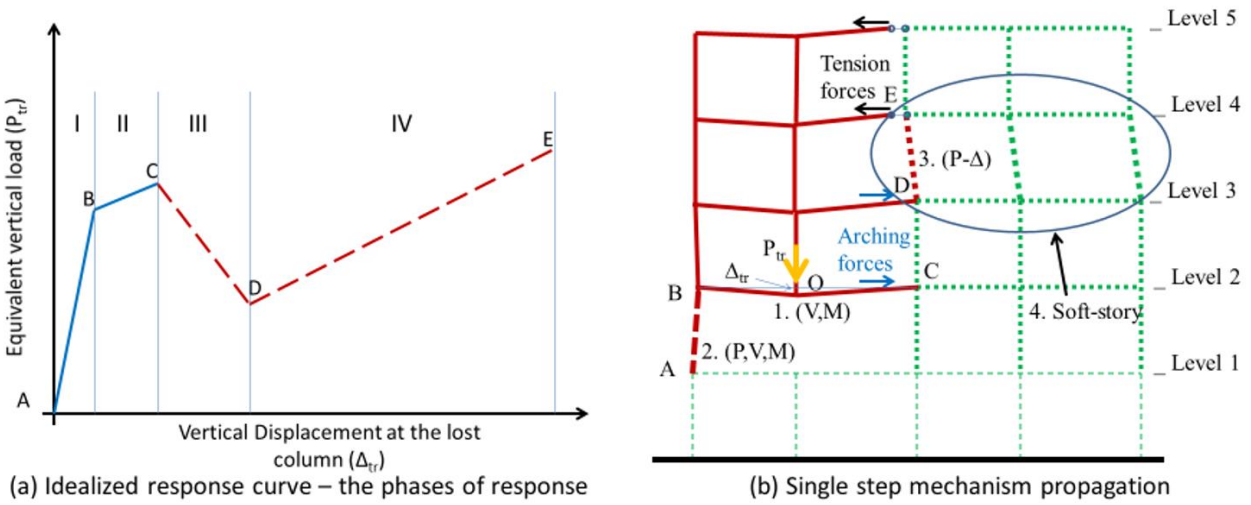

Figure 6.4-4 Illustration of the 'step' column progression of collapse scenario result from the trigger of column loss at point O

Therefore, the progressive collapse simulation, for the single step column case, must be sensitive to both the increase in the loading or the displacement demands/capacity. To date macro models are based on clear distinction between modes of failure in column; whether axial dominant, shear dominant or flexure dominant, before the analytical model cannot be used unless the mechanism is confidently predefined, therefore non-of these techniques is valid here because they are based on pre-decoupled failure mode analysis. Therefore, it is the concern here to find a computationally efficient universal column model that can be used for progressive collapse simulation of the building. Before surveying the options of column failure simulation, let us abstract the key limit states required for the step column from the above example, we will make a distinction between the limits defined by the static stability, denotes by the subscript 's', and the transit stability denoted by the 't'. The limits are summarized in the Table 6.4-1below in association with the level of response as defined by the idealized response curve shown in the figure 1. Before the limits are checked, the column must be classed; either with permitted lateral drift, or not. For example, in the Figure 6.4 4 (b), in the case of the column AB, it is the sole source of lateral stability and it is judged that the drift is permitted, also in the case of the soft-story. In such a case, P-D effects must be included in the simulation of the column.

Table 6.4-1 summary of the limit states of static and transit behavior

No.	The limit-states	Examples column – figure 5	Associated to the response curve
1	Pt	CD	Response phase II
2	Ps		
3	Pt and (Vt, Mt)	DE	Response phase II and IV
4	Ps and (Vs, Ms)		
5	Pt and (Vt, Mt, Dt)	AB and DE if soft-story	Response phase II and IV
6	Ps and (Vs, Ms, Ds)		

The failure of RC columns shall be discussed below, from the simplest case; e.g. axial compression dominant to the most complex cases of the combined loading effects. It worth to note here that not only the static stability must be satisfied, attention must be also to the dynamic increase in loading demand results from the transit nature of both the trigger of collapse and the progression of collapse.

6.4.3.1. Classes of test observed failures in the RC columns

In the following paragraph, prediction of the column strength will be visited through a tour in the most relevant literature. The structure of this tour will be based on first assuming that there is no lateral displacement at the column tip, or no additional shear of flexure is applied, then the role in lateral movement and forces will be reviewed.

6.4.3.1.1. Axial compression dominant RC columns

The dynamic axial compressive failure is tested in (Zeng & Zhang, 2012) under the dynamic axial load result from loading speed of 0.004 and 0.007 s^{-1}. As the results compared to the prediction of AASHTO LRFD Bridge Design Specification, and based on the strain rate effect on the concrete strength proposed by CEB-FIP MODEL CODE (1990), it has been observed that although results match the analytical formula for slender columns, the margin is increased, to the safe side, for the group of tested slender columns. The reported dynamic increase factors in steel are 1.014 and 1.017 respectively to loading speed in test earlier. The reported results give confidence in strength predictions based on similar capacity formulas.

I will refer to the term collapse mechanism to the structural mechanism that forms in collapsing structure, or part of it. The collapse mechanism at which the ultimate strength

can be accurately identified, will be regarded as the ultimate mechanism. The term 'accurate' means getting a result with high level of confidence. The start point of the mechanism is the point at which the very first element, of a structural assembly, drops stiffness although it may not significantly affect the overall stiffness of the assembly. Therefore, the term collapse mechanism is referring to the trip between the mechanism and the ultimate mechanism.

Although the primer purpose of the column is to take the vertical loads, columns take shear and bending forces due to frame action, or because of lateral (horizontal) loads. The most classical horizontal loads result from wind and earthquakes. Earthquakes effects on RC building have been receiving a lot of attention due to the critical role of the column and the reported deficiencies in the post-earthquakes surveys of damage. The recent development in this area have led to the distinction of different models of failure depending on the level of demand in the shear forces and the characteristic ultimate shear strength of the column. More classes have been defined when the post-peak behavior of the column is being observed also based on the shear demand to strength variance (Lodhi M. S., 2010). The reliable derivation of the ultimate shear capacity of the column remains an area of research. In the following paragraphs, the classes of columns response will be reviewed and discussed.

To facilitate the following classes, let us define the following variables;

- Vy is the lateral shear load associated to the point where tension reinforcement reaches yielding.
- Vp is the lateral shear peak load corresponds to the peak moment capacity of the critical section.
- Vn is the shear strength of the cross section

Based on the relationship between the above variables the following classes can be defined;

6.4.3.1.2. Shear dominant RC columns

As the column is subjected to increased lateral load or displacement, the column mode of axial failure is dominated by shear failure when the Vn < Vy.

The total deflection of the column at the peak strength can be evaluated summing up the three components of the deflection;

- the deflection results from slips of tension bars $D_{barslip}$; at the end sections of the columns where the flexure of the column produce tensile stress in reinforcements,
- The deflection results from the flexure of the column D_{flex}; this is can be evaluated from the aggregation of the cracks over the full height of the column depending on curvature at each section,
- The deflection results from the aggregation of the shear deformation, called D_{shr}, over the full height of the column.

Although the shear deflection can be neglected before the peak strength bearing in mind that limited inelastic flexural response is observed, the total deflection, in the post-peak, can be evaluated by adding the shear deflection, to the constant values of deflection resulted from bar slip and flexural evaluated at the peak.

Now if the shear strength of the column is larger from the shear at yield of the column, but not the ultimate flexural strength; $Vy < Vn < 0.95Vp$, the mode of failure still in shear but significant inelastic flexural deflection is expected. This will result in more pronounced shear deflection before the peak, while the rules of the post-peak remain the same.

6.4.3.1.3. Mixed shear and flexure dominant RC columns

Now if the shear strength of the column is close to flexural strength of the column, $0.95Vp < Vn < 1.05Vp$, mixed flexure and shear mode of failure is expected. Where the deflection can be evaluated using the same rules as the previous case, the post-peak deflection is a combination of the post-peak flexural and shear response.

6.4.3.1.4. Flexure dominant RC columns

If the shear strength of the column is higher than the shear force associated to the ultimate flexural strength of the column, $1.05Vp < Vn < 1.4Vp$. The difference is that in the post-peak

response, the deflection result from shear is fixed at the value evaluated at the peak, while both the deflections results from bar-slip and the flexure are continuous in the post-peak.

When the column is ductile, the column mode of axial failure is dominated by flexure failure when the Vn > 1.4Vp. The same rules, above, applies, although the shear deformation remains in the elastic range.

6.4.3.2. Reduced models of the RC columns

The above classification is based on drawing lines of distinction between different patterns of the column response observed by the test. Although empirical equations have been developed well matching test results, the reliability of these questions still in vague beyond the tested examples. The behavior of RC columns can be captured more objectively if the material laws can combine shear, flexure and axial effects in presence of confinement pressure result from the transverse steel. Although these can be modeled by most 3D FEM models to the peak point, it is not only computationally impractical; also models of the post-peak still require advancement. The concept of fiber section analysis permits the combination of the axial and flexural action with 1D confined and un-confined concrete models. The modified compression field theory (MCFT) (Vecchio & Colliins, 1986) provided a method to combine the axial and shear effect in shear panels. The model of (Setzler & Sezen, 2008) based on aggregating the deformations result from bar slip, flexure and shear although these are evaluated independently. An improvement is proposed by (Mostafaei & Kabeyasawa, 2007) through coupling the fiber section with the MCFT in what is called axial-shear-flexure interaction mode or the ASFI. although the three deformations are also aggregated to evaluate the total (axial) deformation, the axial deformation component results from the flexural effects is subtracted from the fiber section analysis in which the pure axial deformation is coupled with shear strain by the MCFT, the MCFT evaluate strain at every step of analysis the analyses based on force based finite element discretization. So the ASFI solve the interaction problem based on the assumption that the axial strain result from flexure is the same that satisfy the balance with the average shear in the discretized element. This first condition is called the compatibility and the second one is called the

equilibrium check. It is important to indicate that this coupling is reflected in the modified softening response of concrete in the 1D material model. The comparison of the empirical approach of (Setzler & Sezen, 2008) and the axial-shear-flexure interaction (ASFI) model based on the MCFT (Mostafaei & Kabeyasawa, 2007) is presented in (Lodhi M. S., 2010). These results show that the monotonic post-peak recorded higher strength than test data using the first approach, and less strength, or steeper inclination, when the second approach is used. However, both models show good peak approximation. In (Lodhi M. S., 2010) and (Lodhi & Sezen, 2010), it was proposed adding the buckling of the reinforcement bar and to delay of the coupling of shear and flexure to the ASFI, even though it only reduces the intense of the computations by single or two iterative steps, it shows good match of the shear response for the post-peak as compared to the fours specimens of (Sezen, 2002). However, when both bending and axial load are changing, in specimem-3, the simulated post-peak response is a lot steeper that the reported test data.

From computer simulation point of view, the empirical equations are implemented in the so called 'limit state material shear spring element' in the OpenSEES (McKenna, Fenves, & Scott, 2000), see for example (LeBorgne & Ghannoum, 2014), the model is relatively simple and computationally efficient. The ASFI model is sounder, from the theory point of view, however, it still computationally expensive to run for every column in 3D building model.

So far, the following conclusion can be drawn; the limit state based on the empirical equations can predict well the column response, although the model is computationally efficient, it cannot be considered safe as the response beyond the peak strength plays significant role in the analysis of the further progression of collapse. In contrast, the ASFI model, based on More-Columb failure criteria and enforced compatibility provide a safe compromise between the 3D-FEM simulation and the line-FEM although it is still computationally cumbersome if full-building model is implemented. However, these are based on well-developed concepts of the MCFT, the theory is developed based on the RC plate elements with uniformly distributed reinforcement in both directions. The thickness of the plate is relatively small compared to the other dimensions of the square plates and

so, the effects of the confinement of concrete of the element failure were net presented. So, it is believed that the MCFT is more suitable to the case of the RC deep beams and RC shear walls, and there for cannot be reliably applied to the reduced FEM structural model.

In order to implement large building models, reduced models are important due to their reduced computational cost. Although the proposed component based models reviewed earlier seems to approach the modelling requirements for seismic response simulation, collaboration of the model is yet a long process with is not only full of expert judgment, it does not seem to naturally replicate the real behavior unless the mode of failure is known

6.5. The modelling uncertainties

As mentioned earlier, Figure 6.4-1 shows two possible *assumed* propagation scenarios; (b) and (c) for the local mechanism (a). However, there are further collapse propagation possibilities; e.g. compressive collapse of the column under the point A, or the shear collapse of the column just above the point A in Figure 6.4-1 (a). These have been excluded to focus on the lateral spread only for illustration, back to assumed scenarios, the structural model required for the correct derivation of the curve in Figure 6.4-3 will gradually expand, evolve, to further proportions undergoing geometrical non-linearity (large displacement). For such model updating, may be a single full-building model is required. Such a model, to date, is not practically available especially when all contributing components are required for the economic scale of the safety decision. So, while the point B, in Figure 6.4-2, can be predicted using contemporary FEM codes, points C, D & E demand experience and judgment, so uncertainty is in present due to many factors, some are discussed below.

To illustrate some of the recognized modelling uncertain parameters, and the propagation of the natural uncertainties, the modeling tool developed in chapter 5 here will be reused.

6.5.1. Prediction of ultimate arching strength at the point C

The location of the point on the response curves is linked to the associated strength and displacement. In the deterministic analysis, the ultimate strength is linked to the strength of concrete, the ratio of the main reinforcement and the level of arching force. The arching

force, in the RC structures, can improve the bending strength while it is within the small eccentricity region of the interaction diagram. In contrast, if high arching force is being to develop in the large eccentricity zone, it can reduce the overall bending strength. In all cases the presences of the arching forced will reduce the value of displacement at which the ultimate strength is obtained when the balanced force equilibrium is applied at the beam element level. The level of confinement, or the transverse reinforcement in beams and columns, is a secondary parameter which can increase the named displacement when confinement is increased. The developed analytical tools in chapter 3 and 5 are both capable in reflecting the listed relationships. However, the used models are all approximate, and considerable safety margin is needed in the case of direct design.

In the case of 2D frame, uncertainty is combined; Figure 6.4-2 (a) proposes the response of the structure to the trigger event. If the model did not accurately consider, for example, the P-Δ at point A, P_{LC} will be overestimated. Another example, if various reinforcement configurations are provided at different levels of the frame, correct force redistribution demand detailed nonlinear model. This uncertainty will be present over the whole following proportion from C onward to E.

6.5.2. Prediction of the proportion CD

At a single beam level (Yu & Tan, 2011), CD proportion varies depending on; the concrete crashing point, or shear-normal-forces-interaction and buckling then fracture of compressive bars or even another concrete crash at the other end of the beam. At local mechanism level, the prediction depends on how many sections are involved. This may also evolve further contribution of stirrups and friction.

Correct prediction of the CD is essential to quantify the DAF defined in the section 3.5 of the chapter 3, and it is believed that this proportion is yet left out by researchers. In the analytical modeling tool of the chapter 3, linear bending damage is assumed. And in the modeling strategy of the chapter 5, the post-peak damage rate is related to the number of

fibers in the section, and to the chosen time step. Therefore, in both of them, artificial assumption is used although good results were presented.

6.5.3. Prediction of the proportion DE

The increased dynamic potential due to some sort of kinetic energy develops with collapse progression from C towards D absorbed by the strain energy via the catenary in the remaining steel reinforcement here. This is connected to the following events:

- At the element level; either a complete fracture of bars' set of reinforcement layer at either ends of the bean, or complete bars pull out, or joint failure at any section.
- At the mechanism level, there will be as many possible, stable bottom locations for the point D, as elements involved evolving along the way to point E until point of stability is reached.

Then, the response curve is subjected to various levels of uncertainties under the current modeling capabilities hinting the need for large number of test data enabling probabilistic analysis for the development of reliable models. However, the discussed dynamic amplification is not yet considered in literature, the work in (Orton S. L., Development of a CFRP System to Provide Continuity in Existing Reinforced Concrete Buildings Vulnerable to Progressive Collapse, 2007) show that simple analytical formulation can describe this proportion of the response curve.

6.6. Summary

In this chapter modelling uncertainties are presented in relation to the definition of the response curve of the collapse mechanism. In additional to well-established statistical mechanical parameters such as the properties of material, embedded and model-based sources of uncertainty are distinguished. Those sources of uncertainty are linked to the response curve based on simplified 2D frame model through which an event based evaluation is employed. Aiming at careful evaluation of the correct collapse mechanism, these uncertainties must be systematically handled to obtain reliable simulation. These

issues are discussed in the next chapter with focus on measuring overall system structural robustness which can be also extended to be used for model reliability assessment.

Chapter 7 Robustness framework

7.1. Aim and abstract

Reliability and robustness is here defined with focus on the disproportionate collapse safety of structures. Linking to previous chapter, these can be redeployed including the reliability of modelling strategy. Then, it is aimed at unified reliability and robustness that consider modelling and structural reliability in an integral framework.

In this section, general robustness criteria are presented and linked to general concepts in *reliability based design*. The proposed index of robustness is built along-side new fit-for-purpose performance functions, or sub-risk functions, which are integrated through logic three, the tree reflect the uncertainty modes of failure in disproportionate collapse analysis. These functions are provided in both deterministic and stochastic form. Where the deterministic form provides a quasi-fuzzy definition of the risk/safety state of the structure, the stochastic form aims at the reliability measurement in line with current trend of the design codes. At last, the model quality can be realized through the minimization of an

objectivity function in presence of a set of modeling uncertain parameters, such parameters discussed in chapter 6.

7.2. Introduction

In earlier sections, proposed analytical techniques for disproportionate collapse analysis are presented and validated. Uncertainty in modeling and analysis are qualitatively presented in earlier chapter. In this chapter, these methods will be redeployed in an integrated safety assessment framework, the framework aims at objectively quantifying the level of structural robustness, or safety. The structural robustness here refers to the versatility and the level of resilience in the structural systems inherited by the structural design to accommodate an abnormal event without having the initial damage to spread disproportional from the trigger event.

The framework developed in the following section is an extension of the work of (Hatahet & Könke, 2014a) and it is applied to the case of a building structures.

Using either the direct analytical method, or the structural FE, it was shown that results of the model is still sensitive to modelling parameters. These parameters require sometimes high level of engineering judgment which make the result uncertain. Also, it has been shown in chapter 6, that many of local failure mechanism cannot be yet captured by the modelling strategy, therefore well-informed judgement is also required which is also another source of uncertainty. To make a reliable decision, then, the following streams of uncertainty need to be systematically covered;

1. Event uncertainties;
    a. Related to the type of the trigger effects e.g. it can be reflected in the uncertain number of the initially damaged supporting elements.
    b. Related to the location of the trigger. It has been shown that the location of the column possesses different level of reacting mechanism.
2. Modelling uncertainties based on;
    a. Assumed material and geometric information; e.g. material properties.

b. The embedded simulation uncertainties; for example, the SFEM approximation of the collapse mechanism; location of the integration points, the error in the length of the plastic hinge, and the tight representation of the failure mode.
c. The method of quantifying the dynamic increase factors and the point of stability.

Although a distinction is made in chapter 6 between the embedded modeling and the modeling uncertainties, we will discuss them here in a single category as modeling uncertainty. Regardless of specific simulation strategy, we presume the interdependence of the embedded modeling and the modeling uncertainties can be established by the well-trained user of the simulation tool.

7.3. The structural reliability analysis

The main steps in system robustness assessment can be taken as a problem of structural reliability against disproportionate collapse. In general, the following steps are needed;

1. Define the target level of reliability, which forms the baes of the performance based design for which the buildings regulation is consulted.
2. Name all possible failure modes, for each the reliability index must satisfy the standard.
3. Decompose the failure modes into elementary events which are the component of the major mode of failure. Event-tree can be used to handle this step.
4. Functional formulation of the failure criteria (limit state functions) for each component in the modes of failure. In the following we propose criteria for the ALP analysis.
5. Isolate the uncertain (stochastic) variables and the deterministic ones by sensitivity analysis.
6. Calculate for each mode of failure the level of structural reliability. A method is proposed below.

7. Improve design to meet target criteria of reliability named in one above.
8. Perform second round of sensitivity analyses, and go back to 5 when targets are not met.

The first item, above, is specified by the design norm. Items 2-5 are discussed in chapter 6, the focus here is on the item number 6.

To achieve a reliable design, or reliability analysis, of the structural system, on the following methods can be followed;

1. Method 1 – the use of characteristic value to represent the uncertain variable; e.g. the coded defined strength of steel and concrete, which is based on the reliability defined in the material parameter directly.
- Method 2 – The uncertain value is represented by the mean and the deviation. e.g. the reliability index method.
- Method 3 – The uncertain value is represented by a specific density and distribution function. e.g. the reliability here is defined by the probability of failure. This is the motivation to present the performance functions in the stochastic form, these are provided in the section 7.3.5 below.
- Method 4 – The sequences of the event is combined with the probability in the same function of which an optimal reliable performance is foreseen through the minimum negative sequences of the maximum value of return/gain. IN support of this method, the risk index is introduced in the section 7.3.7.

While the problem in hand, in most cases, is related to an existing structure, or to the design of a seldom event, path 1 is considered unsuitable because neither additional uncertainty, nor the current level of reliability can be precisely established. However, the other three are all possible alternatives.

While reliability is linked to the probability of failure, let us begin by defining the probability of the disproportionate collapse.

7.3.1. The probability of the disproportionate collapse

A few researchers introduced concepts and probabilistic frameworks to define clear distinction between various risk parameters. In (Starossek & Haberland, 2011) clear boarder between the role of structural engineering in the robustness assessment and other mitigation strategies has been suggested. However, when more information about the location of the hazards in the structure is available, it enables enhanced safety mitigation measure as coupled with awareness of vulnerable collapse mechanism (Asprone, Jalayer, Prota, & Manfredi, 2010).

The push-down collapse mechanism under single column loss received attention by (Xu & Ellingwood, 2011) & (Kapil & Sherif, 2011). However, this is a risk independent approach, in the proposed framework here, the total probability is linked to the type of risk (risk dependent) as more informed assessment decision can be made. An example robustness index is defined using pull-down process (Lin, 2013), or any other set of indexes can be used, as it will be shown in the following sections.

Using the alternate path (AP) approach, various levels of risk result from changing the location of the lost column and there are a few factors that contribute to the inherent safety in the redundant supporting structure after a column is removed. These factors are dependent on the triggering scenario (T) and the failure mechanism, the triggering scenario is defined by each location of the lost column. Bearing in mind that the collapse mechanism can cause local failure or can result in collapse progression (disproportionate collapse), a method for global probability assessment is proposed based on (Baker, Schubert, & Faber, 2008). In this single probability of collapse, the total probability is evaluated aggregating all sources of risk. The main function of this index is to aid the decision of safety assessment being uniformly deployed in a single equation or index conveying the risk level in a redundant building structure, which is based on the alternative load path (ALP) approach.

7.3.2. The structural robustness

According to the EN 1991 1 7 accidental actions (CEN, 2010), the robustness can be defined by;

'Robustness is the ability of a structure to withstand events like fire, explosions, impact, or the consequences of human error, without being damaged to an extent disproportionate to the original cause.' (CEN, 2010)

In the recommendation for the design strategies;

'Adoption of the following recommended strategies should provide a building with an acceptable level of robustness to sustain localized failure without a disproportionate level of collapse.' (CEN, 2010)

In the section of the recommended risk mitigation measures;

'Overcome the hazard by providing, for example, increased reserves of strength or robustness, availability of alternative load paths through structural redundancy, or resistance to degradation, etc. *(CEN, 2010)*

The definition is wide in scope, therefore, an attempt of more precise mean of quantifying disproportionate collapse robustness is made here.

7.3.3. Safety assessment framework

In figure 4-1, adapted from (Starossek & Haberland, 2011), it is proposed that the risk-independent analysis approach does not consider the increased likelihood of trigger event due to the presence of sites-specific risk, e.g. gas supply pipe near a column. Therefore, the probability of the trigger event P_T and the opposability of the site specific risk P_{SR} are here decomposed. It is clear that the change in the position of the trigger point results in change of the risk level of disproportionate collapse. In another word, each site condition defines different level of risk affect the likelihood of progressive collapse when matched to different trigger point of the examined structure, in the proposed frame work, it is referred to be

design/analysis scenario (i). However, this has been discussed by (Asprone, Jalayer, Prota, & Manfredi, 2010), little attention is given to the quality of simulation of the structural mechanisms and the economic implication of its structural parameters. So, no uniform safety assessment can be performed in isolation of the site information, structural character of the facility and the quality of the simulation/analysis technique.

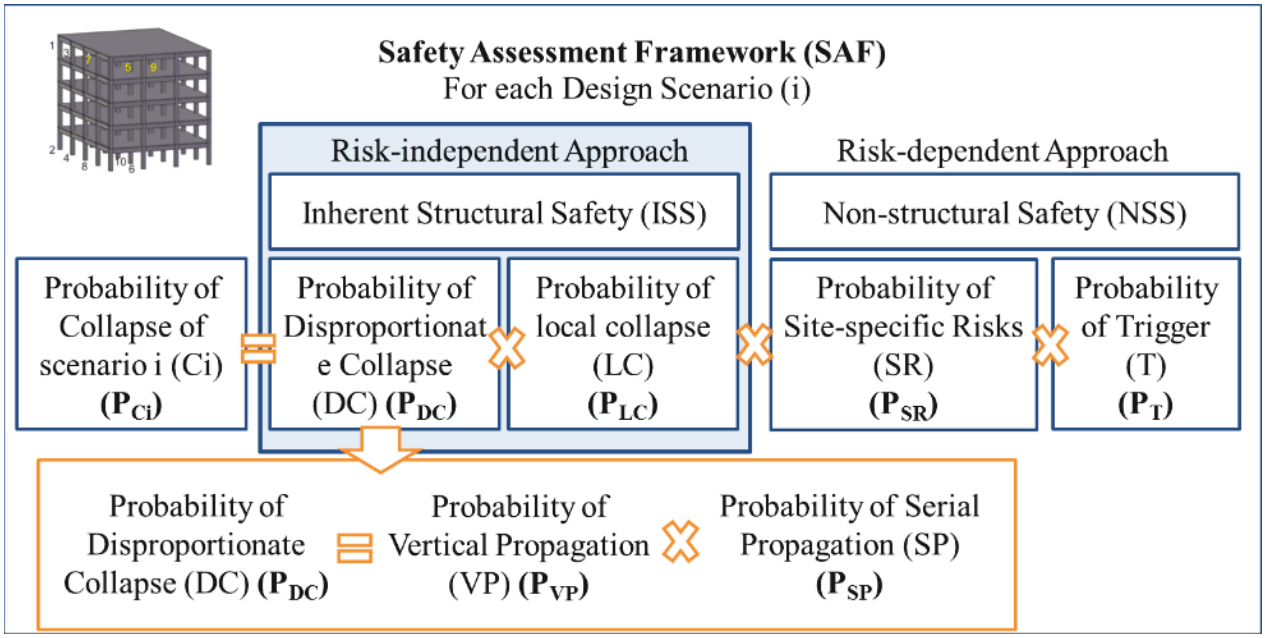

Figure 7.3-1 Outlines of Safety Assessment Framework (SAF)

To consider the link between the direct and indirect risk, assume, for a specific structure, there are number of N_{TS} possible trigger scenarios. For each trigger scenario, with the probability in time P_T, there are; the probability of site-specific risk $P_{SR,}$ the probability of local collapse P_{LC}, and the probability of disproportionate collapse P_{DC}, in this case, for each trigger scenario i, from; 1 to N_{TA}, the probability of collapse of a single scenario i in the life time is P_{Ci} is therefore given by;

$$P_{Ci} = (P_{LC} * P_{PC} * P_{SR} * P_T)_i \dots\dots (7.1)$$

Then, the total probability of structural disproportionate (progressive) collapse is defined by the integration over the full triggers domain;

$$P_C = \sum_i P_{Ci} \dots\dots (7.2)$$

Meaning that the structure can collapse by either trigger scenario i = 1, 2, …, or N_{TS}. Not covered yet are those relating the size of the assumed event, for example the number of columns to be eliminated for a specific scenario such as the flood effects introduced in chapter 1. In the example shows full row of columns were removed due to the full slide of the foundation.

The objective of robust design can be expressed here by increasing the safety of the structural system, or reducing the risk of the disproportionate collapse.

According to (Baker, Schubert, & Faber, 2008), if the risk of trigger, non-structural related, is R_T, and the risk of the structural disproportionate collapse is R_{DC}, the structural robustness can be objectively formulated by the global structural robustness index I_{SR};

$$I_{RS} = \frac{R_T}{R_T + R_{DC}} \dots\dots (7.3)$$

Then, minimizing R_{DC}, or maximizing the I_{SR} is the goal of the analysis, which can be termed by the inherited structural safety or robustness. The terms risk R and the probability P of failure are here antonyms. The same index is also adopted by the (Sørensen, 2010) and (Canisius, 2011).

The problem in the probability measure, as suggested in Eq. (7.2) and (7.3) is that it loses its objectivity when applied to undefined trigger location, e.g. the location of the assumed lost column, see chapter 6. Because, the higher the redundancy of the structure is, the more the trigger points, the higher the accumulated probability, therefore, an alternative quantification measure is required, this is presented in Eq. (7.18) below. And the named measures; P_C and the I_{RS}, shall only be applied on a single trigger location.

At last, the probability of the disproportionate collapse is also decomposed into vertical and serial propagations, because this detection can be identified reviewing the different classes of partial collapses presented in chapter 1.

7.3.4. The inherent structural safety

The focus here is allocated on quantifying P_{LC}* P_{DC}, or the R_{DC}. The other terms are discussed by other researchers see for example (Asprone, Jalayer, Prota, & Manfredi, 2010). It is a challenge to give a quantified probability of local collapse or progressive collapse; it is even less realistic when assessed independently from the trigger.

Before moving to the quantification of the structural safety, inspired by the seismic structural safety, the concept of disaster is here introduced. Popular example is the major floods, just like the those of the North Sea in 1957 and 2007. Another extreme example of the manmade disaster is the war; e.g. the second World War or, the war in Syria. Where the purpose of the structures is to provide a shelter, it is an ethical mandate of the design codes to impose more attention to post disaster human safety. While nothing is impossible, in contrast with controlled demolition, we may be able to extend the time of the structural failure giving the inhabitants more time to evacuate. These terms can be presented as shown in the Figure 7.3-2(Hatahet & Könke, 2017b) .

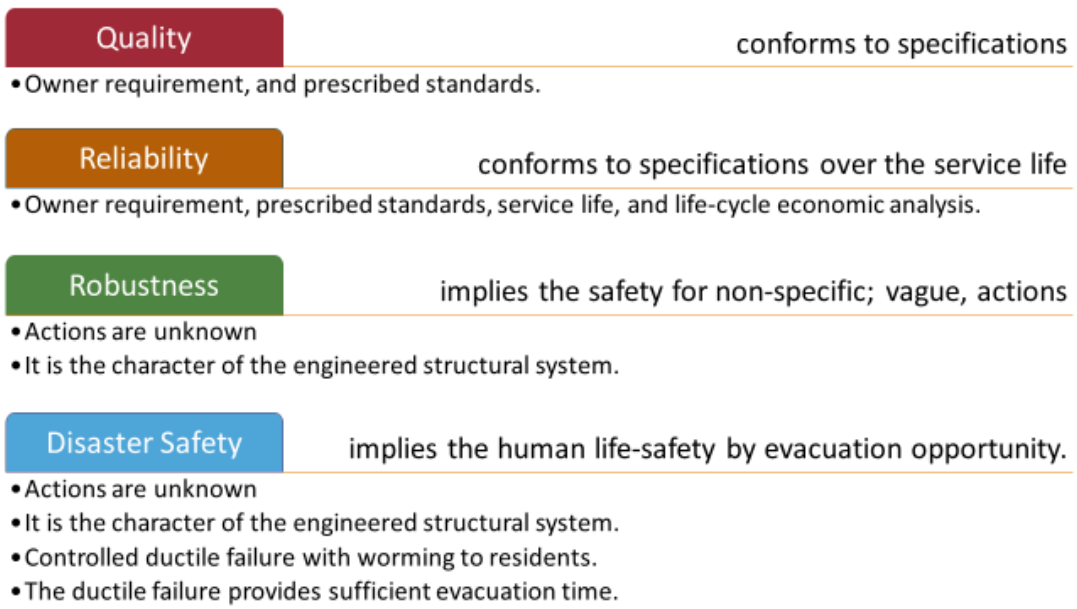

Figure 7.3-2 introducing the mandate of the disaster level of safety for modern design standards

The term 'structural robustness', in (Starossek & Haberlan, 2010), is often used referring to the same concept of the inherited structural safety; as coined with the structure character,

minimizing the P_{DC} is the objective here. It is accepted by standards that if the alternate load path (ALP) was successful to transfer the load through a non-linear dynamic response, the local collapse is unlikely and so the structures are perceived safe. However, the probability associated to abnormal event extends to the what-if scenario. E.g. what if 2 columns where severely damaged, or what if strength was overestimated, especially analyzing an existing structure. Especially, it shown by (Orton & Kirby, 2013), also discussed in chapter 3, the incremental dynamic analysis is unable to predict the right dynamic amplification beyond the arching strength. So; it is useful to find the level of inherent safety available beyond the analyzed scenario and the probability of collapse accompanied by proper handling of the dynamic effect. Subsequently, a quantification method is required. In the following, measures of structural robustness index are proposed, referred to by RI. These are presented in section 7.3.5, and thereafter it is linked to the R_{DC} casting in Eq. (7.3) to obtain a single global measure for a single trigger location.

To aid the presentation of the RI(s), the simple example, used in section 6.4 of the chapter 6, is here reused. A summary of the framework is shown in Figure 7.3-3. In the figure, the first window assumes a trigger scenario; a loss of a single column. In the second window, only two possible collapse progressions are presented. However, due to the limits of current numerical simulation models, varying assumptions can result in switch between different models, as discussed in chapter 6, which can result in more than response scenario, these are shown in the window number 2. In the third window; introducing uncertainties to the points C-D-E identified on the idealized (linear) response curve, variance in the key measures of response is shown. Consequently, the accuracy in the response curve is critical to identify the safety level in the analysis and design. Then depending on the level of articulation of the used simulation models, uncertainties in producing points C, D and F which can be reflected in safety factors deployed in robustness assessment comparing predicted loading to predicted strength with attention to the dynamic (force) increase factor (DIF). The later results from the loading rate (r) expressing the loading speed of the applied load P_{Ap} while reaching the strength points at C and D, these are shown in window 4. To assemble a single

robustness indicator, all possible collapse progression scenarios are structured in decision tree and quantified with the single probability index accumulating single progression probabilities and weighing them up with the severity of the sequences. An example of the decision tree is shown in the window 5. The used terms are explained near the window 5 of the same figure.

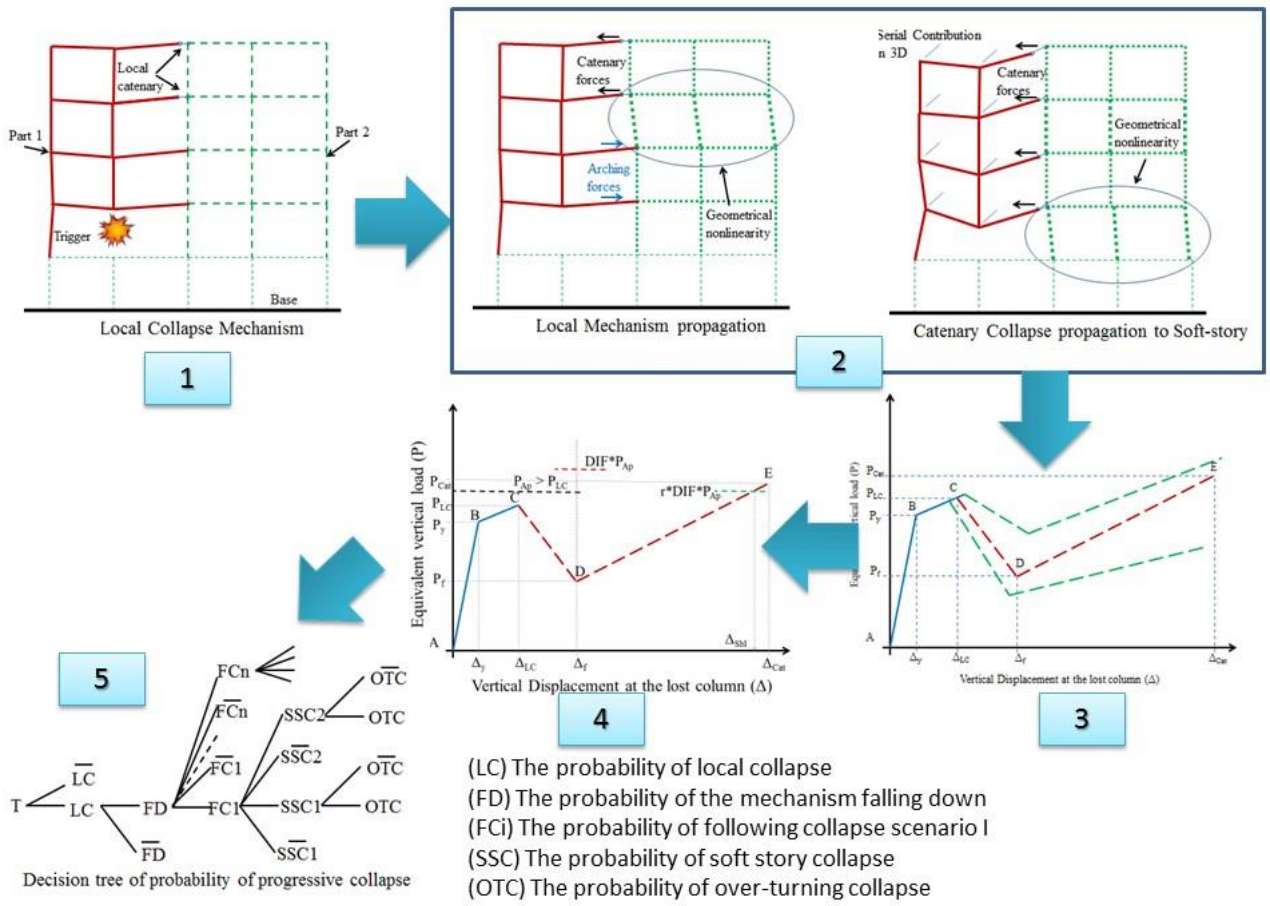

Figure 7.3-3 the framework for structural robustness index (RI), (Hatahet & Könke, 2014a)

While processing the decision tree require careful development which is a challenge in itself. At each exit of the tree, a probability of propagation scenario exists. The sum of all scenarios must be equal to one.

Although the decision tree presents a challenge, an advantage can be also realized in smart algorithm guiding the deployment of the computing effort. For example, due to the uncertainty, alternative collapse progression scenario can be implemented in parallel

computing. And for each scenario, based on the analytical knowledge of collapse mechanism, the domain can be decomposed. Those two strategies can result in significant reduction in computational time. As suggested, it will promote the quality of the modelling strategy, if, for example, multi-scale simulation can be implemented in an adaptive modeling algorithm in which the damage evolution can be reproduced by meso-scale simulation minimizing the error, and promoting the robustness of the model. The last stream is not perused here due to the time-scale of this work.

7.3.5. Indexes of structural robustness

To measure structural safety through structural robustness indexes RIs, the RIs will be defined then the analytical probability is provided in an example decision tree. The following is an extension of the earlier report (Hatahet & Könke, 2014a). Due to the uncertain nature of each of the key point of the response curve, the RIs are also presented in probabilistic form;

In the earlier example the following key events were identified; the trigger (T), the local collapse (LC), the fall–down (FD) of the above structure (this is an example of the vertical collapse propagation named in section 7.3.3), the serial collapse (SC) propagation, and the total collapse (TC). Under each of the sub-class, additional uncertain paths are possible depending on the modelling capabilities, for example, the SC can be caused by a soft-story, or an over turning of the serial structure. In order to handle such modelling uncertainty, aware judgment of the modeling tool alongside a well-structured logic tree is required. The logic tree for the simple example is see in *Figure 7.3-4*.

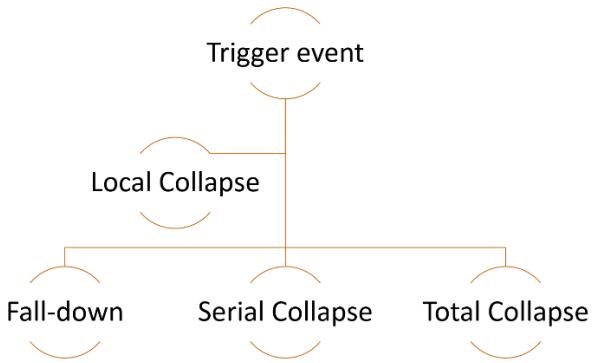

Figure 7.3-4 an example of the logic tree of the level of disproportionate collapse

Each even of the tree is a candidate end-result of the analysis. However, the rout of each of them can be rather complex and required careful modelling consideration. To illustrate this, the logic tree is extended by the rout causes of each of the main events, then the item which has more than one key cause required specific handling. To avoid complexity, in light with example modes of serial propagation shown in Figure 7.3-3, two subsequent events are extended of the main serial even category. This even with multiple cause is then underlined in the *Figure 7.3-5*.

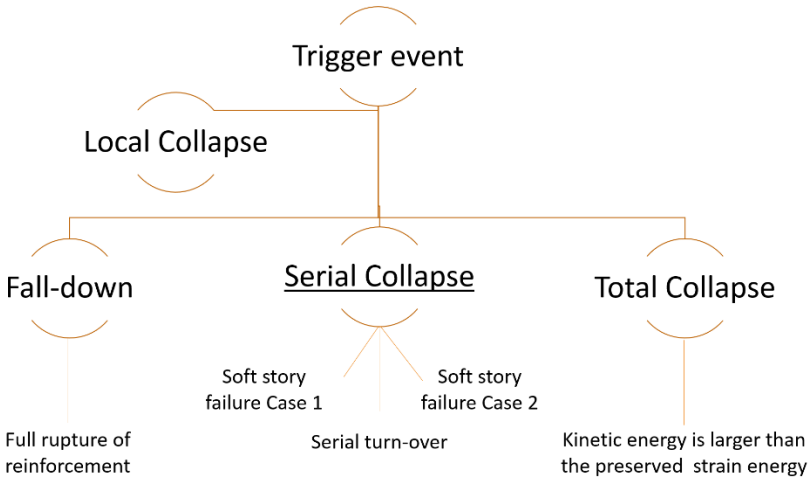

Figure 7.3-5 the example logic tree extended with the rout cause of each event

The degree of inter-dependence between different events must be evaluated because it affects the numerical quantification method. In the given example, the local collapse proceeds each of the three other events. While the FD and the SC can be considered independent, the total collapse can be a result of FD or the SC. Then either of which is a rout cause of a total collapse and shall be then considered. Based on the provided classification presented in the logic tree, relevant robustness indexes are presented in the form of; limit state functions, and the complement probability, which is the probability of failure. The last is useful to judge the quality of limit state function of the RI in light of specific modelling assumptions.

7.3.5.1. The probability of local collapse (LC) and the risk index RI_{LC}

The local collapse (LC) mechanism refers to the minimum, rather inevitable, level of damage directly following the trigger event, therefore, the scalar P(LC), denoting the probability of the local collapse, is the linked to the triggering effect. Where; P(T), is denoting the probability of a trigger or an event. Direct association between the force-based risk index, and the probability of collapse can be made as follows;

$$RI_{LC} = P_{Ap}/P_{LC} \quad if \quad RI_{LC} \geq 1 \leftrightarrow P(LC|T) = 1 \; otherwise \; P(LC|T) = 0 \ldots\ldots (7.4)$$

The P_{Ap} refers to the value of the applied equivalent static applied force, which refers to the load result from the active mass of the mechanism, and the P_{LC} is the strength of the formed local mechanism. Therefore, if $P_{Ap} > P_{LC}$ the trigger event will cause local collapse, and then the probability of local collapse result from trigger event is one.

While both the applied action and the strength of the reaction are uncertain quantities, the probability of the local collapse will then vary between zero and one. The probabilistic version of the deterministic association above can be expressed in terms of the load/strength (P) variation around the two deterministic values of P_{Ap} and P_{LC} by;

$$P(LC|T) = \int_0^\infty F_{LC}(p) \,.\, f_{Ap}(p)dp = 1 - \int_0^\infty f_{LC}(p) \,.\, F_{Ap}(p)dp \ldots\ldots (7.5)$$

Where; the F is the distribution function of Local collapse or applied load, and the f is the density function of them.

The local collapse can be avoided if the structure can react without tangible damage, then there is no local collapse, the local collapse is the failure of parts of the mechanism but the mechanism remains stable. However, if it does not stabilize, there are three alternative scenarios, figure 2-11:

1. The proportion directly above the trigger will fall-down (FD). This can be translational and discontinuous, or rotational and connected.

2. The formed mechanism spreads laterally to cause; either pull down, soft story, or over-turning of the serial structure, call it the serial failure (SF).
3. The momentum generated the FD, and/or with the SF, will cause a total collapse (TC).

Each of the three streams of events can be considered independent or mutually exclusive, and therefore it satisfies the conditions of the axioms event, and their probability is independent.

7.3.5.2. The probability of mechanism falling down (FD) and the RI_{FD}

After the bending, or compressive arching, failure the mechanism transfers into the tensile catenary. Here there is two possible reactions; it stabilizes on catenary, or one of the three scenarios presented in the earlier section will take place. Of the three possibilities, the FD is assumed here to write the deterministic expression as;

$$RI_{FD} = r.DIF.P_{Ap}/P_{Cat} \quad if \quad RI_{Cat} \geq 1 \leftrightarrow P(FD|LC) = 1 \; otherwise \; P(FD|LC) = 0 \; \ldots\ldots (7.6)$$

Here, the r<1 is used to indicate the favorable contribution of material strain rate, in steel in this case. And the DIF, is the dynamic increase factor, the P_{Cat}, is the static strength of catenary force.

Also the probabilistic version can be rearranged in;

$$P(FD|LC) = \int_0^\infty F_{FD}(p) \, . f_{Ap}(p) dp = 1 - \int_0^\infty f_{FD}(p) \, . F_{Ap}(p) dp \; \ldots\ldots (7.7)$$

Where; the F is the distribution function of falling down or applied load, and the f is the density function of them

Intermediate effect can cause the FD mechanism, in which the local mechanism can progress to include another column, e.g. near column fails due to the P-Δ effects, shear in the column, the axial compressive failure or even the failure of the joint A, the point A is shown in the Figure 6.4-1 (a). Each of the named mode of failure can be represented in a unique index, keeping it short, the vertical displacement at point O associated to critical P-

Δ drift of column tip will be defined as $\Delta^{Col}{}_{P\text{-}\Delta}$. To define the limit of the collapse progress to the column at A in Figure 6.4-1 (a).

$$RI_{CC} = \Delta^{Col}{}_{P-\Delta}/\Delta_{Sbl} \quad if \quad RI_{CC} \geq 1 \leftrightarrow P(CC|T) = 1 \; otherwise \; P(CC|T) = 0 \; \ldots\ldots (7.8)$$

If RI_{FC} >1, the mechanism must be updated including the new lost element, column called the collapsed column CC, and so the response curve and the indexes must be reevaluated. It must be noted that the column shear failure above the point A was not explicitly considered here. Similar to the earlier sections, the probabilistic version can be written.

$$P(CC|T) = \int_0^\infty F_{Sbl}(\Delta) \, . f^{Col}{}_{P-\Delta}(\Delta) d\Delta = 1 - \int_0^\infty f_{Sbl}(\Delta) \, . F^{Col}{}_{P-\Delta}(\Delta) d\Delta \; \ldots\ldots (7.9)$$

It is worth to note the DIF, equation, is uncertain derived quantity. This will require further analysis which can expanded, but this will be left short to this end.

7.3.5.3. The probability of serial collapse (SC) progression and the RI_{SC}

For this section the introduction of another serial possible scenarios alternative to FD is required.

7.3.5.3.1. The probability of soft story collapse (SSC) RI_{SSC}

The local mechanism, instead of FD, can progress to involve a soft story of the adjacent part of the supporting structure, in which, depending on the size and the stiffness, part 2 in figure 2-11(a) will cause either; joints failure (stiff Part 2), P-Δ or shear failure of columns or bending mechanism. Each of the possible scenarios defines a new limit state. The associated vertical displacement of point O which triggers the most critical one, keeping it short, will be denoted P-Δ at the soft-story and called $\Delta^{Sty}{}_{P\text{-}\Delta}$, reflecting the point at which negative stiffness is observed and so the RI can be defined by;

$$RI_{SSC} = \Delta^{Sty}{}_{P-\Delta}/\Delta_{Sbl} \quad if \quad RI_{SSC} \geq 1 \leftrightarrow P(SSC|T) = 1 \; otherwise \; P(SSC|T) = 0 \; \ldots\ldots (7.10)$$

Generalizing the studied example, this index must be checked for any possible progression cases (j) other than the two possible scenarios presented in figure 2-11 which is limited to simple 2D frame case. Again, the probabilistic form can be written in the same manner.

$$P(SSC|T) = \int_0^\infty F_{Sbl}(\Delta) \,.\, f^{Sty}{}_{P-\Delta}(\Delta) d\Delta = 1 - \int_0^\infty f_{Sbl}(\Delta) \,.\, F^{Sty}{}_{P-\Delta}(\Delta) d\Delta \quad \dots\dots (7.11)$$

7.3.5.3.2. The probability of over-turning collapse progression RI_{OTC}

When part 2, figure 2-11(a) is weak, e.g. one bay multi-story frame, it is likely that it will turn over. However, it cannot be evaluated using the response curve, simple moment equation around possible points of rotation leads to the following index. Let M be the engineering moment and the M_{Sbl} stands for the stabilizing one.

$$RI_{OTC} = \quad M_{OT}/M_{Sbl} \quad if \quad RI_{OTC} \geq 1 \leftrightarrow P(OTC|T) = 1 \; otherwise \; P(OTC|T) = 0 \quad \dots\dots (7.12)$$

Also the probabilistic form can be derived.

$$P(OTC|T) = \int_0^\infty F_{Sbl}(M) \,.\, f_{OT}(M) dM = 1 - \int_0^\infty f_{Sbl}(M) \,.\, F_{OT}(M) dM \quad \dots\dots (7.13)$$

7.3.5.4. The probability of total collapse (TC) and the RI_{TC}

This can be evaluated mapping the dynamic impact of the falling element to the dynamic vertical strength of the structure beneath the affected story in general. Depending on the level of details in the analytical model, and integration of the kinetic energy E_k can be compared to the total E_s strain energy capacity of the resisting system.

$$RI_{TC} = \quad E_{TC}/E_S \quad if \quad RI_{TC} \geq 1 \leftrightarrow P(TC|T) = 1 \; otherwise \; P(TC|T) = 0 \quad \dots\dots (7.14)$$

And the probabilistic form can be also here derived.

$$P(TC|T) = \int_0^\infty F_S(E) \,.\, f_{TC}(E) dE = 1 - \int_0^\infty f_S(E) \,.\, F_{TC}(E) dE \quad \dots\dots (7.15)$$

Depending on the method of the analysis, for each robustness index, factor of safety can be employed covering uncertainties inherited from each variable discussed in (2.1.5), if the first type of reliability assessment method is used indicated in section 4.3.

7.3.6. Hierarchy of the robustness indexes

In fact, the introduced indexes above are tight to the studied logic tree. Although the example is close to the general case, other indexes may be required to handle more complex logical trees. In this section, therefore, an attempt is made to generalize steps of the structural analysis based on the proposed form of robustness indexes.

To do that, classes of disproportional collapse analysis is here proposed;

1. Class 1; the structure can adapt the trigger without the fall down of the proportional immediately above the trigger point. This is the robust class. Although, the structure may remain stable, the developed mechanism may process from arching to tensile catenary. In the transient phase, body motion and dynamic transit analysis are required. This class also include the case of the full stable response in the arching phase. To distinguish the two levels; these can be named, catenary robustness and arching robustness classes respectively.
2. Class 2; the strain energy of the supporting structure is larger than the kinetic energy of the falling mass result from the trigger scenario. This is the proportional demolition class, which can be full, or partial. The proportional demolition can be mapped to the serial collapse progression in the given example above. And the patronal proportional demolition may represent any level ranging from the fall-down to the complete serial pull down. In all cases it does not include the collapse of the proportion of the structure underneath, or under the point (the story) of the trigger.
3. Class 3; the strain energy of the supporting structure is less than the kinetic energy of the falling mass result from the trigger scenario. This is the demolition class. An example analysis of such collapse can be found (Lalkovski & Starossek, 2016), they have applied this analysis to a steel frame structure.

The classes above can be associated to the introduced indexes in the earlier section in the generalized form. But, in the open design problem, the class of response is not predefined. Therefore, a method for automatic systematic evaluation is required.

7.3.7. Quantifying the structural robustness with sequences

The proposed framework is based here on the Failure Mode and Effect Analysis (FMEA). For that there are three possible ways to quantify the risk; event tree, fault tree and the decision matrix, the problem in hand is suitable for the event tree analysis. The risk explosion to the direct and indirect sequences can be linked through the event three, through which (Baker, Schubert, & Faber, 2008) defined the robustness index for progressive collapse.

7.3.7.1. The risk index of disproportionate collapse for trigger T

Based on (Baker, Schubert, & Faber, 2008), the level of risk can be evaluated alongside possible modes of collapse using single risk index applied here on the disproportionate collapse R_{DC}. Also, additional terms, the C(s), are proposed weighing various levels of the consequences. This term is directly defined by the weighted possibility of only local collapse (C_{LC}), the *indirect* weighted consequences of collapse progression are; fall down C_{FD}, following collapses C_{FCi} & soft-story collapses C_{SSCj} as the collapse progresses to include another load bearing elements, and finally the weighted indirect consequence of the total collapse C_{TC} or any other depending on the examined case. Finding an objective representation of these consequences weights is an art beyond this text. All events and consequences are linked to each other in the decision tree in Figure 7.3-6. Based on the tree, and assuming the conditional probability of an event A as B is happened can be expressed by $P\left(\frac{A}{B}\right)$, the risk index R_{DC} for a single trigger T is defined by;

$$R_{DC} = C_{LC}P\left(\frac{LC}{T}\right)P(T) + C_{FD}P\left(\frac{FD}{LC}\right)P\left(\frac{LC}{T}\right)P(T)$$
$$+ \sum_{i=1}^{N^{FC}} C_{FCi}P\left(\frac{FCi}{\overline{FD}}\right)P\left(\frac{\overline{FD}}{LC}\right)P\left(\frac{LC}{T}\right)P(T)$$
$$+ \sum_{j=1}^{N^{SSC}}\sum_{l=1}^{N^{FC}} C_{SSCj}P\left(\frac{SSC_j}{\overline{FC_l}}\right)P\left(\frac{\overline{\overline{FC_l}}}{\overline{FD}}\right)P\left(\frac{\overline{FD}}{LC}\right)P\left(\frac{LC}{T}\right)P(T)$$
$$+ \sum_{j=1}^{N^{SSC}}\sum_{l=1}^{N^{FC}} C_{TC}P\left(\frac{TC}{SSC_j}\right)P\left(\frac{SSC_j}{\overline{FCl}}\right)P\left(\frac{\overline{FC_l}}{\overline{FD}}\right)P\left(\frac{\overline{FD}}{LC}\right)P\left(\frac{LC}{T}\right)P(T)$$
$$+ \sum_{j=1}^{N^{SSC}}\sum_{l=1}^{N^{FC}} C_{TC}P\left(\frac{TC}{\overline{SSC_j}}\right)P\left(\frac{\overline{SSC_j}}{\overline{FC_l}}\right)P\left(\frac{\overline{FC_l}}{\overline{FD}}\right)P\left(\frac{\overline{FD}}{LC}\right)P\left(\frac{LC}{T}\right)P(T) \ldots\ldots (7.16)$$

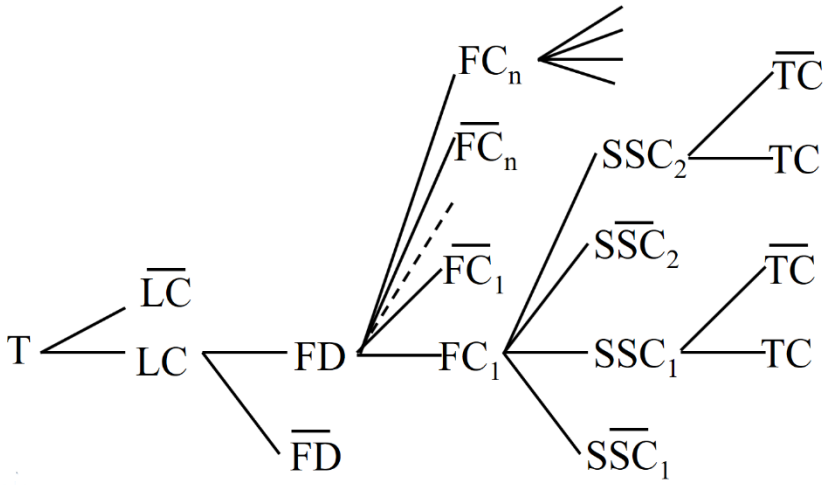

Figure 7.3-6 Decision tree of probability of progressive collapse

Where; the N^{SSC} is the number of possible causes of SSCs, the N^{FC} is the number of the possible FC scenarios where all are disproportionate. And; 'C', or the weights, can be practically reflected by the gross damage; e.g. the damaged area associated to each level of spread of failure.

Other possible modes of following collapses (FCs) of the given example are presumed unlikely and subsequently are not discussed, yet, these have been here generalized using the indexes i and j representing the number of possible alternatives. It is also important to

point out here that the probabilities in Eq. (7.16) may take uncertain (non-deterministic) value, however, when the probability is evaluated by simulation; e.g., SFEM based, single term of the Eq. (7.16) will remain, and then its bounded by a certain value. In other word, the "+" represent the function of "OR" in describing the alternative.

Comparing the proposed structure of disproportionate collapse risk index to (Canisius, 2011), and (Vogel, Kuhlmann, & Rölle, 2014) based on the appendix B of the (CEN, 2010), the code encapsulates the structural failure probability to a single term. While. We propose the modelling tool influences the quality/ the probability, and the level of structural damage can also be seriated. Therefore, the proposed structure of the risk index opens the door for the uncertainty of the modelling tool to be quantified.

7.3.7.2. The risk index of disproportionate collapse for a building B

Proper risk assessment of buildings will require clear analysis of all probable triggers and progressions, so for a specific building (B), the risk index R^{B}_{DC}, become in Eq. (7.17).

$$R^{B}{}_{DC} = 1 - \max(R^{k}{}_{DC}) \dots\dots (7.17)$$

It must be noted that this index $R^{B}{}_{DC}$, will reflect the increase in the structural robustness as a result of the increased redundancy of ALP structural mechanism.

7.3.8. Structural reliability

The reliability of the structural system for a single named trigger point can be defined by maintaining the ability to satisfy the performance objective for a given period of time, life span, under certain service and extreme performance conditions. In the context of the structural robustness against progressive collapse, the structural reliability goes along the line of the structural robustness and therefore can be used to reflect the level of safety. The structural reliability (SR^{TS}), for point of trigger scenario, can be quantified based on the probability of disproportionate collapse, $P(DC)$;

$$SR^{TS} = 1 - P(DC) \dots\dots (7.18)$$

So SR is the probability of no-disproportionate collapse will occur, which is the complement of the probability of failure. The SR can be also defined as the probability of the structure to survive the abnormal event. Such index can be also reflected by the invers of the probability of failure $P(DC)^{-1}$.

Probabilistic reliability can be handled by; probability index method (β Method), time dependent method (e.g. hazard functions), or response surface modelling. The simplest, but demanding high number of samples, is the Monte Carlo simulation (MCS). To reduce the number of samples in MCS, various techniques can be developed depending on the physical nature, and depending on the statistical nature of the uncertain variables. For a give scenario; $P(DC)$= R_{DC}.

7.4. Remarks on seismic collapse analysis

It is proposed here that calculating R_{DC} must be performed for each possible scenario of column loss; this is similar when seismic actions are analyzed however the definition of the key scenarios (KSs) will be led by a superseding non-linear-time history analysis (NLTHA) of the building under the specific design earthquake. The combinations between the seismic actions and the progressive collapse are proposed in line with displacement based analysis (Priestley, Calvi, & Kowalsky, 2007) at three levels A, B, and C:

A. R_{DC} will include another term to combine the probability of seismic action with specific weighted consequence of seismic damage (Asprone, Jalayer, Prota, & Manfredi, 2010). However, such link is normally provided by design codes in load combinations (The Structural Eurocodes, 2008), it must be noted that the combination should be made at each KS, e.g. for each possible column shear failure, as single or in group similar to Eq. (7.16), then for all KS in Eq. (4.17).
B. As for all of the calculated probabilities are based on the robustness indexes, the link can be established through the seismic effects on individual parameter. An earthquake can generally cause either/or form of seismic deficiencies (Venture, 2010); (1) joint failure, normally result in complete failure of the structure however

recent works revealed low probability (Yavari, et al., 2013), (2) the soft-story due to an excessive story drift, (3) column axial force deficiency or (4) column shear failure (Shoraka , 2013). As the first leads to collapse, it is not discussed. The others result respectively in;

1. Reduced story drift capacity of columns due to loading levels and number of cycles after the NLTHA, so it results in a reduced value of; $\Delta^{Sty}{}_{P-\Delta}$.
2. Reduced column P-Δ capacity after the NLTHA, so a reduced value of $\Delta^{Col}{}_{P-\Delta}$.
3. A reduced value of lateral strength of the soft-story as a result of NLTHA which should be an alternate to 1, whichever is more critical.

C. Depending on the strain history of reinforcement results from the NLTHA, Δ_{LC}, Δ_{f}, Δ_{Sbl} and Δ_{Cat} must be also updated increasing the risk index of progressive collapse.

7.5. Summary

Due to uncertainties in the disproportionate collapse analysis and the challenge of modeling, decision tools are required. Framework for risk assessment is developed. The components of risk assessment framework applied to the disproportionate collapse analysis of RC building, key structural parameters can be listed based on the current developments in chapters 2 to 6. The key parameters of structural response associated to various column loss locations are analyzed through an example problem and sources of uncertainties discussed also in chapter 6.

To quantify structural risk indexes, coined to the robustness indexes, are in this chapter proposed and linked to the general probability of the disproportionate collapse based on the alternative load paths principle. These indexes allow for safety factor to be developed by either the deterministic or the probabilistic form. Yet further development of modelling strategy is required.

To integrate the modeling challenge to the proposed framework, Baker's (Baker, Schubert, & Faber, 2008) risk function is applied to an illustrative example, extended from chapter 6.

The association of weighted consequences to various levels of damage is shown with emphasis on a single response indicator for; certain trigger point, or also referred to by a specific scenario (i). The indicator is also presented at the building level as measure of risk/robustness. The last is linked to the concept of system failure probability, or reliability.

Because extreme base excitation is one of the most complex cause of structural collapse. The link between the disproportionate collapse and the seismic trigger is proposed at three levels; load combinations, strength and displacement variables of the key mechanisms, and strain capacity of steel bars. This proposed application opens the door for novel standardized requirements assessing collapse risk of the RC building in the seismically active locations, where a structure undergoes a few base excitations in the period of service.

Chapter 8 Summary and conclusions

8.1. Summary

Facing the need for structural robustness, terms such as redundancy and system ductility are prescribed by standard as design targets which can be proved by either an alternative load path, or the tie force method for less critical buildings. While the structural robustness can be defined as natural property of the structure, in isolation of specific named hazard, means of structural analysis are adopted by the engineering and research communities. An example common approach is the remove of one or more column. Researchers adapted tests to explore the failure mechanism. One major mechanism is beam bridging mechanism in which the beam assembly transfer from the ultimate state of bending failure to the cable tensile catenary when the tensile axial reaction force can develop. Because of axial compressive constrain, or the beam volume locking in presence of strong lateral resistance, the bending mechanism will shift in strength due to so-called arching action. Similar results reported in both frame and slab assemblies.

The bending/arching strength is responsible for the provision of the alternative load path. And the tie force method is based on the presence of the tensile catenary action.

8.1.1. Motivation and scope

Increasing structural robustness is the goal which is of high interest of the structural engineering community. In particular, the partial collapse of RC buildings is rather a new area of interest which was subject of this dissertation. Understanding the robustness of RC buildings will guide the development of safer structure against abnormal loading scenarios. For example; explosions, earthquakes, fine, and/or long-term accumulation effects such as deterioration or fatigue, all may result in local immediate damage, that can propagate to the rest of structure causing what is known by the disproportionate collapse. Although abnormal events are relatively rare, the subject become of high demand under national hazards such as regional floods; e.g. the North Sea 1953 and 2007, or civilians who are threatened by a war, e.g. the second World War or the war in Syria.

Although most of the finding are rather general, the focus; in chapters 2, 3, 4, and 5, is given here to the reinforced concrete structures because it is popular in residential housing and received less attention in the literature compared to the structural steel.

8.1.2. Problem statement

Arching action and the catenary action are described in some harmony in the literature, but the transition between the arching and catenary is less understood. Especially in the presence of strong snap through in the response curve, high dynamic magnifications are reported. It is observed that there is a kind of the body motion phase of response which is disregarded in the analysis of the transfer between the arching and catenary. This will significantly affect the magnification of displacement, or even the increase of the equivalent actions by the point of the stable catenary. In addition, there were incomplete understanding of the interrelations of the key response factors, although there is a few test benchmarks, there is no common agreement of an appropriate modelling strategy. In the absences of a singly coherent and valid analytical framework, an effort is made in this work in this direction.

Also, modeling the progressive collapse remain an open problem, although there are a few successful implementations based on the continuum element based FEM, all suffered from the practical efficiency that hinder the possibility of the development of full building models. The last makes the implementation of sensitivity studies even more impractical. Performing sensitivity analysis is extremely important at the learning phase of the new problem in hand. Hence, an efficient modeling strategy is required which covers all parameters identified by the wealth of recent test reports.

Facing the uncertain nature of the abnormal events, few models were presented in probabilistic equation before. These were linked to some indicators of structural robustness. However, these were made in abstract definition which make them difficult to be implemented in the context of RC buildings due the specific nature of failure mechanisms. Therefore, fit-for-purpose framework for failure analysis is needed.

8.1.3. The implemented approach

An extensive survey of the tested model benchmarks is collected, ordered, and analyzed on purpose of developing modeling benchmark regime that covers the recognized key parameters. With benchmarks in mind, a survey of the wide spectrum of modeling and numerical methods is performed. Along the way, many modeling deficiencies are identified. These deficiencies are then re-evaluated and ranked according to most relevant, until the structural (beam element based) FEM is chosen as a target strategy. The last were studied under the scope of an-open source software with the tool-box relevant to highly non-linear problem in material and geometry. The open source platform was extended to consider some new recognized parameters such as the rupture strain of reinforcement. Then, models are used to explore the validity of the simulation tool, see chapter 5. To do that, and with its help, simplified analytical framework were developed and validated in chapter 3 and chapter 4.

Throughout this work, the uncertainty in modeling is raised into equation, and accumulative deviation of results is found to be misleading in a problem learnt to be very sensitive to molding strategy and inputs, these are discussed in chapter 6.

Structural robustness framework is developed independent from the modelling strategy as learnt from chapter 6, the framework is presented in chapter 7.

8.1.4. Contribution

Extensive survey of vibrant research of progressive collapse is organized. The modeling benchmark regime is formulated on specific modelling targets of quality. Using the developed regime, various reported modeling strategies are grouped and judged. A firm conclusion is made; that none of the reported modeling strategies satisfies all of the modeling targets at once. Therefore, it becomes clear in chapter 2 that more research is required to address the disproportionate collapse simulation problem. This research is begun by identifying key analytical relations in chapter 3, with close look at the results of experiments.

Novel analytical relations were developed relating the key response parameters. These shows good agreement as compared to benchmarks. The relations describe the compressive arching in beams mechanism as well as the tensile catenary in reinforcement. While a few researchers supposed that the arching strength can be significantly higher than the strength of the bending mechanism, it is shown that this arching is limited to the interaction between axial compressive force and the bending moment. The last can be analytically solved by the well-known principles of the section analysis in beams. In addition to the new definition of the plastic hinge, the provided relations provide a structured hierarchy bridging contemporary test in reinforced concrete design to the relative new concepts of; arching, catenary, and the transition in between.

The rule of the body-motion phase explaining the high dynamic amplification factor is explained under the large displacement which result from the transfer of the failure

mechanism from arching to catenary. These relations of chapter 3 are compared well to benchmarks.

A simple method for the slab reinforcement contribution to the kinematic energy absorption were also developed, discussed and validated in chapter 4. It is also found that although the substitution of the slab reinforcement by truss element can simulation energy, the use of beam element may improve the prediction of the force displacement curve.

Efficient modeling strategy is developed based on existing structural finite element method. The careful algorithmic issues; element choice and discretization, in addition to the objectivity of the nonlinear response is successfully handled. The model shows reasonable match to benchmarks. However, the used tool in chapter 5 requires further development to meet all of the recognized targets of modelling named above.

Sources of uncertainty in progressive collapse safety analysis are discussed as related to abstract definition of the repose curve which made the conclusions general in application to frame structures. These included the different levels of uncertain parameters, such as mechanical, embedded and model related uncertainties. Based on these, an alert of some addition key modelling qualities is pointed out. Although none of these is handled in detail, the developed approach can be used alongside the fit-for-purpose performance functions in chapter 6. These functions are then developed in chapter 7.

An overall collapse risk, structural reliability, and robustness framework were developed for the progressive collapse in application to the defined response curve. Novel risk indexes are presented and defined considering the stochastic nature of those uncertain parameters. The risk indexes are related to the definition of the probability of failure, and it has been pulled-out together in new definition of the probability of failure based on system risk index which was proposed by Baker. These are presented in chapter 7.

8.1.5. Important results

- New criterion of tensile catenary is developed based on the inclusion of the dynamic effects of the body motion phase.

- The rapture strain in steel is important parameter in tensile catenary analysis. Therefore, the length of sample steel gage need to be standardized and statistically analyzed. it is also an important uncertain modeling parameter.
- The structural (beam element based) FEM is promising tool, although it requires yet careful development, for example joint, slab and column models must be developed and validated.
- Full shear-axial flexure interaction in column is an important element modeling quality which is useful, recommended, to be implemented in the OpenSEES.
- In RC building structures; it is relevant to distinguish between the vertical and serial propagation scenario of the disproportionate collapse. Especially when calculating the probability of disproportionate collapse, or the robustness index. And, it is highly relevant in the judgement of the reliability of the modeling strategy.
- The link between the disproportionate collapse and the seismic trigger is proposed at three levels; load combinations, strength and displacement variables of the key mechanisms, and strain capacity of steel bars. This proposed application opens the door for novel standardized requirements assessing collapse risk of the RC building in the seismically active locations, where a structure undergoes a few base excitations in the period of service.

8.2. Conclusions and outlook

Modeling of progressive collapse accurately still an open research question. Structural (beam-element-based) FEM, adaptive, multi-scale simulation, or the development of implicit discrete deformable element method can provide the most realistic although achieving mesh independent response is another challenging consideration. Implicit methods are widely adapted for continuous numerical method such as displacement base FEM. The explicit algorithm is more stable from convergence point of view, but these are only useful in the state of body motion. However, when many parts; sections, or elements, goes into large plastic deformation, proving the accuracy of results is not only time step

dependent, it also depends on realistic description of the evolution of the plasticity under different 3D stress state.

In the case of brittle arching failure combined with rupture of the main reinforcement, high dynamic effects are expected in the transfer from the arching to catenary, these high dynamic magnifications suggest that the tensile catenary is unrealistic line of defense in contrast with the assumption of the (CEN, EN 1990 - Basis of structural design, 2002). Therefore, the recommendations summarized in the Figure 8.2-1 is proposed to the committee of the Eurocodes (Hatahet & Könke, 2017b). In these recommendation, a revised version of the tie forces is recommended. For corner located trigger points, peripheral ties will not prevent the vertical propagation of collapse. The other mentioned points in the figure has been already discussed in this summary.

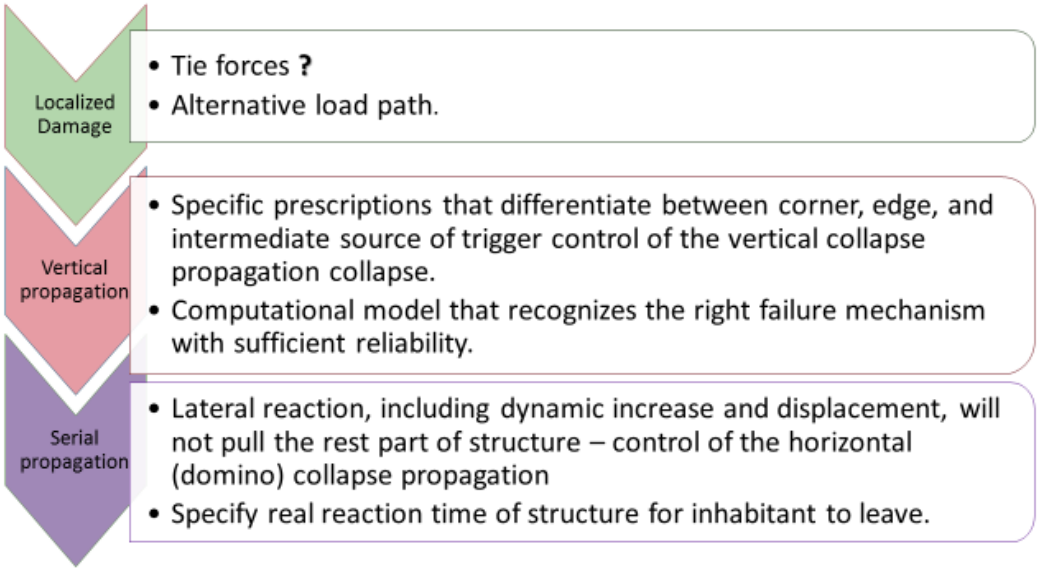

Figure 8.2-1 proposed recommendation to the comities of the Eurocodes (Hatahet & Könke, 2017b)

Modelling progressive collapse using SFEM, as proposed in chapter 5, require careful validation and an awareness of the modeling limits. Therefore, it cannot be relayed on without enough evidence of accuracy tight to the studied problem.

At last, further research in progressive collapse modelling is here proved to be still required and recommended. Having recommended the introduction of the national hazard safety

requirement for the design standards Figure 7.3-2, the current summary of actions and research needs are organized in three groups;

1. Immediate action; to generalize the alternate load path check as standard requirement for all types and category of buildings.
2. With yet needed more computer-based experiments; more articulate criteria for the structural robustness can be developed more fit for reinforced concrete.
3. Laboratory-based experimental program is needed aiming at regulating the disproportionate collapse with real value of reaction time. The reaction time is useful to measure the level of human safety giving inhabitants sufficient evacuation time.

Both 1 and 3 of the above are in consistence having accepted that we need to adapt the need for the disaster safety; such as floods and wars which is along the line of the structural reliability and robustness as shown in the Figure 7.3-2.

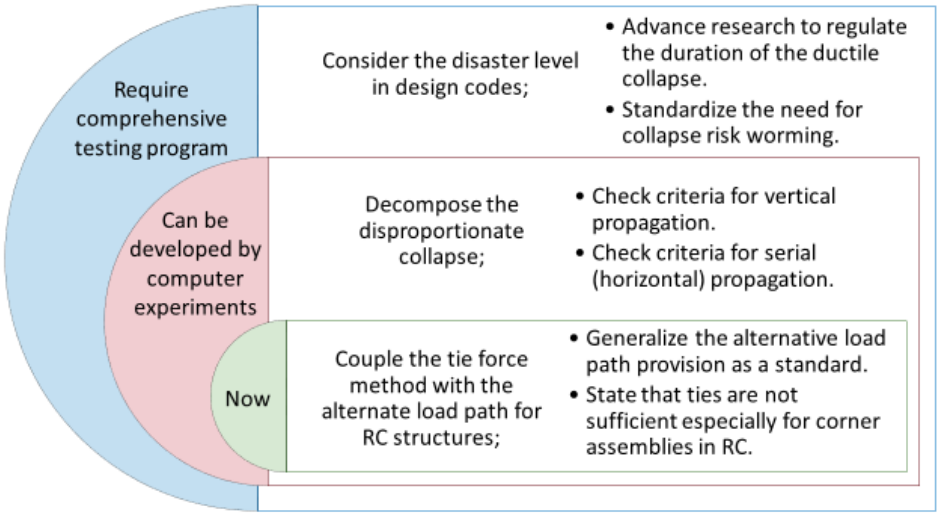

Figure 8.2-2 summary of actions and research needs (Hatahet & Könke, 2017b).

References

2010 Chile earthquake. (2016, July 16). Retrieved from https://en.wikipedia.org: https://en.wikipedia.org/wiki/2010_Chile_earthquake

Alemdar, B. N., & White, D. W. (2005). Displacement, Flexibility, and Mixed Beam–Column Finite Element Formulations for Distributed Plasticity Analysis. *Journal of Structural Engineering, 131*(12), 1811-1819.

Almeida, J. P., Das, S., & Pinho, R. (2011). Adaptive Force-Based Frame Element for Regularized Response. *Thematic Conference on Computational Methods in Structural Dynamics and Earthquake Engineering* (pp. 1-16). Greece: COMPDYN 2011: III ECCOMAS .

Anderson, T. (2012, September 18). *The malignant consensus on Syria*. Retrieved from The Conversation: http://theconversation.edu.au/the-malignant-consensus-on-syria-9565

Arshian, A. H., Morgenthal, G., & Narayanan, S. (2016). Influence of modelling strategies on uncertainty propagation in the alternate path mechanism of reinforced concrete framed structures. *Engineering Structures*, 36–47.

Asprone, D., Jalayer, F., Prota, A., & Manfredi, G. (2010). Proposal of a probabilistic model for multi-hazard risk assessment of structures in seismic zones subjected to blast for the limit state of collapse. *32*(1).

Astarlioglu, S., Krauthammer, T., D. M., & Tran, T. P. (2013). Behavior of reinforced concrete columns under combined effects of axial and blast-induced transverse loads. *Engineering Structures, 55*(0), 26–34.

Ayub, T., Shafiq, N., & Nuruddin, M. F. (2014). Stress-strain Response of High Strength Concrete and Application of the Existing Models. *Research Journal of Applied Sciences, Engineering and Technology, 8*(10), 1174-1190.

Bae, S., & Bayrak, O. (2008). Plastic Hinge Length of Reinforced Concrete Columns. *ACI Structural Journal, V. 105, No. 3,*, 290-300.

Bailey, C. G., Toh, W. S., & Chan, B. M. (2008). Simplified and Advanced Analysis of Membrane Action of Concrete Slabs.

Baker, J. W., Schubert, M., & Faber, M. H. (2008). On the assessment of robustness. *Structural Safety, 30*(3), 253–267.

Bao, Y., Kunnath, S. K., El-Tawil, S., & Lew, H. S. (2008). Macromodel-Based Simulation of Progressive Collapse: RC Frame Structures. *Journal of Structural Engineering, 134*(7), 1079-1091.

Bao, Y., Lew, H. S., & Kunnath, S. K. (2012). Modeling of Reinforced Concrete Assemblies under a Column Removal Scenario. *J. Struct. Eng. (Journal of Structural Engineering)*, 121107211901006.

Bao, Y., Main, J. A., Lew, H., & Sadek, F. (2014). Robustness Assessment of RC Frame Buildings under Column Loss Scenarios. *Structures Congress* (pp. 988-1000). ASCE.

Bazan, M. L. (2008). *Response of reinforced concrete elements and structures following loss of load bearing elements.* Boston, Massachusetts: Northeastern University.

Bazant, Z. P., & Brocca, M. (2000). Compressive failure, large-strain ductility and size effect in concrete: micro plane model. *European Congress on Computational Methods in Applied Sciences and Engineering* (pp. 1-20). Barcelona: ©ECCOMAS.

Bažant, Z. P., & Caner, F. C. (2005). Microplane Model M5 with Kinematic and Static Constraints for Concrete Fracture and Anelasticity. I: Theory. *Journal of Engineering Mechanics,, 131*(1), 31–40.

Binici, B., & Mosalam, K. M. (2007). Analysis of reinforced concrete columns retrofitted with fiber reinforced polymer lamina. *Composites: Part B, 38*(0), 265–276.

Canisius, T. D. (2011). *Structural robustness design for practising engineers.* Prague: COST Action TU0601 – Robustness of Structures.

CEN. (2002). *EN 1990 - Basis of structural design.* Brussels: European Commitee for Standardization.

CEN. (2004). *EN 1992: Design of concrete structures* . Brussels: European Committe for Standardization.

CEN. (2010). *EN 1991-1-7. 'Eurocode 1: Actions on Structures: Part 1–7: Accidental Actions'.* Brussels: European Committe for Standardization.

Chen, S., Zhang, X., Sasani, M., & Sagiroglu, S. (2010). *Gravity Load Redistribution and Progressive Collapse Resistance of 20-Story Reinforced Concrete Structure.* Discussion: Disc. 107-S62/From the November-December 2010 ACI Structural Journal, p. 636.

Choi, H., & Kim, J. (2011). Progressive collapse-resisting capacity of RC beam–column sub-assemblage. *Magazine of Concrete Research, 63*(4), 297–310.

Choi, K.-K., & Park, H.-G. (2010). Evaluation of Inelastic Deformation Capacity of Beams Subjected to Cyclic Loading. *ACI Structural Journal, 107*(5), 507-515.

Coleman, J., & Spacone, E. (2001). Localization Issues in Force-Based Frame Elements. *Journal of Structural Engineering, 127*(11), 1257-1265.

Crisfield, M. A. (1990). A consistent co-rotational formulation for nonlinear, three-dimensional, beam-elements. *Comput. Methods Appl. Mech. Eng., 81*(0), 131–150.

Crisfield, M. A. (1991). *Nonlinear finite element analysis of solids and structures, Vol 1.* New York: Wiley.

Cundall, P. A., & Strack, O. D. (1979). A discrete numerical model for granular assemblies. *Géotechnique, ICE Publishing, 29*(1), 47-65.

Cusatis, G., Mencarelli, A., Pelessone, D., & Baylot, J. (2011). Lattice Discrete Particle Model (LDPM) for failure behavior of concrete. II: Calibration and validation. *Cement & Concrete Composites, 33*(0), 891–905.

Cusatis, G., Pelessone, D., & Mencarelli, A. (2011). Lattice Discrete Particle Model (LDPM) for failure behavior of concrete. I: Theory. *Cement & Concrete Composites, 33*(0), 881–890.

Dat, P. X., & Hai, T. K. (2011). Membrane actions of RC slabs in mitigating progressive collapse of building structures. doi:10.1016/j.engstruct.2011.08.039

Dat, X. P., & Hai, T. K. (2013). Experimental study of beam–slab substructures subjected to apenultimate-internal column loss. *Engineering Structures*, 3-15. Retrieved from http://dx.doi.org/10.1016/j.engstruct.2013.03.026

El-Fouly, A., & Khalil, A. A. (2012). *Progrressive collapse analysis: reinforced concrete assemblies.* Durham: Applied Science International.

Elghazouli, A., & Izzuddin, B. (2004). Realistic Modeling of Composite and Reinforced Concrete Floor Slabs under Extreme Loading II: Verification and Application. *Journal of Structural Engineering, 130*(12), 1985–1996.

El-Tawil, S., Li, H., & Kunnath, S. (2013). Computational Simulation of Gravity-Induced Progressive Collapse of Steel-Frame Buildings: Current Trends and Future Research Needs. *ASCE - Journal of Structural Engineering, 0*(0), A2513001-1-12.

Fadhil, A. T. (2012). *Simplified Analysis to Predict the Behavior of RR Beams Under Collapse.* Columbia, US: the University of Missouri-Columbia, Master Thesis.

FarhangVesali, N., Valipour, H., Samali, B., & Foster, S. (2013). Development of arching action in longitudinally-restrained reinforced concrete beam. *Construction and Building Materials, 47*(0), 7-19.

Filippou, F. C., & Fenves, G. L. (2004). Chpater 6: Methods of Analysis for Earthquake-Resistant Structures. In Y. Bozorgnia, & V. V. Bertero, *Earthquake Engineering: From Engineering Seismology to Performance-Based Engineering* (pp. 6.1-6.66). CRC Press LLC.

Filippou, F. C., D'Ambrisi, A., & Issa, A. (1992). *Nonlinear static and dynamic analysis of reinforced concrete subassemblages.* Berkeley: Earthquake Engineering Research Center, University of California, Report No. UCB/EERC–92/08.

FIP-MC. (2010). *fib Model Code for Concrete Structures.* Lausanne: © 2013 fédération internationale du béton / International Federation for Structural Concrete (fib).

Fu, F. (2009). Progressive collapse analysis of high-rise building with 3-D finite element modeling method. *Journal of Constructional Steel Research, 65*(0), 1269-1278.

Fujikake, K., & Aemlaor, P. (2013). Damage of reinforced concrete columns under demolition blasting. *Engineering Structures, 55*(0), 116–125.

Gharakhanloo, A. (2014). *Distributed and Concentrated Inelasticity Beam-Column Elements used in Earthquake Engineering.* Troundheim: Norwegian University of Science and Technology - Master thesis.

Glösmann, P. (2010). Reduction of discrete element models by Karhunen–Loève transform: a hybrid model approach. *Comput Mech, Springer, 45*(0), 375–385.

Gouverneur, D., Caspeele, R., & Taerwe, L. (2013). Experimental investigation of the load–displacement behaviour under catenary action in a restrained reinforced concrete slab strip. *Engineering Structures, 49*(0), 1007–1016.

Grassl, P. (2004). Modelling of dilation of concrete and its effect in triaxial compression. *Finite Elements in Analysis and Design, 40*(0), 1021–1033.

Grassl, P., & Jiraesek, M. (2006). Damage-plastic model for concrete failure. *International Journal of Solids and Structures, 43*(0), 7166–7196.

GSA. (2003). *Progressive collapse analysis and design guidelines for new federal office buildings and major modernization projects.* Washington (DC): : US General Service Administration.

Hart, R. D. (1989). *Overview of the discontinous methods.* Minnesota: Itasca Consulting Group.

Hartmann, D., Breidt, M., Nguyen, v. V., Stangenberg, F., & Höhler, S. (2008). Structural collapse simulation under consideration of uncertainty – Fundamental concept and results. *Computers and Structures*, 2064–2078.

Haselton, C. B., & Deierlein, G. G. (2008). *Assessing Seismic Collapse Safety of Modern Reinforced Concrete Moment-Frame Buildings, PEER Report 2007/08.* Berkeley: Pacific Earthquake Engineering Research Center.

Hatahet, T., & Könke, C. (2014a). Rational Framework for Probability of Collapse in Buildings. *Vulnerability, Uncertainty, and Risk* (pp. 1685-1695). Liverpol: American Sociatey of Civil Engineers (ASCE).

Hatahet, T., & Könke, C. (2014b, August 17-29). Simple method for the tensile catenary slab contribution in the 2D progressive collapse simulation. *Bauhaus Summer School in Forecast Engineering: Global Climate change and the challenge for built environment*, pp. 1-13.

Hatahet, T., & Könke, C. (2017a). (in press) Criteria for the Partial Collapse Simulation of RC Building. *Advances in Civil engineering,*.

Hatahet, T., & Könke, C. (2017b). (in press) Is the disproportionate collapse of RC frame structures well covered by the Code? *fib Symposium 2017 Maastricht.* Maastricht: Springer.

He, Q., & Yi, W. (2013). Discussion of 'Slab Effects on Response of Reinforced Concrete Substructures after Loss of Corner Column'. *ACI Structural Journal, 110*(5), 893.

Hsu, T. T., & Mo, Y. L. (2010). *Unified Theory of Concrete Structures.* Singapore: A John Wiley and Sons, Ltd., Publication.

Huixian, L., & George W. Housner, X. L. (2016, July 16). *The great Tangshan earthquake of 1976.* Retrieved from http://authors.library.caltech.edu: http://authors.library.caltech.edu/26539/1/Tangshan/Overview.pdf

Izzuddin, B. A., & Einashai, A. S. (1993). Adaptive space frame analysis Part II: a distributed plasticity approach. *Proc. Jnstn Civ. Engrs Structs & Bldgs*, 317-326.

Izzuddin, B. A., Vlassis, A., Elghazouli, A., & Nethercot, D. (2008). Progressive collapse of multi-storey buildings due to sudden column loss - Part I: Simplified assessment framework. *Engineering Structures, 30*(5), 1308–1318.

Izzuddin, B., Tao, X., & Elghazouli, A. (2004). Modeling of Composite and Reinforced Concrete Floor Slabs under Extreme Loading. I: Analytical Method. *Journal of Structural Engineering, 130*(12), 1972–1984.

Jahromi, H. Z., Vlassis, A., & Izzuddin, B. (2013). Modelling approaches for robustness assessment of multi-storey steel-composite buildings. *51*(0).

Jiang, J.-F., & Wu, Y.-F. (2012). Identification of material parameters for Drucker–Prager plasticity model for FRP confined circular concrete columns. *International Journal of Solids and Structures, 49*(0), 445–456.

Jiang, M., Leroueil, S., Zhu, H., Yu, H.-S., & Konrad, J.-M. (2009). Two-Dimensional Discrete Element Theory for Rough Particles. *International Journal of Geomechanics, 9*(1), 20-33.

Jirasek, M. (2013). *Modeling of Localizes Inelastic Deformation - Lecture Notes.* Prague: Short Cource in Czech Technical Univesity.

Kapil, K., & Sherif, E.-T. (2011). Pushdown resistance as a measure of robustness in progressive collapse analysis. *Engineering Structures*(33), 2653-2661.

Kappos, A. J., Panagopoulos, G., Panagiotopoulos, C., & P. P. (2006). A hybrid method for the vulnerability assessment of R/C and URM buildings. *Bulletin of Earthquake Engineering, 4*(4), 391-413.

Kaufmann, P., Martin, S., Botsch, M., & Gross, M. (2008). Flexible Simulationof Deformable Models Using Discontinuous Galerkin FEM. *Eurographics/ ACM SIGGRAPH Symposium on Computer Animation*, 1-11.

Kazerani, T. (2013). A discontinuum-based model to simulate compressive and tensile failure insedimentary rock. *Journal of Rock Mechanics and Geotechnical Engineering, 5*(0), 378–388.

Koenke, C., Eckardt, S., Haefner, S., Luther, T., & Unger, J. (2010). Multiscale simulation methods in damage prediction of brittle and ductile materials. *International Journal for Multiscale Computational Engineering, 8*(1), 1-20.

Kokot, S., Anthoine, A., Negro, P., & Solomos, G. (2012). Static and dynamic analysis of a reinforced concrete flat slab frame building for progressive collapse. *40*(0).

Kolkata. (2013, Marsh 12). Retrieved from TopNews.in: http://www.topnews.in/tree/Kolkata/Kolkata

Kwasniewsk, L. (2010). Nonlinear dynamic simulations of progressive collapse for a multistory. *Engineering Structures, 32*(5), 1223–1235.

Lalkovski, N., & Starossek, U. (2016). Vertical building collapse triggered by loss of all columns in the ground story−Last line of defense. *International Journal of Steel Structures, 16*(2), 395-410.

Le Corvec, V. (2012). *Nonlinear 3d frame element with multi-axial coupling under consideration of local effects.* Berkeley: UC Berkeley Electronic Theses and Dissertations.

Le, J.-L., & Xue, B. (2014). Probabilistic analysis of reinforced concrete frame structures against progressive collapse. *Engineering Structures, 76*, 313–323.

LeBorgne, M. R., & Ghannoum, W. M. (2014). Analytical Element for Simulating Lateral-Strength Degradation in Reinforced Concrete Columns and Other Frame Members. *Journal of Structural Engineering, ASCE, 140*(38), 1-12.

Lee, C.-L., & Filippou, F. C. (2009). Efficient Beam-Column Element with Variable Inelastic End Zones. *Journal of Structural Engineering, 135*(11), 1310-1319.

Lee, S.-C., Chob, J.-Y., & Vecchio, F. J. (2011). Model for post-yield tension stiffening and rebar rupture in concrete members. *Engineering Structures, 33*(0), 1723–1733.

Lew, H., Bao, Y., Sadek, F., Main, J., Pujol, S., & Sozen, M. (2011). *An Experimental and Computational Study of Reinforced Concrete Assemblies under a Column Removal Scenario.* National Institute of Standards and Technology - U.S. Department of Commerce.

Li, J., & Hao, H. (2013). Numerical study of structural progressive collapse using substructure technique. *Engineering Structures*, 101–113.

Li, Y., Lu, X., Guan, H., & Ye, L. (2014). Progressive Collapse Resistance Demand of Reinforced Concrete Frames under Catenary Mechanism. *ACI Structural Journal/, 111*(0), 1225-1234.

Liel, A. B., Haselton, C. B., & Deierlein, G. (2011). Seismic Collapse Safety of Reinforced Concrete Buildings II: Comparative Assessment of Nonductile and Ductile Moment Frames. *Journal of Structural Engineering, 137*(4), 492–502.

Lin, M. (2013). Pulldown Analysis for Progressive Collapse Assessment. *Journal of Performance of Constructed Facilities.* doi:10.1061/(ASCE)CF.1943-5509.0000459

Livingston, E., Sasani, M., Bazan, M., & Sagiroglu, S. (2015). Progressive Collapse Resistence of RC beams. *Engineering Structures, 95*, 61–70.

Lodhi, M. S. (2010). *Response Estimation of Reinforced Concrete Columns Subjected to Lateral Loads.* Ohio, USA: The Ohio State University - Master thesis.

Lodhi, M. S., & Sezen, H. (2012). Estimation of monotonic behavior of reinforced concrete columns considering shear-flexure-axial load interaction. *Earthquake Engineering & Structural Dynamics, 41*(15), 2159-2175. doi:10.1002/eqe.2180

Lu, X., Lin, X., & Ye, L. (2008). Simulation of Structural Collapse with Coupled Finite Element-Discrete Element Method. *Proc. Computational Structural Engineering,* (pp. 127-135). Shanghai: Springer.

Lu, X., Lu, X., Guan, H., & Ye, L. (2013). Collapse simulation of reinforced concrete high-rise building induced by extreme earthquakes. *Earthquake Engng Struct. Dyn., 42*, 705–723.

Main, J. A. (2014). Composite Floor Systems under Column Loss: Collapse Resistance and Tie Force Requirements. *Journal of Structural Engineering*, A4014003-1-15. doi:10.1061/(ASCE)ST.1943-541X.0000952.

Mander, J. B., Priestley, M. J., & Park, R. (1988). Theoretical Stress-Strain Model for Confined Concrete. *Journal of Structural Engineering, ASCE, 114*, 1804-1826.

McKenna, F. (1997). *Object-oriented finite element programming: frameworks for analysis, algorithms and parallel computing.* Berkeley: PhD Thesis, University of California.

McKenna, F., Fenves, G. L., & Scott, M. H. (2000). *Open System for Earthquake Engineering Simulation*. University of California, Berkeley,, CA, US: PACIFIC EARTHQUAKE ENGINEERING RESEARCH CENTER.

McKenna, F., Scott, M., & Fenves, G. (2009). Nonlinear finite-element analysis software architecture using object composition. *Journal of Computing in Civil Engineering, 24*(1), 95-107.

Meguro, K., & Tagel-Din, H. (1997). A new simplified and efficient technique forfracture behavior analysis of concrete structures. *Fracture Mechanics of Concrete Structures Proceedings FRAMCOS-3* (pp. 911-920). Freiburg, Germany: AEDIFICATIO Publishers.

Meguro, K., & Tagel-din, H. (1999). *Simulation of Buckling and Post Buckling Behavior of Structures Using Apllied Lement Method.* Bull. ERS 32.

Meguro, K., & Tagel-din, H. S. (2002). Applied Element Method Used for Large Displacement Structural Analysis. *Journal of Natural Disaster Science, 24*(1), 25-34.

Merola, R. (2009). *Ductility and robustness of concrete structures under accidental and malicious load cases .* Birmingham: PhD Thesis, The University of Birmingham.

Monti, G., & Petrone, F. (2015). Yield and Ultimate Moment and Curvature Closed-Form Equations for Reinforced Concrete Sections. *ACI Structural Journal, 112*(4), 463-475. doi:10.14359/51687747

Morone, D. J. (2012). *Progressive Collapse: Simplified Analysis Using Experimental Data.* Ohio: The Ohio State University, Master Thesis.

Morone, D. J., & Sezen, H. (2014). Simplified Collapse Analysis Using Data from Building Experiment. *ACI Structural Journal, 11*(4), 925-934.

Mostafaei, H., & Kabeyasawa, T. (2007). Axial-Shear-Flexure Interaction Approach for Reinforced Concrete Columns. *ACI Structural Journal/, 104*(0), 218-226.

Mullapudi, R., & Ayoub, A. (2009). Fiber beam element formulation using the Softened Membrane Model. *ACI Special Publication, 265(SP265-13)*, 283-308.

Mullapudi, R., Charkhchi, P., & Ayoub, A. (2009). Evaluation of behavior of reinforced concrete shear walls through finite element analysis. *ACI Special Publication 265 (SP-265—4)*, 73-100.

Munjiza, A. (2004). *The Combined Finite-Discrete Element Method.* London: John Wiley & Sons Ltd.

Net World Directory. (2013, Feb 22). Retrieved from http://www.networlddirectory.com: http://www.networlddirectory.com/blogs/permalinks/3-2007/construction-strategies-to-avoid-collapse.html

Neuenhofer, A., & Filippou, F. C. (1998). Geometrically nonlinear flexibility-based frame finit element. *Journal of Structural Engineering, 124*(0), 704-711.

Neuenhofer, A., & Filppou, F. C. (1997). Evaluation of Nonlinear Frame Finite Element Models. *Journal of Structural Engineering, 123*(7), 958-965.

Ning, N., Qu, W., & Zhu, P. (2014). Role of cast-in situ slabs in RC frames under low frequency cyclic load. *Engineering Structures, 59*(0), 28–38.

Orton, S. L. (2007). *Development of a CFRP System to Provide Continuity in Existing Reinforced Concrete Buildings Vulnerable to Progressive Collapse.* Austin: The University of Texas at Austin, PhD Dissertation.

Orton, S. L. (2007). *Development of a CFRP System to Provide Continuity in Existing Reinforced Concrete Buildings Vulnerable to Progressive Collapse.* Austin: The University of Texas at Austin, Dissertation.

Orton, S. L., & Kirby, J. E. (2013). Dynamic Response of a RC Frame Under Column Removal. *Journal of Performance of Constructed Facilities, 28*(4), 04014010.

Panagiotakos, T., & Fardis, M. (2001). Deformations of RC Members at Yielding and Ultimate. *ACI Structural Journal, 98*(0), 135-148.

Park, R., & Gamble, W. L. (2000). *Reinforced concrete slabs, Second edition.* New York, Chichester: John Wiley & Sons, Inc.

Paulay, T., & Priestley, M. J. (1992). *Seismic Design of Reinforced Concrete and Masonry Buildings.* New York: John Wiley & Sons, Inc.

Popovics, S. (1973). A numerical approach to the complete stress strain curve for concrete." Cement and concrete research. *Cement and concrete research, 3*(5), 583-599.

Potger, G., Kawano, A., Griffith, M., & Warner, R. (2001). Dynamic analysis of RC frames including buckling of longitudinal steel reinforcement. (p. Paper No. 4.12.01). Proceedings of the NZSEE Conference. Retrieved from www.nzsee.org.nz/db/2001/papers/41201paper.pdf

Priestley, M. J., Calvi, G. M., & Kowalsky, M. J. (2007). *Displacement-based seismic design of structures.* Pavia: IUSS Press.

Punton, B. (2014). *Progressive collapse mitgation using CMA in RC framed buildings.* Southampton: Thesis for the degree of Doctor of Philosophy, University of Southampton.

Qian, K. (2012). *Experimental and Analytical Study of Reinforced Concrete Substructures Subjected to a Loss of Ground Corner Column Scenario.* Singapore: PhD thesis submitted to the Nanyang Technological University.

Qian, K., & Li, B. (2012). Dynamic performance of RC beam-column substructures under the scenario of the loss of a corner column—Experimental results. *Engineering Structures, 42*(0), 154–167.

Qian, K., & Li, B. (2012). Slab Effects on Response of Reinforced Concrete Substructures after Loss of Corner Column. *ACI Structural Journal, 109*(0), 845-855.

Qian, K., & Li, B. (2013). Analytical Evaluation of the Vulnerability of RC Frames for Progressive Collapse Caused by the Loss of a Corner Column. *Journal of Performance of Constructed Facilities.* doi:10.1061/(ASCE)CF.1943-5509.0000493

Qian, K., & Li, B. (2013). Analytical Evaluation of the Vulnerability of RC Frames for Progressive Collapse Caused by the Loss of a Corner Column. *Journal of Performance of Constructed Facilities*, 04014025.

Qian, K., & Li, B. (2013). Performance of Three-Dimensional Reinforced Concrete Beam-Column Substructures under Loss of a Corner Column Scenario. *J. Struct. Eng., 139*(4), 584-594.

Qian, K., & Li, B. (2013). Performance of Three-Dimensional Reinforced Concrete Beam-Column Substructures under Loss of a Corner Column Scenario. *J. Struct. Eng.,, 139*(4), 584–594.

Qian, K., & Li, B. (2013). Quantification of Slab Influences on the Dynamic Performance of RC Frames against Progressive Collapse.

Qian, K., Li, B., & Zhang, Z. (2016). Influence of Multicolumn Removal on the Behavior of RC Floors. *J. Struct. Eng., 04016006*, 1-13. doi:10.1061/(ASCE)ST.1943-541X.0001461

Qian., K., & Li, B. (2013). Analytical Evaluation of the Vulnerability of RC Frames for Progressive Collapse Caused by the Loss of a Corner Column. *J. Perform. Constr. Facil.* doi:10.1061/(ASCE)CF.1943-5509.0000493

Qing-feng, H., & Wei-jian, Y. (2008). Experimental Study on Collapse-Resistant Behavior of RC Beam-Column Sub-structure considering Catenary Action. *The 14th World Conference on Earthquake Engineering.* Beijing, China: National Information Centre of Earthquake Engineering .

Rabczuk, T. (2013). Computational Methods for Fracture in Brittle and Quasi-Brittle Solids: State-of-the-Art Review and Future Perspectives. *ISRN Applied Mathematics, Hindawi Publishing Corporation*, 1-38. Retrieved from http://dx.doi.org/10.1155/2013/849231

Rabczuk, T., & Belytschko, T. (2004). Cracking particles: a simplified meshfree method for arbitrary evolving cracks. *International Journal for Numerical Methods in Engineering, 611*, 2316–2343.

Robinson, G. P., Palmeri, A., & Austin, S. A. (n.d.). Appropriateness of Current Regulatory Requirements for Ensuring the Robustness of Precast Building Typologies. Loughborough, UK. Retrieved from http://www.ice.org.uk/ICE_Web_Portal/media/Events/Appropriateness-of-current-regulatory-requirements-for-ensuring-the-robustness-of-precast-building-typologies.pdf

Sagiroglu, S., & Sasani, M. (2014). Progressive Collapse-Resisting Mechanisms of Reinforced Concrete Structures and Effects of Initial Damage Locations. *Journal of Structural Engineering, ASCE*, 04013073.

Salem, H., El-Fouly, & Tagel-Din, H. (2011). Toward an economic design of reinforced concrete structures against progressive collapse. *Engineering Structures, 33*(0), 3341–3350.

Sasani, M. (2008). Response of a reinforced concrete infilled-frame structure to removal of two adjacent columns. *Engineering Structures, 30*(0), 2478–2491.

Sasani, M., & Kropelnicki, J. (2008). Progressive collapse analysis of an RC structure. *The Structural Design of Tall and Special Buildings*, 757-771.

Sasani, M., & Sagiroglu, S. (2008). Progressive Collapse Resistance of Hotel San Diego. *Journal of Structural Engineering , 134*(3), 478–488.

Sasani, M., & Sagiroglu, S. (2010). Gravity Load Redistribution and Progressive Collapse Resistance of 20-Story Reinforced Concrete Structure following Loss of Interior Column. *ACI Structural Journal, 107*(6), 636-644.

Sasani, M., Bazan, M., & Sagiroglu, S. (2007). Experimental and Analytical Progressive Collapse Evaluation of Actual Reinforced Concrete Structure. *ACI Structural Journal, 104*(6), 731-739.

Sasani, M., Werner, A., & Kazemi, A. (2011). Bar fracture modeling in progressive collapse analysis of reinforced concrete structures. *Engineering Structures*, 401–409.

Scawthorn, C., & Johnson, S. G. (2000). Preliminary report: Kocaeli (Izmit) earthquake of 17 August 1999. *Engineering Structures, 22*(7), 727–745.

Scott, M. H., & Hamutceuogelo, O. M. (2008). Numerically consistent regularization of force-based frame elements. *Int. J. Numer. Meth. Engng, 76*(0), 1612–1631.

Setzler, E. J., & Sezen, H. (2008). Model for the Lateral Behavior of Reinforced Concrete Columns Including Shear Deformations. *Earthquake Spectra, 24*(2), 493-511.

Sezen, H. (2002). *Seismic Behavior and Modeling of Reinforced Concrete Building Columns, PhD Thesis.* Berkeley, USA: Department of Civil and Environmental Engineering, University of California.

Sezen, H., & Moehile, J. (2004). Strength and deformation capacity of reinforced concrete columns with limited ductility,. Vancouver, Canada: Proceedings of the 13th World Conference on Earthquake Engineering.

Shoraka , M. B. (2013). *Collapse assessment of concrete buildings: an application to non-ductile reinforced concrete moment frames.* Vancouver: PhD Thesis, the University of British Columbia.

Sørensen, J. D. (2010). *Theoretical framework on structural robustness .* http://www.cost.eu/: COST Action TU0601 – Robustness of Structures.

Sourceable industry news analysis. (2016, July 15). Retrieved from https://sourceable.net/: https://sourceable.net/wp-content/uploads/2013/07/Ronan-Point-Explosion.jpg

Souza, R. M. (2000). *Force-based Finite Element for Large Displacement Inelastic Analysis of Frames.* Berkeley: University of California, Ph.D. Thesis.

Starossek, U., & Haberland, M. (2010). Disproportionate Collapse: Terminology and Procedures. *Journal of Performance of Construction Facility*, 519-528.

Starossek, U., & Haberland, M. (2011, 7-8). Aproaches to measures of structural robustness. *Structure and Infrastructure Engineering, 7*, 625-631.

Stinger, S. M. (2011). *Evaluation of Alternative Resistance.* Columbia, US: the University of Missouri-Columbia, Master Thesis.

Stinger, S. M., & Orton, S. L. (2013). Experimental Evaluation of Disproportionate Collapse Resistance in Reinforced Concrete Frames. *ACI Structural Journal, 110*(3), 521-530.

Structural Safety. (2013, Marsh 22). Retrieved from http://www.structural-safety.org/: http://www.structural-safety.org/view-report/cross104/

Stylianidis, P., Nethercot, D., Izzuddin, B., & Elghazouli, A. (2016). Study of the mechanics of progressive collapse with simplified beam models. *Engineering Structures, 117*, 287–304.

Su, Y., Tian, Y., & Song, X. (2009). Progressive Collapse Resistance of Axially-Restrained Frame Beams. *ACI Structural Journal,, 106*(5), 600-607.

Talaat, M. M., & Mosalam, K. M. (2008). *Computational Modeling of Progressive Collapse in Reinforced Concrete Frame Structures.* University of California, Berkeley: Pacific Earthquake Engineering Research Center, PEER Report 2007/10.

Taucer, F. F., Spacone, E., & Filippou., F. (1991). *A Fiber Beam-Column Element for Seismic Response Analysis of Reinforced Concrete Structures.* Berkeley: Report No.

UCB/EERC-91/17. Earthquake Engineering Research Center, College of Engineering, University of California,.

Tsai, M.-H., & Chang, Y.-T. (2015). Collapse-resistant performance of RC beam–column sub-assemblages with varied section depth and stirrup spacing. *Structural Design of Tall and Special Buildings, 24*(0), 555–570.

Tsai, M.-H., Lu, J.-K., & Chang, Y.-T. (2013). Experiemenatal investigation of the collapse resistence of RC beam-column subassemblages. *Proceeding the 6th Civil Engineering Conference in Asia Region: Embracing the Future through Sustainability* (p. 247). Jekarta: Wordpress.

UFC. (2009, July 14). Deaign of Buildings to Resist Progressive collapse. *Design of Buildings to Resiste Progressive Collapse*. Unified Facilities Creterien, Department of Defence, USA.

Usmani, A. S., & Cameron, N. J. (2004). Limit capacity of laterally restrained reinforced concrete floor slabs in fire. *Fire Resistance, 26*(2), 127–140.

Valipour, H., FarhangVesali, N., & Foster, S. (2013). A generic model for investigation of arching action in reinforced concrete members. *Construction and Building Materials, 38*(0), 742–750.

Valipour, H., Vessali, N., & Foster, S. (2015). Fibre-reinforced concrete beam assemblages subject to column loss. *Magazine of Concrete Research*, Paper 1500095.

Valipour, H., Vessali, N., Foster, S., & Samali, B. (2015). Influence of Concrete Compressive Strength on the Arching Behaviour of Reinforced Concrete Beam Assemblages. *Advances in Structural Engineering, 18*(8), 1199.

Vanadit-Ellis, W., Gran, J. K., & D. Vaughan. (2015, August 4). *US Army Centrifuge: Progressive Collapse Testing of a 4-Story Reinforced Concrete Structure at 1/18-Scale.* Retrieved from researchgate: https://www.researchgate.net/publication/265795717_US_Army_Centrifuge_Progressive_Collapse_Testing_of_a_4-Story_Reinforced_Concrete_Structure_at_118-Scale

Vecchio, F. J., & Colliins, M. P. (1986). The Modified Compression-Field Theory for Reinforcememt Concrete Elements Subjected to Shear. *American Concrete Institute (ACI) journal, 83*(0), 219-231.

Venture, N. C. (2010). *Program Plan for the Development of Collapse Assessment and Mitigation Strategies for Existing Reinforced Concrete Buildings.* Gaithersburg: National Institute of Standards and Technology.

Vogel, T., Kuhlmann, U., & Rölle, L. (2014). Robustheit nach DIN EN 1991-1-7. In U. Kuhlmann, *Stahlbau Kalender 2014* (pp. 559-610). Wiley-VCH Verlag GmbH & Co. KGaA.

Wang, T., Chen, Q., Zhao, H., & Zhang, L. (2015). Experimental Study on Progressive Collapse Performance of Frame with Specially Shaped Columns Subjected to Middle Column Removal. *Journal of Shock and Vibration, Hindawi Publishing Corporation.*, Accepted.

Wellmann, C., & Wriggers, P. (2012). A two-scale model of granular materials. *Comput. Methods Appl. Mech. Engrg.*, 46-58.

Wieczorek, G., Larsen, M., Eaton, L., Morgan, B., & Blair, J. L. (2016, July 17). *Debris-flow and flooding hazards associated with the December 1999 storm in coastal Venezuela and strategies for mitigation.* Retrieved from USGS Publications Warehouse - U.S. Geological Survey, Open File Report 01-0144, (2001): http://pubs.usgs.gov/of/2001/ofr-01-0144/

wikipedia. (1996, June 25). *Khobar Towers bombing*. Retrieved from https://en.wikipedia.org/: https://en.wikipedia.org/wiki/Khobar_Towers_bombing

Wikipedia. (2011, September 21). *[online] Available at: <> [Accessed on]*. Retrieved from Wikipedia, the free encyclopedia,: http://en.wikipedia.org/wiki/Progressive_collapse

Wood, C., Lodhi, M., & Sezen, H. (2014). Progressive Collapse Experiments, Modeling and Analysis of Existing Frame Buildings. *Structures Congress 2014* (pp. 909-919). ASCE.

Worakanchana, K., & Meguro, K. (2008). Voronoi applied element method for structural analysis: theory and application for linear and non-linear materials. *The 14th World Conference on Earthquake Engineering*, (pp. 1-8). Beijing, China.

Wu, C. T., Ma, N., Takada, K., & Okada, H. (2016). A meshfree continuous–discontinuous approach for the ductile fracture modeling in explicit dynamics analysis. *Computational Mechanics, Springer*, 1-19.

Xiao, L., Xin Zheng, L., Wan Kai, Z., & Lie Ping, Y. (2011). Collapse simulation of a super high-rise building subjected to extremely strong earthquakes. *SCIENCE CHINA - Technological Sciences*, 2549–2560.

Xiao, Y., Kunnath, S., Li, F. W., Zhao, Y. B., Lew, H. S., & Bao, Y. (2015). Collapse Test of Three-Story Half-Scale Reinforced Concrete Frame Building. *ACI Structural Journal, 112*(4), 429-438.

Xu, G., & Ellingwood, B. (2011). An energy-based partial pushdown analysis procedure for assessment of disproportionate collapse potential. *Journal of Constructional Steel Research*(67), 547-555.

Xuan Dat, P., & Hai, T. K. (2011). Membrane actions of RC slabs in mitigating progressive collapse of building structures. *Engineering Structures, 55*, 10-115. doi:10.1016/j.engstruct.2011.08.039

Xuan Dat, P., & Hai, T. K. (2013). Experimental study of beam–slabsubstructures subjected to apenultimate-internal column loss. *Engineering Structures, 55*(0), 2–15. Retrieved from http://dx.doi.org/10.1016/j.engstruct.2013.03.026

Xuan Dat, P., Hai, T. K., & Jun, Y. (2015). A simplified approach to assess progressive collapse resistance of reinforced concrete framed structures. *Engineering Structures*, 45-57.

Yavari, S., Elwood, K., Wu, C.-L., Lin, S.-H., Hwang, S.-J., & Moehle, J. (2013). Shaking Table Tests on Reinforced Concrete Frames without Seismic Detailing. *ACI Structural Journal/, 110*(06), 1001-1012.

Yi, W.-J., He, Q.-F., Xiao, Y., & Kunnath, S. K. (2008). Experimental Study on Progressive Collapse-Resistant Behavior of Reinforced Concrete Frame Structures. *ACI Structural Journal,, 105*(4), 433-439.

Yu, J. (2012). *Structural Behavior of Reinforced Concrete Frames Subjected to Progressive Collapse.* Singapore: A thesis submitted to the Nanyang Technological University.

Yu, J., & Tan, K. (2013). Structural Behavior of RC Beam-Column Subassemblages under a Middle Column Removal Scenario. *Journal of Structural Engineering, 139*(2), 233–250.

Yu, J., & Tan, K. H. (2010). Progressive collapse resistance of RC beam-column subassemblages. *Design and Analysis of Protective Structures (3rd:2010:Singapore).* Singapore: DR-NTU, Nanyang Technological University Library. Retrieved from This

document is downloaded from DR-NTU, Nanyang Technological: http://dr.ntu.edu.sg/bitstream/handle/10220/7034/Session%202%20Paper%203%20Yu.pdf?sequence=1

Yu, J., & Tan, K. H. (2014). Analytical model for the capacity of compressive arch action of reinforced concrete sub-assemblages. *Magazine of Concrete Research, 66(3),* , 109–126.

Yu, J., & Tan, K.-H. (2011). Experimental and numerical investigation on progressive collapse resistance of reinforced concrete beam column sub-assemblages. *Engineering Structures*(0), 90–106. doi:10.1016/j.engstruct.2011.08.040

Yu, J., Rinder, T., Stolz, A., Tan, K.-H., & Riedel, W. (2014). Dynamic Progressive Collapse of an RC Assemblage Induced by Contact Detonation. *Journal of Structural Engineering, 140*(6), 04014014.

Yu, X., Lu, D. G., Qian, K., & Li, B. (2016). Uncertainty and Sensitivity Analysis of Reinforced Concrete Frame Structures Subjected to Column Loss. *Journal of Performance of Constructed Facilities*, 04016069:1-15. doi:10.1061/(ASCE)CF.1943-5509.0000930

Zeng, X., & Zhang, B. X. (2012). Experimental Study on Axial Compression Behavior of RC Columns Under Rapid Loadings. *15th World Conference in Earthquake Engineering.* Lisbon, Portugal.

Zhao, J., & Sritharan, S. (2007). Modeling of Strain Penetration Effects in Fiber-Based Analysis of Reinforced Concrete Structures. *ACI Structural Journal, 104*(2), 133-141.

Zhao, X., Wu, Y.-F., Leung, A., & Lam, H. F. (2011). Plastic Hinge Length in Reinforced Concrete Flexural Members. *Procedia Engineering, 14*(0), 1266–1274

[i] No pictures have been provided reporting example from Syria because of the political nature of the sources. Interested readers can use the google images' search tool typing 'Syria buildings' viewing example regardless of the source